

# *Very Large-Scale Fires*

*N. R. Keltner, N. J. Alvares,  
and S. J. Grayson, editors*

*STP 1336*



STP 1336

# *Very Large-Scale Fires*

*N. R. Keltner, N. J. Alvares, and S. J. Grayson, Editors*

ASTM Stock #: STP1336



ASTM  
100 Barr Harbor Drive  
West Conshohocken, PA 19428-2959

Printed in the U.S.A.

## Library of Congress Cataloging-in-Publication Data

Very large-scale fires / N.R. Keltner, N.J. Alvares, and S.J. Grayson, editors.

p. cm. -- (STP ; 1336)

"ASTM stock number: STP1336."

Includes bibliographical references and index.

ISBN 0-8031-2481-3

1. Fires. 2. Fire extinction. 3. Tall buildings--Fires and fire prevention. 4. Wildfires--Prevention and control. I. Keltner, N. R. (Ned R.), 1942-. II. Alvares, Norman J. III. Grayson, S. J. IV. Series: ASTM special technical publication ; 1336.

TH9448.V47 1998

628.9'25--dc21

98-45728

CIP

Copyright © 1998 AMERICAN SOCIETY FOR TESTING AND MATERIALS, West Conshohocken, PA. All rights reserved. This material may not be reproduced or copied, in whole or in part, in any printed, mechanical, electronic, film, or other distribution and storage media, without the written consent of the publisher.

### Photocopy Rights

**Authorization to photocopy items for internal, personal, or educational classroom use, or the internal, personal, or educational classroom use of specific clients, is granted by the American Society for Testing and Materials (ASTM) provided that the appropriate fee is paid to the Copyright Clearance Center, 222 Rosewood Drive, Danvers, MA 01923; Tel: 508-750-8400; online: <http://www.copyright.com/>.**

### Peer Review Policy

Each paper published in this volume was evaluated by two peer reviewers and at least one editor. The authors addressed all of the reviewers' comments to the satisfaction of both the technical editor(s) and the ASTM Committee on Publications.

To make technical information available as quickly as possible, the peer-reviewed papers in this publication were prepared "camera-ready" as submitted by the authors.

The quality of the papers in this publication reflects not only the obvious efforts of the authors and the technical editor(s), but also the work of these peer reviewers. The ASTM Committee on Publications acknowledges with appreciation their dedication and contribution of time and effort on behalf of ASTM.

# Foreword

This publication, *Very Large-Scale Fires*, contains papers presented at the symposium of the same name, held in St. Louis, MO on 16 June, 1997. The symposium was sponsored by Committee E5 on Fire Standards. Ned R. Keltner, with Ktech Corporation in Albuquerque, NM; Norman J. Alvares, with Fire Science Applications in San Carlos, CA; and Stephen J. Grayson, with Interscience Communications in London, U.K., served as symposium co-chairmen and are editors of the resulting publication.

# Contents

<b>Overview—N. R. KELTNER</b>	1
<b>RAPID OR LARGE STRUCTURE FIRES</b>	
<b>Fire Development and Fatality Analysis of the April 19, 1993 Fire at the Branch Davidian Mt. Carmel Center, Waco, Texas—G. J. HAUSSMANN</b>	7
<b>Analysis of Full-Scale Fire Tests of Wall Linings in Ranch House— M. M. HIRSCHLER</b>	20
<b>High-Temperature Accelerant Arson—Revisited—N. R. KELTNER, H. K. HASEGAWA, AND J. A. WHITE, JR.</b>	41
<b>Large Compartment Fire Tests on a Full-Scale Eight Storey Building— T. LENNON</b>	55
<b>INDUSTRIAL AND WILD LAND FIRES</b>	
<b>Time-Dependent Model of Forest Fire Spread in Turbulent Gusting Winds— V. E. GARZÓN, J. M. McDONOUGH, AND K. SAITO</b>	73
<b>Estimates of the Extent and Character of the Oxygen-Starved Interior in Large Pool Fires—L. A. GRITZO, W. GILL, AND V. F. NICOLETTE</b>	84
<b>Reconstruction of Very Large-Scale Fires—K. SAITO</b>	99
<b>Boiling Liquid Expanding Vapor Explosions (BLEVE): Possible Failure Mechanisms—J. E. S. VENART</b>	112
<b>MARINE FIRES</b>	
<b>Experimental Measurement of a Shipboard Fire Environment with Simulated Radioactive Materials Packages—J. A. KOSKI, S. D. WIX, AND D. E. BEENE, JR.</b>	135

**Evaluation of Large-Scale Marine Fire Protocols—R. L. HANSEN**

AND G. G. BACK

150

**Full-Scale Model Tests of Smoke Movement in Ship Passenger  
Accommodations (First Report)—K. YOSHIDA**

163

# Overview

---

Time and again, it has been observed that the rules governing fire behavior appear to change as the intensity and scale of the fire increase. Sometimes, conditions combine to produce events that surprise and amaze all of us, often with tragic results. Well known examples of such severe fires include:

- a) The Dupont Plaza hotel fire—hot, fire gases from a growing, ventilation-controlled fire in one part of the hotel/casino complex were transported to another part of the complex. This resulted in a rapid flashover in that area.
- b) The Piper Alpha offshore platform—a sequence of explosions and fires eventually caused this platform to sink in the North Sea.
- c) The Apollo Space Capsule fire—an oxygen-enriched atmosphere accelerated burning.
- d) In Mississauga, Ontario—a tankcar fire generated a boiling liquid/expanding vapor explosion that destroyed a large area.
- e) The Berkeley Hills fire—this fire in a wildland/urban interface demonstrated the importance of more fire resistive construction and the need to control vegetation near structures.
- f) The Storm King Mountain wildfire in Colorado—a number of fire fighters were killed when the fire jumped over their position.

The keynote address for the symposium was appropriately titled “A Review of Very Severe Fires.” Dr. John R. Hall, Jr. Assistant Vice President of the National Fire Protection Association, described a study of the 36 largest-loss fires of the quarter century from 1971 through 1995. In all of these fires, direct property damage equaled or exceeded \$100 million in 1995 dollars. These incidents demonstrated several common situations—fires in the wildland/urban interface, a vapor cloud or other very large initiating explosion, gaps in sprinkler coverage or other sprinkler problems, or fires in areas where there was extremely high value per square foot of exposed space. In the study, special attention was given to the physical area involved in the fire and the distance over which the effects of the fire were felt. Such distance factors are important considerations in our ability to model or otherwise represent these important fires for purposes of performance-based design or other calculation-supported decision-making. The 36 fires ranged in size from a low of 1200 square feet for a cable fire in a telephone switching station to a high of 5.1 billion square feet (184 square miles) in a wildfire.

Fire losses in North America are high when compared to other developed countries. According to the Building and Fire Research Laboratory at the National Institute of Standards and Technology, the economic cost of fire safety and fire losses in the United States exceeds \$100 billion per year. One of the keys to saving lives and reducing dollar losses is improved understanding of complex fire phenomena. Very large-scale fires, as described above, generally cause the greatest number of deaths, or the largest monetary losses, or both. As a result of their spectacular nature, they also generate the most headlines. The publicity produces calls for action on the part of government and fire safety organizations.

Fires involve several highly nonlinear physical phenomena, such as combustion and turbulence and radiation heat transfer. Individually, these phenomena are difficult to understand. Coupling of these nonlinear phenomena make understanding any fire a very challenging proposition. However, the changing rules in very large-scale fires is believed to be a result of strong coupling between these nonlinear phenomena.

Very large-scale fires are difficult, if not impossible, to replicate completely. Studying or modeling the accidents and conducting large-scale experiments provides insight into the coupling between the various fire phenomena. Large-scale experiments are needed to capture the important physics. However, these experiments are very costly. Given their complexity and volume, they are difficult to instrument and understand.

We use a variety of experimental and analytical tools in our attempt to understand the special hazards and risks associated with these fires. The tools of fire science include:

- 1) Developing scaling laws, correlations, and parametric models.
- 2) Developing numerical models ranging in complexity from zone models based on differential equations up to three-dimensional field models based on computational fluid dynamics codes.
- 3) Using forensic techniques to attempt to reconstruct the events in fires as well as guide both our models and experiments.
- 4) Conducting large numbers of laboratory experiments to study the physics and the materials' reaction-to-fire.
- 5) Conducting smaller numbers of intermediate and large-scale experiments as a means of validating scaling laws and analytical/numerical models as well as for evaluating fire protection techniques.

The Table of Contents indicates some of the many and varied types of fires that occur. We attempt to model and understand these diverse fires using this whole arsenal of tools because the events and phenomena are so complex. Although it would be desirable to have models that could accurately predict the complex behavior of fires, this is a long way off. Given the complexity and diversity of fires along with the assumptions and limitations inherent in any model, it is no surprise we often disagree. In this respect, studies of fire are no different than many other walks of life. Even though our models are not perfect, one thing must be remembered. *The purpose of all of these models is insight.*

What is important? To improve our understanding of fire behavior and translate this understanding into public practice to help reduce fire-related injuries and deaths. Through a lot of hard work, we keep learning and keep improving the tools in our arsenal. As documented in these proceedings, the capabilities of our experimental and analytical models are improving steadily.

ASTM Committee E-5 on Fire Standards sponsored this symposium to promote communication and aid progress in this important area of fire safety. All of the tools mentioned above were touched on during this symposium. In fact, a number of the papers demonstrated the effectiveness of using more than one type of tool in an interactive fashion. As in other areas of fire science, significant progress has been generated by using experiments to help develop analytical models and analytical models to help design experiments.

The symposium program was organized into three areas:

### **Rapid or Large Structure Fires**

This section includes fires that develop rapidly, such as the wind-driven fire at the Branch Davidian Complex, fires in high-rise apartment buildings, techniques for extracting additional information from earlier test burns, and the High Temperature Accelerant Arson Demonstration Burn. In particular:

“Fire Development and Fatality Analysis of the 19 April, 1993 Fire at the Branch Davidian Mt. Carmel Center, Waco, Texas”—Fires were started in several locations in a large wooden structure; they were driven by the wind into a conflagration. Seventy-six people perished in the fire. This paper describes the results of an independent investigation into the events that occurred.

“Analysis of Full-Scale Fire Tests of Wall Linings in Ranch House”—Large-scale experiments of any kind are expensive. This paper looks at techniques for extracting and correlating additional information from the numerous test burns of houses that have been conducted over the years.

“High-Temperature Accelerant Arson—Revisited”—A series of unusual fires in the Pacific Northwest were eventually called the High-Temperature Accelerant Arson Fires. These were unusual fires given their extremely rapid development in large structures, even those with low fuel loads. They melted steel and caused premature collapse of heavy timber construction. The unusual fire characteristics resulted in the deaths of two fire-fighters. This paper describes a demonstration burn conducted in a 1900-square-meter, single-story, strip shopping center building to support the Seattle Fire Department’s arson investigation. The burn produced flashover in approximately two minutes and a large backdraft event.

“Large Compartment Fire Tests on a Full-Scale Eight Storey Building”—A purpose built, high-rise, steel frame structure was used to study the behavior of multi-storey buildings subjected to real fires. The fire data are being used to validate models for structural analysis at elevated temperatures and evaluate parts of the forthcoming Eurocodes.

## Industrial and Wild Land Fires

This session looks at the causes and character of fires and explosions. Topics include boiling liquid—expanding vapor explosions (BLEVE) which have caused massive damage in both LPG storage facility and railcar accidents, the development of a scale model experimental facility for studying the generation of dangerous fire whirls, characterization of large petrochemical fires, and the use of CFD modeling for studying fire brand transport in forest fires. In particular:

“Estimates of the Extent and Character of the Oxygen-Starved Interior in Large Pool Fires”—Large hydrocarbon pool and spill fires have very different characteristics than structural fires. There has been a concerted effort over a number of years to define the thermal exposure of objects engulfed by or adjacent to these fires. This paper describes experimental data from JP8 fires (19 meter diameter—heat release rate of 800–900 MW) and the use of CFD codes to help interpret the results.

“Time-Dependent Model of Forest Fire Spread in Turbulent Gusting Cross Winds”—Forest fires can produce tremendous updrafts and transport burning embers long distances. These fire-brands can cause spot fires well beyond the current fire line and pose a significant danger to fire fighters. This paper examines the development of a CFD model for predicting the trajectories of fire-brands. The purpose is to develop tools for forest fire management and reduce the risk of fighting these fires.

“Reconstruction of Very Large-Scale Fires—Fire whirls have been generated following earthquakes as well as in wars and forest fires. These whirls can produce tornado-like winds. A mass fire broke out following a severe earthquake in Tokyo; winds in a fire whirl generated by the mass fire were estimated to be over 70 m/s (157 miles/hour). This paper covers the development of a dimensional analysis and scale model test facility for studying the production of fire whirls.

“Boiling Liquid Expanding Vapor Explosions (BLEVE): Possible Failure Mechanisms”—BLEVEs can produce devastating explosions and highly radiative fireballs. A series of experiments exposed 2-ton, pressure liquefied gas vessels to jet fires. Based on an analysis of the catastrophic vessel failure, this paper postulates a two-step process. First, there is initiation of a crack in the vapor-wetted area of the vessel. Nearly instantaneous release of the contents results from rapid crack propagation (unzipping) in the tank wall.

## **Marine Fires**

This session covers testing of Halon replacement agents such as water mists, the thermal exposure of radioactive material shipping containers in marine fires, and smoke movement in passenger ships. In particular:

“Evaluation of Large-Scale Marine Fire Protocols”—International agreements require the replacement of Halon-based fire suppression systems. Water mist or gaseous agent systems are potential replacements. This paper reviews large-scale experimental evaluations of the effectiveness of such systems for protecting critical machinery spaces.

“Experimental Measurement of a Shipboard Fire Environment with Simulated Radioactive Material Packages”—The public is concerned about the potential release of hazardous materials in fires. This paper describes a series of experiments used to define the potential thermal exposure of radioactive material shipping containers due to fires in a ship’s hold. Large pipe calorimeters were used to simulate containers and measure heat fluxes generated by pool, spray, and wood crib fires. The experiments were conducted at the U.S. Coast Guard’s large test facility in Mobile, Alabama.

“Full-Scale Model Tests of Smoke Movement in Ship Passenger Accommodations”—Ships and offshore platforms share special fire safety concerns because their relative isolation means they need to control fires by themselves for more extended times. In passenger ship fires, smoke has been identified as one of the major threats to the passengers and crew. This paper describes experiments, conducted in a specially built test facility, to study smoke transport away from the point of fire origin.

## **Rapid or Large Structure Fires**

Gregory J. Haussmann<sup>1</sup>

**Fire Development and Fatality Analysis of the 19 April, 1993 Fire at the Branch Davidian Mt. Carmel Center, Waco, Texas**

---

**REFERENCE:** Haussmann, G. J., “Fire Development and Fatality Analysis of the 19 April, 1993 Fire at the Branch Davidian Mt. Carmel Center, Waco, Texas,” Very Large-Scale Fires, ASTM STP 1336, N. R. Keltner, N. J. Alvares, and S. J. Grayson, Eds., American Society for Testing and Materials, 1998.

**ABSTRACT:** On 19 April, 1993, fire broke out and spread rapidly through the Mt. Carmel Center of the “Branch Davidians”, located near Waco, Texas. Seventy-six occupants of the structure perished in the resulting inferno. In sharp contrast to most large fires, a substantial amount of information is available regarding the origin and spread of this fire. This information clearly establishes multiple origins and documents rapid fire spread through the structure. Analysis of fatality records shows that fire related factors accounted for 80% of reported causes of death. Factors identified as contributing to the high casualty rate include multiple fire origins, rapidly spreading fires, structural collapse of critical egress points, the clustering of women and children in a perceived area of refuge (a fortified “bunker”), and the use of chemical agents in this area.

**KEYWORDS:** Large scale fires, fire cause and origin, fire egress, Waco

---

On 28 February, 1993, agents of the Bureau of Alcohol, Tobacco, and Firearms (ATF) went to the Mt. Carmel Center of the Branch Davidians, located near Waco, Texas, to serve an arrest warrant for David Koresh and a search warrant for the Mt. Carmel Center. Gunfire was exchanged during an attempted forced entry to the facility, resulting in the deaths of four ATF agents and five members of the Branch Davidians. Following this initial confrontation, the Federal Bureau

---

<sup>1</sup>Senior Managing Engineer, Thermal Sciences Department, Failure Analysis Associates, Inc., 149 Commonwealth Dr., Menlo Park, CA 94025.

of Investigation (FBI) took over control of the scene and a 51-day standoff began.

On the morning of 19 April, 1993, the FBI executed a plan to deliver tear gas into the Mt. Carmel Center, with the intent of forcing the occupants to leave the building. The initial plan anticipated the incremental use of tear gas over a period of several days. Modified M60 tanks, known as Combat Engineering Vehicles, (CEVs) were fitted with battering rams and tear gas delivery systems. The CEVs used their battering rams to break into the structure and deliver tear gas to the first and second floors. ISPRA Protectojet Model 5 (M5) Anti-Mob Fog Ejectors were mounted on the CEVs [ 1 ]. The M5 system is a pressurized bottle containing 30 g of CS tear gas dissolved in 1070 g of methylene chloride, with 700 g of carbon dioxide propellant. In addition to the CEVs, Bradley infantry carriers were used to deliver 40-mm liquid filled "Ferret" tear gas rounds into the structure. This 40 mm barricade-penetrating plastic projectile, delivered using M79 grenade launchers, can penetrate a hollow core door at a distance of 100 m [ 1,2 ]. Each 40-mm Ferret round contains 3.7 g of CS dissolved in 33.25 g of methylene chloride. These devices represent nonpyrotechnic delivery systems.

At approximately 6:00 AM, the CEVs began to break into the structure and deliver CS tear gas. Within a few minutes, shots from inside the structure were reported. At this point the gas assault was accelerated, and tear gas rounds were fired into all windows and through a side wall of the structure [ 1 ]. Four separate assaults using CEVs to deliver larger quantities of CS gas were carried out, resulting in the demolition of significant portions of the structure. Shortly after the fourth and final round of tear gas delivery by the CEVs was completed at approximately 12:06 PM, fire broke out in the structure. This fire spread rapidly through the building, and the Mt. Carmel Center burned completely to the ground. Of the 85 occupants, only 9 escaped.

## DESCRIPTION OF THE MT. CARMEL CENTER

As part of an independent investigation into events that occurred on 13 April, 1993, Failure Analysis Associates, Inc. (FaAA) constructed a three-dimensional computer model of the Mt. Carmel Center based on data from an FBI Laboratory report (photogrammetric analysis and site survey), careful examination of numerous photographs of the center, testimony of survivors, and other government reports [ 1,3 ]. The Mt. Carmel Center was a multistory wood frame building constructed by the Branch Davidians, primarily using combustible materials [ 3,4 ]. The ground floor consisted of a gymnasium and chapel attached to the main building, an approximately 54 m long by 7.3 m wide two-story structure containing living quarters (Fig. 1). Each end of the main building had a three-story tower, and a four-story tower was attached to the rear of the structure, adjacent to the dining room. The first floor of the four-story central

tower was a concrete bunker, approximately 9.5 by 6.4 m. Adjacent to the bunker was an attached dining room which encompassed the remainder of the first floor of the center.

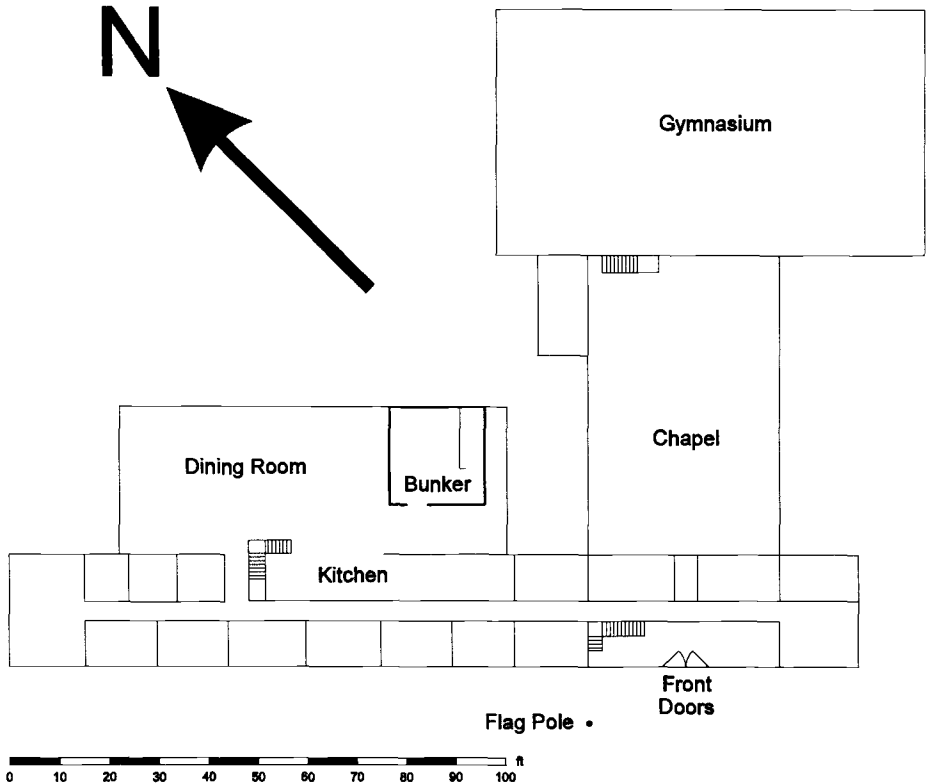


FIG. 1--Layout of the Mt. Carmel Center.

**FIRE INITIATION**

A substantial amount of information is available regarding the origin and spread of this fire, including videotape from multiple angles, aerial photographs, aerial forward looking infrared (FLIR) video, and interviews with survivors. Synchronization of the various video and infrared images allows a detailed timeline of events to be constructed for events leading up to and including the spread of fire through the structure, as found in Table 1.

A careful review of overhead infrared video and continuous television coverage of the standoff from several sides of the building allows this detailed fire timeline to be developed. The aerial FLIR video was taken from an aircraft orbiting the

building, and as such views from all sides of the building are available. The first indication of a fire is observed in the FLIR at 12:07:41 PM as a moderate heat indication in a second floor window in the southeast corner (Fig. 2). Although a CEV injected a bottle of tear gas at the first floor level in this location approximately 90 s before the start of this fire, there is no evidence of a direct connection between these two events, which occurred on separate floors. A larger, well-established fire was later observed at 12:08:11 PM at the rear of the dining room. This is seen in both FLIR and conventional video, as a large heat signature on the FLIR and a moderate quantity of white smoke on video. These two fires were nearly simultaneous, in separate and distinct portions of the building. A third fire was observed on the FLIR at 12:09:44 PM, near the east wall in the central portion of the chapel. Although the person or persons responsible for starting these fires have not been identified, the use of liquid accelerants was documented by the arson investigation team [ 3 ]. Furthermore, punctured one gallon camping fuel containers were uncovered in the fire debris (Fig. 3).

TABLE 1 --Timeline of events, 19 April 1993.

Time	Events
6:00 AM	Initial tear gas application
11:45 AM	Tear gas discharged at bunker entrance
12:06 PM	Fourth CS gas application completed
12:07:41 PM	FLIR reveals onset of fire in second floor, southeast corner (origin #1)
12:08:11 PM	FLIR and video reveals established fire in dining room (origin #2)
12:09:44 PM	FLIR reveals onset of fire in approximate middle of chapel (origin #3)
12:14 PM	Dining room, chapel, gymnasium, and second floor of southeast tower fully involved
12:27 PM	Large fireball observed immediately adjacent to the bunker; structure fully involved

## FIRE DEVELOPMENT

Strong winds contributed significantly to the rapid spread of fire through the Mt. Carmel Center. The National Oceanic and Atmospheric Administration weather station in Waco recorded high winds beginning at noon on 18 April, 1993. These winds continued unabated through the day on 19 April, 1993. At the time of the fire, winds were recorded from the south-southeast at 39 km/h, with gusts to 48 km/h. The Mt. Carmel Center had experienced substantial structural damage at this time, as CEVs had breached major sections along the front and right hand

side of the structure, and had completely collapsed one-half of the gymnasium (Fig. 4). The dining room and chapel fires grew at an extremely rapid pace, shown in Fig. 5 [ 4 ].

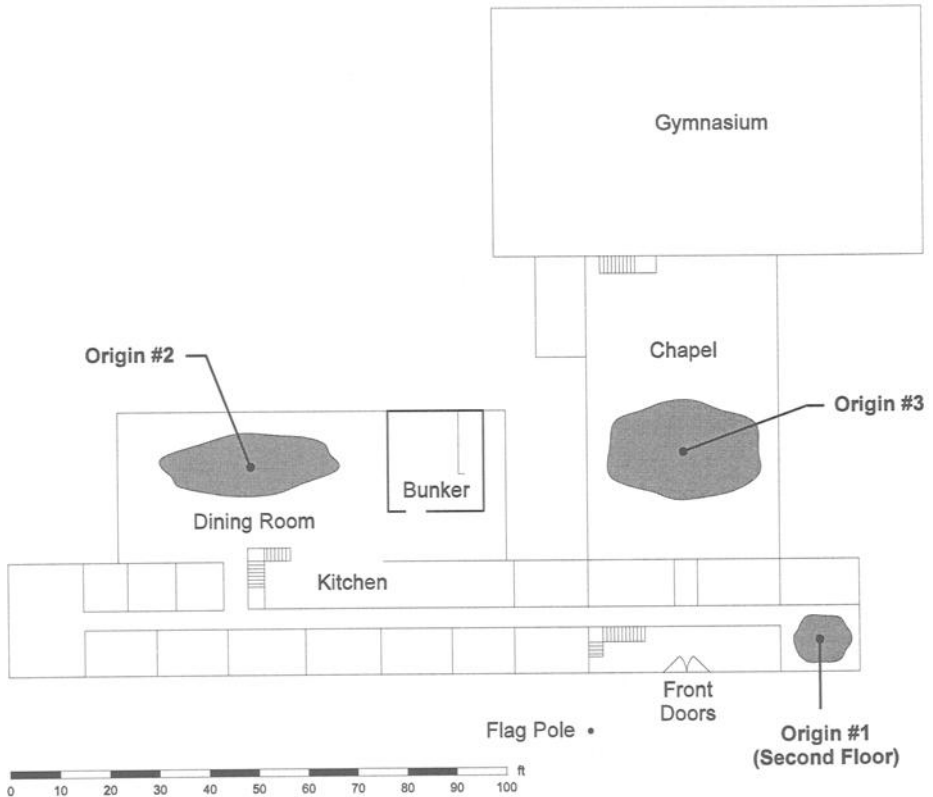


FIG. 2--Location of independent fire origins.

High winds, coupled with the reported penetration of all windows by 40-mm Ferret tear gas rounds and the large openings and structural damage caused by the CEVs, significantly increased ventilation to the fire and the rate of fire spread through the structure [ 3 ]. This is most clearly seen in the spread of fire through the chapel and gymnasium, which experienced severe structural damage on both upwind and downwind faces prior to the fire. Structural damage was present at the Mt. Carmel Center to an extent uncommon to most large structural fires (other than those preceded by internal gas explosions). Experimental test burns have been found to demonstrate a marked increase in structural fire spread rates under windy conditions simply by opening the windows. Additionally, structural damage has been found to increase the rate of fire spread [ 5 ].



FIG. 3--Punctured fuel containers recovered in fire debris.



FIG. 4--Pre-fire structural damage to the Mt. Carmel Center.

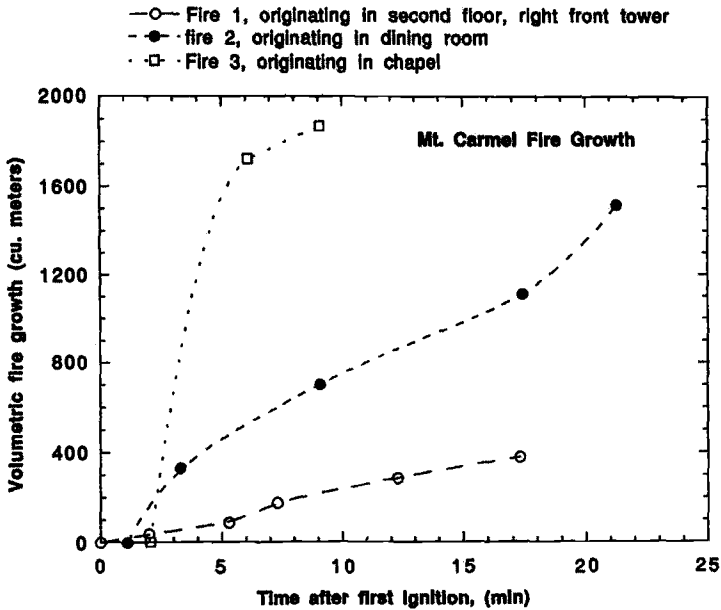


FIG. 5—Volumetric fire growth rates [ 4 ].

Many theories about the cause and spread of fire have surfaced, many of them involving alleged governmental conspiracies against the Branch Davidians. One example involves allegations that flame-throwing tanks (CEVs) were used by the government to start fires in the building [ 6 ]. This documentary shows a video excerpt containing “evidence” of such tanks, with a flash observed as the vehicle backs away from the structure. A complete analysis of this video reveals that the “flames” emitted from the CEV are in fact reflections from insulation material which fell on the CEV during demolition activities. Furthermore, the FLIR has been synchronized with this video, revealing that the “flames” generate no heat.

Additional allegations have been raised regarding a large fireball observed during the fire, in the immediate vicinity of the bunker. Many of the victims were found in this location. Analysis of photographs taken from the southern (front) side of the building and video taken from the east allows the location of this fireball to be determined. The fireball emanated from the courtyard area on the east side of the bunker. Propane tanks of 100 lbs (45 kg) are observed in this location in post-fire photographs. Although the safety relief valves on several tanks appear to have prevented explosions, one was reported to have ruptured during the fire [ 3 ]. Calculations indicate that such a release is consistent with the size of the fireball observed [ 4 ].

One final hypothesis regarding the origin and spread of the fire involves the potential role of methylene chloride, the solvent in which the CS chemical agent is dissolved. Two means of tear gas delivery were used in the assault, the M5 systems mounted to CEVs and 40-mm Ferret rounds launched from Bradley infantry carriers. A total of 20 M5 bottles and approximately 375 Ferret rounds were delivered [ 1 ], representing a combined total of approximately 1,900 g of CS and 33,000 g of methylene chloride. Tear gas was delivered over a period of 6 hours, with the maximum methylene chloride concentration calculated as approximately 1%, substantially below the lower flammability limit of 12% [ 7 ]. Furthermore, no indications of internal gas explosions were observed associated with the origin of any fire. The amounts used were insufficient to play a significant role in either the ignition or spread of the fire.

## FATALITY ANALYSIS

Our investigation of the official causes of death included evaluation of autopsy reports, death certificates, toxicological test results, and the forensic examination report which includes the location of each set of remains [ 8 ]. Autopsy reports and death certificates were available for 75 of the 76 victims, and are summarized in Appendix A.

Out of 85 people present in the structure when the fires started, only 9 survived. Of the survivors, one was in a room attached to the adjacent water tower, four exited through the East wall of the chapel, and four exited the front (South) side. The high casualty rate raises questions regarding factors responsible for impeding egress from the structure. Although several possible egress routes were potentially demolished by the CEVs [ 3 ], many routes to safety were available during the early stages of the fires. Eight people escaped in the upwind direction during later stages of the fire, through areas kept free of smoke and flames by strong prevailing winds blowing into the structure.

Although it has been widely reported that many of the Branch Davidians died from gunshot wounds, only 18 of the 76 victims were found to have gunshot wounds as a cause of death (Appendix A). The distribution of victims who died as a result of gunshot wounds is illustrated in Fig. 6. The majority of victims died as a result of fire related injuries. Thirty-four victims, primarily women and children, died inside the first floor bunker, with many others found near the only exit to this bunker. The distribution of victims who died as a result of fire related injuries is illustrated in Fig. 7. This pattern of fatalities strongly indicates that many of the victims were trapped inside the bunker, with an attempt to exit the bunker made only after egress was untenable. Note that the only door to the bunker was a blanket covering the opening, and therefore physical barricading of the victims inside the structure did not occur.

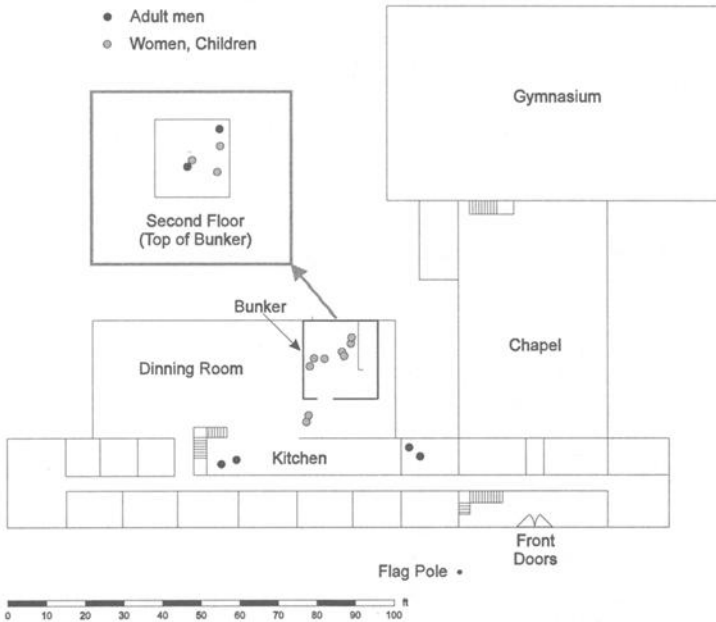


FIG. 6-- Location of victims with gunshot wound as cause of death.

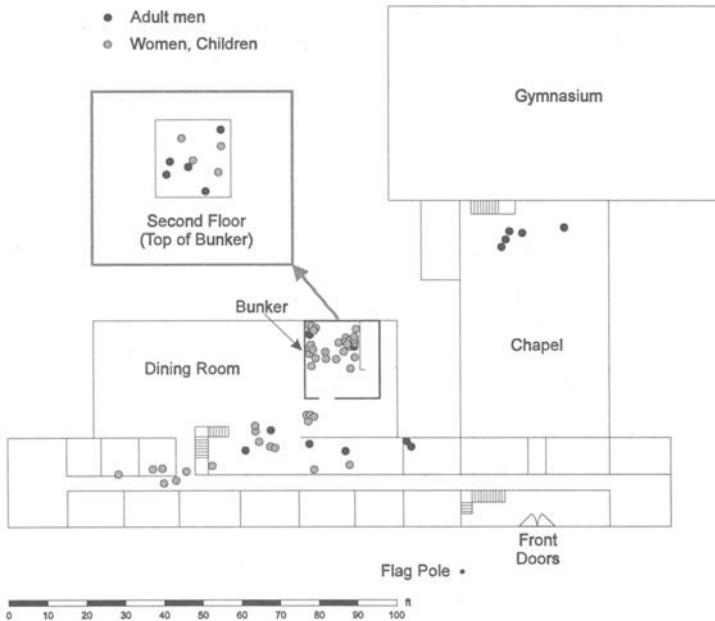


FIG. 7--Location of victims with fire-related causes of death.

The tear gas agent used by the FBI was CS "tear gas". This chemical is dissolved in a liquid solvent, methylene chloride (dichloromethane) in this case, and dispersed as an aerosol. A CS concentration of 10 mg/m<sup>3</sup> is sufficient to deter trained soldiers [ 9 ]. Use of the M5 delivery system indoors produced extremely high concentrations of both CS and the methylene chloride carrier agent. M5 bottles were discharged into individual rooms as small as 3 by 3 m, yielding CS concentrations as high as 90 times that required to deter trained soldiers. Methylene chloride concentrations are calculated to be as high as twice the level considered immediately dangerous to life and health (IDLH), and nearly to the level that would render a person unconscious [ 7 ].

The fourth and final use of tear gas involved a total of four M5 bottles. Of these, two were discharged after a CEV had penetrated deep into the structure, following instructions to attempt to penetrate to the base of the central tower (bunker) [ 10 ]. At this time, many women and children were seeking refuge from the tear gas assault in the bunker. Two bottles were discharged near the entrance to the bunker, generating a methylene chloride concentration of 0.1% in the kitchen and dining room area, which is well below levels considered to be a fire or health threat. The resulting CS concentration, however, was approximately 90 mg/m<sup>3</sup> (9 times that required to deter trained soldiers), representing a significant impediment to egress. Although fire spread in this area was rapid, safe egress was likely possible at the time of fire detection absent other impeding factors, such as this presence of CS gas. Later in the fire, high levels of toxic materials found in post-flashover fires would additionally restrict the possibility of egress. Smoke toxicity in large post-flashover fires is typically dominated by carbon monoxide (CO) in the smoke [ 11 ]. Under post-flashover ventilation-limited conditions, a production rate of approximately 0.2 kg CO per kg of fuel burned is typically reached, generating high levels of CO inside the building.

Blood carboxyhemoglobin saturation levels were reported for 56 of the victims, with values of up to 79% reported (Appendix A). Postmortem carboxyhemoglobin saturations above 30% are potentially hazardous to most humans, and levels above 50% are likely to be lethal [ 12 ]. In addition to fire-related causes of death, 8 victims are reported to have died solely as a result of asphyxiation by suffocation as they were physically trapped inside the collapsing bunker (Appendix A). Escape from the bunker was difficult if not impossible due to high CS gas levels prior to the fire, and was compounded by smoke toxicity following flashover several minutes into the fire. Although the possibility of an enforced (by threat of firearms) stay inside the bunker has been raised by some; no direct evidence to support or deny this allegation has been found in the present investigation.

## CONCLUSIONS

The fire that destroyed the Mt. Carmel Center of the Branch Davidians on 19 April, 1993 was watched live on television by millions. This sparked much controversy regarding events that occurred on that day. Despite the substantial amount of information available regarding the origin and spread of this fire, numerous and wildly conflicting theories surfaced regarding the fire origin, fire development, and casualties, many of which persist to this day. A rigorous scientific approach allows an evaluation of such theories, sorting out fact from fiction. Available information clearly establishes multiple origins and rapid fire spread through the structure, with three separate and distinct fires developing in a period of less than 2 min. Many factors combined to generate conditions under which fire represented a singularly severe threat to occupants of the building, including rapidly spreading fires driven by unusually high ventilation as a result of to high winds coupled with severe structural damage, potential structural collapse of critical egress points, clustering of women and children in a perceived area of refuge (a fortified "bunker"), and the use of large quantities of chemical agents in this area.

## GLOSSARY

ATF	Bureau of Alcohol, Tobacco, and Firearms.
Bradley	Armored infantry carrier.
CEV	Combat Engineering Vehicle (modified M60 tank).
CS	Orthochlorobenzylidene Malononitrile (a form of tear gas).
Ferret	Tear gas projectile (40-mm).
ISPRA	Israel Product Research Co. Ltd.
M5	Projectojet model 5 tear gas delivery system (manufactured by ISPRA).
M79	Grenade launcher.

## REFERENCES

- [ 1 ] Scruggs, R., Gonzalez, V., Zipperstein, S., Cousins, H., Lyon, R., and Beverly, R., "Report to the Deputy Attorney General on the Events at Waco, Texas February 28 to April 19, 1993," United States Department of Justice, 8 Oct. 1993.
- [ 2 ] Mace Security International Products Catalog, Federal Laboratories Division, Chemical Munitions & Accessories - projectiles for confined area use, Bennington, Vermont, 1994.
- [ 3 ] Gray, P., C., Ricketts, J. T., Cass, W. S., and Hitchings, T. W., "Fire Investigation Report, Branch Davidian Compound, Waco, Texas, April 19, 1993," 13 July 1993.

- [ 4 ] Quintiere, J. G. and Mowrer, F., "Fire Development Analysis, Mount Carmel Branch Davidian Compound, Waco, Texas, April 19, 1993," University of Maryland, 8 September 1993.
- [ 5 ] Waterman, T.E., "Experimental Structural Fires," Report AD/A-001 134, IIT Research Institute, July 1974.
- [ 6 ] Thompson, L., "Waco: The Big Lie," American Justice Federation, 1993.
- [ 7 ] Material Safety Data Sheet for methylene chloride (CAS No. 75-09-2), Revision G, Genium Publishing Corp., Schenectady, NY, June 1994.
- [ 8 ] Peerwani, N., "Summary Report on Forensic Examination of Human Remains from the Branch Davidian Compound, Mount Carmel, McLennan County, Texas," Tarrant County Medical Examiner's Office, 29 Sept. 1993.
- [ 9 ] Himsworth, H., Black, D. A. K., Crawford, T., Dornhorst, A. C., Gilson, J. C., et al., "Report of the Enquiry into the Medical and Toxicological Aspects of CS (Orthochlorobenzylidene Malononitrile), Part 11. Enquiry into the Toxicological Aspects of CS and its Use for Civil Purposes," Home Office, Her Majesty's Stationery Office, London, Sept. 1971.
- [ 10 ] Testimony of FBI Special Agent R.J. Craig, United States of America vs. Brad Branch, Kevin Whitecliff, Clive Doyle, et al., Criminal Action No. W-93-CR-046, United States District Court for the Western District of Texas, Waco Division, 8 Feb. 1994, pp. 5525-5530.
- [ 11 ] Clarke, F. B., "Physiological Effects of Smoke: Managing Escape," American Society of Heating and Refrigeration Engineers Journal, March 1997, pp. 47-56.
- [ 12 ] National Fire Protection Association, Fire Protection Handbook, 17<sup>th</sup> edition, 1991, p. 3-4.

Appendix A - Summary of Autopsy Results

Doe #	Case #	Location (Medical Examiner Summary Report)	Age (yrs)	Sex	Reported Causes of Death:							Carboxyhemoglobin Level	
					Gunshot Wound	Thermal Injury	Asphyxiation (CO)	Asphyxiation (Suffocation)	Smoke Inhalation	Trauma	(% Sat)	Source	
1	930001	Stage-Auditorium	76	M		X	X		X				
2	930003	Stairways-Auditorium	27	M			X		X			26	Blood
3	930004	Stairways-Auditorium	61	M		X			X	X		3.75	Blood
4	930005	Stairways-Auditorium	36	M		X			X			15	Blood
5	930006	Stairways-Auditorium	42	M		X			X			ND	Blood
6	930007	Communication Room	37	M		X			X			ND	Blood
7	930008	Communication Room	43	M	X				X			35	Blood
8	930009	Communication Room	33	M	X				X			24	Blood
9	930010	Kitchen/Serving Area	33	M		X	X		X			66	Blood
10	930011	Kitchen/Serving Area	31	F		X	X		X			79	Blood
11	930012	Kitchen/Serving Area	43	F		X	X		X			15	Blood
12	930013	Front of "Bunker"	20	F		X	X		X			43	Liver
13	930014	Front of "Bunker"	41	F		X	X		X	X		37.5	Blood
14	930015	Kitchen/Serving Area	47	F		X	X		X			33	Blood
15	930016	Kitchen/Serving Area	35-50	M		X			X			ND	Blood
16	930017	Kitchen/Serving Area	22-28	F		X	X		X			29	Blood
17	930018	Kitchen/Serving Area	27	F		X	X		X			38	Blood
18	930019	Kitchen/Serving Area	17-35	F		X	X		X			26.5	Blood
19	930020	Kitchen/Serving Area	48	F		X	X		X			29/35	Liver/Spleen
20	930021	Stairways-Kitchen	32	M	X							ND	Blood
22	930023	Stairways-Kitchen	23	M	X							ND	Blood
23	930024	Hallways	31	F		X	X		X			59	Blood
24	930025	Hallways	31	F		X	X		X			15	Blood
25	930026	Hallways	32	F		X	X		X			68	Blood
26	930027	Hallways	15-19	F		X	X		X			58	Blood
27	930028	Hallways	60	F		X	X		X			29	Blood
28	930029	Hallways	55	F		X	X		X			38	Blood
29	930030	Hallways	27	F		X	X		X			15	Blood
30	930031	"Bunker" (surface)	14	F		X	X		X			52.5	Liver
31A	930032	"Bunker" (surface)	17	F	X		X		X			46	Blood
32	930033	"Bunker" (surface)	27	M		X	X		X				
33A/B	930034	"Bunker" (surface)	3.5	M		X	X			X			
34	930035	Top of "Bunker"	34	F	X	X	X		X			37.5	Blood
35	930036	Top of "Bunker"	18	F	X	X	X		X			50/43.7	Liver/Spleen
36	930037	Top of "Bunker"	39	M	X	X						ND	Blood
37	930038	Top of "Bunker"	36	M		X	X		X			24	Blood
38	930039	Top of "Bunker"	24	F		X	X					ND	Blood
39	930040	Top of "Bunker"	37	F	X	X	X					3.75	Blood
40	930041	Top of "Bunker"	28	M		X	X		X			20	Blood
41	930042	Top of "Bunker"	37	M	X	X			X			66	Blood
42	930043	Top of "Bunker"	28	M		X	X		X			50/37.5	Liver/Spleen
43	930044	Kitchen/Serving Area	24	F	X	X	X		X			41	Blood
44	930045	Kitchen/Serving Area	31	M	X								
45	930046	Kitchen/Serving Area	49	F	X	X	X		X			37.5	Blood
47A	930048	"Bunker" (surface)	24	F	X							ND	Blood
49	930051	"Bunker" (surface)	20	M		X	X		X			46	Blood
51A	930112	"Bunker" (excavation)	2	F					X	X			
51B	930053	"Bunker" (excavation)	41	F					X			ND	Blood
52	930055	"Bunker" (excavation)	8	M		X	X		X			72.5	Blood
53	930056	"Bunker" (excavation)	5.5-6.5	F	X		X		X			37.5	Liver
54	930057	"Bunker" (excavation)	30	F		X	X		X	X		33	Blood
55	930058	"Bunker" (excavation)	13	F	X		X		X			ND	Blood
56	930059	"Bunker" (excavation)	11	F	X				X			ND	Blood
57	930060	"Bunker" (excavation)	6	F					X				
59	930062	"Bunker" (excavation)	14-19	F						X			
61	930064	"Bunker" (excavation)	30	F					X				
62	930065	"Bunker" (excavation)	1	F					X				
63	930066	"Bunker" (excavation)	1.3-1.8	F			X			X		46	Liver
64	930067	"Bunker" (excavation)	1	F		X	X		X				
65	930068	"Bunker" (excavation)	Toddler	F		X	X		X	X		73	Blood
66	930069	"Bunker" (excavation)	40	F	X	X							
67-1	930070	"Bunker" (excavation)	6	F		X	X		X				
67-2	930103	"Bunker" (excavation)	8	M					X				
67-3	930104	"Bunker" (excavation)	23	F					X				
67-4	930105	"Bunker" (excavation)	1-2	F		X	X		X				
67-6	930107	"Bunker" (excavation)	13	F					X				
67-7	930108	"Bunker" (excavation)	2.5	UNK									
67-8	930109	"Bunker" (excavation)	Infant	UNK	X								
69/67-5	930072	"Bunker" (excavation)	1.5	F		X	X			X		50	Blood
70	930073	"Bunker" (excavation)	2	F					X				
71	930074	"Bunker" (excavation)	18	F		X	X		X			8.75	Liver
72	930075	"Bunker" (excavation)	4.1-5	F		X	X		X			50	Liver
73	930076	"Bunker" (excavation)	1.5	F			X		X			52.5	Liver
74	930077	"Bunker" (excavation)	6	F									
75	930078	"Bunker" (excavation)	25-35	F				X		X		50	Chest fluid

Marcelo M. Hirschler<sup>1</sup>

## **ANALYSIS OF FULL-SCALE FIRE TESTS OF WALL LININGS IN RANCH HOUSE**

**REFERENCE:** Hirschler, M. M., "Analysis of Full-Scale Fire Tests of Wall Linings in Ranch House," *Very Large-Scale Fires, ASTM STP 1336*, N. R. Keltner, N. J. Alvares, and S. J. Grayson, Eds., American Society for Testing and Materials, 1998.

**ABSTRACT:** A total of 4 tests were conducted, in the 1960's, in a three room arrangement, in a ranch house. The structure was 3.9 m wide and 13.6 m long, and contained three rooms, designated living room, dining room and bedroom, which were all of equal length, in a row, starting with the living room. All windows were closed during the tests, but interior doors were open. All rooms were fully furnished. The exterior walls and roof were fir plywood, and the exterior siding was gypsum board nailed to the "2 x 4" studs. The tests were all initiated by ignition of a 4.4 kg wood crib, in the living room, near an easy chair, which itself ignited very soon afterwards. Measurements made included temperatures, in °F, at 24 locations throughout the structure (including one measuring ambient temperature). Concentrations of three gases were also measured throughout the tests with continuous analyzers: carbon monoxide, carbon dioxide and oxygen. The gas measurements were made in sequence, so that concentrations at each location were measured at different times, but all gases were measured simultaneously at each location. The tests were conducted using 4 different wall lining products: (a) 13 mm (0.5 in) thick painted gypsum board, nailed to the studs; (b) 6 mm (0.25 in) thick pre-finished plywood panels nailed over 13 mm (0.5 in) gypsum board, itself nailed directly to the studs; (c) 16 mm (0.25 in) thick pre-finished plywood panels nailed directly to the studs and (d) 6 mm (0.25 in) thick pre-finished fire-retardant (pressure-treated core) plywood panels nailed directly to the studs. The original data interpretation was restricted to a consideration of whether flashover was or was not reached and little else. A new analysis of the data, however, has permitted determination of broad approximations to heat release (both comparative values and rough average data), and comparisons with data from other standard fire test methods, such as the Steiner tunnel (ASTM E84) and the cone calorimeter (ASTM E1354). This type of analysis is very important because (a) it recovers information which is often lost and (b) it allows significant information to be obtained from existing tests conducted at earlier dates, for semi-qualitative reasons. In this way, cost savings can be achieved in decreasing the need for repeated testing.

**KEYWORDS:** carbon monoxide, fire, fire tests, flashover, heat release, smoke obscuration, temperature measurement, wall linings

---

<sup>1</sup>GBH International, 2 Friar's Lane, Mill Valley, CA, 94941.

One of the greatest difficulties with fire safety is the high cost of the large scale tests which are often essential to understand the phenomena occurring in real fires. Such tests are also needed to help develop correlations with modern small scale tests, known to be able to predict full scale test results, but for which proper correlating equations have not yet been found.

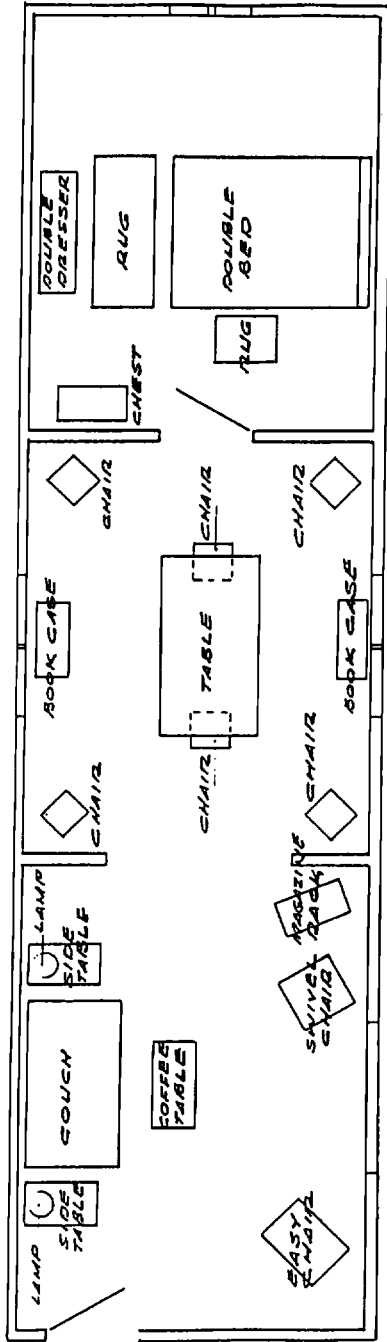
It has now become clear that heat release measurements are essential to determine quantitatively a number of aspects of a fire [1-2]. In order to assess heat release rates accurately, modern techniques for measuring it (by oxygen consumption or by carbon dioxide generation), had to be developed. Moreover, it was not until the promulgation, by Huggett, of the oxygen consumption principle, in 1980 [3], that the era of routine heat release measurements in large scale tests actually began. However, the time has now come to try to rescue and reappraise the extensive amount of quantitative information that has been developed between the 1950's and the 1980's from large scale fire tests wherein measurements were made, but heat release was not directly assessed.

The present study will focus on an investigation by the Hardwood Plywood Manufacturers Association, between September 12, 1967 and November 25, 1968, of fire development in fully furnished manufactured housing, as a function of the type of interior wall finish used [4-5]. These tests were uncommonly detailed as to the amount of information gathered and are worthy of further analysis.

## Experimental

A total of 4 tests were conducted in a three room arrangement, in a ranch house. The structure was 3.9 m (12 ft 9 in) wide and 13.6 m (44 ft 8 in) long, and contained three rooms, designated living room, dining room and bedroom, which were each 4.2 m (13 ft 9 in) long, in a row, starting with the living room. There was one outside door, from the living room at the East end, and windows in every room: one single hung aluminum frame 0.7 x 1.1 m (28 x 42 in) window in the bedroom; 2 twin similar size ones in the dining room and a plate glass picture window (1.5 x 1.8 m; 5 x 6 ft) in the living room. The dining room and bedroom were separated by a 2.0 m (6 ft 8 in) high 0.9 m (3 ft) wide 35 mm (1 3/8 in) thick hollow core interior door. The living room and dining room were separated by a 1.8 m x 2.1 m (6 ft x 7 ft) opening. All windows were closed during the tests, but doors were open. All rooms were furnished, as indicated in the table of furnishings (Table 1). The exterior walls were construction grade Douglas fir plywood on 38 x 89 mm (nominally 50 x 100 mm; 2 x 4 in) wood studs, with a plywood roof. Exterior siding was 13 mm (0.5 in) gypsum board nailed to standard nominally 50 x 100 mm (2 x 4 in) studs. The layout is shown in Fig. 1.

The tests were all initiated by ignition of a 4.4 kg (9 lb 12 oz) wood crib, through 85 g (3 oz) of methyl alcohol, in the living room, near the easy chair, which itself was the second item ignited, and did so very soon afterwards. Measurements made were temperatures (with 24 AWG Type K Chromel-Alumel thermocouples, connected to a mechanical data acquisition system), in °F, at 24 locations centrally spread throughout the structure (including one measuring ambient temperature): 2 thermocouples in each room at heights of 2.1, 1.5 and 0.3 m (7, 5 and 1 ft), a third thermocouple in the dining room and in the bedroom at a height of 1.5 m (5 ft), as well as one at 15 mm (6 in) above the bed pillows and 2 at 25 mm (1 in) above the large rug



Living Room (4.2 x 3.9 m) Dining Room (4.2 x 3.9 m) Bedroom (4.2 x 3.9 m)

FIG. 1 --Ranch House (Dimensions: 13.6 x 3.9 m)

TABLE 1 – *Interior Furnishings***Living room:**

- \* Couch: hardwood frame, felted cotton filler, polyurethane foam cushions, rayon-acetate cover: 42.6 kg (94 lb).
- \* Easy chair: hardwood frame, felted cotton filler, polyurethane foam cushions, rayon-acetate cover: 24.4 kg (53 lb 14 oz).
- \* Swivel chair: swivel platform rocker, hardwood base and frame, felted cotton filler, steel, springs, cotton tweed fabric: 16.3 kg (36 lb).
- \* Coffee table: chip-board base, plastic top, hardwood legs: 8.2 kg (18 lb).
- \* Side tables: chip-board base, plastic top, hardwood legs; 2 tables: 15.6 kg (34 lb 8 oz).
- \* Lamps: hydrocal molded base, plastic shade; 2 lamps: 3.6 kg (8 lb).
- \* Magazine rack: (simulated) varnished Douglas fir plywood; 4.5 kg (10 lb).
- \* Drapes: antique satin, 70% rayon, 30% acetate, cotton lined: 1.8 kg (4 lb).
- \* Pictures: (simulated) Douglas fir, paper, varnish; 3 pictures: 5.9 kg (12 lb 15 oz).
- \* Magazines: on coffee table (1.8 kg; 3 lb 15 oz) and one magazine rack (2.6 kg; 5 lb 10 oz): 4.3 kg (9 lb 9 oz).
- \* Flooring: 100% nylon face carpet, installed with tackless stripping over foam rubber pad.

**Dining Room:**

- \* Table: chip-board base, plastic top, hardwood legs: 28.4 kg (62 lb 8 oz).
- \* Chairs: hardwood frame and back, felted cotton filler, plastic covered seat; 6 chairs: 26.5 kg (58 lb 7 oz).
- \* Bookcases: hardwood and "hardboard"; 2 bookcases: 21.8 kg (48 lb 2 oz).
- \* Drapes: cotton; 2 sets of drapes: 1.5 kg (3 lb 4 oz).
- \* Books: in both bookcases; 22.9 kg (50 lb 6 oz) in south bookcase; total: 43.9 kg (96 lb 14 oz).
- \* Pictures: (simulated) Douglas fir, paper, varnish; 4 pictures: 5.3 kg (11 lb 11 oz).
- \* Clothes: One cotton shirt hung on chair at east end of table: 0.6 kg (1 lb 6 oz).
- \* Flooring: Service grade 1.6 mm (1/16 in) thick vinyl asbestos tiles, 3 x 0.3 m (12 x 12 in).

**Bedroom**

- \* Double bed: hardwood frame, hardboard headboard; hardwood frame, hardboard footboard; metal rails, four pine slats, box spring with 63 coils, felted cotton, 1.5 g/m<sup>2</sup> (6 oz/yd<sup>2</sup>) ticking; innerspring mattress, 252 coils, felted cotton, button tufted: 163.3 kg (360 lb).
- \* Chest: chest of drawers, hardwood hardboard: 29.8 (65 lb 10 oz).
- \* Double dresser: dresser and mirror, hardwood hardboard: 44.5 kg (98 lb 0 oz).
- \* Drapes: cotton: 0.6 kg (1 lb 4 oz).
- \* Pictures: (simulated) Douglas fir, paper, varnish; 3 pictures: 5.2 kg (11 lb 6 oz).
- \* Rugs: 100% rayon cut pile, latex backing, 0.6 x 0.9 m (1.4 kg; 2 x 3 ft; 3 lb) and 0.9 x 1.5 m (4.1 kg; 3 x 5 ft; 9 lb): 5.4 kg (12 lb).
- \* Clothes: various clothing materials in dresser: 5.3 kg (11 lb 12 oz), various materials in chest: 6.6 kg (14 lb 10 oz); total: 12.0 kg (26 lb 6 oz).
- \* Bedding: 2 cotton sheets, acrylic blanket, chenille (cotton) bedspread, two chicken feather pillows, two cotton pillowcases: 8.9 kg (19 lb 10 oz).
- \* Flooring: laminated hardwood tiles 0.23 x 0.23 m (9 x 9 in).

Room	Weight furnishings kg/lb	Floor area m <sup>2</sup> /ft <sup>2</sup>	Floor load kg m <sup>-2</sup> /lb ft <sup>-2</sup>
Living	131.46/ 289.81	15.37/165.40	8.59/1.76
Dining	128.23/ 282.69	15.35/165.25	8.35/1.71
Bedroom	269.75/ 594.69	15.35/165.25	17.58/3.60
Overall	529.44/1167.19	46.07/495.90	11.47/2.35

in the living room. Concentrations of three gases were also measured throughout the tests with continuous analyzers: carbon monoxide, carbon dioxide (both with non dispersive infrared analyzers) and oxygen (with a paramagnetic analyzer). The gas measurements were made in sequence at six locations (2 in each room), so that concentrations at each location were measured at different times. However, all gases were measured simultaneously at each location. Exit signs were posted to make visual observations of smoke obscuration.

The wall lining products used were:

- Test 1: 13 mm (0.5 in) thick painted gypsum board. The gypsum board was nailed, taped, floated and painted with 3 coats of standard vinyl base latex paint. All interior trim was of standard pine and painted with latex paint.
- Test 2: 6 mm (0.25 in) thick pre-finished hardwood panels nailed over 0.5" gypsum board. The gypsum board (untaped) was nailed directly to the nominally 50 x 100 mm (2 x 4 in) wall studs.
- Test 3: 6 mm (0.25 in) thick pre-finished hardwood panels nailed directly to the nominally 50 x 100 mm (2 x 4 in) wall studs.
- Test 4: 6 mm (0.25 in) thick pre-finished fire-retardant (pressure-treated core) hardwood panels nailed directly to the nominally 50 x 100 mm (2 x 4 in) wall studs.

## Results and Discussion

The ignition source in these tests was sufficiently intense to cause a very intense fire in the living room in all tests, so that untenable conditions (both in terms of temperature and of toxicity) existed, even at the lowest level (0.3 m above the floor). In the first test, flashover was not reached, but conditions in the living room remained tenable for almost 10 min, while they become untenable at about 6 min in the other tests. In the other three tests, flashover conditions were reached.

Curves of temperature, heat release and gas concentration against time all show that, as was to be expected, the living room (where the ignition source was located) is where the fire becomes most intense, followed by the dining room, with the bedroom being involved to a small extent only (and virtually not involved in the first test). In fact, in Test 1 (gypsum board wall linings) the bedroom temperature never rises significantly, and in the other tests it does so only after about 25 min.

The observations made during the tests, and the sequence of events are summarized in Tables 2-5, one for each test. Figures 2 and 3, corresponding to the original data from Tests 1 and 4, indicate that the repeatability of the measurements made at replicate locations is adequate, so that using one of the sets of measurements is sufficient. Figures 4 and 5 show that the time-dependent curves for the various gases have similar features, both among themselves and with respect to temperature (original measurements). Figures 6 and 7 show that the oxygen measurements, in two of the rooms at a height of 1.5 m, can indicate the overall broad results: (a) the test with

**TABLE 2 -- Sequence of Events During Test 1, With 13 mm Painted Gypsum Board**

Min:Sec

0:00	Ignition of crib in living room
0:05	Chair ignited
1:00	Flames 3 ft above crib
1:45	Light smoke coming out dining room windows
2:30	Living room window fogging
3:00	Flames 5 ft above crib
3:50	Warm combustion products coming out dining room windows-windows fogging
4:25	Smoke visible in dining room
4:50	Heavy smoke visible in dining room
5:30	Opaque smoke visible in dining room
6:00	Flames lapping living room ceiling over crib and easy chair
6:30	Picture burning on east living room wall
7:00	Smoke density increased - no flames visible
7:10	View through dining room completely blocked by smoke
10:00	Odor of smoke coming out bedroom window, but no smoke visible
11:00	Visible smoke coming into bedroom: temperatures and gas concentrations in living and dining rooms steadily dropping
11:30	Maximum temperatures in structure are near 300 °F
12:00	Living room door opened 4 in
15:00	Temperatures and gas concentration steadily dropping-maximum temperatures in structure below 300 °F
15:40	Living room door open 12 in
16:00	Easy chair in living room flaming
16:15	Window frames in dining room warm to the touch
19:30	Visibility improved
20:00	No flames visible
20:45	Living room drapes fallen to floor
23:45	Living room plate glass window cracked, small piece fell out
24:00	Fallen living room drapes burning
24:35	Strong increase in smoke and reduction in visibility
25:00	Smoke continually building up in bedroom, noted below level of open window
25:45	Weatherstripping on dining room windows fell out
28:00	Smoke in bedroom obscured upper area of east wall as viewed through west window, dining room windows on north side cracked
29:30	Visibility somewhat improved
30:30	flames at floor level visible in living room
34:00	Temperatures and gas concentrations falling steadily (since 28:00), living room door shut
60:00	Temperatures and gas concentrations continue to drop, test terminated.

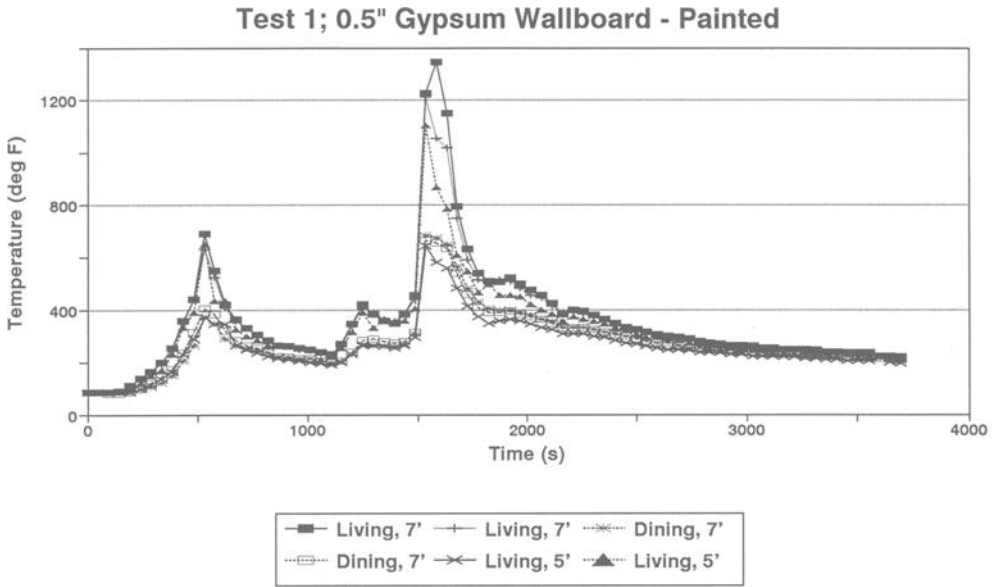


**Fig. 2 --Temperatures Measured in the Living and Dining Rooms in Test 1**

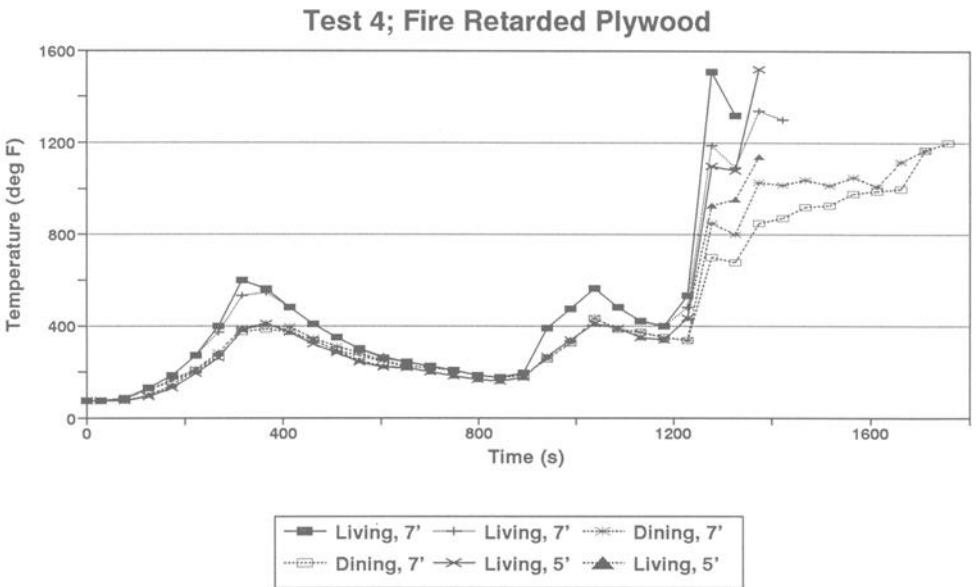


**Fig. 3 --Temperatures Measured in the Living and Dining Rooms in Test 2**

TABLE 3 – *Sequence of Events During Test 2, With Plywood on Gypsum Board*

Min:Sec

0:00	Ignition of crib in living room
0:06	Chair ignited
1:00	Flames 3 ft above crib, smoke scent coming out dining room windows
1:30	Flames 4 ft above crib
2:30	Flames 5 ft above crib
3:00	Living room window fogging, dining room windows fogging
3:20	Smoke beginning to obscure furnishings in living room
3:30	Flames 6 ft above crib
3:55	Visible smoke coming out dining room windows
4:00	Visibility reduced to 10 ft in living room (at 7-ft height)
4:36	Visibility reduced to 6 ft in dining room (at 3-ft height)
5:00	Visibility reduced to 2 ft in dining room (at 7-ft height)
6:00	Flaming localized to crib and easy chair; occasionally flames are visible and seen reaching ceiling. Visibility reduced to 4 ft (at 3-ft height) in dining room
6:10	Smoke scent at bedroom window
7:00	Temperatures in living and dining rooms have peaked and have started to drop
9:15	Visible smoke (gray) coming out bedroom window
11:30	Maximum temperatures in structure are near 250 °F and continuing to drop; gas concentrations have leveled off since 7:00
12:00	Living room door open 4 in
12:30	Visibility slightly increased; fire appears to be confined to crib and easy chair
13:00	Flames from crib and easy chair have increased; flames flash over ceiling
13:43	Living room plate glass window cracked, smoke pouring from eaves at northwest corner of building
14:20	Dark smoke seen coming through door into bedroom
14:30	Flames from crib and easy chair reaching ceiling and spreading halfway across living room above window
15:00	Heavy smoke coming out open living room door, heavy smoke coming from all around door into bedroom
15:20	Visibility markedly reduced again
15:30	Visibility reduced to 10 ft in bedroom (at 5-ft height)
15:40	Living room door opened 12 in
16:00	Weatherstripping on dining room windows fell out; black smoke being forced out all openings in living and dining rooms, observers unable to approach windows
16:12	Bedroom door obscured from view through west window
16:15	Visibility reduced to zero in living room and dining room
17:45	Dining room windows cracked
17:50	Living room window disintegrating
18:12	Visibility in bedroom reduced to 6 ft (at 5-ft height)
18:30	Flames pouring out full living room window opening
20:00	Loud popping and crackling noise heard from dining room, living room completely involved in flame
21:00	Visibility in bedroom reduced to 4 ft (at 3-ft height); eaves burning over living room door and the living and dining room windows
21:06	Dining room windows falling out
22:48	Plywood completely burned away on east wall of living room
24:23	Flashover in dining room
25:45	Smoke and heat coming out bedroom window forced observer back, curtains blown out window opening
26:12	Dining room completely involved in flame
28:38	Temperatures and gas concentrations in bedroom above acutely tolerable levels
29:30	Fire extinguished - test terminated.

TABLE 4 -- *Sequence of Events During Test 3, With Plywood on Studs*

Min:Sec

0:00	Ignition of crib in living room
1:00	Flames 3 ft above crib
1:30	Flames 5 ft above crib, smoke scent coming out dining room windows
3:30	Flames 6 ft above crib
4:10	Easy chair flaming
5:00	Visible smoke coming out dining room windows
5:30	Visibility reduced to 10 ft, flames 7 ft above crib
5:40	Swivel chair ignited
6:00	Visibility reduced to 4 ft
6:35	East wall ignited
6:50	Living room window cracked
7:47	Visibility reduced to 2 ft
8:00	Living room window cracking again, gray smoke coming into bedroom around door
9:00	No visible flames
9:30	Temperatures in living and dining rooms peaked at 9:00 and have started to drop
10:35	4 x 12-in piece fallen out of living room window
11:00	Temperatures steadily dropping nearing 400 °F
12:00	Living room door opened 4 in
12:30	Weatherstripping on dining room windows fallen out
12:40	Easy chair in living room actively burning
13:40	East wall of living room burning, flames reaching ceiling over easy chair and crib
14:15	Flames halfway across living room ceiling
14:30	Crackling, popping and bubbling noise coming from dining room, visible smoke coming from gable over bedroom
15:30	Black smoke coming around door into bedroom
15:40	Living room door open 12 in
15:45	Flames coming out living room windows
16:00	Flames coming out living room door
17:00	Living room doorway nearly filled with flames, carpet burning only in immediate area of crib and easy chair
17:30	Dining room windows cracked
19:30	Loud crackling and popping noise coming from dining room
19:45	Heavy black smoke coming around door into bedroom
22:00	Visibility reduced to 8 ft in bedroom
23:00	Visibility reduced to 4 ft in bedroom, living room door falls off top hinge
23:30	Flashover in dining room
23:50	Flames coming out dining room windows, room totally involved in flame
24:15	Flames burning through wall between living and dining room
25:00	Visibility reduced to 3 ft in bedroom
25:30	Flames noted in bedroom
28:30	Lower pane in bedroom window cracked
29:00	Upper pane in bedroom window cracked
30:00	Test terminated, fire extinguished.

**TABLE 5 -- Sequence of Events During Test 4, With Fire Retarded Plywood on Studs**

Min:Sec

0:00	Ignition of crib in living room
2:00	Flames 5 ft above crib
3:20	Smoke building
3:45	Chair ignited in living room
4:40	Picture above burning chair in living room ignited
4:45	Visible smoke issuing from dining room windows
5:10	Visibility reduced to 7 ft in dining room, north windows
5:15	East wall ignited opposite chair
5:30	Visibility in living room reduced to less than 8 ft
5:30	Visibility reduced to 5 ft in dining room, north windows
5:50	Visibility reduced to 3 ft in dining room, north windows
5:55	Visibility reduced to 1 ft in dining room, north windows
6:05	Drape on east side of living room window ignited
6:10	Living room window cracked, visibility 5 ft from south dining room window
6:30	East living room drape falls
7:75	Visibility reduced to zero in living room, no flames visible
8:00	Smoke visible in bedroom
9:10	Smoke emitting from eave at northeast corner
10:00	Smoke coming out bedroom window
12:00	Living room door opened 4 in, chair and crib burning, no activity on walls
12:30	Dining room table now visible from south windows
14:20	Visibility somewhat improved, 12 in flames visible but confined to northeast corner of living room
15:00	Picture on east wall of bedroom no longer visible from bedroom window
15:20	Burning activity in corner of living room increasing
15:40	Living room door open 12 in
16:00	Picture over bed no longer visible, flames confined to northeast corner of living room 2 to 3 ft in height walls no burning
16:45	Walls ignited in northeast corner living room spreading flames up and along ceiling
17:10	Flames issuing out living room door at top
17:30	Flame activity markedly reduced, confined to chair and crib, no burning on walls
17:45	West living room drape ignited
18:50	Chair in northwest corner of living room ignited
20:10	Flame activity continues but is confined to remains of chair and crib in northeast corner of living room and chair in northwest corner
20:40	Flame activity increasing noticeable from chair and crib
21:00	Northeast corner of living room completely on fire, flames coming out living room door
21:15	Living room window blown out
21:45	Dining room windows cracking, plastic glazing dripping out
21:55	Flames coming out living room window and door, living room completely afire
22:00	Visibility reduced to 6 ft in bedroom
22:30	Visibility reduced to 4 ft in bedroom
23:00	Loud crackling and popping audible from dining room
25:10	Living room door falls inward
27:55	Dining room flashed over
28:22	Flames issuing from north dining room windows
29:00	Dining room filled with flame
30:05	Heavy smoke issuing from bedroom window
33:00	Fire extinguished - Test terminated.

**Test 1: Painted Gypsum Board; Living**

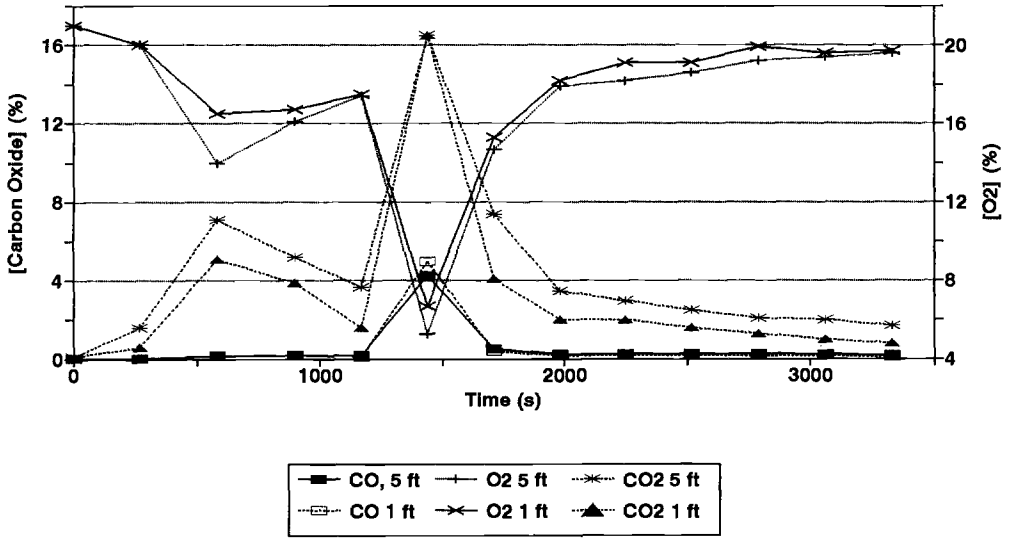


**Fig. 4 --Gas Concentrations Measured in the Living Room in Test 1**

**Test 2: CO and Temperature, at 5 ft**

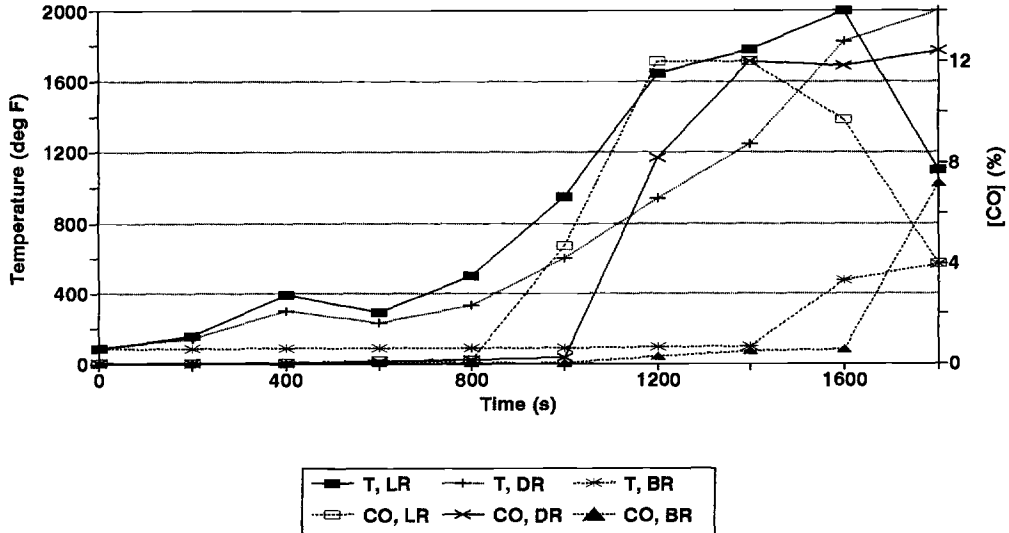


**Fig. 5 --Gas Concentrations Measured in All Rooms in Test 2**

### Oxygen in Living Room - 5 ft

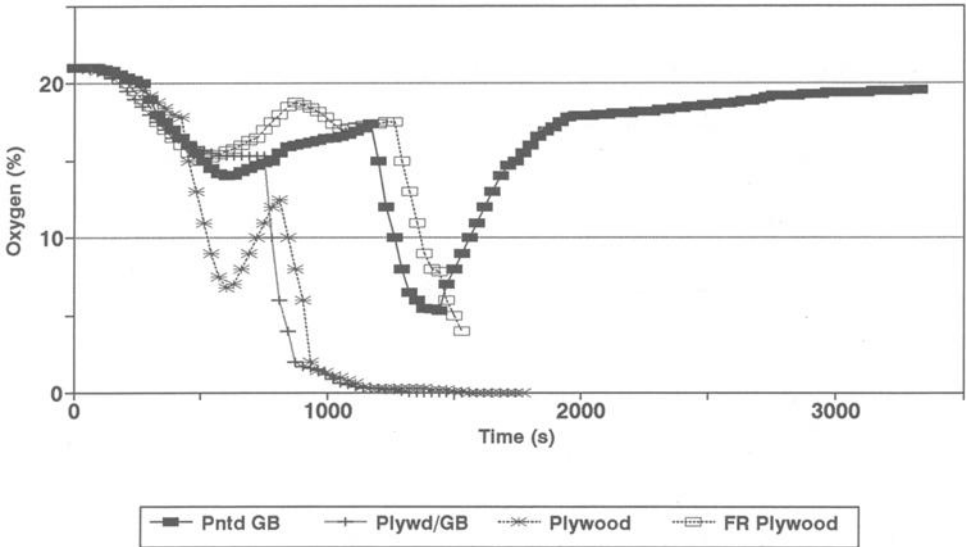


**Fig. 6 --Oxygen Concentrations Measured in the Living Room in All Tests**

### Oxygen in Bedroom - 5 ft

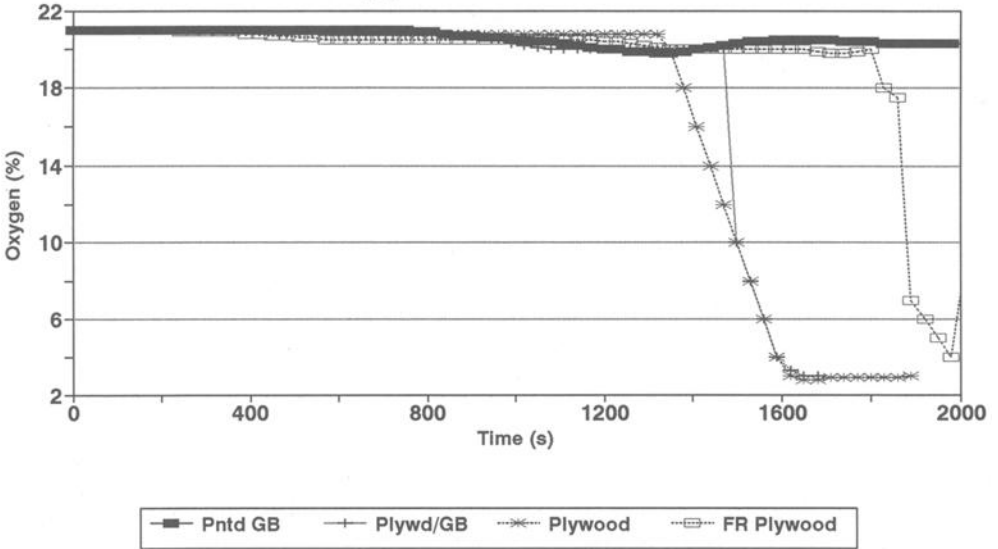


**Fig. 7 --Oxygen Concentrations Measured in the Bedroom in All Tests**

gypsum board does not reach flashover, while the other three do; (b) the fire retarded plywood maintains viability, even in the room of fire origin (living room) for a considerable period longer than the non-fire retarded plywood, and (c) conditions in the bedroom eventually become similar to those in the living room, but only for the 3 tests where flashover occurs, while virtually nothing of significance happens in the bedroom in Test 1.

With these results, it is possible to estimate the heat released in each test, and conduct comparative analyses between the tests and within each test. The heat released can be estimated in three ways:

(a) Relative (qualitative) values based on the increase in temperature (and Figures 8 and 9 show results assessed in that way). In this analysis, the analysis is as follows: differences in temperature are calculated between the measuring site and ambient temperature; these differences are then normalized and a summation is made up to 30 min. The equation is shown as Equation (1):

$$Av\ RHR = \frac{\sum (\Delta Temp\ (F) * \Delta time\ (s))}{1800\ (s)} \quad (1)$$

where Av RHR is the average relative rate of heat release (in arbitrary units),  $\Delta Temp\ (F)$  is the increase in temperature at every site and for every scan (in °F),  $\Delta time$  is the time between scans (in s).

The results indicate that there is very little difference between the results of Tests 2 and 3 (where non fire retarded plywood is used attached to gypsum board or directly to the studs), while the other two tests present a much safer environment, with the fire retarded plywood being responsible for more heat release. Overall rankings can be established: Test 1 (gypsum board) is best, followed by Test 4 (fire retarded plywood), with the two non fire retarded plywood wall linings exhibiting similar performance (Tests 2 and 3). It is also clear that the heat released in the bedroom is very much smaller than that released in the other rooms.

(b) Semi-quantitatively, on the basis of the oxygen consumption principle [6] (i.e the statement that the rate of heat release is directly proportional to the difference between the mass of oxygen present before and after; the proportionality constant is 13.1 MJ/kg), where it is assumed that the mass of oxygen is based on the room volume, and that the oxygen can continually flow into the room (see also the guidance provided in ASTM E 603, Standard Guide for Room Fire Experiments and [6-7]). The

**Average Heat Release Rate Per Room**

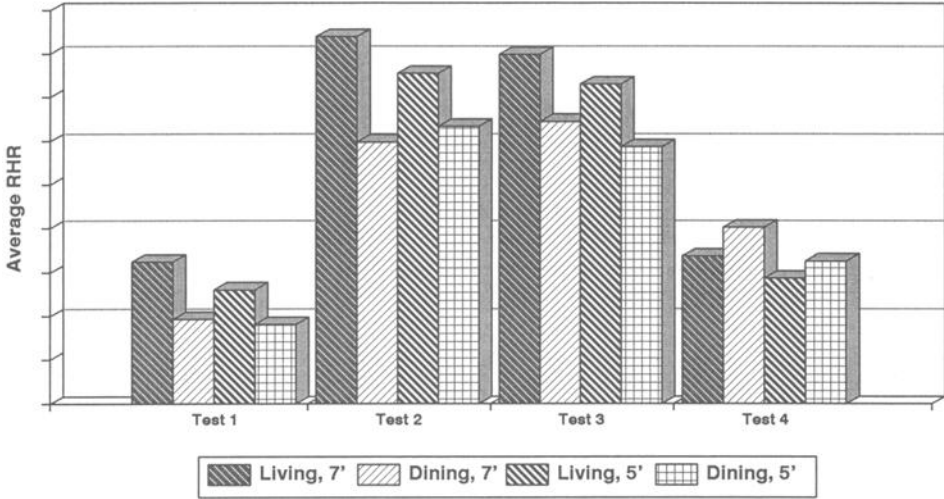


**Fig. 8 --Average Relative Rate of Heat Release for Several Locations in All Tests**

**Test 3: Plywood on Studs**

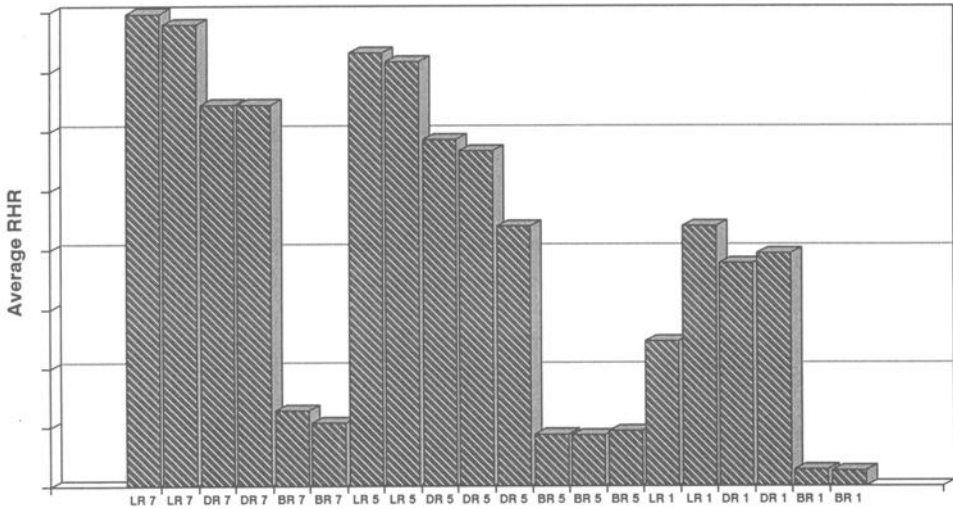


**Fig. 9 --Average Relative Rate of Heat Release for All Locations in Test 3**

calculation method, which is applied at each time interval, is based on Equation (2):

$$Av\ RHR\ (kW) = \frac{13.1\ (MJ/kg) * Mass\ House\ Air\ (kg) * \frac{Mw\ O_2}{Mw\ air} * \Delta O_2\ (\%) * 10}{\Delta time(s)} \quad (2)$$

where Av RHR is the average semi-quantitative rate of heat release from oxygen consumption (in kW), Mass House Air is the mass of air contained in the house under the assumption that it is completely sealed (in kg),  $M_w\ O_2$  is the molecular mass of oxygen (32.0 kg/mol),  $M_w\ air$  is the molecular mass of standard air (28.8 kg/mol),  $\Delta O_2(\%)$  is the change in oxygen concentration (in %) and  $\Delta time$  is the time period (in s).

Figures 10-13 show the heat release rate at a height of 1.5 m for all four tests and all three rooms using this analysis. These Figures show the features of the heat release in the tests, and allow the various stages of the fire to be identified.

(c) Semi-quantitatively, on the basis of the temperature increase at each scan and the Stefan-Boltzmann constant and the equation for black body radiation (where heat release per unit surface is proportional to the fourth power of the temperature measured), followed by calculations based on the surface areas of each room. This follows Equation (3), as shown below:

$$Av\ RHR\ (kW) = \sigma \left( \frac{W}{m^2\ K^4} \right) * \Delta T^4\ (K^4) * Area\ (m^2) \quad (3)$$

where Av RHR is the average semi-quantitative rate of heat release from temperature increase (in kW),  $\sigma$  is the Stefan-Boltzmann constant ( $5.67 \times 10^{-8}\ W\ m^{-2}\ K^{-4}$ ),  $\Delta T^4$  is the change in temperature, raised to the fourth power (in  $K^4$ ) and area is the floor area of the house (in  $m^2$ ).

In Fig. 14 is shown a comparison between the two semi-quantitative methods, for test 4, with fire retarded plywood.

This analysis shows that the methods are not as precise as modern heat release technology, but that the trends appear similar in both sets of calculations, and that they can be used for understanding the phenomena.

RHR in All Rooms - 5 ft - Gypsum Board

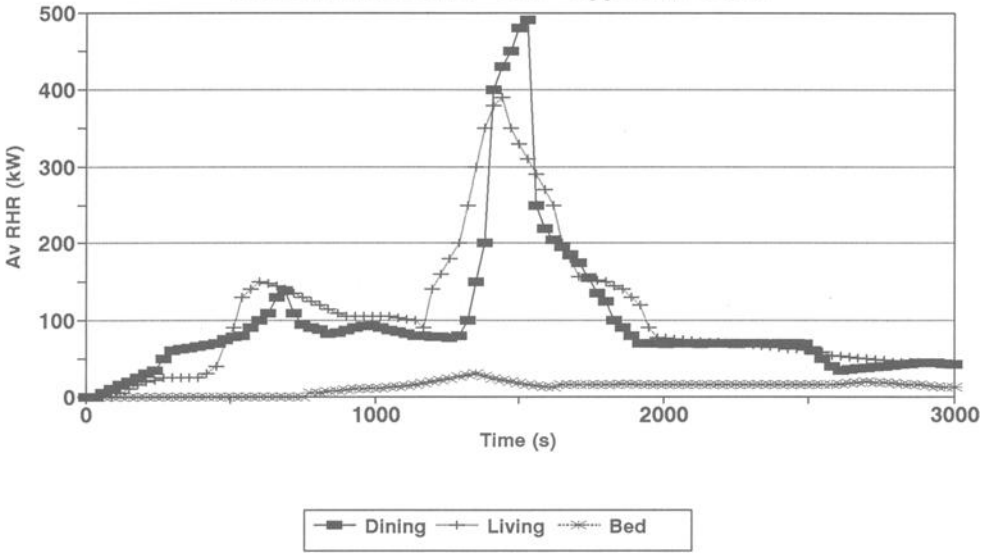


Fig. 10 --Rate of Heat Release Calculated From Oxygen Concentration in Test 1

RHR in All Rooms - 5 ft - Plywood/G Brd

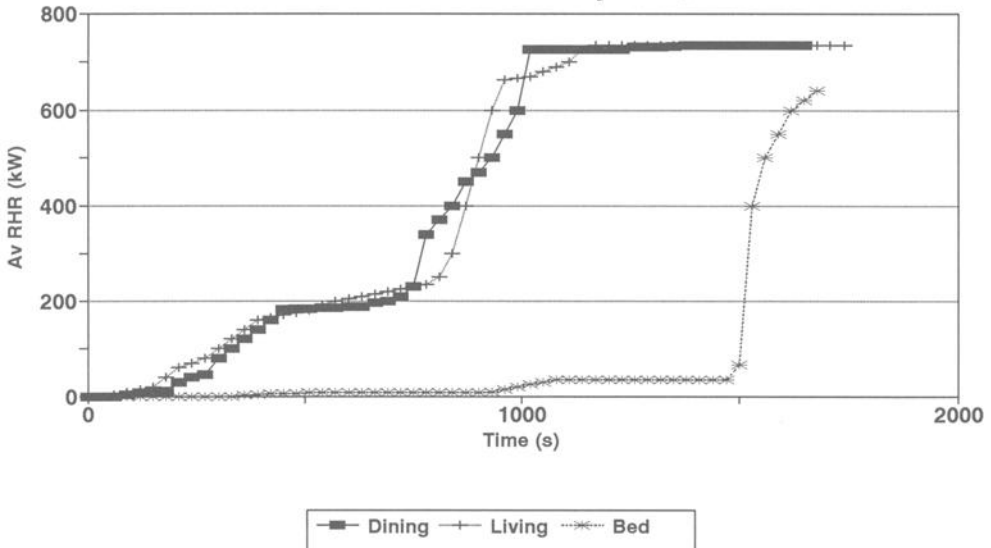


Fig. 11 --Rate of Heat Release Calculated From Oxygen Concentration in Test 2

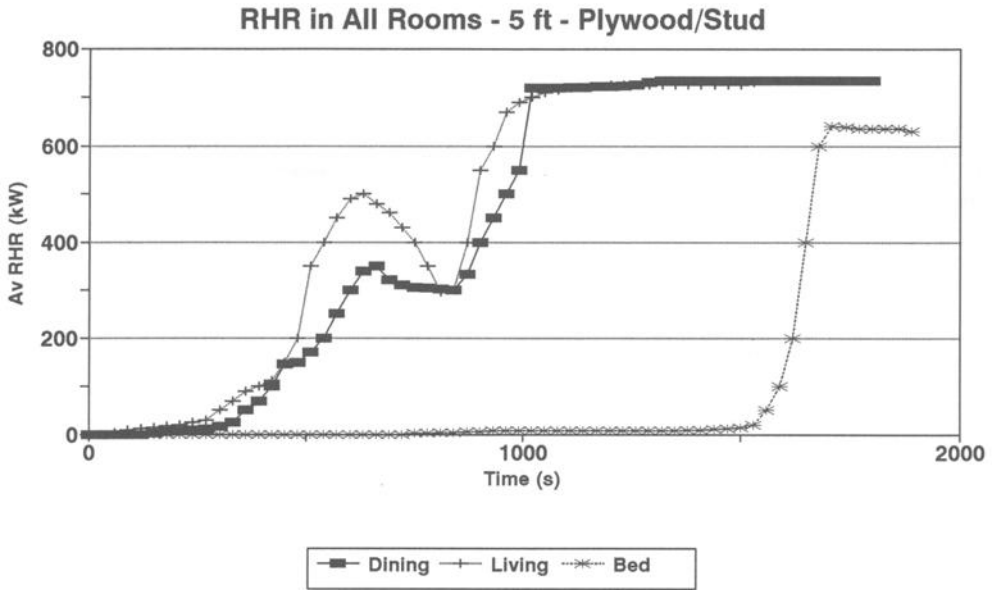


Fig. 12 --Rate of Heat Release Calculated From Oxygen Concentration in Test 3

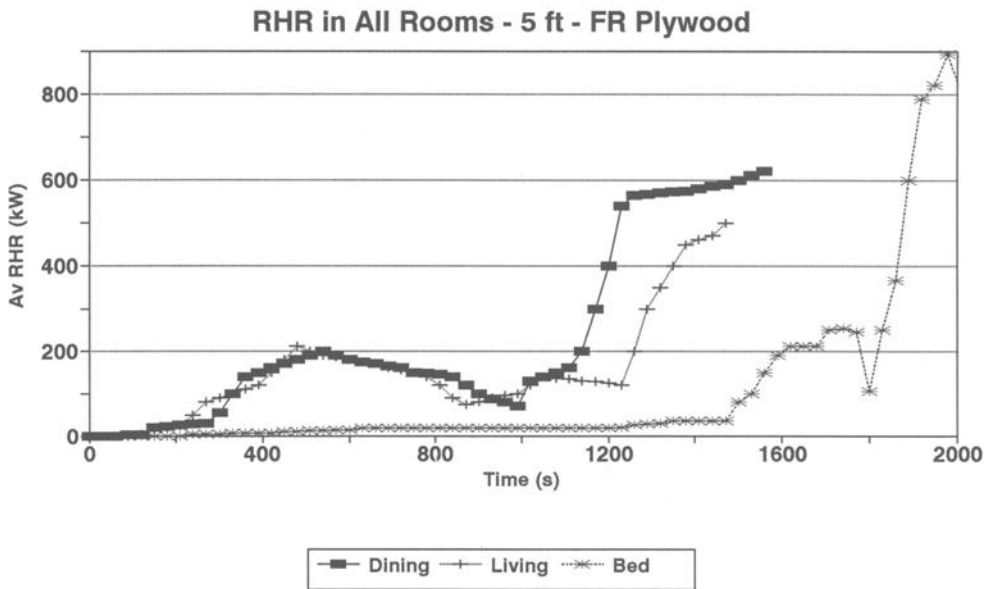


Fig. 13 --Rate of Heat Release Calculated From Oxygen Concentration in Test 4

RHR in All Rooms - 5 ft - FR Plywood

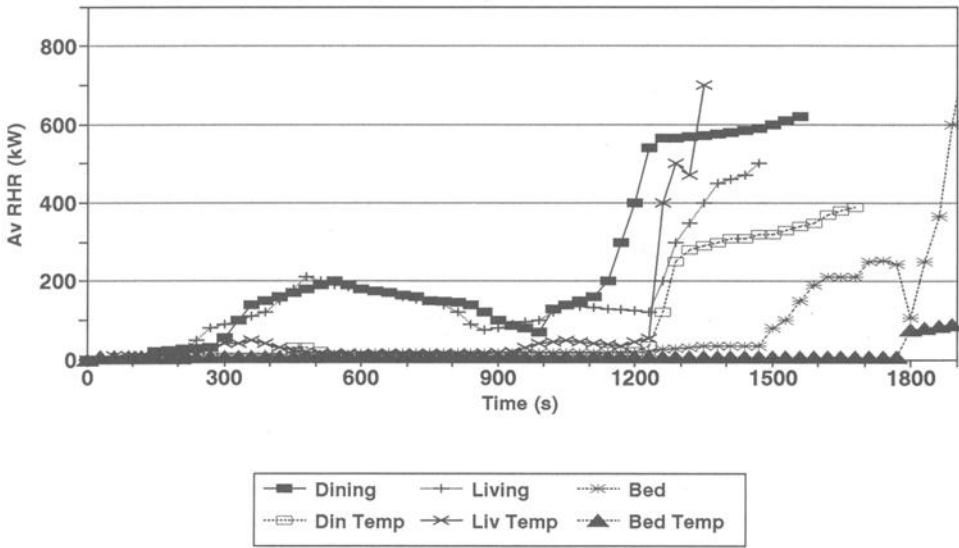


Fig. 14 --Rate of Heat Release Calculated From Both Oxygen & Temperature in Test 4

Correlations with ASTM E84 & ASTM E1354

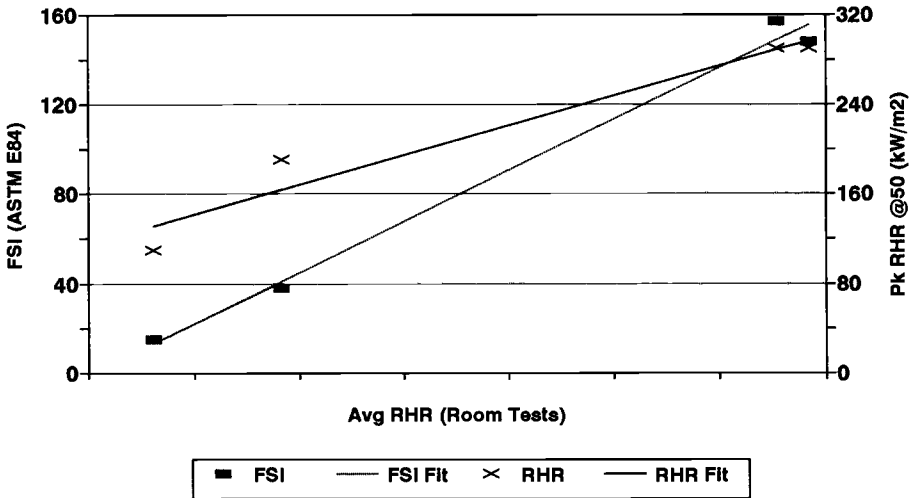


Fig. 15 --Correlation Between Heat Release in Full Scale & Small Scale Test Results

The Figures presented are illustrative examples of the type of results that can be obtained, and show the importance of using such old test data for developing new information.

Table 6 shows the first occurrence of several untenable conditions, namely a temperature in excess of 150 °C (300 °F), carbon monoxide levels of 1% and oxygen levels of 7%. The table also includes a determination of the time required to reach a low visibility (determined empirically by observation), the principal test results from ASTM E 84, Standard Test Method for Surface Burning Characteristics of Building Materials (Steiner tunnel), on flame spread index (FSI) and smoke developed index (SDI) and the peak rate of heat release in the cone calorimeter at 50 kW/m<sup>2</sup>. It is noticeable that the untenable levels are not reached consistently in either test 2 or test 3, but that there is crossover between the two.

Figure 15 is of particular interest in that it shows that the relative values of average heat release calculated for all tests correlate extremely well (correlation coefficients of well over 90%) with both the ASTM E 84 data and with the cone calorimeter data (ASTM E 1354, Standard Test Method for Heat and Visible Smoke Release Rates for Materials and Products Using an Oxygen Consumption Calorimeter). This is not unexpected for cases where solid wood or gypsum board is being tested.

The average RHR calculated for use in Figure 15 is based on Equation (1). The data for the abscissa of Figure 15 has been omitted purposefully because the calculation method is arbitrary and thus it is essential to prevent misuse of the data. The correlation found is not a function of the exact magnitude of the average RHR values used, but of their relative magnitudes.

## Conclusions

- \* Gypsum board wall linings offer more protection than plywood, as does fire-retarded plywood. In particular, the heat released in Test 1 is about 1/3 of that released in Tests 2 or 3, while the heat released in Test 4 is only ca. 50% higher than that in Test 1.
- \* High temperatures are reached very soon in the living room and dining room, even with fire retarded plywood. Also, flashover in the dining room is reached in all tests with plywood, even fire-retarded. Low visibility is also reached early in the living room and dining room with fire retarded plywood. Thus, the fire-retarded plywood used in this particular test does not offer as much additional protection as other fire retarded products in comparison with their non fire retarded analogues.
- \* There is very little difference between the fire performance of the two non fire-retarded plywood panelling wall linings. In terms of detailed comparisons, Test 2, with gypsum board behind the plywood, released more heat than Test 3, with the plywood nailed directly to studs. Similarly, in the same test, higher temperatures are reached earlier in the living room and dining room. Also, in Test 3, low oxygen levels and high carbon monoxide levels are reached earlier than in Test 2. Finally, the time to reach low visibility in the living room and dining room is the same for Test 2 and Test 3, but is reached somewhat earlier

**TABLE 6 – First Occurrence of Untenable Conditions in Each Test**

Criterion	Test 1	Test 2	Test 3	Test 4
	Gypsum	Plywood/GB	Plywood/stud	FR Plywood
$T \geq 159 \text{ } ^\circ\text{C}$ (300 $^\circ\text{F}$ )				
LR 5	7:26	5:50	6:22	4:30
DR 5	8:18	6:42	8:04	5:30
BR 5	-	26:24	26:06	30:00
$\text{CO} \leq 1\%$				
LR 5	21:00	13:20	7:20	21:00
DR 5	21:00	14:20	8:30	19:00
BR 5	-	24:32	25:30	29:20
$\text{O}_2 \leq 7\%$				
LR 5	24:00	15:00	10:08	>24:00
DR 5	25:30	15:00	15:45	21:30
BR 5	-	26:30	26:40	31:30
Visibility $\leq$ 1.2 m (4 ft)				
LR 5	Not Determ.	6:00	6:00	5:30
DR 5	9:00	6:00	6:00	5:50
BR 5	-	21:00	23:00	22:30
Flashover in DR	-	24:23	23:30	27:55
<b><u>Steiner</u></b> <b><u>Tunnel</u></b>				
FSI	15	148	163*	38
SDI	12	77	81*	14
<b><u>Cone @ 50</u></b> <b><u>[kW/m<sup>2</sup>]</u></b>				
Pk RHR	110	290**	290**	190

\* Averages of two tests: FSI: 169 and 157; SDI: 64 and 98.

\*\* The tests conducted did not have gypsum board backing.

in Test 2 in the bedroom. In conclusion, the lack of difference between the tests with the plywood on gypsum board or nailed directly to the studs is consistent with the results of the ASTM E 84 (Steiner tunnel) test, which is, often, a good indicator of flame spread results for wood products.

- \* The results of this investigation indicate that the additional safety resulting from the incorporation of gypsum board behind this particular type of fire retarded plywood is marginal, at best. This investigation indicates that properly fire retarded plywood wall panels offer a significant improvement over non fire retarded panels. However, mildly fire retarded panels may not offer sufficient improvement in some fire properties.
- \* The more important conclusion is that old data can be reanalyzed and used for developing fire safety information without requiring the added expense of conducting new tests.

## References

- [1] Babrauskas, V. and Peacock, R. D., "Heat Release Rate: The Single Most Important Variable in Fire Hazard", *Fire Safety Journal*, 1992, Vol. 18, pp. 255-72.
- [2] Hirschler, M. M., "Tools Available to Predict Full Scale Fire Performance of Furniture", in *Fire and Polymers II. Materials and Tests for Hazard Prevention* (Ed. G. L. Nelson), ACS Symposium Series 599, Developed from ACS Symposium in 208th ACS National Meeting, Aug. 21-25, 1994, Washington, DC, Chapter 36, American Chemical Society Washington, DC, 1995, pp. 593-608.
- [3] *Heat Release in Fires*, Babrauskas, V. and Grayson, S. J. Eds, Elsevier, London, UK, 1992.
- [4] Pryor, A. J., "Full Scale Evaluation of the Fire Hazard of Interior Wall Finishes", Southwest Research Inst. Project No. 03-2167, for Hardwood Plywood Manufacturers Association, San Antonio, TX, May 1977.
- [5] Pryor, A. J., "Full Scale Evaluation of the Fire Hazard of Interior Wall Finishes", Southwest Research Inst. Project No. 03-2363, for Hardwood Plywood Manufacturers Association, San Antonio, TX, May 1977.
- [6] Parker, W. J., "Calculations of the Heat Release Rate by Oxygen Consumption for Various Applications", *Journal of Fire Sciences*, Vol. 2, September/October, 1984, pp. 380-95.
- [7] Janssens, M. L., "Measuring Rate of Heat Release in Full-Scale Fire Tests by Oxygen Consumption", *Fire Technology*, Vol. 27, August 1991, pp. 237-249.

Ned R. Keltner<sup>1</sup>, Harry K. Hasegawa<sup>2</sup>, James A. White, Jr.<sup>3</sup>

## HIGH-TEMPERATURE ACCELERANT ARSON—REVISITED

---

**REFERENCE:** Keltner, N. R., Hasegawa, H. K., and White, J. A., Jr., “**High-Temperature Accelerant Arson—Revisited,**” *Very Large-Scale Fires, ASTM STP 1336*, N. R. Keltner, N. J. Alvares, and S. J. Grayson, Eds., American Society for Testing and Materials, 1998.

**ABSTRACT:** In the 1980's, there were a number of unusual arson fires involving very fast fire growth and in some cases premature structural failure. These characteristics posed great risks for fire fighters. The evidence, such as melted steel, indicated that a high temperature accelerant was involved. To support their investigation into these fires, the Seattle Fire Department organized a large scale demonstration. An accelerant with characteristics similar to rocket propellant was used to initiate a fire in a 1900 m<sup>2</sup> room in a single story building. The accelerant produced peak heat fluxes of 250-300 kW/m<sup>2</sup> in approximately five seconds. Approximately two minutes after ignition of the accelerant, there was an apparent backdraft event and then flashover occurred. The building was heavily involved within four minutes.

From this demonstration, the Seattle Fire Department developed and distributed information to help other fire departments recognize certain characteristics of this type of arson and modify their procedures to protect their personnel.

**KEYWORDS:** arson, high temperature accelerant, backdraft, flashover, heat flux

---

In the 1980's there were eight fires in the state of Washington and over twenty nationwide, suspected of involving an unusual type of arson. Fire fighters were killed in two of these fires; one fatality was due to a premature structural collapse. In the second case, a survivor described spontaneous ignition of a material that produced intense flames after firefighters had entered the building.

There were a number of features that distinguished these fires from arson fires involving a liquid fuel accelerant.

---

<sup>1</sup>Senior Engineer, Ktech Corporation, 901 Pennsylvania NE, Albuquerque, NM 87110.

<sup>2</sup>Principal Fire Consultant, Fire Quest, 1220 Oakland Blvd., Suite 200, Walnut Creek, CA 94596-4337.

<sup>3</sup>President, Western Fire Center, 2204 Parrott Way, Kelso, WA 98626.

Unique characteristics noted during the fires included:

1. Bright, orange-yellow-white flames were observed within the structures at times accompanied by pyrotechnic displays;
2. There was rapid, total involvement of the building within minutes of discovery, even with a small internal fuel load; and,
3. Structural failure occurred in heavy timber constructions much faster than expected by experience or reaction to fire models.

Unique characteristics discovered during the post-fire investigations included:

1. Cast iron and steel structural members appeared melted and/or burned;
2. There were areas of severe concrete damage with deep spalling or rubblization;
3. There was a blue-green discoloration of the concrete; and
4. Little or no trace of an accelerant was ever found.

The Arson Squad of the Seattle Fire Department suspected that an accelerant with unusual characteristics was being used because normal evidence of accelerants was not found at suspected arson sites. From on-scene evidence, such as damage to cast iron and steel, and from witness accounts, they concluded that a very high temperature accelerant was being used. They coined the phrase High Temperature Accelerant (HTA) Arson.

The Seattle Fire Department organized a project to try to replicate this type of arson on a relatively large scale. For this demonstration, a shopping center building (~2600 m<sup>2</sup>) was used.

The goals of the demonstration were to provide detailed information on the characteristics of these fires and a documented setup for a complete forensic investigation. The demonstration was used to develop a report and a video to warn other fire departments of the unusual hazards involved in this type of fire. These suggested modifications to normal fire suppression techniques to protect the fire fighters from the hazards posed by the rapid flame spread and the chance of premature structural collapse. These were distributed nationwide. Information was also publicized in journals [1].

Information related to this type of arson has been presented in a number of forums. Some of the technical details were presented in a conference paper [2]. Additional analyses carried out by the Bureau of Alcohol, Tobacco, and Firearms indicated that other potential causes could explain some but not all of the suspected HTA fires [3]. The U. S. Fire Administration also reviewed the information; however, no report was provided. There were articles related to the investigation in the Wall Street Journal and the television show Unsolved Mysteries. The purpose of this paper is to review some of the prior work and present additional technical information on the demonstration.

### Small Scale Tests

To help develop an accelerant recipe and to design appropriate techniques for instrumenting the large scale demonstration, a number of tests were conducted using kilogram quantities of fuel-oxidizer mixes. The tests were conducted at the Weyerhaeuser

Fire Technology Laboratory in Longview, Washington. The potential accelerants were placed in a small metal can and set at the base of a wooden column. The intent was to look for bright, white flames described by some witnesses and to make limited thermal and combustion product measurements. Results obtained from these small tests include:

1. Heat fluxes of up to 700 kW/m<sup>2</sup> were measured adjacent to the flame plume; these are four to five times those produced by liquid hydrocarbon accelerants;
2. An apparent erosion rate of up to 10 mm / minute was produced in wood columns by a flame plume flowing along the face of a column this is an order of magnitude greater than generally observed in structure fires; and,
3. The appearance of the flames and the smoke / gas release varied significantly among the fuel-oxidizer mixes with at least one producing the desired bright, white flame plume.

### Large Scale Demonstration

The large scale HTA demonstration had several goals:

1. To attempt to replicate the rapid fire development and structural damage characteristics;
2. To develop a basic understanding of the temperature and heat flux exposures;
3. To provide a documented experimental setup for post-test forensic examination; and,
4. To develop training materials for fire departments nationwide to help them quickly identify this type of fire and modify their techniques to prevent injuries from the unusual hazards posed by these fires.

The demonstration was set up in a one story, shopping center building that was scheduled to be demolished. The building was a wooden structure, approximately 73 m (240 ft) by 36 m (118 ft) by 5 m (16 ft). Most of the front of the building was 3.7 m high plate glass windows. The roof was exposed 2 x 6 (nominally 51 mm by 153 mm) double tongue and groove wood. Glue laminated beams 6 x 28 (153 mm by 711 mm) ran from the front to the back of the building; these beams figured prominently in the fire modeling described later in the paper. Part of the floor was carpeted; the remainder had linoleum tile. There was plywood wainscoting on part of the walls; the rest had a wall covering over gypsum board. The layout of the building and the instrumentation are shown in Figure 1. The room in the northeast corner (approximately 700 m<sup>2</sup>) was closed off during the demonstration burn.

The building was instrumented with thermocouples, heat flux sensors (radiometers, thin-skin calorimeters, and slug calorimeters), gas sensors (oxygen and carbon monoxide), and pressure sensors. The layout of the instrumentation is shown in Figure 2. Video cameras were set up at several locations along the front of the building; there was also a camera in a helicopter overhead.

Based on the small tests, the accelerant mixture was ammonium perchlorate, aluminum, eutectic salts, and diesel fuel. Approximately 200 kg of the mixture was put in plastic buckets and placed adjacent to three columns as shown in Figure 2. Two buckets

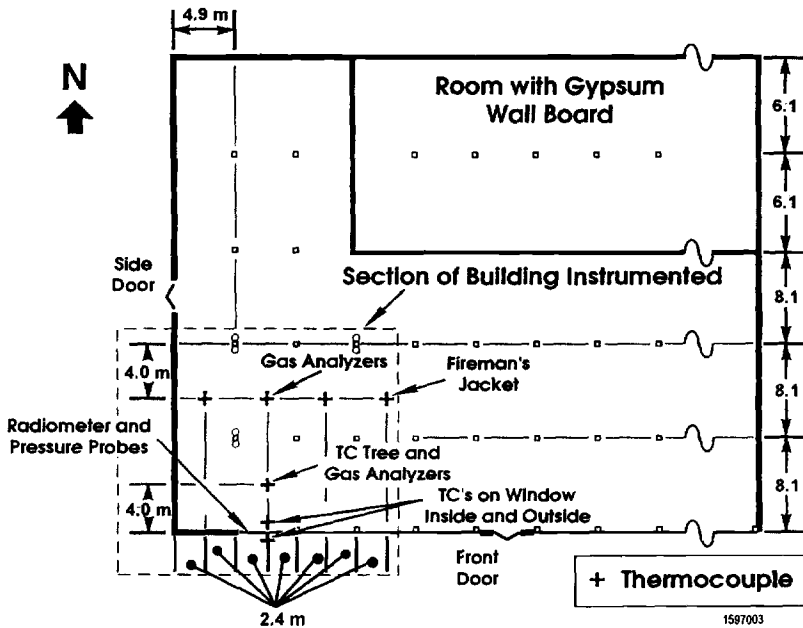


Fig. 1--Overall layout of the test building.

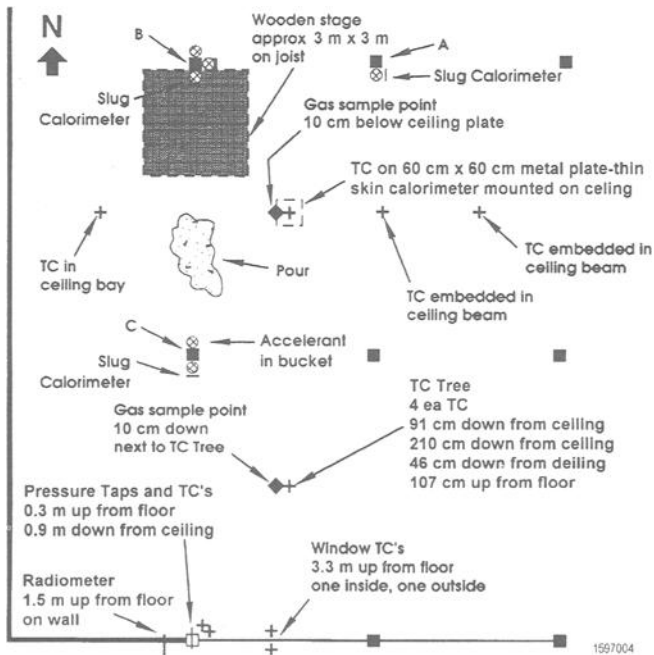


Fig. 2--Layout of the accelerant and instrumentation locations.

were stacked next to Column A; buckets were placed on three sides of Column B; buckets were placed on opposite sides of Column C. The intent was to ignite all of the buckets simultaneously. Additional accelerant was spilled on the floor and left to ignite spontaneously during the fire.

### Test Observations and Measurements

On the initial attempt, the accelerant was ignited at two locations; the third location was ignited approximately forty seconds later after a firing circuit was fixed. The accelerant produced intense, white flame plumes. An analysis of the measurements and the videotapes indicates that flashover occurred between one hundred twenty (120) and one hundred forty (140) seconds after the initial ignition of the accelerant. At approximately the same time there was an apparent backdraft event after the side door broke or opened [3]. The building was heavily involved in three to four minutes. A summary of the video observations with description of the events is contained in Table 1.

**TABLE 1--Large Scale HTA Demonstration Video Observations.**

<b>Time min:sec</b>	<b>Event Description</b>
01:10	Ignition of accelerant at columns A and C
01:30	Hot gas layer reaches the top of the windows
01:48	Ignition of accelerant at column B
02:01	Bucket(s?) at column A comes apart
02:14	Front door opens from interior pressure; large amplitude waves occur in the hot gas layer
02:15	Accelerant spill ignites
02:35	Smoke obscures the front of the building
03:10	<u>Apparent backdraft event</u> jets flame out of side (west) door; carpeting ignites
03:10-03:30	<u>Flashover occurs</u> in the southwest quadrant of the building
03:33	Front windows begin to break; flame plumes well above roof
04:10	Accelerant mix burns out
05:50	Carpet is still burning
06:30	Water cannon applied to the front of the building

Figures 3-5 show some of the temperature measurements made during the test. On the plots, the first ignition occurred at approximately 70 seconds. All channels in Figures 3 and 4 show a rapid temperature rise at approximately 180 seconds. Figure 3 shows temperature measurements made at ceiling level in the first four bays; the bays are defined as the areas between the large, glue laminated, structural beams that run North to South (or front to back) in the building and are approximately 5 m wide. Approximately two minutes after ignition, the test indicated temperatures from the three bare thermocouples (channels 4,6,11) rose to over 1000°C within a 20-40 second period. Figure 4 shows measurements made at different elevations on the 'thermocouple tree'

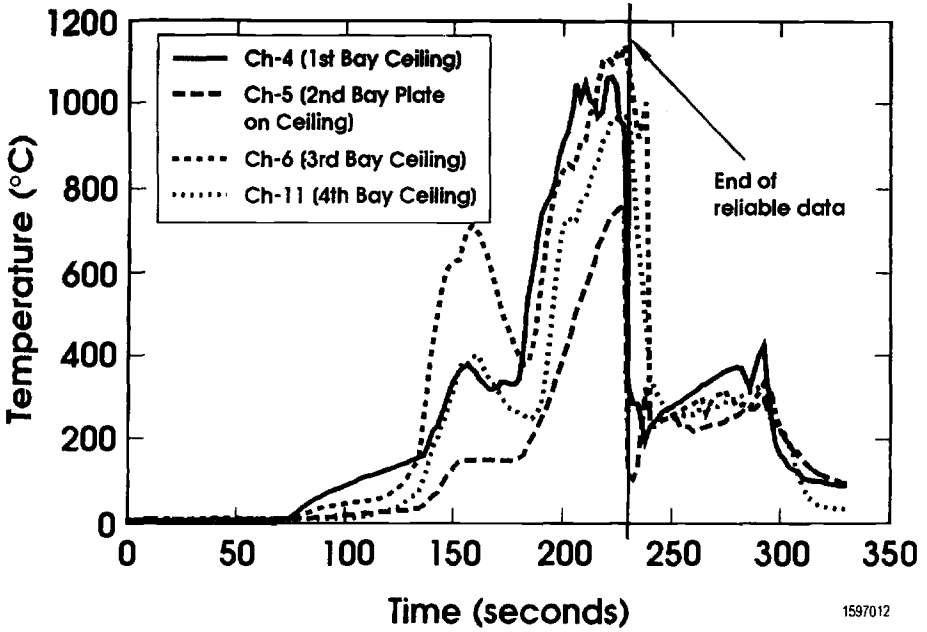


Fig. 3--Temperature histories in four ceiling bays.

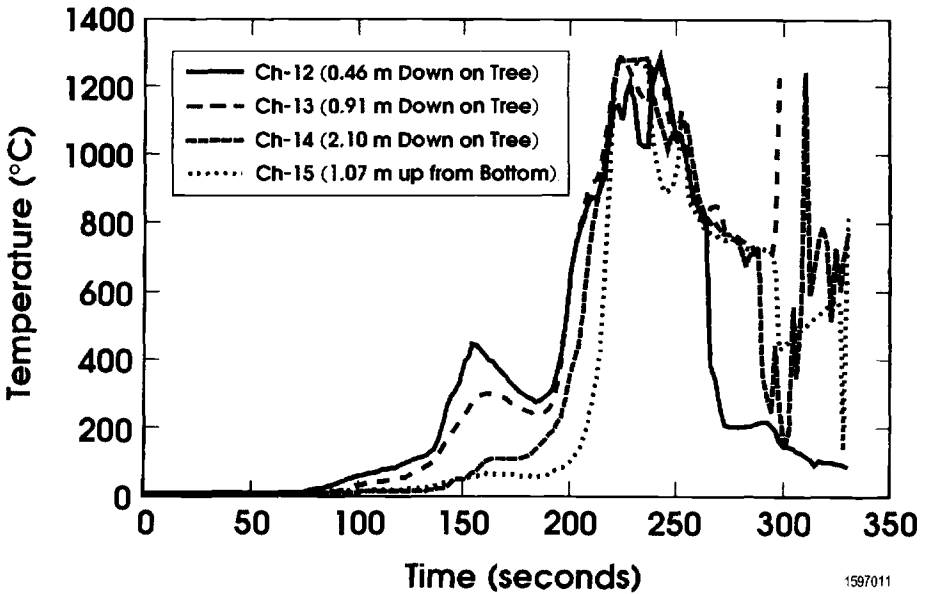


Fig. 4--Temperature histories on the thermocouple tree.

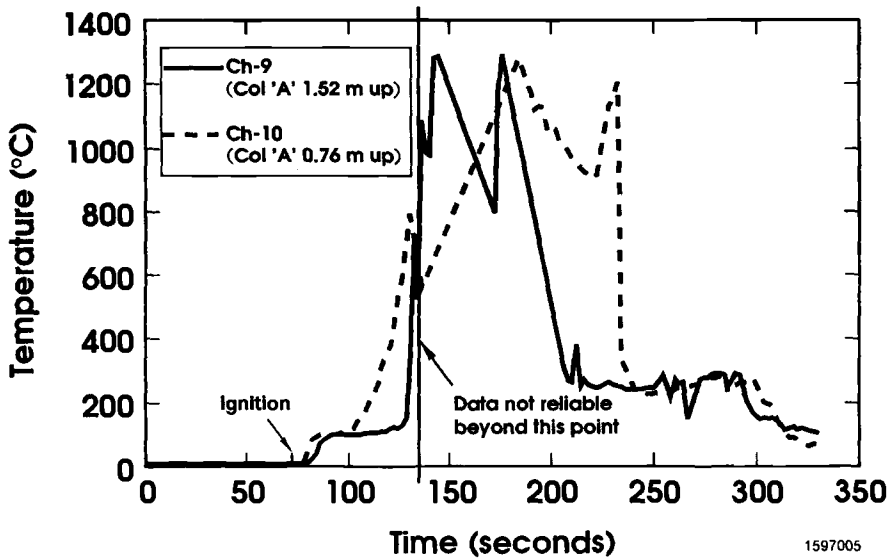


Fig. 5--Temperature histories in a wooden support column.

shown in Figure 2. These are similar to measurements near the ceiling although there is a progressive delay from the ceiling to the floor. Figure 5 shows the temperatures measured by thermocouples imbedded approximately 6.3 mm (0.25 in) beneath the surface of Column C at elevations of 0.76 m and 1.52 m. As noted on the figure, both thermocouples failed when the temperature exceeded 800°C. It is believed that the wood had charred to the thermocouple depth and they were exposed directly to the flame plumes at this time. Thermocouples mounted on the inside and the outside of the southwest window spiked up at approximately 140 seconds; the indicated temperature difference across the window was approximately 200°C although radiant loading on the interior thermocouple would cause it to read too high.

Slug (6.3 mm steel plate) calorimeters were set next to the accelerant buckets [ASTM E 457, Standard Test Method for Measuring Heat-Transfer Rate Using a Thermal Capacitance ( Slug ) Calorimeter]. An inverse heat conduction code (SODDIT) was used with the measured plate temperatures to predict absorbed heat fluxes [4]. In the second bay, heat flux measurements were made with a thin-skin calorimeter attached to the ceiling [ASTM E459, Standard Test Method for Measuring Heat-Transfer Rate Using a Thin-Skin Calorimeter]. Remember, ignition of the accelerant occurs at approximately 70 seconds on the data plots. Analysis of the heat flux data shows:

1. After an initial pulse of 250-300 kW/m<sup>2</sup>, the absorbed heat flux measured with all three of the slug calorimeters mounted by the buckets was in the 100- 250 kW/m<sup>2</sup> range. Figure 6 shows the estimated heat flux for the slug calorimeter near Column A. The incident heat flux would depend on the absorptivity of the surface; for oxidized steel, the initial absorptivity is around 0.7-0.8. The

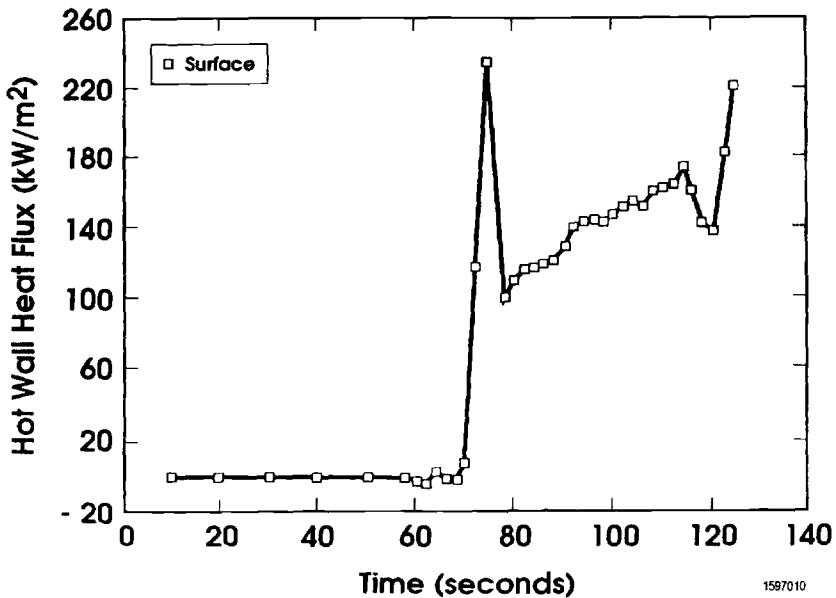


Fig. 6--Heat flux measured with a slug calorimeter at column A.

plates may have been coated with aluminum oxide from the burning mix; if so, the absorptivity would be significantly less than 0.8. After the fire, the steel calorimeter near Column C was found folded in half and welded together along with some burn holes. This damage was similar to some evidence.

- For the thin-skin calorimeter in the 2nd ceiling bay, Figure 7 shows the heat flux was low for approximately a minute after ignition, picked up to between 30 and 50 kW/m<sup>2</sup> for 15-20 seconds, and then went to near zero ( i.e., the temperature remained approximately constant around 150°C ) until flashover. The plate temperature history also shows what appears to be flashover at approximately the same time as the 1st bay thermocouple. After flashover, the absorbed heat flux increased steadily to over 120 kW/m<sup>2</sup>. The plate used for the thin skin calorimeter appeared to be cold rolled steel, which would have an absorptivity of 0.6-0.7.
- The readings from the radiometer mounted in the southwest corner remained low for approximately 110 seconds, then rose to 50 kW/m<sup>2</sup> over a period of 30 seconds, and then spiked up to 160 kW/m<sup>2</sup> before dropping back down into the 40 - 80 kW/m<sup>2</sup> range.

Figure 8 shows that the O<sub>2</sub> measurements undergo dramatic changes in the time from shortly before to shortly after flashover. The measurements were made near the ceiling plate in the second bay and 1.2 m ( 4 ft ) below the ceiling adjacent to the

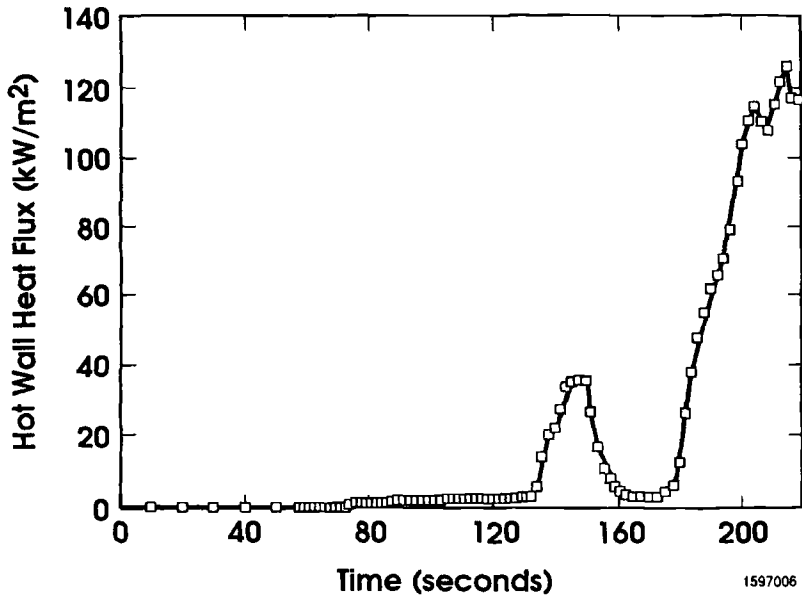


Fig. 7--Heat flux measured at the ceiling with a thin-skin calorimeter in the 2<sup>nd</sup> ceiling bay.

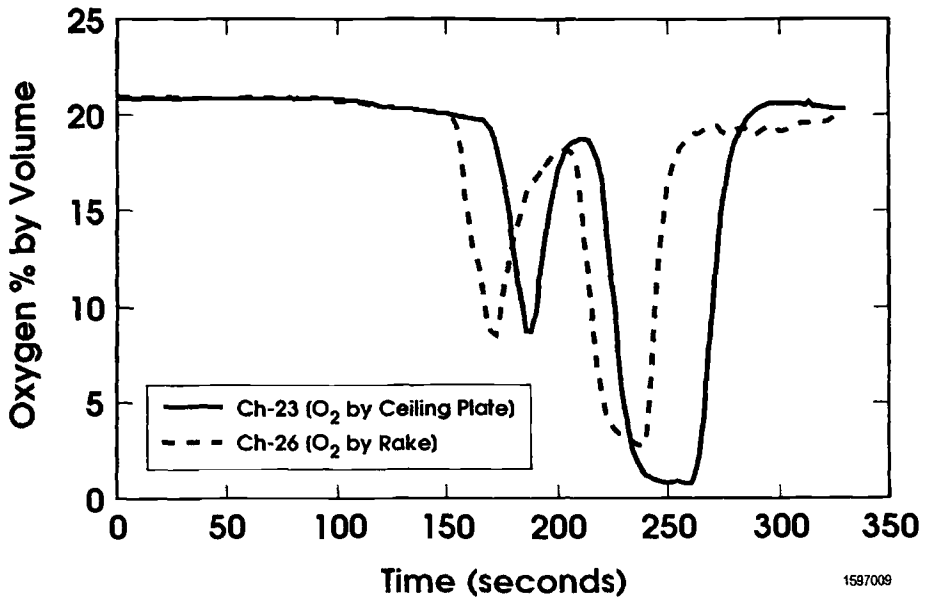


Fig. 8--Oxygen level measurements.

thermocouple tree. The time shift between the two readings is due to the different lengths of tubing used for gas sampling. The carbon monoxide levels, which are not shown, underwent similar dramatic changes.

Figure 9 shows the pressure histories measured near the floor and the ceiling. The pressure increased to approximately 80 Pa and then dropped when the front door opened; this caused a large amplitude, rolling wave motion in the ceiling smoke layer that was readily visible through the front windows. The pressure had built back up to approximately 150 Pa when the glass side door either opened or broke. Immediately, a flame jet, almost horizontal and 20-30 m long, shot out of the double wide personnel door on the west side of the building in an apparent backdraft event [5]. A group of fire fighters was stationed directly opposite of that door, approximately 50 m from the building. When they observed the flame jet they immediately took cover; afterwards, they described the jet's appearance as that of a glowing, fast moving, freight train.

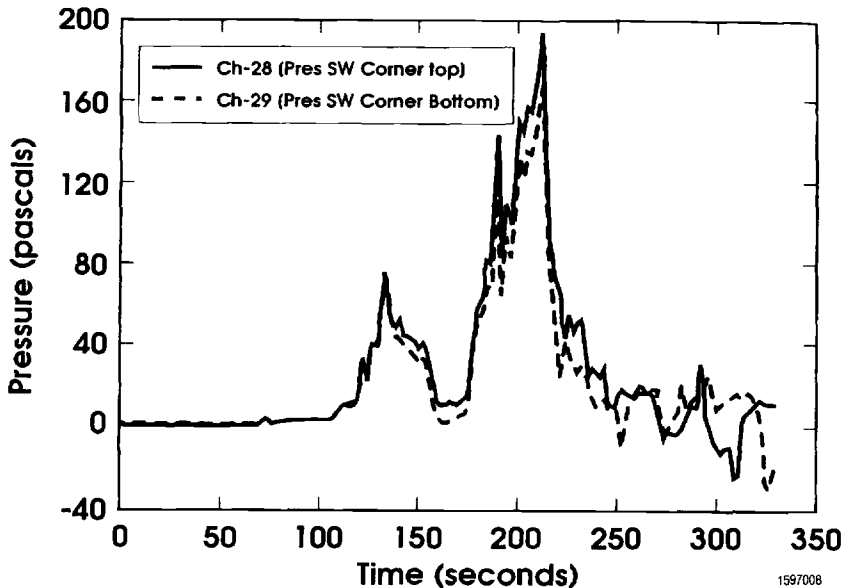


Fig. 9--Pressure histories inside the building.

### Heat Release Rate Estimates

Analysis of the accelerant mixture was done using the TIGER code [6]. TIGER calculates the thermochemical state ( combustion products, temperature, and heat release ) for an initial mixture of known composition. Using the nominal mixture formulation, the flame temperature was estimated to be approximately 2500 K (4000 F); the heat release from the reacting mix was estimated to be approximately 2800 J / g.

Review of the videotapes indicated the accelerant burned out in approximately three minutes. Assuming a uniform burn rate, the heat release rate would be approximately 3.5 MW. It is difficult to determine an exact burn time from the videos.

For a shorter or longer time, the estimated heat release rate would be adjusted up or down. In addition, ignition around Column B was delayed approximately 40 seconds. This would argue for a lower heat release rate until ignition of the third bucket was achieved. The estimate treats the spill material as burning uniformly over this time.

The accelerant mixture was fuel rich. As a result, there are many combustible gases ( e.g., hydrogen, carbon monoxide, etc. ) in the plume; burning of these gases along with the metal oxide combustion products produce the bright ( high temperature ), white appearance of the flame plume. These combustible gases are also thought to promote the rapid flashover that often occurs in the arson fires.

The analysis shows that there are 13.5 gram-moles of hydrogen (i.e., slightly over 27 grams) released per kilogram of mix. If all of this were burned to form water, the heat release rate would be slightly greater than that from the initial reaction of the accelerant mixture. However, there is a significant amount of OH also being released; if this reacts with part of the hydrogen to form water it will reduce the amount of heat released by the hydrogen burning in the plume. Measured carbon monoxide levels were in the 3-5 % range immediately prior to flashover. After trying to account for the various uncertainties, combustion of these gases was estimated to increase the total heat release rate to approximately 7 MW. This gives a heat release rate of 10 MW/m<sup>2</sup>.

For a point of comparison, the heat release rate in 9 m x 18 m pool fires conducted at Sandia National Laboratories is approximately 3 MW/m<sup>2</sup> using JP-4 as the fuel with a consumption rate of approximately 82 g/m<sup>2</sup>/s [7 & 8]. The average and peak temperatures in this type of fire are in the 1250-1450 K range. The peak heat flux is approximately 150 kW / m<sup>2</sup>.

To match the total heat release of the accelerant used in the demonstration test would require a pool area of about 2.5 m<sup>2</sup>. A fire of this size burning at an air/fuel ratio of 15:1 would consume approximately 4 % of the oxygen in the building in three minutes.

### Supplementary Tests

To help evaluate the wooden column data obtained in the demonstration, small scale radiant heat and solid rocket propellant tests were conducted. Douglas fir 4 X 4's were used to simulate the columns. The Weyerhaeuser Fire Technology Laboratory instrumented the test pieces. Temperatures were measured at four depths, including the 6.3 mm depth used in the demonstration.

The small propellant burns were conducted with the sample mounted at the top edge of the canister with the burning plume flowing parallel to the sample, as in the demonstration or with the sample mounted horizontally above the canister with the flame plume impacting the sample. Each burn used six kilograms of a commercially available solid propellant and lasted approximately 105 s. At the 6.3 mm depth from the heated surface, maximum temperatures ranged from 900°C in the vertical orientation to 1100-1300°C in the horizontal orientation. This propellant composition has a higher flame temperature than the accelerant used in the large scale demonstration. The maximum expected heat fluxes for the vertical orientation were in the 600-1000 kW / m<sup>2</sup> range and the 1000-1300 kW / m<sup>2</sup> range for the horizontal orientation [9].

A series of radiant heating tests were conducted based on the heat flux measurements made in the large scale demonstration and in other tests with a solid propellant fire plume impacting a calorimeter. The Douglas fir 4 x 4's were mounted vertically with one face exposed to heat fluxes of 150, 300, and 600 kW/m<sup>2</sup> for five minutes using a 1.0 m by 1.2 m quartz lamp, radiant panel at Sandia National Laboratories Radiant Heat Facility. At the highest flux, the surface ignited in a few seconds with an audible pop. Temperatures exceeded 500°C at the 6.3 mm depth in approximately 135 s at 150 kW / m<sup>2</sup>, 115 s at 300 kW / m<sup>2</sup>, and 65 s at 600 kW / m<sup>2</sup>. In the demonstration, the column temperature measurements exceeded 500°C in 50-60 seconds as Shown in Figure 5. Peak temperatures at 6.3 mm from the heated surface ranged from 1000°C to 1400°C<sup>4</sup>.

### Fire Modeling

Numerical simulations of the demonstration were made with a multi-compartment zone model: Consolidated Compartment Fire Model (CCFM) [10]. The building was modeled as both a single room and as nine separate compartments. The deep ceiling beams, that ran from the front to the back of the building, were used to define openings between the eight compartments ( or ceiling bays ) closest to the accelerant locations; the final compartment was the remainder of the building. Heat release rates of 3.5 MW and 7 MW were used for a period of three minutes to simulate the estimates of heat release from just the reacting mixture and the total heat release rate which includes burning in the plume. Given the short duration of the accelerant burn, heat loss to the ceiling and walls was set at 10% of the total.

With a heat release rate of 3.5 MW, the predicted hot gas layer temperatures in the ceiling bags (compartments) close to the accelerant locations peaked at approximately 300°C this is well below 500°C assumed for flashover to occur. With a heat release rate of 7 MW, the predicted hot gas layer temperatures in the first two compartments ( i.e., those close to the accelerant locations ) exceed 400°C after 60 seconds. The predicted temperatures in the first two ceiling bays reached 500°C in a period of 120-150 seconds and correlates with the apparent flashover time of approximately 120-130 seconds. These results, shown in Figure 10, are in good agreement with the measurements, shown in Figures 3 and 7<sup>5</sup>.

Using the data developed from the demonstration test, CCFM was used to estimate the accelerant quantities for another suspected high temperature accelerant arson fire. Concrete damage patterns were used to locate the accelerant. The simulations indicated that heat release rates in the 4-8 MW range would produce flashover within the timelines developed in the investigation<sup>5</sup>.

---

<sup>4</sup>Sobolik, K. B., Sandia National Laboratories, private communication, 1990.

<sup>5</sup>Nicolette, V. F., Sandia National Laboratories, private communication, 1991.

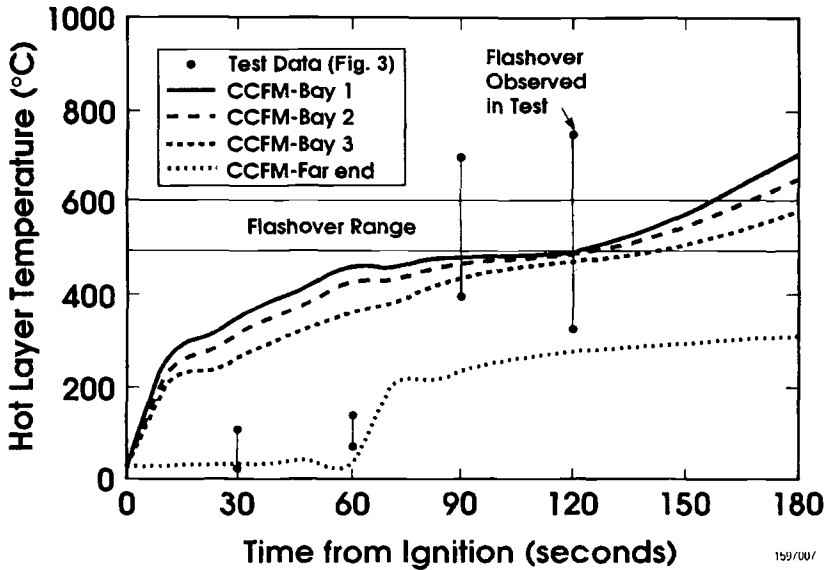


Fig. 10--Comparison of Predicted and Measured Ceiling Temperatures

### Summary

To support an arson investigation, a shopping center building was used for a large scale demonstration involving high temperature accelerants. The accelerant mixture is similar to solid rocket propellant. It ignites quickly; structural columns were exposed to heat fluxes of 250-300 kW/m<sup>2</sup> in five seconds. Over a three minute period the average estimated heat release from the accelerant was approximately 7 MW. There was an apparent backdraft event and then flashover occurred in the building approximately 2 minutes after ignition. The structure was heavily involved after four minutes. This rapid fire development was in line with witness reports from some of the suspected arson fires. Simulations with a multi-compartment, zone type of fire model provided good agreement with experimental results up to flashover.

The wealth of scientific evidence obtained from the small scale tests, the demonstration, and the post-test examinations supported the Seattle Fire Department's conclusion. They were dealing with an arsonist who was using an accelerant resembling solid rocket fuel to destroy buildings.

### References

- [1] Russo, W. P., "Northwest Battles High-Tech Arson," NFA Journal, November-December, 1992, pp.67-73.
- [2] Keltner, N. R., et al, "Investigation of High Temperature Accelerant Arsons," Proceedings of the Sixth International Interflam Conference ( INTERFLAM'93 ), University of Oxford, March 30 - April 1, 1993, InterScience Communications Limited, London.

- [3] Carmen, S. W., "High Temperature Accelerants," Bureau of Alcohol, Tobacco and Firearms, Sacramento, CA, (October 1994).
- [4] Blackwell, B. F., R. W. Douglass, and H. Wolf. "A User's Manual for the Sandia One-Dimensional Direct and Inverse Thermal (SODDIT) Code," SAND85-2478, Sandia National Laboratories, Albuquerque, NM (May, 1987).
- [5] Fleischmann, C. M., P. J. Pagni, and R. B. Williamson, "Quantitative Backdraft Experiments," Fire Safety Science - Proceedings of the Fourth International Symposium, Editor T. Kashiwagi, Ottawa. Ontario, Canada, June 13-17, 1994.
- [6] Cowperthwaite, M. and W. H. Zwisler, "TIGER - Computer Program Documentation," SRI Publication No. Z106, Stanford Research Institute, Menlo Park, CA, January, 1973.
- [7] Gregory, J. J., N. R. Keltner, and R. Mata Jr. "Thermal Measurements in Large Pool Fires," Journal of Heat Transfer, Vol. 111, May, 1989, pp. 446-454.
- [8] Gregory, J. J., R. Mata Jr., and N. R. Keltner. "Thermal Measurements in a Series of Large Pool Fires," SAND85-0196, Sandia National Laboratories, Albuquerque, NM (August, 1987).
- [9] Gill, W., L. A. Kent, N. R. Keltner, and W. Schimmel, "Preliminary Model for Heat Transfer from an Uncontained Solid Rocket Propellant Burn, JANNAF, 1994.
- [10] Cooper, L. Y. and G. P. Forney, "The Consolidated Compartment Fire Model (CCFM) Computer Model, Parts I-IV," NISTIR 4342-4345, National Institute of Standards and Technology, Center for Fire Research ( now the Building and Fire Research Laboratory ), Gaithersburg, MD (July, 1990)

**Acknowledgments:**

The authors want to acknowledge the substantial contributions made by numerous people and organizations who volunteered to support this effort.

R. Gehlhausen, D. Fowler, B. L. Hansen, W. T. Hepburn, C. Harris, Seattle Fire Department  
 K. Staggs, Lawrence Livermore National Laboratory, Livermore, CA  
 R. U. Acton, V. F. Nicolette, and K. B. Sobolik, Sandia National Laboratories, Albuquerque, NM  
 J. Shaw, N. Pataansu, J. Leubbers, Weyerhaeuser Corporation, Longview, WA  
 K. Farmer, Naval Air Warfare Center, China Lake, CA.  
 W. Dietz, Bureau of Alcohol, Tobacco, Firearms, Walnut Creek, CA  
 J. deHann, California Criminalistics Institute, Sacramento, CA  
 J. Mars, Rocket Research Co., Redmond, WA  
 M. Fitz, Machine Design Engineers, Seattle, WA  
 D. Mann, Washington State Patrol Crime Laboratory, Seattle, WA  
 R. Anderson, San Jose State University, San Jose, CA

Tom Lennon<sup>1</sup>

## **LARGE COMPARTMENT FIRE TESTS ON A FULL-SCALE EIGHT STOREY BUILDING**

---

**REFERENCE:** Lennon, T., “Large Compartment Fire Tests on a Full-Scale Eight Storey Building,” *Very Large-Scale Fires, ASTM STP 1336*, N. R. Keltner, N. J. Alvares, and S. J. Grayson, Eds., American Society for Testing and Materials, 1998.

**ABSTRACT:** A series of fire tests have been undertaken on a purpose built eight storey, three bay by five bay steel frame building with composite floors and overall dimensions 33.5m by 21m by 45m. The building has been constructed at the BRE’s Large Building Test Facility at Cardington, near Bedford, England. As part of the overall fire programme, BRE have carried out fire tests on a compartment (9m x 6m) representative of a corner office and a large compartment (21m x 18m) representative of a large open plan office. The objectives of the programme are to examine the behaviour of multi-storey steel-framed buildings subject to real fires and to use the data from the tests to validate computer models for structural analysis at elevated temperatures. The work will provide substantial benefits and produce high quality data which will inform decisions on the degree of fire protection required for steel framed buildings, which could significantly reduce costs while maintaining existing levels of safety.

**KEYWORDS:** fire resistance, natural fires, structural behaviour, steel structures, composite structures, full scale testing

---

There is a growing opinion that the structural contribution of composite steel deck floor systems is under-utilized in current design procedures particularly for the fire limit state.

---

<sup>1</sup>Senior Scientific Officer, Metal Structures Section, Building Research Establishment, Watford WD2 7JR, UK

This, together with evidence from three dimensional numerical models and investigations from real fires such as that which occurred in Broadgate in the UK on the 23rd June 1990, suggest that the fire resistance of complete structures is significantly better than that of the single elements from which fire resistance is universally assessed. The fire at Broadgate is particularly significant as it occurred during construction and much of the steelwork in the area of the fire was unprotected. In order to verify these observations full scale tests were required.

Available computer programs for predicting structural behaviour at elevated temperatures have developed beyond the available experimental data. However, before such analytical techniques can be used with any confidence it is necessary to verify them against test results from real buildings subject to real fires. While it is possible to study structural behaviour by examining fire damaged buildings, interpretation of the findings is complicated by the lack of information on heating rates, temperatures and the stresses imposed on the members at the time of the fire.

The concept of equivalent time of fire exposure which relates the duration of heating in a standard test furnace to the thermal loading received in a real post-flashover fire has recently been introduced into the fire part of Eurocode 1 [1]. However, this approach has only been validated on compartments with dimensions significantly smaller than found in modern office buildings. Large compartment fire tests in real buildings will complement work recently carried out by the Fire Research Station and British Steel on natural fires in small to medium compartments [2].

It is therefore desirable to carry out a series of full-scale large compartment fire tests in real structures to improve the design procedures for modern steel framed buildings and to quantify safety margins. The development of the Building Research Establishment's Large Building Test Facility at Cardington has given researchers a unique opportunity to carry out a series of controlled fire tests on a building designed and built to current practice.

This paper describes the philosophy and objectives of the programme. The type and location of the instruments used to measure the response of the building to the fires are enumerated. Preliminary results from both the corner fire test and the large compartment fire test are presented. In both cases the fuel source was timber cribs having a fire load density of  $40\text{kg/m}^2$ . An applied loading of  $5.48\text{KN/m}^2$  representing the dead load plus one third of the imposed load was present on all floors. The response of the structure was measured using a wide range of instrumentation - the thermal response was monitored using thermocouples and heat flux transducers whilst the structural response was recorded using strain gauges, displacement transducers and clinometers. In addition a video recording of each test has been made. The influence of glazing, a highly unpredictable parameter, on the development of the fire has been investigated.

### **Large Building Test Facility (LBTF)**

The opening of the BRE's LBTF on 23rd March 1993 represented an ideal opportunity for researchers interested in the full scale testing of large structures. The tests described in this paper were carried out on the first building to be erected on the facility, an eight storey, three bay by five bay steel frame building with composite floors. The building was designed and constructed to resemble a typical modern city centre office development. A typical floor plan

of the building is shown in fig. 1. Further information on the design and construction of the compartment may be found in [3].

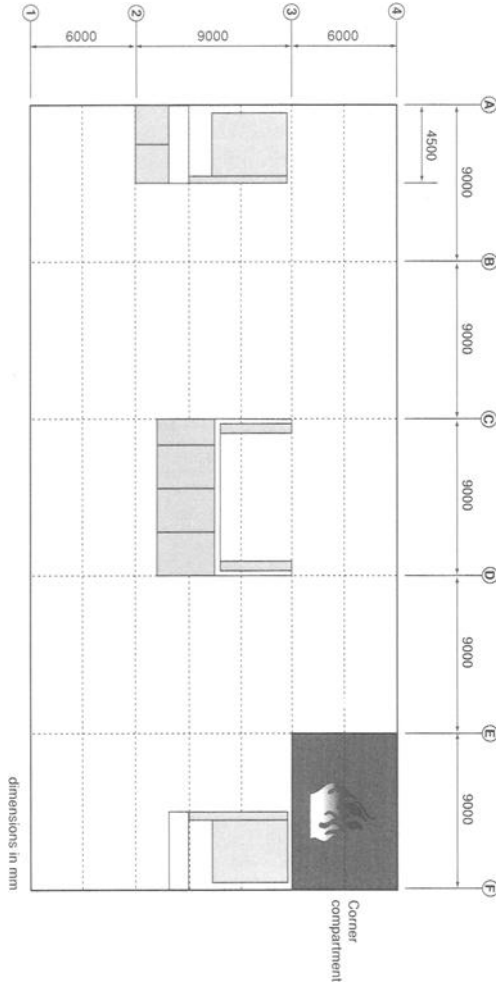


Fig.1 Typical Floor Plan Showing Location of Corner Fire Test

### Fire Test Programme

A wide range of tests have been carried out on the building. Among these is a programme of fire tests summarized in Table 1:

*Table 1 Cardington Frame Fire Test Programme*

Test No.	Description	Date
1	column tests, bare steel frame	September 93
2	column tests, composite floors	November 93
3	restrained beam	January 95
4	2D plane frame	May 95
5	BST corner test	July 95
6	BRE corner test	October 95
7	large compartment test	April 96
8	demonstration test	June 96
9	column tests, failure	to be arranged

This extensive programme of work has been carried out with the co-operation of a number of organisations. The BRE has overall responsibility for tests 1,2,6,7 and 9. The remaining tests have been carried out by British Steel's Swinden Technology Centre [4]. This paper is concerned only with tests 6 and 7.

### Corner Fire Test

The BRE corner fire test took place on the evening of the 23rd October 1995. The fire was ignited from a single source on the second floor of the eight storey building in a corner compartment bounded by gridlines E to F and 3 to 4 (see Fig. 1). Adjacent cribs were connected by fibre board soaked in paraffin. Figure 2 is a three dimensional view of the compartment. The choice of the third floor as the location for the fire test was made in order to minimize the heat rise on the structural members of the hangar itself and to facilitate observations during the test. The first and second floors were not typical of the building due to the presence of a central concourse. The location was also dictated by the need to ensure that, as far as possible, the results of a test in one location do not adversely affect subsequent tests.

The compartment itself was created using fire resistant board running between the columns forming the boundaries of the compartment. The internal column on gridline E3 was fully protected. Protection was also provided to the two external columns E4 and F4. The two

remaining columns were outside the compartment behind the shaft walling used to protect the stairwell at the Eastern end of the building. The secondary beam running through the centre of the compartment was unprotected. The presence of the glazing formed the only protection to the edge beam running between gridlines E4 to F4.

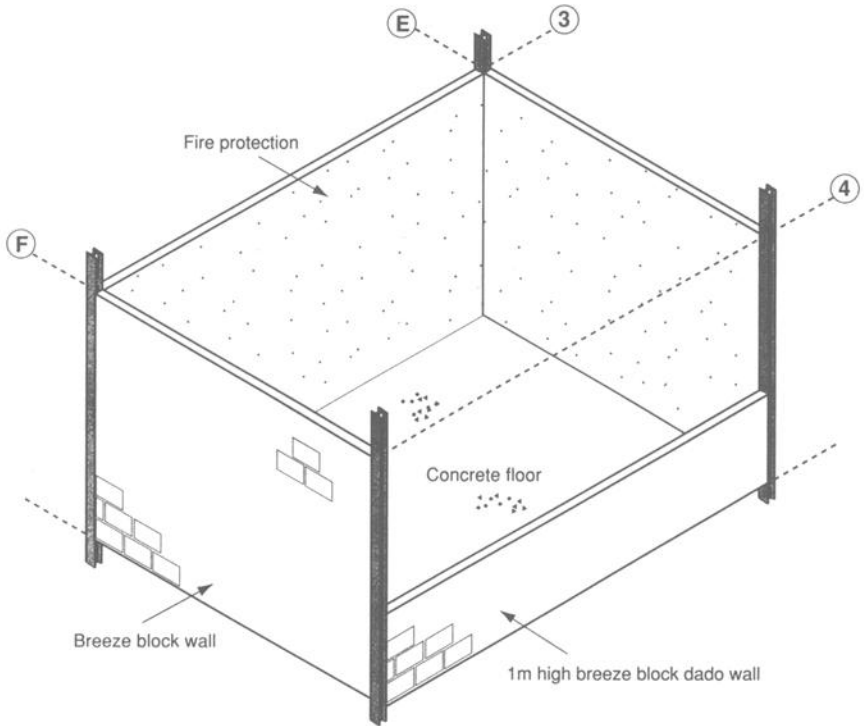


Figure 2, 3D View of the Compartment

As mentioned above the compartment was bounded on the Southern end by a fire resistant partition extending from the shaft walling to the column on gridline E3. The western boundary was similarly formed by constructing a fire resistant partition between columns E3 and E4. In both cases the protection was built up to the underside of the beams with a deflection allowance of 50mm. The Northern boundary was formed by constructing double glazed aluminium screens between columns E4 and F4 while the Eastern boundary was the gable wall already in existence. No attempt was made to provide any additional restraint to the wall. No additional ventilation was provided to the compartment and no attempt was made to artificially seal the compartment. One of the purposes of the test was to investigate the influence of the glazing on the development of the fire. The glazing comprised one 9 metre wide by 3 metre high 12 pane aluminium grid. Each pane consisted of two 6mm thick glass panels separated by a 12mm air gap. Each double glazed sealed unit measured 1.5 metres by 1.5 metres. For the purposes of design it is assumed that all the glass has cracked at the outset and that the amount of ventilation present is the maximum possible. Results from the test would suggest that this is an over-simplification.

Twelve timber cribs were placed in the compartment. The fire load was 40kg/m<sup>2</sup> over a floor area of 54m<sup>2</sup> giving a total fire load of 2160kg. Each crib was constructed from 200 sticks of 50x50mm rough sawn softwood with 10 sticks in each of 20 layers giving a crib height of 1 metre. Ignition was from a single point close to the stairwell at the back of the compartment. Floor loads were provided by sandbags on all floors other than the second. On the second floor the sandbags were split and their contents spread uniformly over the floor area. The bags on the floor above were suspended from slings attached to the steelwork which were designed to support the bags should the displacement exceed a pre-determined value of 400mm. The sandbags applied a loading of 5.48kN/m<sup>2</sup> representing the dead load plus one third of the imposed loading.

### *Instrumentation*

A number of thermocouples were used to monitor the temperature of the steel columns and beams within the compartment, the temperature profile through the depth of the concrete slab and the atmosphere temperature within the compartment. Additional instruments were used to record the temperature immediately outside the compartment, the temperature of the hangar steelwork, indicative temperatures of unprotected column sections suspended from the ceiling of the compartment and the internal and external temperatures of the gable wall. In total 278 thermocouples were used. Strain gauges were used to measure the response of the structure to the fire. Eight columns on the fire floor, the floor below, the floor above and the seventh floor were instrumented in addition to four beams on the fire floor. Additional strain gauges were used to measure the response of the reinforcing mesh and the concrete surface on the third floor. A total of 300 strain gauges were used. A total of 23 1000mm displacement transducers were used to measure the deformation of the concrete slab on the third floor. An additional 24 100mm travel transducers were used to measure the axial and lateral movement of columns E3 and E4. Twelve clinometers were used to measure the major axis rotations of the connections within the compartment while an innovative laser system monitored the movement of the gable wall.

In addition to the instrumentation mentioned above the University of Ulster monitored heat transfer through the floor while the Fire Research Station measured heat transfer in the plane of the window. A comprehensive audio visual record of the test was made including both stills photography and video. More detailed information on the location of the instrumentation is available in [5].

### *Preliminary Results*

The development of the fire was largely influenced by the lack of oxygen within the compartment. After an initial temperature rise the fire died down and continued to smoulder until the fire brigade intervened to vent the compartment. The removal of a single pane of glazing resulted in a small increase in temperature followed by a decrease. Flashover did not occur until a second pane, immediately below the first, was removed. This initiated a sharp rise in temperature which continued as the fire spread throughout the compartment. The maximum recorded atmosphere temperature in the centre of the compartment was 1051°C 1200mm from the ceiling after 102 minutes. The maximum atmosphere temperature recorded was 1060°C to the South of the compartment 1500mm below the ceiling. Figure 3 shows the average atmosphere time/temperature response.

The maximum recorded steel temperature of 903°C occurred after 114 minutes on the bottom flange of the unprotected beam B2 in the middle of the member. The maximum temperature reached by the edge beam was 690°C after 114 minutes despite being completely engulfed in flames. The maximum temperature of the beam framing into the stairwell was 629°C on the web of the section at mid-length. Figure 4 shows the time/temperature curve for the unprotected beam B2.

The maximum recorded value of slab displacement occurred in the centre of the slab after 130 minutes where it reached a value of 269.4mm. However, by the next morning the slab had recovered to a displacement of 160mm. Figure 5 shows the time/displacement curve for the centre of the slab.

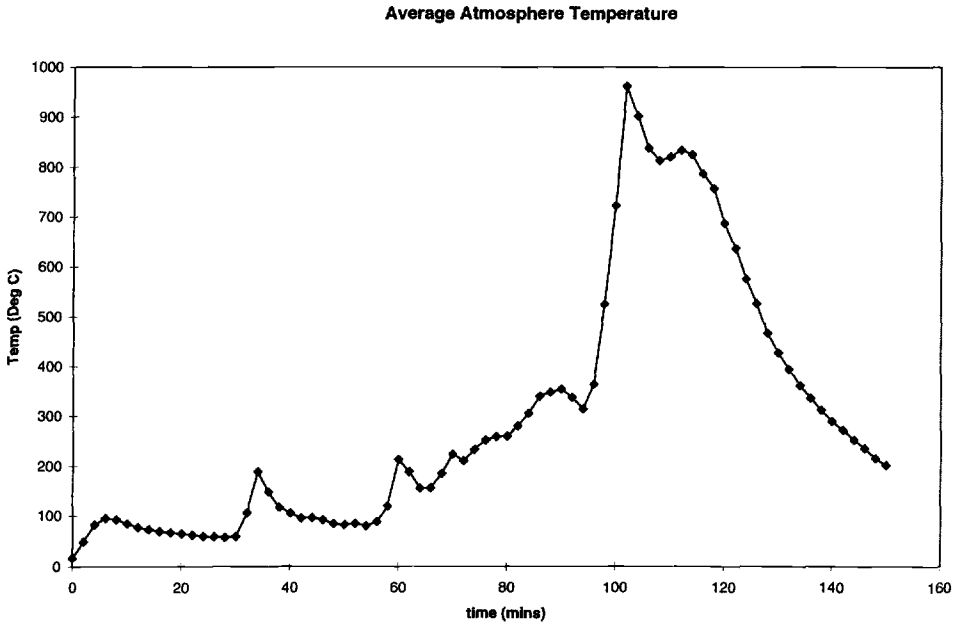


*Fig. 3 Atmosphere Temperature Corner Fire Test*

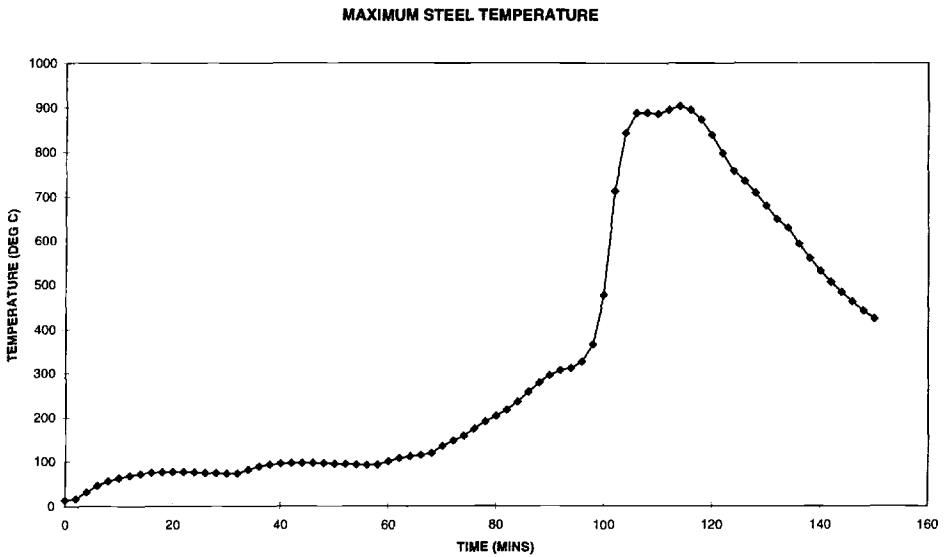


*Fig. 4 Maximum Steel Temperature Corner Fire Test*

## MID-SPAN DEFLECTION CORNER FIRE TEST

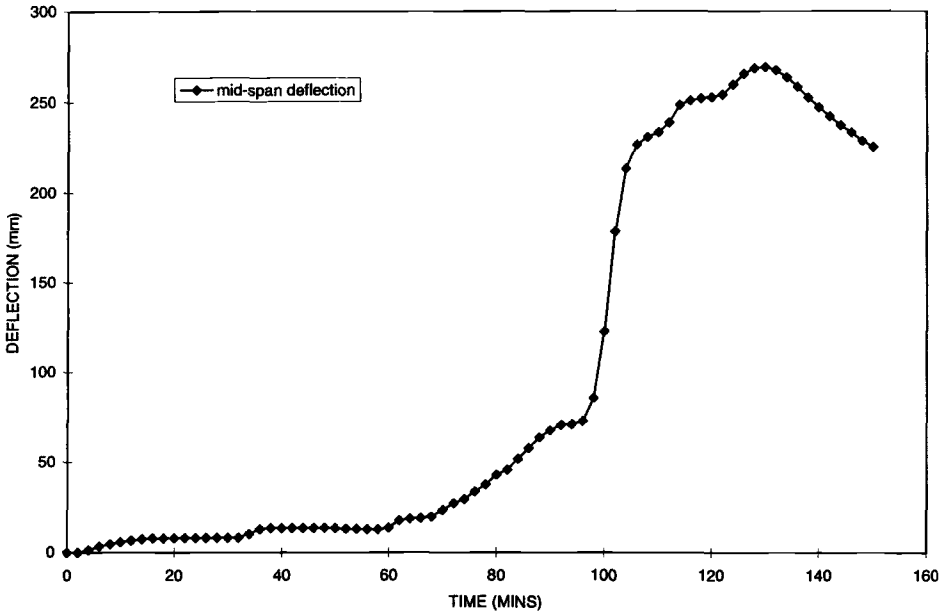


*Fig. 5 mid-span deflection corner fire test*

### *Discussion*

Initial observations have highlighted a number of areas worthy of consideration. The influence of glazing on the development of the fire requires further study. It is clear from the tests that the opening factor is not a constant for the compartment but varies with time. Unfortunately no measurements of glazing temperatures or strains were made for this test. The masonry wall forming the Eastern boundary of the compartment retained its integrity despite a significant thermal gradient across the wall and substantial lateral deformation. The fire resistant partitions performed adequately and prevented any appreciable heat rise outside the boundaries of the compartment.

There was significant lateral-torsional deformation of the secondary beam running through the shaft walling while the primary beam forming the Western boundary of the compartment remained virtually straight. While this may in part be due to the relative position of the partitions to the underside of the lower flange of the beams it is more likely that the enhanced performance of the primary beam was due to the restraint provided by the secondary beam framing into the web of the member halfway along its length.

That any damage was limited to the area within the compartment demonstrates the integrity of the structure. The performance of the structure was significantly better than that of the individual members which comprise the compartment. An initial comparison with analytical techniques suggests that a simplified theory of tensile membrane action provides a quick and accurate method of predicting the behaviour of a composite slab subject to a fire [6]. Comparisons with formulae in the Eurocode and elsewhere [7] for predicting the temperature-time response of the compartment have shown that it is possible to predict post-flashover fire behaviour with reasonable accuracy.

### **Large Compartment Fire Test**

The BRE large compartment fire test took place on the evening of the 2nd April 1996. The fire was ignited on the second floor of the eight storey building in a corner compartment bounded by gridlines A to C and 1 to 3 (see Fig. 6). All columns, both internal and external, were protected up to and including the connections. All beams including edge beams were left unprotected. The compartment was bounded on the Southern edge by the existing 1m high wall and double glazed aluminium screens similar to those used for the previous test. The middle third of the open area was not glazed to allow sufficient ventilation for the fire to develop. Therefore, before the glass broke the initial ventilation was an area of approximately 6m x 3m on either side of the building. The Western boundary was formed by constructing a fire resistant wall across the full width of the building. The Northern boundary was identical to that on the Southern side. The Eastern boundary was the existing gable wall together with a shaft wall system to provide protection to the passenger hoist.

Forty two timber cribs were placed within the compartment. The fire load was again 40kg/m<sup>2</sup> over a floor area of approximately 342m<sup>2</sup> giving a total fire load of approximately 13680kg. Each crib was constructed from 10 layers of grouped sticks (four per group at a spacing of 1:0.5) and 6 layers of individual sticks at a spacing of 1:1. The composite crib was designed to limit the speed of burning by altering the effective stick size and crib porosity. Ignition was achieved by lighting a number of cribs. Each crib was connected to the adjacent cribs by means of fibre board soaked in paraffin.

As for the corner fire test, the sandbags were similarly suspended although this time the allowable deformation of the slab was 1 metre before the load would be removed from the floor. The instrumentation was similar to the previous test although due to the size of the compartment it was not possible to maintain the density of instrumentation. More detailed information on the extent and location of the instrumentation used is given in [8].

As with the previous test the ventilation condition governed the development and severity of the fire. Rapid ignition resulted in the windows breaking during the early part of the test. This resulted in much lower peak temperatures although it gave a fire of much

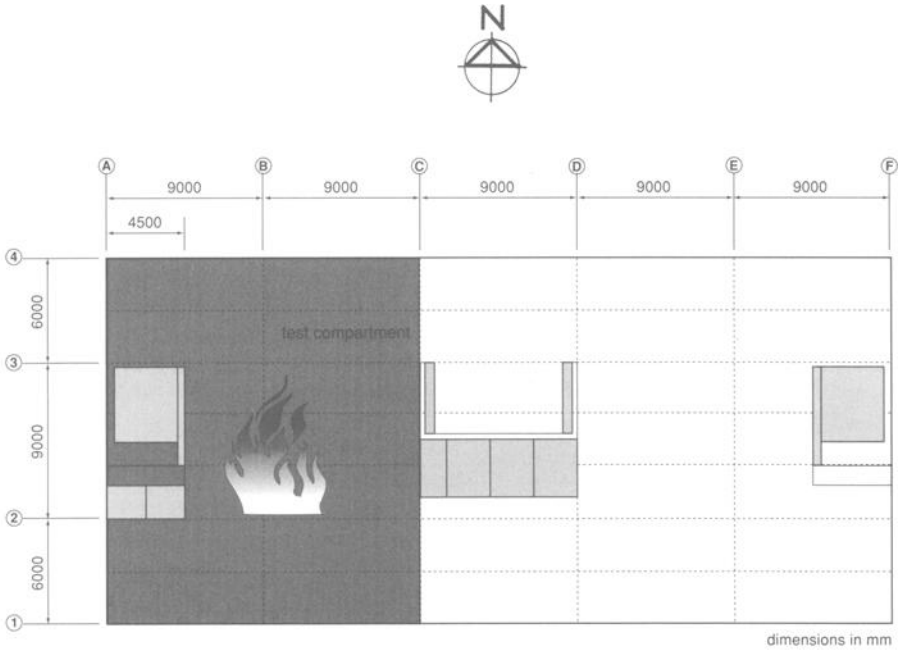


Fig. 6 Location of Large Compartment Test

**Maximum Atmosphere Temperature**

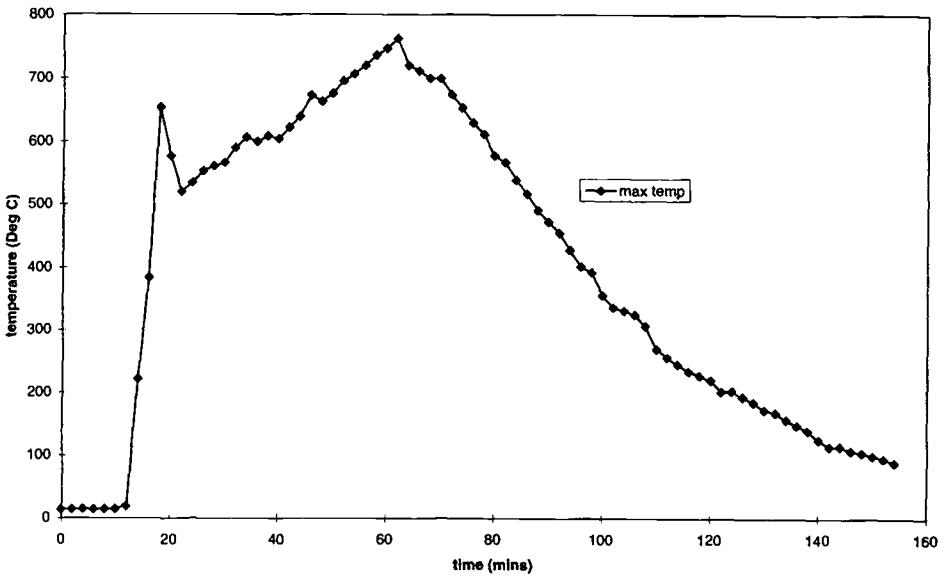


Fig. 7 Maximum Atmosphere Temperature Large Compartment Test

longer duration. The maximum temperature was 763 °C occurred towards the centre of the compartment approximately 62 minutes from ignition. Figure 7 shows the time/temperature curve for the location of maximum temperature. Figure 8 is a comparison of the average values of atmosphere temperature for the corner fire test and the large compartment fire test where “demo” refers to the large compartment test.

The maximum steel temperature of 691 °C occurred on the bottom flange of the deep beam running between gridlines B2 and B3 close to the connection at B3. The maximum temperature in the secondary beams was 685 °C after 68 minutes on the bottom flange of the long span secondary beam framing into gridline B2 in the middle of the section. The maximum temperature in the edge beams was 536 °C on the top flange of the beam running between gridlines A4 and B4 again in the middle of the section. The beams to the West of the compartment which had the gable wall framing into them reached a maximum value of 346 °C after 76 minutes. Figure 9 shows the time/temperature curve for the location of the maximum steel temperature.

The maximum recorded value of the displacement of the floor slab was 557mm although an exact figure can only be approximated as during the test some of the instruments stopped working. Figure 10 shows the time/displacement relationship for the location of maximum measured displacement.

### *Discussion*

Again the influence of the ventilation characteristics was the determining factor in terms of the intensity and duration of the fire. In this test measurements were made of the temperature and strains in the glazing as part of a separate research programme conducted by the University of Ulster. As far as structural behaviour is concerned the fire tests described in this report represent two extreme cases. One an intense fully developed fire of short duration the other a fire of lesser intensity and longer duration. In this test the greater displacements associated with the much larger spans involved imposed severe deformations on the fire protection. This phenomenon clearly requires further study.

As with the corner test comparison with predictive methods for determining the temperature-time response of the compartment such as the parametric equations used in Eurocode 1 show good agreement despite the fact that the dimensions of the test compartment are outside the scope of validity of the equations.

As in the previous test the limiting of any damage to within the compartment boundaries and the floor immediately above the compartment demonstrates the integrity of the structure and the benefits of continuity and member inter-action. An investigation is underway to look at the enhanced load carrying capacity of the floor slab at large deflections. This investigation will also consider alternatives to composite construction.

The fire tests have demonstrated the inherent fire resistance of modern composite steel framed buildings while highlighting the importance of protecting key elements within the structure. Such a strategy based on high quality data will allow a more rational approach to the passive fire protection strategy for buildings without constraining innovation through prescriptive legislation.

Comparison of Averaged Atmosphere Temperatures

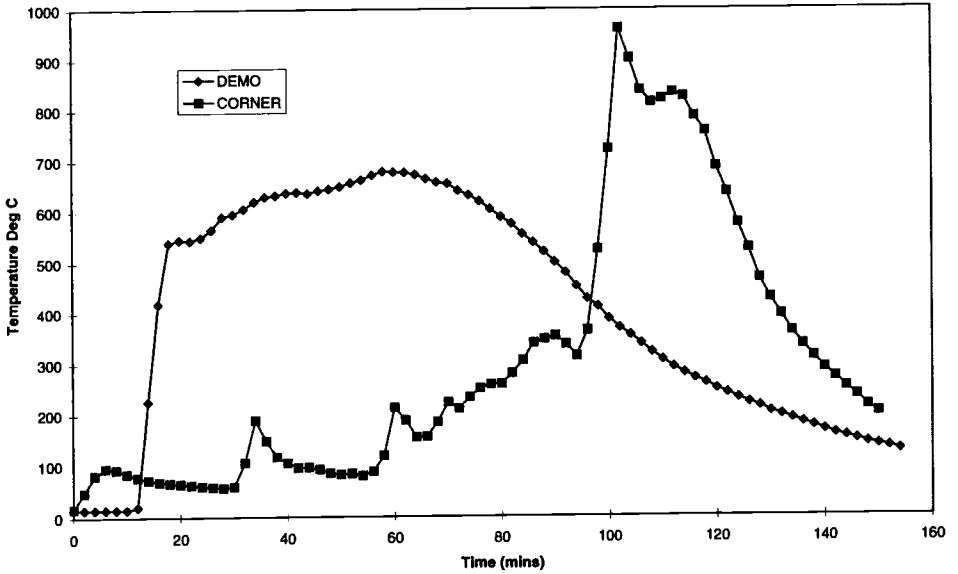


Fig. 8 Comparison of Atmosphere Temperatures

MAXIMUM STEEL TEMPERATURE LARGE COMPARTMENT TEST

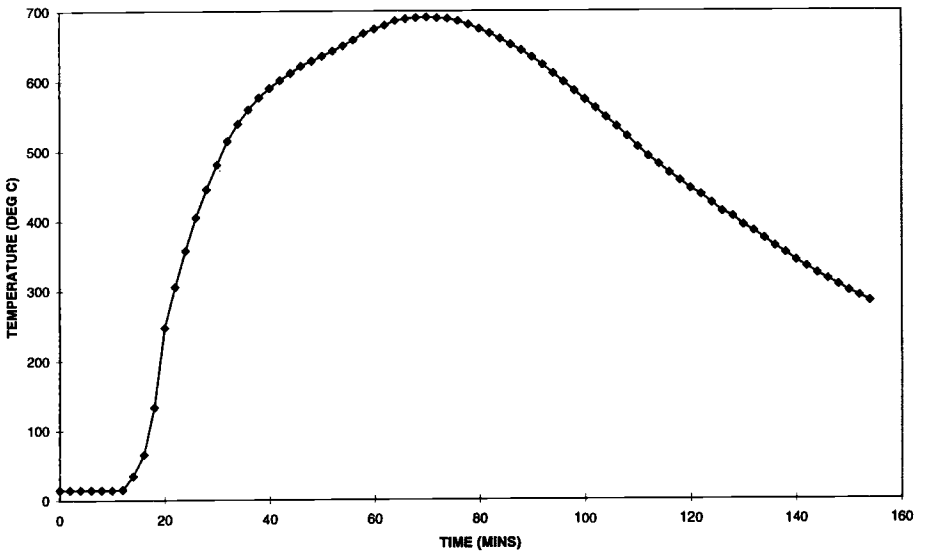


Fig. 9 Maximum Steel Temperature Large Compartment Test

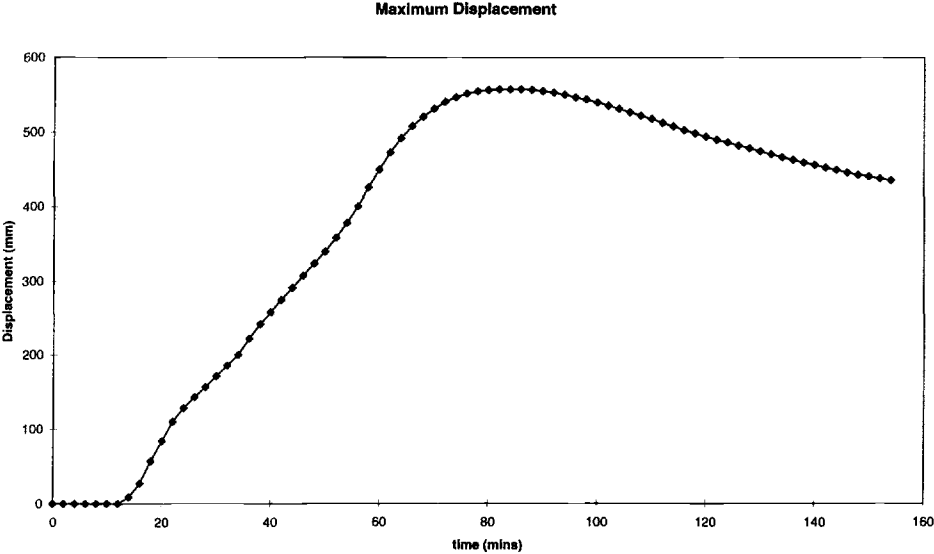


Fig. 10 Maximum Displacement Large Compartment Test

## Future Work

Following completion of the fire test programme on the building work is currently underway to analyse the results from the test with the aim of producing comprehensive design guidance for the fire engineering design of multistorey steel framed office buildings. The results from the tests will be used to assess predictive methods for determining the temperature-time response of compartments in buildings. The structural response of the building will be assessed by evaluating the extent of load and moment redistribution and by extending and verifying the theory of tensile membrane action to utilise the enhanced load carrying capacity of lightly reinforced floor slabs.

The fire tests described in this report form part of an overall programme of research to consider actual structural behaviour rather than that predicted from tests on individual elements with idealised boundary conditions and subject to a standard heating regime which bears little relation to the often more severe temperatures encountered in real fires. As such it forms part of an overall fire engineering approach to meeting the fire resistance requirements for buildings. The introduction of a new generation of standards such as the recently introduced British Standard Draft for Development [9] will allow a more rational less prescriptive approach to the overall fire safety design solutions for modern buildings.

## References

- [1] Eurocode 1: Basis of Design and Actions on Structures; ENV 1991-2-2 (1994) Actions on Structures Exposed to Fire
- [2] Latham, D. J., Kirby, B. R. and Thomson, G., "The Temperature Obtained by Unprotected Steelwork in Experimental Natural Fires", Fire Safety Journal 12, 139-152, 1987
- [3] Armer, G. S. T. and Moore, D. B., "Full Scale Testing on Complete Multistorey Structures", The Structural Engineer Volume 72 No2 pp. 30-31, 1994
- [4] Kirby, B. R., "British Steel European Fire Test Programme - Design, Construction, Results" Proceedings of the second Cardington Conference, 1996
- [5] Lennon, T., "Cardington Fire Tests: Instrumentation Locations for Corner Fire Test", BRE Internal Note N 152/95, BRE 1995
- [6] Wang, Y. C., "Tensile Membrane Action in Slabs and its Application to the Cardington Fire Tests", Proceedings of the Second Cardington Conference, 1996
- [7] Lennon, T., "Cardington Fire Tests: Analysis of Atmosphere Temperatures", BRE Internal Note N 38/97, BRE, 1997

[8] Lennon, T., "Cardington Fire Tests: Instrumentation Locations for Large Compartment Fire Test", BRE Internal Note N 100/95, BRE 1996

[9] British Standards Institution, British Standard Guide to Fire Safety Engineering, DD240, London: BSI 1997

# **Industrial and Wild Land Fires**

Víctor E. Garzón<sup>1</sup>, James M. McDonough<sup>2</sup> and Kozo Saito<sup>3</sup>

## TIME-DEPENDENT MODEL OF FOREST FIRE SPREAD IN TURBULENT GUSTING WINDS

---

**REFERENCE:** Garzón, V. E., McDonough, J. M., and Saito, K., “**Time-Dependent Model of Forest Fire Spread in Turbulent Gusting Winds,**” *Very Large-Scale Fires, ASTM STP 1336*, N. R. Keltner, N. J. Alvares, and S. J. Grayson, Eds., American Society for Testing and Materials, 1998.

**ABSTRACT:** In this paper we describe a model for simulating the spread of large-scale forest fires based on three novel concepts related, respectively to the three main features of the forest-fire problem that make it essentially intractable to simulate from first principles—namely, *i*) inhomogeneity and irregularity of forest fuel materials, *ii*) chemistry and radiation, and *iii*) turbulence. In particular, the complex structural features of the forest are treated as an inhomogeneous, very permeable porous medium; effects of chemistry and radiation are included as a source term in the thermal energy equation, and turbulence is modeled via the standard  $k-\epsilon$  model. Firebrand trajectories are computed at the end of any given flowfield calculation to estimate maximum spotting distances.

**KEYWORDS:** Forest fires, porous media, turbulence, firebrands.

---

Large-scale forest fires result in billions of dollars in financial losses annually in the United States alone. They can locally disrupt complete ecosystems and in cases of extremely large fires can produce significant meteorological effects. Computer models capable of detailed simulation of forest-fire spread under various topographical, meteorological and vegetation conditions including firebrand transport could be invaluable in a priori development of fire-fighting strategies.

In the remainder of this introductory section we will discuss the important physical aspects of forest fires. We will then present a survey of previous studies and subsequently introduce the essential features of a new computational model we are proposing in this work.

---

<sup>1</sup>Graduate research assistant,

<sup>2</sup>Associate Professor,

<sup>3</sup>Professor, Department of Mechanical Engineering, University of Kentucky, Lexington, KY 40506-0108, USA

## Forest-Fire Physics

From the standpoint of physics, a large-scale forest fire is an extremely complicated natural phenomenon [1]. It is actually a collection of many different phenomena, each of which is itself quite complex [2, 3]. The fire is an instance of combustion of a complicated nonhomogeneous environment of poorly understood fuels (mainly trees and underbrush) whose composition is not known in detail. Thus, the chance of developing accurate models of chemical kinetics from which to predict burning rates, flame temperatures and heat release is very small.

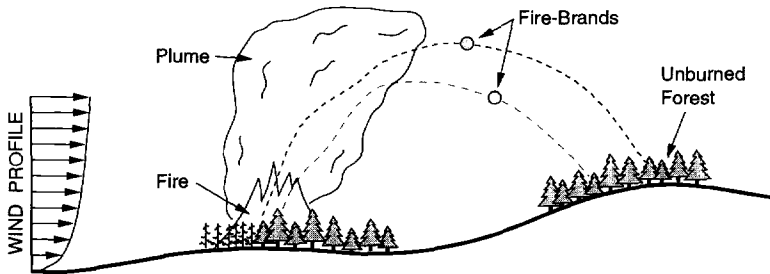


FIG. 1: *Forest Fire Schematic.*

As Fig. 1 suggests, the forest fire will generally be burning over irregular terrain of mixed vegetation (fuel), and driven by generally unsteady meteorological effects which may, themselves, be influenced by the fire. All modes of heat transfer are of significance, and the convective heat transfer will usually be a combination of forced and free.

In addition, the spread rate is significantly altered by so-called firebrand (lofted burning debris) "spotting" far downwind of the actual fireline. Spotting distances are among the most important quantities to predict in forest fire analysis, and several crude models have been in use for years [4]. But it has been extremely difficult to make accurate predictions because of the complicated turbulent flow fields created by interactions of cross winds and large-scale vortices in the thermal plumes that loft the firebrands, and there is the additional issue of whether the firebrand will still be burning when it lands downstream.

The foregoing discussion suggests that a considerable amount of modeling will be necessary to attack the forest-fire problem. Considerable work along these lines has been carried out previously, and results have been in use in the field. In the next subsection we will summarize some of this work.

### Survey of Previous Forest-Fire Modeling Efforts

Fons presented the first model of forest fire spread in 1946, based on convective and radiative heat transfer to unburned parts of the fuel bed [5]. Vogel and Williams

studied the spread of fire along lines of vertically oriented matchsticks [6]. The flame spread in more complex porous fuel beds was studied by Pagni and Peterson [7]. In 1972 Rothermel presented a semi-empirical fire spread model which has been widely used in the United States and other countries to predict behavior of wildland fires [8, 9]. Many computer programs have been written using Rothermel's model and used in forest fire management. An example of such computer codes was produced by Andrews [10]. Albini proposed a one-dimensional model for wind-blown turbulent flame from a line fire [11] and also developed a spread model based on radiative heat transfer [12]; he has also developed one-dimensional models to estimate the spotting distance from wind-driven surface fires [4, 11, 13]. Venkatesh and Saito modified Albini's spotting distance model to predict maximum spotting distance from running crown fires by applying correlations from experiments and calculations [14, 15].

### Overview of Proposed Porous-Medium Model

With the continuing increase in computer power and rapid communication over the Internet it is becoming possible to consider the next step beyond the phenomenological models discussed in the preceding section and now in wide use in the USDA Forest Service. Parallel supercomputers are beginning to approach Tflops ( $10^{12}$  floating-point operations per second) performance, and even personal computers suitable for field use will have Gflops processing speeds. It is thus time to begin using more sophisticated and realistic models of forest fire spread —models based on the full equations of motion and utilizing more details of the heat transfer and chemical kinetics than has heretofore been possible. At the same time, however, we must keep in mind the extreme complexity of the overall problem and recognize that rather crude models will still be necessary in specific parts of the problem in order to achieve useful processing speeds.

In the present study we will model the forest as a porous medium with very high porosity, permitting us to solve the Navier-Stokes (N.-S.) equations with Darcy and Forchheimer terms to account for trees and brush in an averaged way.

The remainder of this paper is organized as follows. In the next section we will provide detailed discussions of the modeling aspects noted above. Following this discussion will be a section indicating computational results obtained with this procedure, and in a final section we will provide a short summary.

### The Porous-Medium Forest Model

The basic ideas underlying use of a porous-medium model for air flow in a forest fire will be discussed; the governing equations will be presented, and details of various submodels will be considered.

#### The Forest Viewed as a Porous Medium

One of the specific features of the forest fire problem making rigorous analysis difficult is the presence of individual trees, shrubs, bushes, etc. and possibly human

dwellings. A detailed simulation would require that the flow field around each of these be computed with sufficient accuracy to generate the vortical motions leading to turbulence generation and/or enhancement with its attendant effects on mixing (thermal and species) and thus fire development and spread. From a computational fluid dynamics (CFD) standpoint this is an intractable problem. Even over a region only a few acres in extent there will be thousands of individual unequally sized and spaced trees of different kinds, and the corresponding grid generation problem would simply be impossible—even if the coordinates associated with all these objects were known, which could not possibly be the case.

Furthermore, at ground level there will in general be shrubs, bushes, leaves and other matter contributing to a completely inhomogeneous mixture of material, distributed in a nonuniform and possibly even time-dependent manner. At somewhat intermediate heights, say below 3 to 5 meters, the main flow obstructions will be tree trunks (and possibly human dwellings), also nonuniformly distributed in size, shape and relative locations, and also material composition and condition. Above approximately 5 meters is the leafy part of the trees; again, this is a very nonhomogenous, nonuniform region. It is easily seen that detailed modeling of even a single tree for purposes of predicting effects on fluid motion in its neighborhood on length scales ranging from tens of feet down to a few inches is essentially impossible. So modeling thousands of such trees, even if real-time simulations are not required, is completely inconceivable.

The situation, however, is not as bleak as it might at first seem. Upon a little reflection, one immediately recognizes that the foregoing description of a local region of the forest closely resembles our intuitive notions of porous media, albeit ones of very high porosity and inhomogeneity, and this provides the underpinnings of our basic flow field model. In particular, trees, for example, represent obstructions to the fluid flow, and since we have argued the difficulty of treating each of these individually we must attempt to construct a global model that introduces the effects of the trees on the flow field without actually predicting flow around individual trees. Based on the physics governing forest fires, we observe that trees, or any other obstructions, will tend to decelerate the flow, create vortices and irregular pressure distributions, thus leading to turbulence and drag. Thus, we expect to introduce terms into the equations of fluid motion to account for these effects, and this is precisely what is done in treating flows in porous media.

In this context, we expect from the preceding description of the forest that there are at least three different levels of porosity. Very near the ground, porosity will be quite high, but generally less so than in the intermediate heights where there are mainly only tree trunks, and thus very high porosity. Finally, at the upper leafy (forest crown levels) the porosity can be expected to be lowest of the three regions, but still very high.

We now want to quantify these ideas so that they might be incorporated in a computational model. Our discussion here will follow Nield and Bejan [16]. First, we note that the porosity  $\varphi$  is defined to be the fraction of the overall medium that is open to flow. We shall assume that there are no disconnected (“dead-end”) flow paths. Moreover, we comment that hair (on mammals) which might be viewed as

having porosity no greater than that of a forest has porosity in the range 0.95 – 0.99 from Table 1.1 of [16]. It is thus reasonable to expect that  $\varphi \gtrsim 0.98$  will hold for our cases.

We next remark that since the fluid flow is viewed to take place throughout the porous medium even though some portions of the medium are, in fact, blocked, it is necessary to define two velocity fields. One is the actual velocity averaged over only those volumes that are open to flow, and the other is a velocity averaged over all volumes. If we denote these by  $\mathbf{U}_f$  and  $\mathbf{U}$ , respectively, then they can be related through the porosity via the Dupuit-Forchheimer relationship,

$$\mathbf{U} = \varphi \mathbf{U}_f . \tag{1}$$

From the standpoint of modeling, we will want to express our equations in terms of  $\mathbf{U}$ , the “effective” velocity. This velocity is often termed “seepage” velocity, but we will not employ this terminology in the present context.

For low-speed flows, within a porous medium, the main effect on the flow is retardation which can be modeled as a linear damping proportional to the fluid viscosity  $\mu$  and inversely proportional to the porosity. This concept is based on an experimental observation known as Darcy’s law which typically is expressed in terms of a pressure gradient, and permeability rather than porosity. In particular, the term  $-\frac{\mu}{K}\mathbf{U}$  is added to the right side of the momentum equations. Here  $K$  is permeability.

There are numerous formulas relating permeability  $K$  with porosity  $\varphi$ , essentially all of which have been obtained from empirical data. For beds of particles or fibers one has the formula

$$K = \frac{D_{p2}^2 \varphi^3}{180 (1 - \varphi)^2} \tag{2}$$

with

$$D_{p2} \equiv \frac{\int_0^\infty D_p^3 f(D_p) dD_p}{\int_0^\infty D_p^2 f(D_p) dD_p} , \tag{3}$$

as given in [16]. Here  $D_p$  is an effective average particle or fiber diameter, and  $f(D_p)$  is a diameter density distribution function. The factor 180 in the denominator of (2) is empirical, and Eqs. (2, 3) are found to work best for nearly spherical particles in a narrow range of diameters. Clearly, this does not correspond well to our present situation, but Nield and Bejan [16] report that it is a widely used approximation.

It is clear from (2) that  $K \rightarrow \infty$  as  $\varphi \rightarrow 1$ , and this implies that linear damping will probably be relatively unimportant in the forest model. It should also be observed that  $f(D_p)$  will be different in each of the three porous regions discussed above. In particular, values on the order of  $10^{-1}$  to  $10^{-2}$  m would be reasonable near the ground where the function  $f(D_p)$  should be heavily weighted in the direction of the branches of shrubs, twigs, etc. In the midlevels where tree trunks are dominant, we would expect  $D_p \sim \mathcal{O}(1)$ , and at the highest levels where branches and leaves comprise the main obstacles to flow we would expect  $D_p \sim \mathcal{O}(10^{-1})$ . From these estimates it

follows that  $K$  could be sufficiently small to have a significant effect near the ground, and in some cases also at the higher levels, at least for very dense forests.

We next consider effects of higher-speed flows. In this case the linear Darcy term must be augmented by a quadratic drag formula often attributed to Forchheimer, but which in the form presented here is due to Ward [17]. It is given by  $-c_F K^{-\frac{1}{2}} \rho |\mathbf{U}| \mathbf{U}$ , where  $|\cdot|$  denotes the Euclidean length of the vector  $\mathbf{U}$ , i.e., the velocity magnitude. In this expression  $c_F$  is a friction factor commonly known as Ergun's coefficient. Generally we expect  $c_F \sim \mathcal{O}(1)$ , and a value of  $\sim 0.55$  is widely used although it is known that  $c_F$  is not a universal constant, as first thought, but it is instead a function of the porous medium.

At this point we have developed all of the model aspects needed to modify the fluid momentum equations except to note, as can be implied from Fig. 1, that over parts of the flow field buoyancy driven flow will be a dominant aspect of the physics. We will introduce this via a body force in the usual way. This permits us to express the equations of fluid motion as

$$\nabla \cdot \mathbf{U} = 0, \quad (4a)$$

$$\rho_0 \left( \frac{1}{\varphi} \frac{\partial \mathbf{U}}{\partial t} + \frac{1}{\varphi^2} \mathbf{U} \cdot \nabla \mathbf{U} \right) = -\nabla p + \frac{\mu}{\varphi} \nabla^2 \mathbf{U} - \frac{\mu}{K} \mathbf{U} - c_F K^{-\frac{1}{2}} \rho |\mathbf{U}| \mathbf{U} + \delta \rho g \mathbf{e}_3, \quad (4b)$$

$$\rho_0 c_p \left( \frac{\partial T}{\partial t} + \frac{1}{\varphi} \mathbf{U} \cdot \nabla T \right) = k \Delta T + S. \quad (4c)$$

In (4)  $\rho_0$  is a reference density and  $\delta \rho \equiv \rho - \rho_0$ ;  $g$  is gravitational acceleration, and  $\mathbf{e}_3$  is the "vertical" unit vector;  $\rho$  is local fluid density,  $c_p$  is specific heat at constant pressure,  $T$  is temperature, and  $S$  is a general source term accounting for heat release due to combustion, and to thermal radiation effects. Finally,  $\nabla$  and  $\Delta$  are, respectively, the gradient and Laplace operators in an appropriate coordinate system.

## Trajectory Calculations

The equation of motion of a rigid particle immersed in a moving fluid is commonly known as the Basset-Boussinesq-Oseen (BBO) equation [18]. In the present formulation we neglected the effects due to the Basset history term (additional drag caused by the unsteady motion of a particle in a viscous flow) and apparent mass (surface pressure increase during particle acceleration) since the ratio of fluid to particle density is much less than unity [19]. In addition, Saffman lift (sideways force due to shear at low particle Reynolds number) is assumed to be negligible compared to Stoke's drag [20]. Furthermore, we are assuming a one-way coupling between the fluid and particle phases—i.e., the fluid acts upon the firebrands but not conversely—in order to simplify the equations of motion. In this manner the equations for firebrand velocity and position reduce to the following initial value problem:

$$\frac{d\mathbf{X}_p}{dt} = \mathbf{u}_p, \quad (5a)$$

$$m_p \frac{d\mathbf{u}_p}{dt} = \mathbf{F} - m_p g \mathbf{e}_3, \quad (5b)$$

where  $\mathbf{X}_p$ ,  $\mathbf{u}_p$  and  $m_p$  denote firebrand position, velocity and mass respectively. Initially the particles are taken to be at rest and located within the burning region of the domain.

In (5b) the force  $\mathbf{F}$  is the drag force exerted on the particle by the moving fluid, defined in this case by

$$\mathbf{F} = C_D \frac{1}{2} A_p \rho |\mathbf{u}_f - \mathbf{u}_p| (\mathbf{u}_f - \mathbf{u}_p), \quad (6)$$

where  $\mathbf{u}_f$  is the flow velocity and  $A_p$  is the cross sectional area of the particle. The drag coefficient  $C_D$  can be estimated using empirical correlations based on the particle Reynolds number. Examples of such correlations are given in [19].

We note that with this approach, we can perform the time integration of firebrand trajectories in a transient flow field, and that time dependent mass or geometry can also be considered. However we limit the present study to computation of firebrand trajectories in fully evolved flow fields—i.e., after the buoyancy forces in the plume are able to sustain firebrand transport. We also concentrate for now on constant particle properties (density and geometry). In particular, the results presented in the next section are for spherical firebrands of constant diameter  $D_p = 0.05$  m and density  $\rho_p = 50$  kg/m<sup>3</sup>. The particle density was selected from tabulated data for Ponderosa pine wood [4]. Several different particle diameters were computed, but only those corresponding to  $D_p = 0.05$  are presented and discussed herein. Yet these results are representative of the qualitative behavior observed for other density values.

## Results And Discussion

A typical computational grid used in this study is shown in Fig. 2. The physical dimensions of the computational domain are 1000 by 800 meters. The burning region corresponds to a porous medium blockage with heat-generation. The unburned part of the forested region is modeled simply as a porous medium. A velocity profile is prescribed as the boundary condition on the left boundary of the computational domain. On the right and top boundaries the pressure is set to the atmospheric condition and the velocity components are computed to satisfy mass conservation. At the bottom boundary a no-slip condition ( $u = v = 0$ ) is enforced and a temperature value of 290 K is prescribed. The initial condition for temperature on the entire domain is 290 K. The flow field calculations were carried out with the commercial package CFD2000.<sup>4</sup>

A constant heat flux of 50 Kw/m<sup>2</sup> [14] is imposed on the burning region. The buoyancy force is modeled via a Froude number scaling and the ideal gas law. Effects due to turbulence are introduced in the calculation through the  $k$ - $\epsilon$  model provided in CFD2000.

The flow velocities are time advanced until a “reasonable” flow field is achieved—i.e., the plume has evolved sufficiently to sustain firebrand transport. Then this

<sup>4</sup>Adaptive Research, Santa Monica CA, <http://www.adaptive-research.com/>

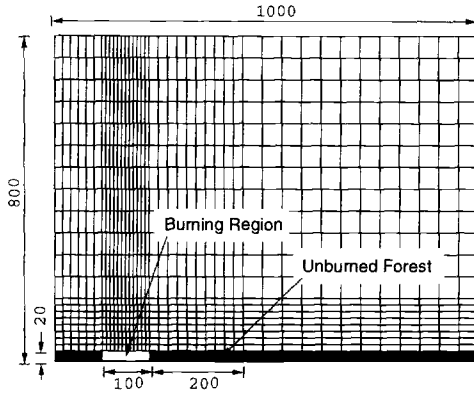


FIG. 2: Computational grid (all dimensions in meters).

solution is fed to a program for integrating the firebrand trajectories. Results from two different flow patterns are shown in Figs. 3 and 4. Figure 3 shows plume evolution—depicted by shaded temperature contours—, velocity vectors, and computed firebrand trajectories for a 10 m/s cross wind. The horizontal velocity component on the left

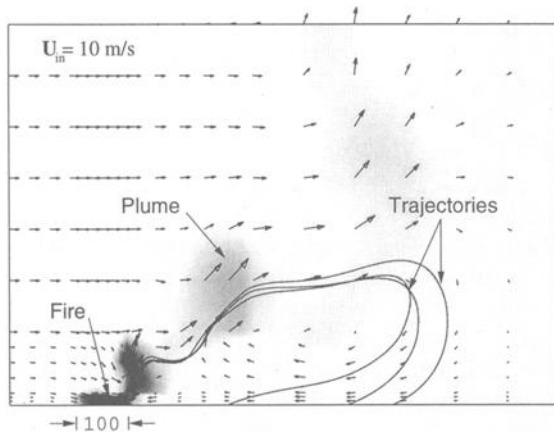


FIG. 3: Computed flow field, temperature contours (buoyant plume) and firebrand trajectories for  $U_{wind} = 10 \text{ m/s}$ , with peak flow velocity  $U_{max} \approx 26 \text{ m/s}$  in the plume.

boundary is prescribed so as to roughly approximate a planetary boundary layer profile. The difference in the trajectories is due to changes in the initial position and diameter of the particles.

As should be expected, the flow speed through and around the forest region de-

creases as the porous medium terms in the momentum equation take effect. Figure 4 shows similar results for wind velocity  $U_{wind} = 13 \text{ m/s}$ . Although both flow field solutions were integrated to the same physical time using time accurate procedures, they look very different. The variations in the velocity flowfields in turn translate into significant changes in the firebrands paths. In particular, the faster cross wind causes the firebrands to travel further, even though similar particle properties were used in both calculations. These results are qualitatively in agreement with observations indicating that as the cross wind increases and the forest fire changes from plume-dominated to wind-driven, the maximum spotting distances increase [9] accordingly. It should be noted however, that this is not necessarily the case in general since as the cross wind velocity increases past a certain point, the relative magnitude of the buoyancy forces decreases and the initial lift required to loft the firebrands becomes less dominant—i.e., the particles are not lofted sufficiently high into the convective plume to be carried away by the cross wind.

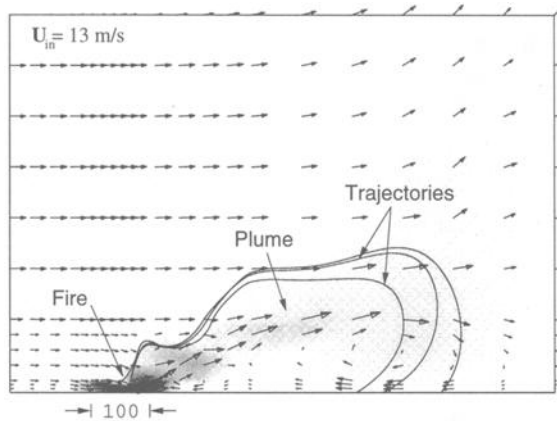


FIG. 4: Computed flow field, temperature contours (buoyant plume) and firebrand trajectories for  $U_{wind} = 13 \text{ m/s}$ , with peak flow velocity  $U_{max} \approx 22 \text{ m/s}$  in the plume.

Also, we note that firebrand trajectories are affected (sometimes significantly) by the recirculation zone behind the porous blockage, formed as the plume evolves and interacts with the incoming wind. This effect is somewhat more poignant in these results than in observed fires since we are restricting our computations to only two spatial dimensions.

## Summary

In this paper we have outlined the construction of a forest fire model whereby the forest is treated as a highly inhomogeneous and very permeable porous medium. The heat generated in the burning part of the forest was simulated through the addition

of a general source term to the equation of thermal energy. The buoyancy forces caused by temperature gradients in the flow were modeled using a modified Froude number scaling. The resulting velocity field was then used to estimate the position and velocity of the firebrands. Sample results from the application of the present method to the calculation of firebrand trajectories were discussed.

We note that in order to obtain more accurate estimates of maximum spotting distances, we need to incorporate the firebrand trajectory calculations into the flow field simulation, so as to properly account for the inherent time dependency of the problem. In addition, firebrand aerodynamics and their effects need to be addressed further—i.e., accurate  $C_D-Re$  correlations for complex firebrand geometries are needed in order to produce more realistic simulations. Furthermore the flowfield structures under consideration are obviously three-dimensional and should be modeled as such. However moving to three dimensions would imply a significant increase in the computational expenditure of typical simulations, making them less appealing for practical (real-time) implementation. It is hoped that as computational resources improve (e.g., increased availability of massively parallel hardware, faster networks, etc.) real-time three-dimensional simulations over complex terrain will be possible, and will in time become a practical tool in forest-fire management. These and other concerns are an integral part of the authors ongoing investigation.

## Acknowledgments

This study was supported by the Center for Computational Sciences, University of Kentucky and the Kentucky NASA EPSCoR Program through grant WKU 522761-95-0.

## References

- [1] Pyne, S., Andrews, P. L., and Laven, R. D. *Introduction to Wildland Fire*. Second edn. John Wiley & Sons, Inc., New York, NY, 1996.
- [2] Williams, F. A. "Urban and Wildland Fire Phenomenology." *Progress in Energy and Combustion Sciences*, vol. 8, 1982:pp. 317–357.
- [3] Soma, S. and Saito, K. "Reconstruction of fire whirls using scale models." *Combustion and Flame*, vol. 86, 1991:pp. 269–284.
- [4] Albini, F. A. "Spot Fire Distance From Burning Trees: A Predictive Model." General Technical Report INT-56, USDA Forest Service, Intermountain Forest and Range Experiment Station, Ogden, UT, 1979.
- [5] Fons, W. L. "Analysis of Fire Spread in Light Forest Fuels." *Journal for Agricultural Research*, vol. 72(3), 1946:pp. 93–121.
- [6] Vogel, M. and Williams, F. A. "Flame Propagation Along Matchstick Arrays." *Combustion Science and Technology*, vol. 1, 1970:pp. 429–436.

- [7] Pagni, P. I. and Peterson, T. G. "Flame Spread Through Porous Fuels." Tech. rep., In proceedings of 14<sup>th</sup> Intern. Symp. on Combustion, The Combustion Institute, Pittsburgh, PA, 1972.
- [8] Rothermel, R. C. "A Mathematical Model for Predicting Fire Spread in Wildland Fuels." Research Paper INT-115, USDA Forest Service, Intermountain Forest and Range Experiment Station, Ogden, UT, 1972.
- [9] Rothermel, R. C. "Predicting Behavior and Size of Crown Fires in the Northern Rocky Mountains." Research Paper INT-438, USDA Forest Service, Intermountain Forest and Range Experiment Station, Ogden, UT, 1991.
- [10] Andrews, P. L. "BEHAVE: Fire behavior prediction and fuel modeling system—BURN Subsystem. Part 1." Gen. Tech. Rep. INT-194, USDA Forest Service, Intermountain Forest and Range Experiment Station, Ogden, UT, 1986.
- [11] Albini, F. A. "A Model for the Wind-Blown Flame from a Line Fire." *Combustion and Flame*, vol. 43, 1981:pp. 155–174.
- [12] Albini, F. A. "A Model for Fire Spread in Wildland Fuels by Radiation." *Combustion Science and Technology*, vol. 42, 1985:pp. 229–258.
- [13] Albini, F. A. "Potential Spotting Distance from Wind-Driven Surface Fires." Research Paper INT-309, USDA Forest Service, Intermountain Forest and Range Experiment Station, Ogden, UT, 1983.
- [14] Hirano, T. and Saito, K. "Fire Spread Phenomena: The Role of Observation in Experiment." *Progress in Energy and Combustion Science*, vol. 20, 1984:pp. 461–485.
- [15] Venkatesh, S. and Saito, K. "Maximum Spotting Distances in Wind-Driven Crown Fires (SDWCF)." Final Report No. INT-91586-RJVA, Department of Mechanical Engineering, University of Kentucky, Lexington, KY, 1992.
- [16] Nield, D. A. and Bejan, A. *Convection in Porous Media*. Springer-Verlag, New York, NY, 1992.
- [17] Ward, J. C. "Turbulent Flow in Porous Media." *Journal of the Hydraulics Division, American Society of Civil Engineers*, vol. HY5(90), 1990.
- [18] Ounis, H. and Ahmadi, G. "Motions of Small Rigid Spheres in Simulated Random Velocity Field." *J. Eng. Mech.*, vol. 115(10), October 1989:pp. 2107–2121.
- [19] Kladas, D. D. and Georgiou, D. P. "A Relative Examination of  $C_D$ - $Re$  Relationships Used in Particle Trajectory Calculations." *Journal of Fluids Engineering*, vol. 15, 1993:pp. 162–165.
- [20] Aggarwal, S. K., Yapo, J. B., Grinstein, F. F., and Kailasanath, K. "Numerical Simulation of Particle Transport in Planar Shear Layers." *Computers and Fluids*, vol. 25, 1996:pp. 39–59.

Louis A. Gritzo<sup>1</sup>, Walter Gill<sup>2</sup>, Vernon F. Nicolette<sup>1</sup>

## ESTIMATES OF THE EXTENT AND CHARACTER OF THE OXYGEN-STARVED INTERIOR IN LARGE POOL FIRES<sup>3</sup>

---

**REFERENCE:** Gritzo, L. A., Gill, W., and Nicolette, V. F., "Estimates of the Extent and Character of the Oxygen-Starved Interior in Large Pool Fires," *Very Large-Scale Fires, ASTM STP 1336*, N. R. Keltner, N. J. Alvares, and S. J. Grayson, Eds., American Society for Testing and Materials, 1998.

**ABSTRACT:** Based on data from large pool fire experiments and computational fire field model simulations, the size, shape, and character of the oxygen-starved interior in large pool fires is estimated. In the interior of the fire and near the pool surface, low average and low mean deviation temperatures were noted in experimental data for low wind conditions. These trends tend to indicate the presence of a non-combusting region. Using average and mean deviation temperature distributions (supplemented by heat flux measurements) from several data sets, the spatial extent of the vapor dome is estimated for a range of wind conditions. These estimates are compared with fire field model results of temperature and fuel/air concentration distributions. Predicted and measured temperature trends, supported by heat flux data, illustrate the importance of object placement within the fire during system fire survivability testing. The presence of this region also supplements conventional pool fire representations which are based on a continuous flame zone which extends to the pool surface.

**KEYWORDS:** Large Pool Fires, Thermocouple Temperature, Heat Flux, Fire Models

---

The thermal hazard posed by large fires is primarily determined by the heat flux from the fire to an engulfed or adjacent object. Test methods and procedures with the intent of assessing the fire survivability of engineered systems to very large fires must therefore be founded on a knowledge of the heat fluxes over the range of credible scenarios. As a consequence of the high (1300 K) temperatures and relatively low (~ 10 m/s) velocities, the primary mode of heat transfer to significant sized (dimensions ~ 1m or greater) objects either engulfed by a large fire, or in the

---

1. Senior Member of the Technical Staff, Unsteady and Reactive Fluid Mechanics, Sandia National Laboratories, Albuquerque, NM 87185-0836

2. Senior Member of the Technical Staff, Mechanical and Thermal Environments, Sandia National Laboratories, Albuquerque, NM 87185-0865

3. This work was performed at Sandia National Laboratories, Albuquerque, NM under U.S. Department of Energy Contract DE-AC04-94AL85000

vicinity of a large fire, is radiation from high temperature soot and gases. Assessment or prediction of these radiative heat loads requires a knowledge of the temperature and radiative property distribution over a hemispherical domain adjacent to the surface of interest. The size of this domain is approximately equal to a multiple of 2-3 times the radiative path length (the inverse of the extinction coefficient) associated with the soot and gas concentration field. Temperature distribution trends are therefore needed to assess credible fire scenarios for the development of test methods.

Numerous correlations exist in the literature and in standard practice handbooks to assess the temperature, flame height, flame tilt, and flame surface emissive power of fires [1]. These relationships represent the data acquired to date reasonably well and can serve as first order estimates for fire behavior. For very large scale fires, the spatial distribution of temperature within the flame zone has only been experimentally investigated in a limited sense [2,3]. Although several works have addressed heat fluxes to fire-engulfed objects [4,5], thorough experimental characterization of these fires, and the hazards they pose to objects, has not been achieved. This challenge has not been overcome most likely due to the cost associated with acquiring a sufficient number of measurements to obtain spatial distributions of the relevant parameters in the fire. Efforts have therefore been applied to characterize the continuous flame zone for the purpose of improved understanding which can be used to develop and validate fire field models. These models, in conjunction with a reduced set of experimental data, provide the spatial distributions required to improve our ability to assess the hazard posed by these fires and to develop improved test methods.

The mixing of air into very large fires with a sufficient fuel vapor generation rate to form a single, vertical, continuous flame zone in the shape of a buoyant plume, is defined by the eddies formed on the exterior of the flame zone due to density gradients. Accordingly, very little air is transported into the interior of these fires until an elevation is reached where the eddies have sufficiently increased in size, and the flame zone has necked due to the momentum of the entrained air. An oxygen-starved, non-combusting region therefore exists near the fuel surface in the interior of these fires. This region, sometimes referred to as the vapor dome, is a unique characteristic of large fires and is generally characterized by reduced temperatures and hence lower heat fluxes. Very high heat fluxes, and hence an increase in the hazard posed by the fire, are observed when the vaporized fuel which resides in this region is mixed with air and burned due to the effects of wind and/or objects within the fire. Characterization of this oxygen-starved region is an important aspect of fire phenomenology since 1) the physical extent of the vapor dome will strongly influence the radiative feedback to the pool which, in turn, influences the burning rate, 2) it is expected that large quantities of soot are formed in the vapor dome due to fuel pyrolysis, and 3) heat fluxes to objects located in the vapor dome will be significantly reduced. The presence of this region also supplements previously observed features of fire structure which were based on a continuous flame zone which extended to the pool surface. McCaffrey [6] outlines three distinct fire regimes. The results presented here illustrate the presence of a fourth oxygen-starved regime in some large fires.

**EXPERIMENTAL RESULTS**

To characterize the hazard posed by large pool fires and for the purposes of assessing the ability of a test item to satisfy regulatory criteria, many large fire tests have been performed at Sandia's Lurance Canyon Burn Site. Recently, several series of large (18.9 m diameter) pool fires have been conducted at the Naval Air Warfare Center, Weapons Division for the purposes of characterizing large fire hazards, and to obtain data needed for fire field model development and validation. These unique experiments are sponsored by the Defense Special Weapons Agency and coordinated by Sandia National Laboratories.

Measurements performed during these experiments include heat flux to engulfed objects, heat flux to the fuel surface, local pressures, and optical soot emission temperature and soot volume fraction. The overall temperature of the lower region of the flame zone (where an object of interest is most likely located) is estimated using 0.16 cm inconel-sheathed, ungrounded, type-K thermocouples. It is acknowledged that, due to several mechanisms including radiative transport and thermal inertia, the temperature measured by a thermocouple is not, in general, equal to the local media temperature [7]. Cost and robustness limitations, however, continue to dictate the use of thermocouples for spatial characterization of large fires.

Thermocouple temperatures, time-averaged over a period of quasi-steady state fire behavior, are shown in Fig. 1 for an 18.9 m JP4 pool fire under low (< 0.5 m/s) winds. The approximate total potential heat release of this fire (assuming complete fuel combustion) is 860 MW. To obtain sufficient resolution, and to limit the potential interaction of

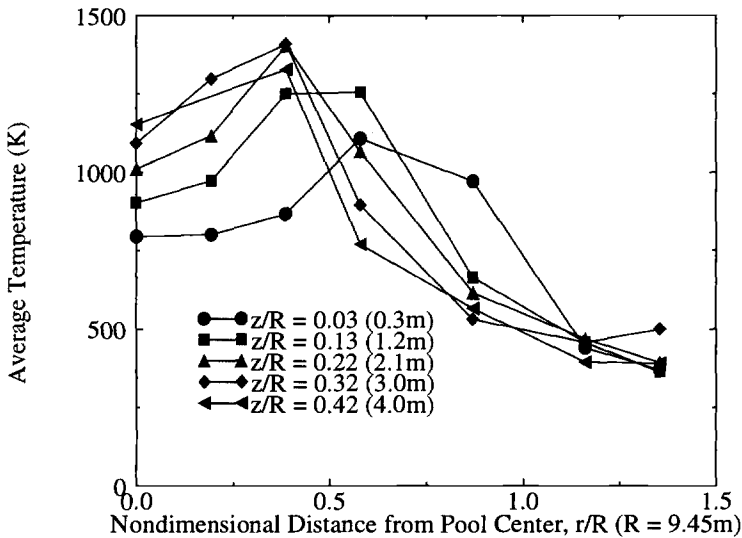


FIG. 1 -- Time-Averaged Thermocouple Temperature Profile for JP4 Pool Fire

diagnostic hardware with the fire dynamics, temperature measurements are only performed at 5 elevations at each of 7 locations along an expected prevailing wind direction. At low elevations ( $z/R = 0.03$ ), the data show a low temperature (800 K) region in the center of the fuel pool. The temperature increases to values representative of flame exposure (1250 K) with increasing distance from the centerline before decreasing to approximately ambient temperatures outside the fuel pool. The same trend is shown with increasing elevation. The centerline temperature continues to increase over the range of the data (up to  $z/R = 0.42$ ). For  $z/R < 0.13$ , the location of the maximum temperature becomes closer to the pool center with increasing elevation representative of the “necking” of the flame zone produced by the momentum of the entrained air. A maximum temperature of 1450 K is observed which becomes essentially invariant with elevation for  $z/R > 0.2$ . These temperature profiles clearly show the existence of a cold region in the center of large pool fires. The most plausible explanation for this reduction in temperature is a lack of oxygen in the interior of the fire due to limited mixing of air into the fire. The main components of the mixing process in these fires are the eddies on the exterior of the fire (which are produced by baroclinic vorticity) and the vorticity which is produced in the vertical direction due to combination of entrained air and the highly buoyant flame sheets which comprise the flame zone.

Additional insight into the structure of these fires is provided by examining the transient trends in the data. Thermocouple temperature as a function of time is presented in Fig. 2 for thermocouples close to the fuel surface at the center of the fire, and significantly above the fuel surface near the exterior of the fuel pool where visible flame cover is observed. In addition to the reduction in mean temperature, significantly smaller deviations from the mean are observed in the data acquired in the interior and near the fuel surface. Large deviations from the mean, consistent with those expected from a thermocouple exposed to radiation and convection from turbulent flame sheets, are observed in the thermocouple temperature measured in the continuous flame zone where active combustion is expected. The trends illustrated in the previous data are summarized

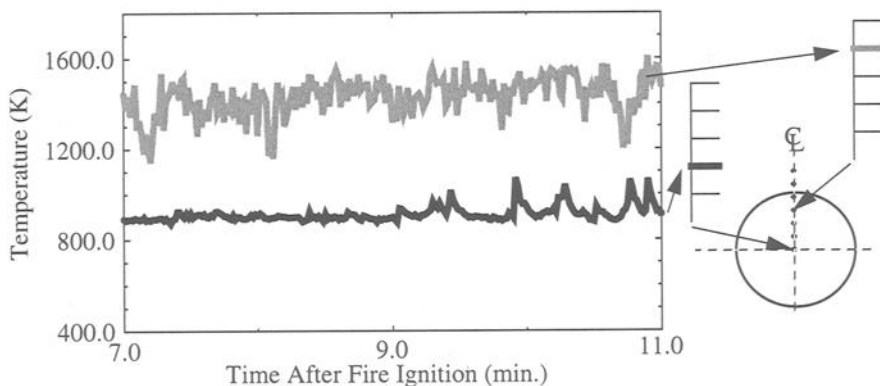


FIG. 2 -- Thermocouple Temperature as a Function of Time, Two Different Locations

in Fig. 3. Low average temperature ( $T_{avg}$ ) and small mean deviation temperature ( $T_{md}$ ), as defined by

$$T_{md} = \frac{\sum |T_i - T_{avg}|}{n}, \tag{1}$$

for a set on  $n$  data points, are observed in the oxygen-starved zone and even lower values are observed in the ambient environment. High average values and large mean deviations are observed in the temperature data acquired within the active combustion zone. Since the oxygen-starved interior is characterized by both low mean deviation and low average temperatures, an indicator variable, given by

$$I = \frac{1/(T_{md} \times T_{avg})}{[1/(T_{md} \times T_{avg})]_{cl}}, \tag{2}$$

which is the inverse of the product of  $T_{avg}$  and  $T_{md}$ , normalized by the value measured closest to the fuel surface at the pool center, has been formed to allow quantitative estimation of the minimum extent of the oxygen-starved interior. The *inverse* of the product of  $T_{avg}$  and  $T_{md}$  was selected in the numerator such that low values of these variables increase the value of  $I$ . Normalization by the value measured closest to the fuel surface at the pool center was chosen to improve the ability to compare values from different fires. The trends evident in the data form the sole physical basis for the form of this variable.

As mentioned previously, and discussed in detail in [7], thermocouples can read temperatures significantly different from the local temperature due to radiation from nearby media. Low average and small mean deviation of temperatures therefore implies

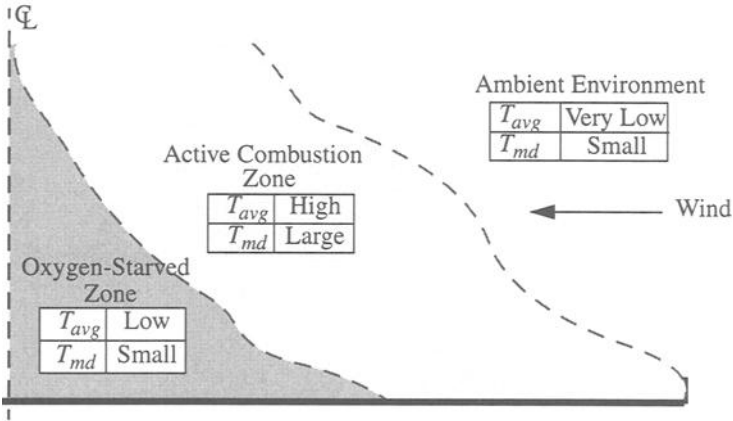


FIG. 3 -- Schematic of Thermocouple Temperature Trends Observed in Large Pool Fires

that the thermocouple is greater than two optical path lengths from the turbulent combusting region. Otherwise, radiative heat transfer from nearby combusting media would raise the temperature and increase the mean deviation. It is also feasible for low temperatures to be measured by thermocouples low in the fire as a consequence of the presence of the cold (approximately 550 K) fuel pool. Although a contributing factor, large temperatures have been measured very close to the pool in regions where active combustion is observed. The presence of the cold fuel is therefore not expected to have a dominant effect on the measured temperatures.

The result of applying the above indicator variable is shown in Fig. 4 and Fig. 5 for two separate JP4 experiments performed under low wind conditions. In these figures, values of  $I$  greater than 0.1 are considered to be a relative indication of the oxygen-starved interior since 1) values consistently less than 0.1 are observed in regions where active combustion is visually observed and, 2) values of  $I$  within the region of active combustion are approximately equal. Values of  $I$  from both figures show an oxygen-starved region which extends from the centerline to  $r/R = 0.5$  at  $z/R = 0.03$ , and from the centerline to  $r/R = 0.25$  at  $z/R = 0.13$ . Temperatures measured at an elevation of  $z/R = 0.22$  do not exhibit trends indicative of the oxygen-starved interior for locations where  $r/R > 0.1$ . The same trends are observed outside the continuous flame zone (i.e. low  $T_{avg}$  and small  $T_{md}$ ) as within the oxygen-starved interior. Values of  $I$  therefore increase sharply at all elevations for radial positions near the edge of the fuel pool.

Plots of the indicator variable for data acquired from fires subject to medium (1.2 m/s) winds, aligned at a  $50^\circ$  angle from the plane of the measurements, are shown in Fig. 6. Overall larger values of  $I$  are observed in these data. Deflection of the flame zone due to the wind, changes in the wind speed and direction during the period the data were averaged, and the position of the thermocouple at the center of the pool relative to the

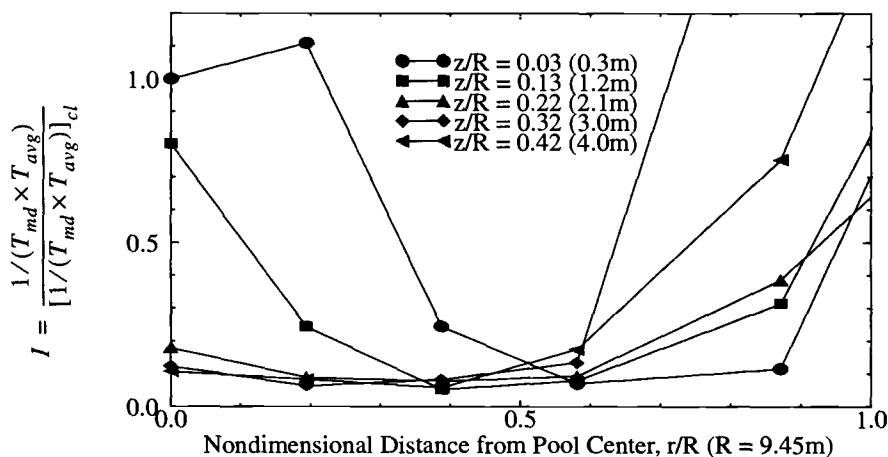


FIG. 4 -- Oxygen-Starved Interior Indicator, JP4 Test 1, Low (< 0.5 m/s) Winds

actively combusting region (as identified from the video record), combine to result in an overall increase in values of  $I$ . Furthermore, results of the indicator variable are not as consistent within the actively combusting region as the results presented in Fig 5. Relative trends in the results, can, however, still be used to estimate the extent of the oxygen starved interior. Using values of  $I$  greater than 0.5 as a metric, these results show the presence of an oxygen-starved interior which extends from the centerline to  $r/R = 0.8$  at  $z/R = 0.03$ , and from  $r/R = 0.4$  to  $r/R = 0.8$  at an elevation of  $z/R = 0.13$ . In agreement with

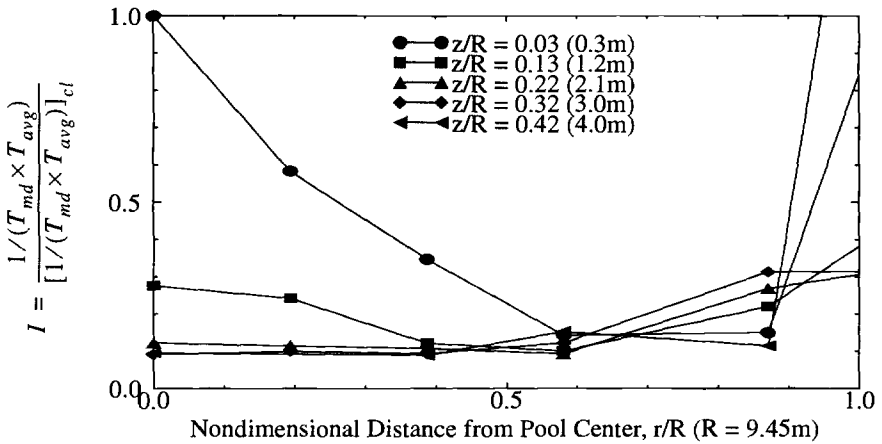


FIG. 5 -- Oxygen-Starved Interior Indicator, JP4 Test 2, Low (< 0.5 m/s) Winds

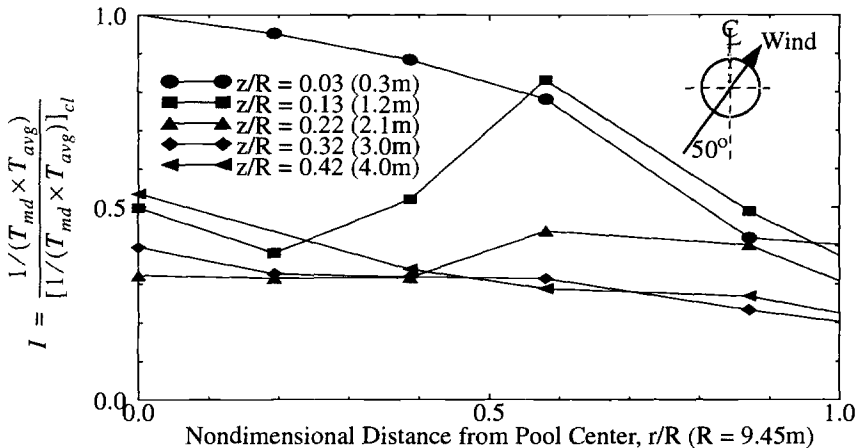


FIG. 6 -- Oxygen-Starved Interior Indicator Variable, JP4 Test 3, 1.2 m/s Winds

the results obtained during lower wind conditions, the data indicate an oxygen-starved interior does not exist for  $z/R = 0.22$ .

Data from a JP8 fire in the same size pool are presented in Fig. 7 for the case of a 1.4 m/s wind  $6^\circ$  from the measurement plane. In this case, data were acquired upwind of the pool centerline and therefore the scale of the axis is slightly different. Again, values of  $I$  are approximately the same for all locations where active burning is expected via visual observation. In particular, the similar values of  $I$  at  $r/R = 0.3$ , located with the region where active burning is expected, should be noted. From these data, the oxygen-starved region extends from the centerline to between  $r/R = 0.2$  and  $r/R = 0.3$  up to an elevation of  $z/R = 0.13$  based on  $I$  greater than 0.5. At greater distances from the pool center, the trends in the indicator variable are reversed from previous results (i.e., decreasing values of  $I$  are observed with increasing elevation) due to the wind-induced tilting of the flame zone which placed the upper thermocouples in an actively combusting region. It should also be noted that the value of  $I$  at  $z/R = 0.13$  is greater than the value at  $z/R = 0.03$  as a consequence of differences in the mean deviation that can not be explained given the available data. Additional experimental data for JP8 pool fires of similar size under calm conditions are not available. A comparison of Fig. 7 with previous data from JP4 pool fires indicates that the size of the oxygen-starved interior is much smaller in radial extent for the lower volatility (JP8) fuel.

## FIRE MODEL PREDICTIONS

Numerical fire simulations were performed using the VULCAN fire field model (under joint development at Sandia and at SINTEF/NTNU, Norway). VULCAN is derived from the KAMELEON Fire model [8] and uses an extension of the SIMPLEC method of

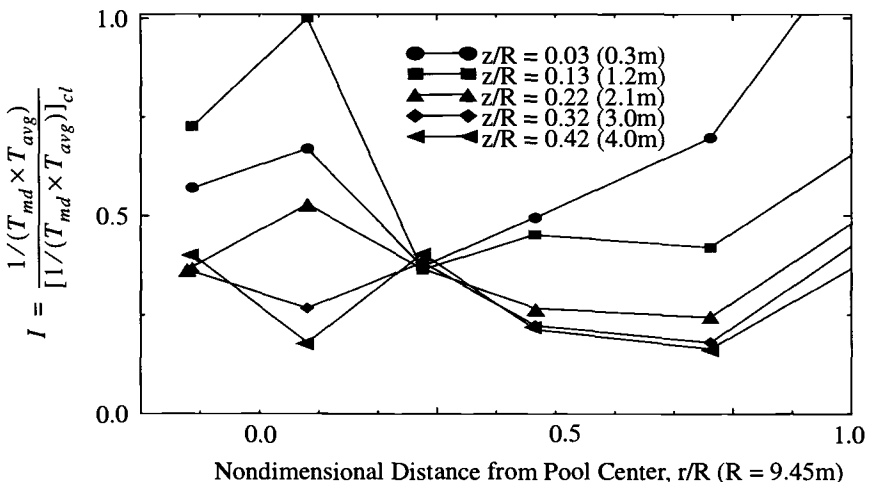


FIG. 7 -- Oxygen-Starved Interior Indicator Variable, JP8 Pool Fire, 1.4 m/s Winds

Patankar and Spalding [9] to solve the conservation equations on a structured, staggered, 3-dimensional Cartesian finite difference grid. First- and second-order accurate upwind schemes can be used for the convective terms. Turbulence can be modeled using either a standard two equation  $k-\epsilon$  model, or with a large eddy simulation (LES) formulation. Combustion is based on Magnussen's Eddy Dissipation Concept [10] with infinitely fast combustion assumptions. Local extinction is assumed to occur when the time scale for turbulent mixing is less than a user-specified chemical time scale. Soot formation is based on the fuel dependent modification by Magnussen [11] of the two step process first proposed by Tesner [12]. Thermal radiation is modeled using the Discrete Transfer Method [13]. Soot and combustion gases are treated as a gray gas with a mean absorption and emission coefficient based on the local concentrations and temperature. The eddy viscosity near solid surfaces and convective heat transfer to solid surfaces is calculated using the logarithmic wall function method of Launder and Spalding [14].

A calculation was performed of an 18.9 m diameter JP8 pool fire in a 1.4 m/s wind. The computational domain was 100 m by 100 m by 60 m high, corresponding to a finite difference grid of 30 by 30 by 20 cells. A fixed velocity boundary condition was applied along the upwind boundary (using a logarithmic profile), and constant pressure boundaries were applied downwind and on the remaining free boundaries. Second order accurate upwind differencing was used for the convective terms in the governing equations, and turbulence was modeled using the  $k-\epsilon$  turbulence model. The CPU time required for the calculations was 2-3 days on a Silicon Graphics Indigo R3000 workstation.

The numerical results for the temperature field are shown in Fig. 8. This figure represents a vertical slice through the center of the pool, with wind from the left. Relatively cooler temperatures are observed along the flame zone centerline near the pool surface. The gradients in the calculated temperature field provide an estimate of the extent of the vapor dome. Gradients along the flame zone centerline extend to a height of

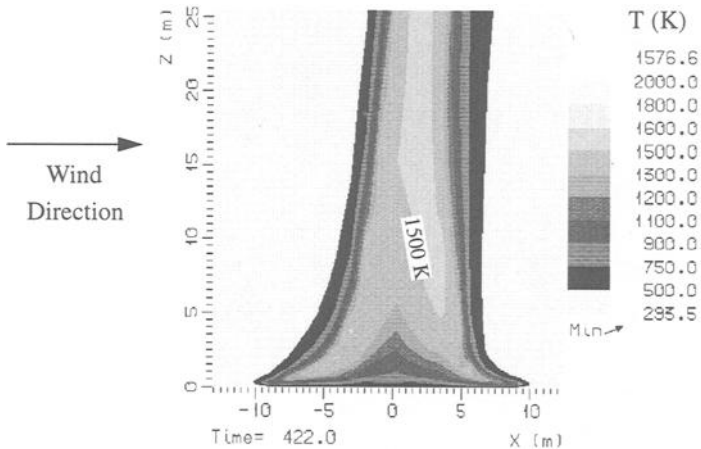


FIG. 8 -- Predicted Temperature Field, JP8 Pool Fire, 1.4 m/s Wind From Left

approximately 6 m, or  $z/R = 0.63$ . A direct comparison of the magnitudes cannot be made with the experimental data, since the thermocouples are influenced by the local radiation field. In general, rendering of the temperature field from thermocouple measurements should follow the same overall trends as, but be smoother than, the actual media temperature distribution. The numerical predictions presented in Fig. 8, however, show trends which are clearly consistent with the experimental measurements. The vapor dome is approximately centered along the pool centerline and a decrease in the spatial extent of the vapor dome is observed with increasing elevation above the pool. In agreement with the experimental measurements, these results suggest that air is not mixed into these regions in sufficient amounts to support combustion.

The numerical results for the distribution of fuel mass fraction throughout the fire are shown in Fig. 9. Very high concentrations of fuel are observed at the pool centerline, especially within the lower region. Such high fuel concentrations inhibit the combustion process locally, resulting in lower temperatures. This figure graphically illustrates the limited mixing of air into this region of the flame zone.

In agreement with the thermocouple temperature data presented earlier, additional simulations [15] show significant differences in the size of this region for high (JP4) and low (JP8) volatility fuels. Although the two fuels have approximately the same heat of vaporization, the larger vapor pressure and lower range of distillation temperature for JP4 tends to produce a larger oxygen-starved interior. Preliminary results also indicate that the burning rate for JP4-fueled fire is slightly greater than those burning JP8.

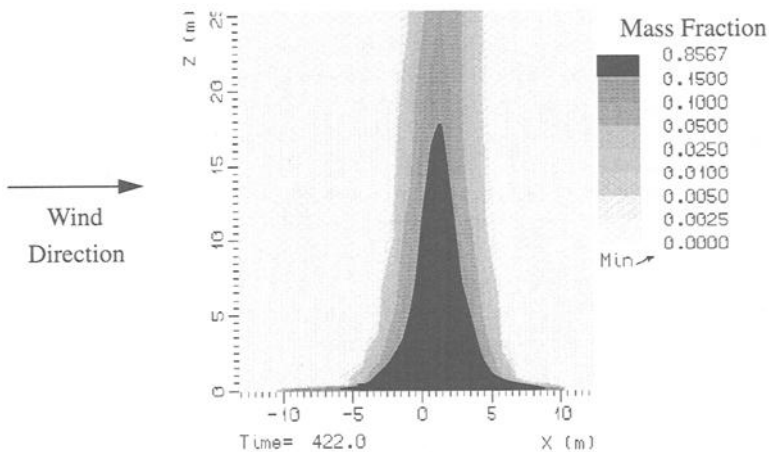


FIG. 9 -- Predicted Fuel Concentration Field, JP8 Pool Fire, 1.4 m/s Wind From Left

## DISCUSSION

### Scaling Issues

Many fire features including flame height, air entrainment, and regimes of fire behavior (such as continuous and intermittent flaming regions) have been scaled in terms of nondimensional parameters derived from or related to a form of the Froude number [1]. Preliminary scaling of the results presented here for the extent of the oxygen-starved interior in fully turbulent pool fires can be based on the fuel vapor Froude number as given by

$$Fr = \frac{V^2}{gD} \quad (3)$$

where  $V$  is the velocity of the fuel vapor (which can be estimated by the fuel composition, bulk vaporization temperature and burn rate),  $D$  is the diameter of the fuel pool, and  $g$  is a gravitational constant. Physically, the fuel vapor Froude number represents the ratio of the inertia of the fuel vapor leaving the fuel surface to the buoyancy generated by burning the fuel over a given dimension. Froude numbers for large fuel fire experiments performed to date tend to be in the range of  $10^6$ . Although not exhaustive due to limits in the number of tests and the complications of winds and engulfed objects in some tests, data from experiments show significantly greater burn rates (and hence Froude numbers) for pool fires burning fuels above their flash point. In contrast, a large reduction in Froude number is expected to result in continuous flame zones with a smaller oxygen-starved interior. It is important to emphasize that these trends and observations are limited to very large fires since smaller (i.e., laminar and transitionally turbulent) fires involve different mixing phenomena.

Scaling of flame zone characteristics, including the extent of the oxygen-starved interior, based on Froude number is proportional to the ratio of heat release to the square root of the fuel bed diameter as proposed by Heskestad [16] and others [1] to determine the transition from a single buoyant flame to a series of flamelets burning over the fuel surface (i.e. a mass fire). The constant of proportionality between the two scaling parameters is the product of the fuel density and the fuel heat of combustion. It is important to note that these properties (fuel density and the fuel heat of combustion) are approximately the same for JP4 and JP8 (i.e. low and high volatility fuels), yet significant differences are observed in the extent of the oxygen-starved interior when these fuels are burned in the same size pool. These differences therefore imply that the inclusion of the fuel density and the fuel heat of combustion to form the ratio of heat release to the square root of the fuel bed diameter do not aid in defining the extent of the oxygen-starved interior. The dominant mechanisms which result in the formation of the oxygen-starved interior are therefore given by the ratio of physical effects represented by the fuel vapor Froude number.

The fuel vapor Froude number is defined by the burning rate of fuel, which in turn is driven by the radiative heat flux from the fire to the fuel surface (a large portion of which is expected to be absorbed within the fuel vapor above the liquid surface.) Previous

measurements of the heat flux to the fuel surface [17] show a significant spatial variation, with a minimum near the center of the fuel pool. Differences can therefore be expected between the total potential heat release and the fuel vapor velocity with increasing pool size due to a reduction in the average heat flux to the fuel surface. Limited available data [18] presently show an approximately constant burn rate with increasing pool size in the fully turbulent regime. However, measured non-uniform heat flux distributions, in conjunction with the presence of an oxygen-starved interior shown here, suggest a reduction in burn rate with increasing pool diameter.

### Implications for Test Methods

The reduction in temperature due to the presence of the oxygen-starved interior has a pronounced effect on the procedures used in fire survivability tests. Fig. 10 shows a map of time averaged temperature in a JP4 “regulatory fire” conducted at the Sandia Lurance Canyon Burn Site [19]. The fuel is floated on a pool of water in a 1 m deep, 6 x 6 m square tub placed above ground level. The map was interpolated from data acquired over a 30 minute period with thermocouples located on towers and supported from the test fixture within a vertical plane through the center of the fire. Wind speeds averaged less than 0.5 m/s during the test. The estimated heat release was 75 MW with a vapor Froude number of about  $4 \times 10^{-6}$ . The lightest and darkest regions correspond to average temperatures of approximately 1350 K and 450 K, respectively.

The pool is fitted with a number of devices intended to stabilize the fire in low wind conditions to ensure the test package is engulfed in flames during the 30 minute test

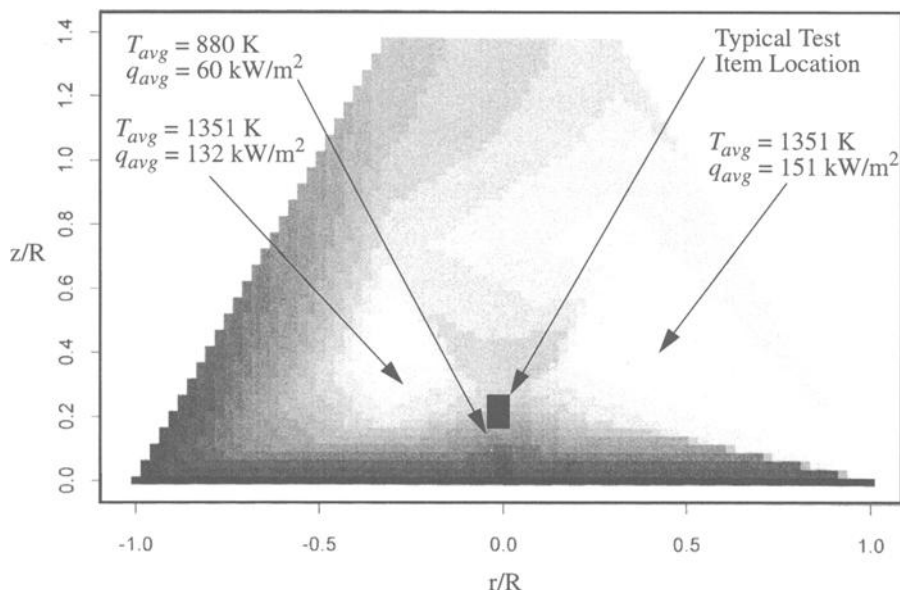


FIG. 10 -- Temperature Contours & Selected Heat Fluxes, “Regulatory” JP4 Pool Fire

to satisfy regulatory requirements. The pool is centered within a 30 meter diameter arena formed by 6 m high wind fences. The wind fences are constructed of chain link and steel slats to provide a 50% blockage. Wind velocities in the arena have been shown to be reduced by a factor of 3 with this system. The pool or tub sides are ramped inward at approximately 60 degrees with respect to the ground with the intent of inducing an upward momentum in the air flow at the edges of the pool. Without the ramps, even very light breezes will cause the fuel vapor to spill over the sides of the tub and carry the fire plume away from the test object. A set of steel baffle plates placed in the middle of the pool directly under the test item also serve to hold the fuel vapor in the center of the pool.

The effect of these devices can be seen in Fig. 10. The vapor dome (as shown by the dark regions in the temperature map) extends across the entire pool and coincides vertically with the non-dimensional limits suggested for the extent of the vapor dome in the large circular pool fire experimental results. A test package would normally sit in the center ( $r/R = 0$ ) at 1 m above the fuel surface and occupy the region  $0.17 < z/R < 0.25$ . At this location, the test item is at the upper boundary of the vapor dome. Average temperatures in this region are about 850 K. An average heat flux of  $60 \text{ kW/m}^2$  was measured using a thick wall steel calorimeter located within this area. Although these conditions meet the criteria set out in 10CFR71 [20], it is easy to see that one could shift the test package towards the edge of the fire and subject the package to a much more intense fire environment. Calorimeters placed at  $r/R = 0.31$  and  $z/R = 0.37$  registered average cold wall fluxes of  $150 \text{ kW/m}^2$ , or more than a factor of two greater than those observed in the fire center.

## SUMMARY AND CONCLUSIONS

If the goal of fire survivability tests to satisfy regulatory requirements is to ensure acceptable system performance in actual fires, then the object placement, and the associated magnitudes and variations in heat flux due to spatial variations in temperature must be considered. Experimental data acquired to date, in conjunction with numerical fire field models, provide the basis for revising test methods and regulatory requirements to ensure adequate system response in actual large fire scenarios.

Data are presented which show the presence of large, noncombusting regions in the interior of very large fires with a sufficient fuel vapor Froude number to form a single continuous flame zone. The data indicate that the minimum (due to radiation effects on measured thermocouple temperatures) extent of this region for an 18.9 m diameter pool fire is from the centerline to  $r/R = 0.5$  at  $z/R = 0.03$  and from the centerline to  $r/R = 0.25$  at  $z/R = 0.13$ . The extent of this region observed in the experimental data is qualitatively similar to fire field model predictions, supporting the utility of these tools in representing large fire phenomena.

Within the oxygen-starved region, temperatures are significantly lower than in the actively burning regions. Accordingly, much smaller heat fluxes are observed. Temperature and heat flux data, and model predictions emphasize that tests of packaging containers, where the container is aligned with the center of the fuel pool and placed near

the fuel surface, will be subject to localized reduction in temperature, and hence heat flux. Although it is commonly thought to be the most conservative case due to the maximum amount of flame cover on the test item, the placement of the item at an elevation 1m above the fuel surface may be subjected to a less severe environment due to the presence of the oxygen-starved interior. For pools greater than 9 m in diameter, the data acquired to date indicate that the specified 1 m elevation results in the package being located within the low temperature vapor dome. These results suggest that large packages, which require large fires to ensure adequate flame cover, should be placed at an elevation of  $z/R > 0.22$ . Consideration should be given to this phenomena during the development of future test methods for fire survivable systems.

Existing prescriptive regulations can be attributed to an incomplete characterization of large fire phenomena. Large fire tests are expensive to perform and difficult to thoroughly instrument. Therefore, the database which might allow such characterization is sparse. The development of fire field models, founded on the physical phenomena observed during well-controlled fire experiments and validated with experimental results, promises to provide the ability to explore fire behavior by yielding results with high spatial and temporal resolution. The estimates of the extent of the oxygen-starved interior presented here are among the most important physical phenomena which must be represented by models. The physical extent of the vapor dome will strongly influence the radiative feedback to the pool which, in turn, influences the burning rate. It is also expected that large quantities of soot are formed in the vapor dome due to fuel pyrolysis.

The presence of the oxygen-starved region in the interior of large fires supplements previously observed features of fire structure which were based on a continuous flame zone which extended to the pool surface. Computational models have demonstrated the ability to reflect the structure of this region, therefore extending predictive ability beyond present analytical models which neglect this lower region.

## ACKNOWLEDGEMENTS

This work was supported by the Sandia Engineering Sciences Research Foundation and the Defense Special Weapons Agency Fuel Fire Techbase Program. The views expressed in this article are those of the authors and do not reflect the official policy or position of the Department of Defense or the U.S. Government.

## REFERENCES

1. *The SFPE Handbook of Fire Protection Engineering, First Edition*, National Fire Protection Association, Quincy, MA, 1988.
2. Mansfield, J.A., and Linley, L.J., "Measurement and Statistical Analysis of Flame Temperatures From Large Fuel Spill Fires," Naval Air Weapons Center NWC TP7061, 1991.

3. Longenbaugh, R.S. and Matthews, L.K., "Experimental and Theoretical Analysis of the Radiative Transfer within a Sooty Pool Fire," SAND86-0083, Sandia National Laboratories, Albuquerque, NM, 1986.
4. Russell, L. H. and Canfield, J. A., "Experimental Measurement of Heat Transfer to a Cylinder Immersed in a Large Aviation Fuel Fire," *Journal of Heat Transfer*, Vol. 95C, 1973, pp. 397-407.
5. Gregory, J., Keltner, N. R., and Mata, R., "Thermal Measurements in Large Pool Fires," *Journal of Heat Transfer*, Vol. 111, 1989, pp. 446-454.
6. McCaffrey, B. J., "Purely Buoyant Diffusion Flames: Some Experimental Results," National Bureau of Standards, NBSIR 79-1910.
7. Gritzo, L.A., Gill, W. and Keltner, N. "Thermal Measurements to Characterize Large Fires," Proceedings of the 41st International Instrumentation Symposium, Denver, CO, May 7-11, 1995, pp. 337-346.
8. Holen, J., Brostrom, M., and Magnussen, B. F., "Finite Difference Calculation of Pool Fires," *Proceedings of the 23rd International Symposium on Combustion*, The Combustion Institute, 1990, pp. 1677-1683.
9. Patankar, S. V., and Spalding, D. B., "A Calculation Procedure for Heat, Mass, and Momentum Transfer in Three-Dimensional Parabolic Flow," *International Journal of Heat and Mass Transfer*, Vol. 15, 1972, p. 1787.
10. Magnussen, B.F., Hjertager, B.H., Olsen, J.G., and Bhaduri, D., "The Eddy Dissipation Concept," *The Seventeenth Symposium (International) on Combustion*, The Combustion Institute, Pittsburg, 1979, p. 1383.
11. Magnussen, B.F., "The Eddy Dissipation Concept," Proceedings of Eleventh Task Leaders Meeting, IEA Working Group on Conservation in Combustion, Lund, Sweden, 1989.
12. Tesner, P.A. Snegiriova, T.D., and Knorre, V.G., "Kinetics of Dispersed Carbon Formation," *Combustion and Flame*, Vol. 17, 1971, pp. 253-260.
13. Shah, N. G., "The Computation of Radiation Heat Transfer," Ph.D. Thesis, University of London, Faculty of Engineering, 1979.
14. Launder, B.E., and Spalding, D.B., "The Numerical Computation of Turbulent Flows," *Computer Methods in Applied Mechanics and Engineering*. Vol. 3, 1972, pp. 269-289.
15. Nicolette, V.F, Gritzo, L.A., Moya, J.L., and Tieszen, S.R. "Comparison of Large JP4- and JP8-Fueled Pool Fires," Proceedings of the International Conference on Fire Research and Engineering, Orlando, Florida, September 10-15, 1995, SFPE, Quincy, MA, 1995, pp.461-468.
16. Heskestad, G., "A Reduced Mass Fire Experiment," *Combustion and Flame*, Vol. 83, 1991, pp. 293-301.
17. Gritzo, L.A., Nicolette, V.F., Tieszen, S.R. and Moya, J.L. "Heat Transfer to the Fuel Surface in Large Pool Fires," *Transport Phenomenon in Combustion*, S.H. Chan, ed., Taylor and Francis, 1996.
18. Blinov, V.I., and Khudyakov, G. N. "Diffusion Burning of Liquids," English Translation: U.S. Army Engineering Research and Development Labs, Fort Belvoir, VA, Report AERDL-T-1490-A, 1961.
19. Gill, W., and Strait, B.G., Test Report for the 9970/9971 Pool Fire Test, Central Technical File, Sandia National Laboratories, Albuquerque, NM, 1992.
20. 10CFR71.73c(3) Code of Federal Regulations. U.S. Government Publication.

Kozo Saito<sup>1</sup>

## RECONSTRUCTION OF VERY LARGE-SCALE FIRES

---

**REFERENCE:** Saito K., “Reconstruction of Very Large-Scale Fires,” *Very Large-Scale Fires*, ASTM STP 1336, N. R. Keltner, N. J. Alvares, and S. J. Grayson, Eds., American Society for Testing and Materials, 1998.

**ABST. 'ACT:** This paper describes scale modeling of very large scale fires as a practically useful means to investigate thoroughly their mechanisms in laboratory. A good example of very large scale fires is “fire whirls”. If they are generated in urban and wildland fires, they can be dangerous for the fire fighters nearby the fire whirls and will cause extensive damage in environments. For over 20 years we have collected information and conducted experimental studies of fire whirls in mass fires using scale models. These studies indicated that a large mass fire often broke out when a large earthquake hit a city of dense population. The mass fire-related casualties and destruction were far more serious than those caused by destruction of buildings and houses by the earthquake itself. A good example is the 1938 Tokyo earthquake which caused mass fires and fire whirls claiming 38,000 deaths.

**KEYWORDS:** accident reconstruction, combustion, forest fire, scaling laws, scale models.

### NOMENCLATURE

- A a characteristic fire area ( $L^2$ )  
c specific heat of air ( $M^{-1} q^{-1} Q$ )  
f frequency ( $T^{-1}$ )  
Fr Froude number  $V_m(gL)^{-1}$   
g gravitational acceleration ( $LT^{-2}$ )  
h fire depth (L)  
H height of fire whirl (L)

---

<sup>1</sup>Professor, Department of Mechanical Engineering, University of Kentucky, Lexington, KY 40506-0108.

- $k$  a constant ( $T^{-1}$ )
- $l$  length of fire (L)
- $L$  length
- $M$  mass
- $P$  difference between pressure at a specified relative point in the whirl core and ambient (Pa)
- $q$  heat generated per unit surface and unit time ( $L^2T^{-1}Q$ )
- $Q$  heat
- $r$  radial distance in cylindrical polar coordinates (L)
- $R$  average radius of fire whirl core (L)
- $R_c$  radius of fire whirl core at ground level (L)
- $Re$  Reynolds number  $DV_mL^{-1}$
- $R_m$  visually observed maximum radius of whirl (L)
- $Ro$  Rossby number  $V_m(2fL)^{-1}$
- $t$  duration of fire whirl (T)
- $T$  time
- $u$  velocity component in the  $r$  direction ( $LT^{-1}$ )
- $U_a$  lateral (mean) velocity component of wind ( $LT^{-1}$ )
- $U_f$  lateral (fluctuating) velocity component of wind ( $LT^{-1}$ )
- $U$  characteristic velocity in the  $r$  direction ( $LT^{-1}$ )
- $v$  velocity component in the  $\phi$  direction ( $LT^{-1}$ )
- $V$  characteristic velocity in the  $\phi$  direction ( $LT^{-1}$ )
- $V_m$  maximum value of  $V$  ( $LT^{-1}$ )
- $w$  velocity component in the  $z$ -direction ( $LT^{-1}$ )
- $W$  characteristic velocity in the  $z$  direction ( $LT^{-1}$ )
- $z$  rectangular coordinate (L)
- $Z$  average height of fire-whirl column (L)
- $Z_m$  visually observed maximum height of whirl column (L)

Greek Symbols

- $\alpha$   $R/Z$
- $\Gamma$  scaling ratio of model to prototype ( $L/L$ )
- $\phi$  azimuthal angle in cylindrical polar coordinates
- $\nu$  kinematic viscosity of gas ( $L^2/T$ )
- $\theta$  temperature of combustible gas and air [ $\oplus$ ]
- $\Delta\theta$  difference between gas temperature at a specified relative point in the fire and temperature of ambient air [ $\oplus$ ]
- $\rho$  density of combustible gas and air ( $ML^{-3}$ )
- $\Delta\rho$  difference between gas density at a specified relative point in the fire and ambient air ( $ML^{-3}$ )
- $\oplus$  temperature
- $\Omega$  constant angular velocity of rotation of the earth ( $T^{-1}$ )

## FIRE WHIRLS

Turbulent diffusion flames are widely used in industrial operations. They produce both solid and gaseous incomplete combustion products, which pollute the environment and reduce combustion efficiency [1]. Spinning the diffusion flame by introducing rotation into the air flow around it can increase the mixing of air and gaseous and liquid fuel. The enhanced mixing leads to higher flame temperature which increases combustion efficiency by reducing the products of incomplete combustion to those of complete combustion, H<sub>2</sub>O and CO<sub>2</sub>. This mechanism, called fire whirl, has broad application (but the mechanism is not well understood [2,3]) to combustion systems in industries using fluidized bed combustion chambers, incineration chambers, and internal combustion engines as well as for fire-safety engineering and evacuation strategies in urban areas [4]. Also, researchers at Princeton University were able to build a low NO<sub>x</sub> burner by using fire whirl enhanced combustion [5].

The fire-safety-engineering aspects of fire-whirl studies are detailed by Pitts [6] and Soma and Saito [4] therefore, we summarize their studies in the following. Williams [7] discussed the possible use of scale models in order to simulate the behavior of mass fires, some progress has been made in how to reconstruct fire whirls in the laboratory. We have collected information and conducted a series of experimental studies of fire whirls in mass fires. Our results were published and some of them are listed in the reference section [4,8,9].

These studies indicated that a large scale mass-fire often broke out when a large scale earthquake hit a city of dense population. The mass fire-related casualties and destruction were far more serious than those caused by destruction of buildings and houses by the earthquake itself. Following is an excerpt from our 1991 paper [4].

"On September 1, 1923, a magnitude 7.9 earthquake hit the downtown Tokyo area and a mass fire quickly broke out because it was almost lunch time and cooking stoves provided a fire source. To escape from the threat of fire, people were gathered in a 0.16-km<sup>2</sup> open area, called Hifukusho-Ato, where hardly any combustible materials were located. Wind was nearly calm (less than 5 m/s) at that time. Despite the fact that the people seemed safe from the threat of fire, a fire whirl that carried burning debris and flames suddenly appeared at the north corner of the Hifukusho-Ato and moved in a tortuous path to the south corner. The maximum velocity of the fire-whirl wind was estimated to be over 70 m/s (157 miles/hour). 38,000 casualties were claimed by the fire whirl within 15 minutes."

Following the tragedy, Terada [10] investigated the cause of the whirl and suggested two possible causes:

1. A tornado that had no association with the fire was generated at the place by chance as a result of weather conditions.

2. A fire whirl was generated by an interaction between a buoyancy driven hot convective plume produced by the mass fire with a wind-shear effect generated by a moderate wind.

Almost 18 years ago, we decided to pursue the second possibility. After a series of experiments, we succeeded in developing scaling laws for reconstructing the fire whirls in our laboratory [4]. As a result of this reconstruction, we are able to conduct an investigation that enables us to understand conditions under which fire whirls can be generated. A whole or partial city may be reconstructed in a reduced scale model. Effectiveness of a fire zone or a fire wall may be tested to prevent the generation of fire whirls. Results from these scale model experiments can be used to develop models that can predict behavior of mass fires caused by earthquakes. We feel the scale model studies are extremely useful and beneficial for explaining these tragic phenomena.

Fire-Whirl Experiment

This experiment consists of (1) a platinum-10%Rh vs. platinum of 50µm diameter thermocouple coated with silica to measure flame and hot gas temperature by traversing axial and radial directions, the accurate measurement of which is very important in assessing the performance of combustion systems; (2) a thermal anemometer for the measurement of air entrainment velocity; (3) a water-cooled Gardon-type heat flux meter to measure a total heat flux from the flame; (4) a laser-sheet particle tracking technique for visualization of the flame-induced flow [11]; (5) infrared and normal video cameras for both instantaneous and average flame-height measurements [12]; and (6) micro probe sampling and gas chromatographic (GC) analysis of combustion by-products in a post-combustion zone [13].

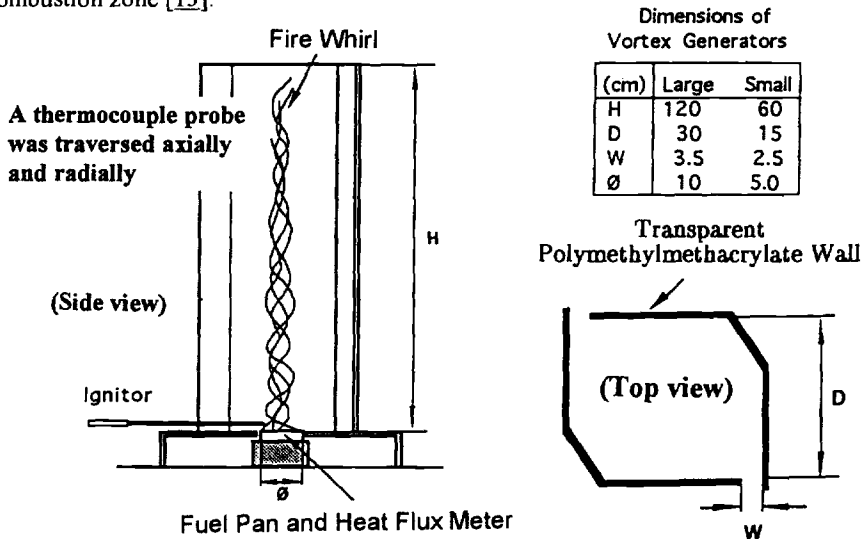


FIG. 1--Schematic of fire whirl generator.

A liquid-pool fire is used as a typical diffusion flame because it is simple, easy to handle, and its characteristics are relatively well known. Two different open top fuel-containers of diameters 5 and 10 cm were designed. The two corresponding fire-whirl generators were made of polymethylmethacrylate. Figure 1 shows a schematic of the vortex generator and schematic of a fire whirl. The aim of using two different size apparatuses is to develop scaling relationships by studying results from the two different size models. It is very important to find proper scaling laws before applying the laboratory results to a full scale phenomenon [6,9,14].

### Scaling Laws

The following considerations were given to simplify the problem and dimensional analysis was applied to obtain parametric relationships:

1. Assume that the whirls are incompressible turbulent vortices that on the average are axisymmetric. Take cylindrical polar coordinates ( $r$ ,  $N$ ,  $z$ ) with the  $z$  axis directed vertically upwards along the axis of the whirl and velocity components ( $u$ ,  $v$ ,  $w$ ). Suppose that ( $R$ ,  $Z$ ,  $U$ ,  $V$ ,  $W$ ) represent typical magnitudes of the variable quantities.
2. The flow in the fire-whirl core is turbulent; thus the viscous forces are small in relation to inertial forces for the mean motion. Hence, (inertial forces)/(viscous forces)  $\sim (1/\alpha)(UZ/v) \gg 1$  in the azimuthal direction and  $(R/Z)(RW/v) = \alpha Re \gg 1$  in both the  $z$  and the  $r$  directions, where  $R$  is distance (vertical) from the fire surface or ground, and  $\alpha$  is a measure of the semi-angle of spread for the core flow measured relative to the fire source (the value of  $\alpha$  is approximately between 0.1 and 0.01, and  $Re$  is a local Reynolds number for axial flow along the core).
3. Although the viscous forces are small in magnitude, they may play an important role in initiation mechanisms of the fire whirl formation which are currently unknown. We do not include the initiation mechanisms of the fire whirl in the scaling laws.
4. The effects of eddies existing in the wind near the earth's surface is minor [15]. The estimated  $Ro = V/2fL$  - (local acceleration)/Coriolis force) is  $10^4$  for fire whirls (characteristic length,  $L = 10$  m; characteristic velocity,  $V = 10$  m/s), and  $Ro = 10^2$  for a large fire whirl ( $L = 3000$  m;  $V = 50$  m).
5. Heat conducted through the ground is negligibly small compared to heat generated by the fire.
6. A fire seldom burns uniformly-some areas are burning intensely while the fire in adjacent areas is dying out, and the strong upsurge of gases over the hot areas can create fire whirls. These "hotspots" in the fire area may be attributed to differences in slope, fuel type, fuel loading, or fuel arrangement. To simplify the problem, however, we assume fires are on a horizontal plane.

With the above considerations, parameters related to the fire whirls can be listed as follows (for the symbols and their dimensions, see the Nomenclature section):

$$[c, f, g, h, l, p, q, R, t, U_a, U, V, W, Z, \theta, \Delta\theta, \rho, \Delta\rho].$$

Applying the pi-theorem, 13 pi-numbers can be formed of which 3 possess a strict physical meaning and the rest restrict similarity of geometry, air flow profiles, air temperature profiles, air density profiles, and frequency of the repeating pattern for fire whirl movement.

The requirement for similarity between model and full-scale systems is that all the pi-numbers must be identical in both. The process of deriving pi-numbers is well established. For readers who are interested in scale modeling technique, see refs. [16,17].

Applying experimental conditions, (1) the geometrical shape of the fuel bed is kept similar in the prototype and the scale models, (2) the scale model experiment is performed under the same ambient/gravity conditions and the same fuel is used (under these conditions, the temperatures at corresponding points and parameters,  $c$ ,  $g$ , and  $\rho$  remain the same [18]), and (3) air and hot combustion products satisfy the equation of state for an ideal gas, the rest of the pi-numbers must obey functional relationship of the form

$$\phi(R/Z, R/h, Rf/V, ft, U/U_a, U/V, W/V, W^2/gZ, \alpha p/\delta W^2, c\delta W\Delta\theta/q) = 0 \tag{1}$$

The following relationships can be automatically deduced:

$$R/R' = Z/Z' = h/h' \tag{2}$$

$$U_a/U'_a = U/U' = V/V' = W/W' \tag{3}$$

$$V/V' = (Z/Z')^{1/2} = (lh/l'h')^{1/4} = (A/A')^{1/4} \tag{4}$$

$$p/p' = (W/W')^2 = (h/h') = (A/A')^{1/2} \tag{5}$$

$$q/q' = (W/W') = (A/A')^{1/4} \tag{6}$$

where  $A$  is a characteristic fire area and prime (') indicates "scale model."

Sometimes, the occurrence of the fire whirl was observed to be periodical [4]. Frequency of the repeating pattern and time period that the fire whirl exists can be respectively deduced from  $Rf/V$  and  $ft$  in Eq 1:

$$Rf/R'f' = V/V' \tag{7}$$

and

$$t/t' = \underline{f}/\underline{f}' \quad (8)$$

whence through Eqs 2 and 4, the frequency of the repeating pattern becomes inversely proportional to the square root of the fire depth or fourth root of the characteristic fire area, that is,

$$\underline{f}/\underline{f}' = (\underline{h}/\underline{h}')^{1/2} = (\underline{A}/\underline{A}')^{1/4} \quad (9)$$

Thus, the model experiments are to be performed with wind velocities and heat-generation rates proportional to square root of the fire widths or one-fourth power of the fire area. Then the scaling predicts variations of fire-whirl characteristics, such as whirl-core diameter, whirl-column height, and tangential velocity of the whirl.

### RECONSTRUCTION OF A FOREST FIRE WHIRL

The objectives of this study are to apply the above scaling laws to a forest fire and design a scale model similar to a real forest fire. The forest fire being modeled herein, called the prototype, caused serious injuries to several fire fighters [8]. The report regarding the forest fire states that the injuries occurred at the mid-point of the valley's slope. The fire suddenly changed its spreading direction at that point and increased both its spreading velocity and its flame height. Because of this rapid change, fire fighters lost their escape route and received serious injuries.

The prototype fire broke out at Mt. Nuki in Japan in 1977, and the fire spread with high velocity driven by heavy wind. Fire fighters were suddenly engulfed by the fire. The accident happened at a spot on the mountain downwind from the fire, with the wind blowing directly downhill. Figure 2 shows a geographical figure of Mt. Nuki and the accident spot. The velocity of fire spread was approximately determined by the observations of fire fighters involved in the extinguishing work. The wind velocity data used was measured at an observatory 50 km (32 miles) away from Mt. Nuki. It is known from daily weather records that the data measured at the observatory are applicable to Mt. Nuki. The data for turbulent intensity, the ratio of fluctuating velocity components to mean velocity components, were used as that obtained for the atmospheric flow near the surface with large roughness.

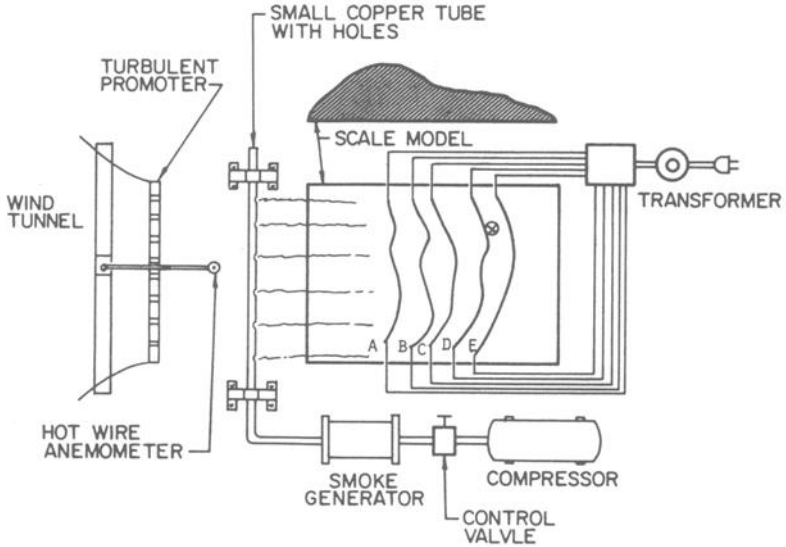
To simulate the conditions of this accident in a scale model, all of the significant parameters were collected in the similar manner as mentioned in the section of scaling laws. In collecting the significant parameters among many existing parameters, the concept of partial modeling [7,19] was introduced, and our interest was focused on the fluid dynamical aspects. Some previous works [19] were also used to make this job easier.

Scale Model Experiment

The designed scale model is geometrically similar to the real forest fire with the scale ratio of 1/2500. The mean air velocity and the fluctuating wind component are adjusted to follow the scaling laws. A wind tunnel equipped with a turbulent grid promoter generates these air movements. The heat generated from the fire was simulated by heating nichrome wire strips placed along the flame position in the model fire. The flame position of the actual fire at equal time intervals was known from the observations of fire fighters [8].

TABLE 1. Scaling relationship between prototype and scale model.

Variable	Prototype	1/2500 Scale model
$l$	2500	1
$h$	30	0.012
$U_a$	15	0.3
$\frac{\sqrt{U_f^2}}{ U_a }$	0.2	1.16-0.20
$q$	630	12.6



Wind tunnel exit dimension:  
0.8m wide x 1.0m long x 0.8m high

FIG. 2--Experimental apparatus of flow visualization for a 1/2500 scale model of Mt. Nuki (A~E = nichrome wire strips, ⊕ = accident location).

$$\frac{\sqrt{U_f^2}}{|U_a|} \cong 0.20 \tag{10}$$

In the prototype, the heat generated per unit surface area and unit time is calculated using information on fire spreading velocity, density of tree growth and heat generated from burning wood.

As a result,

$$q = 630 \text{ kW/m}^2 \tag{11}$$

Although this value is almost twice as high as the value that Byram [20] used, this value is thought to be reasonable. The discrepancy results because the prototype heating value is for windy conditions whereas Byram's heating value is for calm ambient conditions.

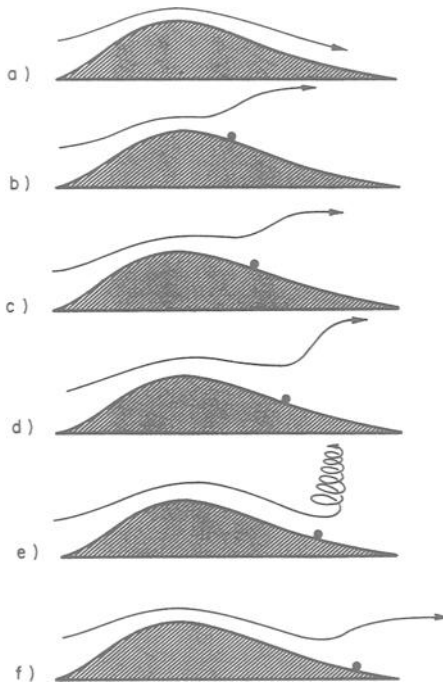


FIG. 3--Schematics of flow patterns observed in the 1/2500 scale model:  
 • = the location of heated nicrome wire,  
a = without heating, and b through f = with heating.

The designed scale model is geometrically similar to the prototype with the scale ratio of 1/2500. With this choice of scale ratio, estimates of the Froude and Reynolds numbers were made. The Froude number is dominant in the prototype but in the small-scale model, the Reynolds number becomes predominant by overwhelming the Froude number in the ratio of  $(1/1')^{3/2}$  as mentioned earlier [7,18]. The minimum size of the scale model can be determined in order to keep the Froude number dominant. Because the heat conducted through the ground was ignored, it was possible to use plaster rather than dirt as the material for the scale model. A turbulent grid promoter was used to generate the velocity components required by the relation in Eq 10. A hot wire probe system was used to measure the turbulent intensity and the mean flow velocity. To satisfy the relation in Eq 11, that is,  $q/q' = \sqrt{2500} = 50$ , nichrome wires were set along the flame position at equal flow time intervals and heat from the nichrome wire was adjusted using a transformer connected to an electrical source. The scaling relationships obtained are summarized in Table 1. The airflow pattern was visualized by smoke tracers coming from small holes drilled in a copper tube which was connected to a smoke generator as shown in Fig. 2.

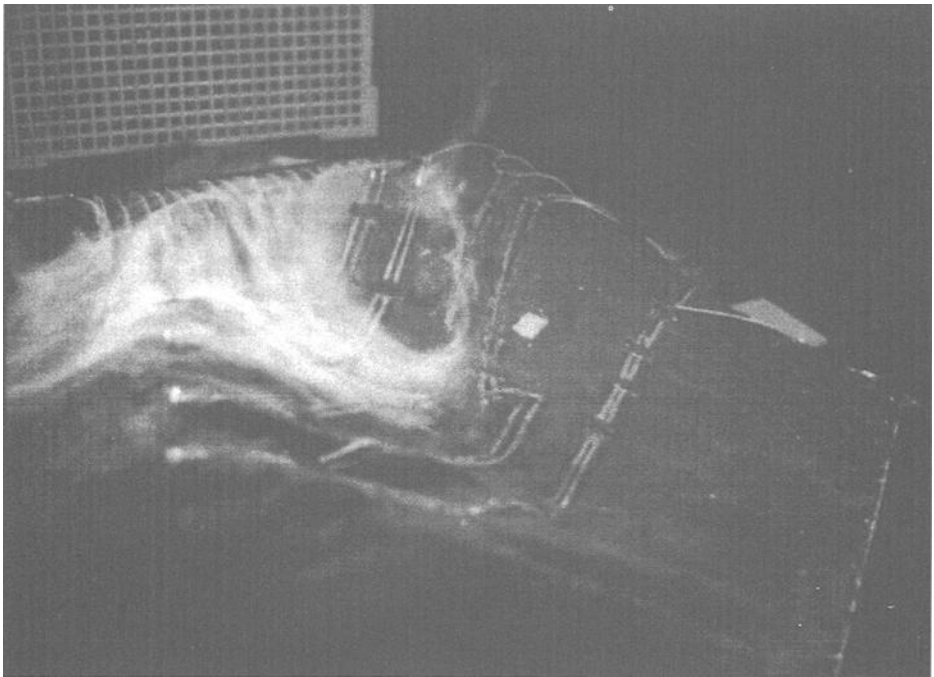


FIG. 4--A picture of a 1/2500 scale-model fire-whirl.

## Results

The experiment was performed in the following order. Firstly, the flow pattern without heating was inspected. Secondly, nichrome wire (A) was heated. The flow pattern was visualized by smoke tracers and pictures were taken. This step was repeated in order from (B) to (E). The observed flow patterns are graphically shown in Fig. 3. The flow pattern without heating is shown in (a) of Fig. 3. The air is flowing smoothly along the slope of the mountain. The flow pattern with heating is shown in (b) to (f) of Fig. 3. The flow patterns are changed by the effects of buoyancy generated from the heated nichrome wires. Most importantly, in case of (e) in Fig. 3, which corresponds to the accident time, a whirl was produced. A picture of this whirl is provided in Fig. 4. To investigate the potential generation of fire whirls, some additional experiments were performed under conditions of various air velocities. The results showed that a whirl appeared for case (e) in Fig. 3, only when the air velocity was between 15 and 50 cm/s. This velocity range corresponds to 7.5 m/s to 25 m/s in the prototype. As shown in Table 1, the estimated velocity at the time of the accident was 15m/s. No whirl appeared outside of this velocity range.

## CONCLUSIONS

This study showed how to reconstruct fire whirls using scale models. In general, when scale models are properly designed, they can be a powerful tool to investigate prototype phenomena. However, the scale models could generate entirely different results from prototype, if the scaling laws fail. Thus, a confirmation experiment, which validates the similarity between the scale model and prototype, is important prior to applying the scale model results to prototype.

The first part of this study showed that the Froude number scaling is valid to reconstruct fluid dynamic aspects of prototype fire whirls in laboratory. This study also revealed three different types of fire whirls and one of them was applied to the accident investigation for the 38,000 deaths caused by the 1938 Tokyo earthquake fire whirl. There may be further interesting aspects of fire whirls can be found. For example, combustion by-products formation and fire brands which are more directly related to chemical and thermal aspects of fire whirls. Thus, further studies are required in the future.

The second part of this study, a scale model investigation of the prototype forest fire showed that a fire whirl may have been generated in the original fire. In the model, a fire whirl appeared in a specific place when the airflow velocity ranged between 15 and 50 cm/s. This indicates that a fire whirl may have been generated in the real fire if the air velocity was in the range of 7.5 to 25 m/s. In general, the scaling laws and the technique of scale model experiments described in this paper are useful in predicting the generation of fire whirls.

## ACKNOWLEDGMENTS

Cheng Qian, Ghassan Tashtoush, and Seog-Shin Lee helped to design vortex generators and conducted fire-whirl experiments. Dale Hall typed this manuscript. This study was supported in part by Kentucky-NASA EPSCoR program and in part by NIST Grant under 60NANB4D1674. Ned Keltner provided me with valuable comments on temperature and radiation measurement techniques.

## REFERENCES

- [1] Williams, F. A., Combustion Theory, Benjamin/Cummins, 2<sup>nd</sup> ed., 1985.
- [2] Albini, F. A., "Wildland Fires," American Scientist, Vol. 72, 1984, pp 590-597.
- [3] Emmons, H. W. and Ying, S. J., "The Fire Whirl," in Eleventh Symposium (International) on Combustion, The Combustion Institute, 1967, pp. 475-488.
- [4] Soma, S., and Saito, K., "Reconstruction of Fire Whirls using Scale Models," Combust. Flame, Vol. 86, 1991, pp. 269-284.
- [5] Glassman, I., Yetter, R. A., Gabler, C., and Sivo, J., "Asymmetric Whirl Combustion - A New Phenomenon?," presented at the Eastern States Section/The Combustion Institute, Florida, November, 1994.
- [6] Pitts, W. M., "Wind Effects on Fires," Prog. Energy Combust. Sci., Vol. 17, 1991, pp. 83-134.
- [7] Williams, F. A., "Scaling Mass Fires," Fire Res. Abst. Review, Vol. 11, 1969, pp. 1-23.
- [8] Emori, R. I. and Saito, K., "Model Experiments of Hazardous Forest Fire Whirl," Fire Technology, Vol. 18, 1982, pp. 319-327.
- [9] Emori, R. I. and Saito, K., "A Study of Scaling Laws in Pool and Crib Fires," Combust. Sci. Tech., Vol. 31, 1983, pp. 217-230.
- [10] Terada, T., "Whirls Generated on September 1, 1923," Report of the Earthquake Prevention Committee No. 100, Tokyo, Japan (in Japanese), 1925.
- [11] Venkatesh, S., Ito, A., Saito, K., and Wichman, I.S., "Flame Base Structure of Small-Scale Pool Fires," Twenty-Sixth Symposium (International) on Combustion, The Combustion Institute, 1996, pp. 1437-1443.
- [12] Arakawa, A., Saito, K., and Gruver, W.A., "Automated Infrared Imaging Temperature Measurement," Combustion and Flame, Vol. 92, 1993, pp. 222-230.
- [13] Saito, K., Williams, F.A., and Gordon, A.S., "Structure of Laminar Co-flow Methane-Air Diffusion Flames," J. Heat Transfer, Vol. 108, 1986, pp. 640-648.
- [14] Hirano, T. and Saito, K., "Fire Spread Phenomena: The Role of Observation in Experiments," Prog. Energy Combust. Sci., Vol. 20, 1995, pp. 461-485.
- [15] Morton, B. R., "Geophysical Vortices," Progress in Aeronautical Series, Kuchman ed., Pergamon, New York, Vol. 7, Chap. 6, 1966.
- [16] Emori, R.I. and Schuring, D.J., Scale Models in Engineering, Pergamon, 1977.
- [17] Saito, K., Edited, Proceedings of International Symposium on Scale Modeling, Lexington, Kentucky, 1997.

- [18] McCaffrey, B.J., "Purely Buoyant Diffusion Flames; Some Experimental Results," National Bureau of Standards, NBSIR 79-1910.
- [19] Saito, K., "Scaling Laws and Model Experiments in Fire Research," Section 2, Chapter IV, Fire Res. Handbook, Kyoritsu, Japan, 1984.
- [20] Byram, G. M., "Scaling Laws for Modeling Mass Fires," Pyrodynamics, Vol. 4, 1966, pp. 271-290.

J.E.S. Venart<sup>1</sup>

## **BOILING LIQUID EXPANDING VAPOR EXPLOSIONS (BLEVE): POSSIBLE FAILURE MECHANISMS**

---

**REFERENCE:** Venart, J. E. S., "Boiling Liquid Expanding Vapor Explosions (BLEVE): Possible Failure Mechanisms," *Very Large-Scale Fires, ASTM STP 1336*, N. R. Keltner, N. J. Alvares, and S. J. Grayson, Eds., American Society for Testing and Materials, 1998.

**ABSTRACT:** Detailed re-analysis of the catastrophic failures of four 2-tonne LPG vessels subjected to jet fire attack indicates that the severity of the event and the intensity of the fireballs formed may be a function of the initiating mode of vessel failure and the thermo-hydraulic state of the contents. The mechanism of vessel failure appears to be a two-step process; the formation of an initiating overpressure crack in the high temperature vapor wetted walls of the vessel, followed by a final catastrophic 'unzipping' of the containment and the nearly instantaneous release of its contents. The distribution and flashing of the lading causes a fireball. The surface emissive power of the BLEVE fireball does not appear to be directly related to the 'superheat' of the contents at failure. Possible reasons for the final rapid failure of the vessel are either crack instability or the rapid quenching of the crack tip, due to its two phase discharge, that results in large local thermal stresses.

**KEYWORDS:** Jet fires, Boiling Liquid Expanding Vapor Explosions (BLEVE), fireballs, pressure liquified gases, LPG, catastrophic pressure vessel failure, loss of containment, LOC, large scale experiments.

---

It is the intent of this contribution to advance a possible explanation for the very complex fluid structure interaction (FSI) observed in the BLEVE event and to support the hypothesis by a detailed re-examination of recent experimental data [1-6], new physical interpretation and further metallurgical measurements for these same experiments.

A major objective of many current research programs in pressure liquefied gas (PLG) safety has been to develop, verify and validate models for the loss of containment (LOC) failures in partially filled, externally heated or otherwise mechanically damaged, PLG storage and process vessels.

Some current work has seen the conduct of extensive and carefully designed and conducted large scale field trials [7, 8] and less well characterized small experiments [9, 10] as well as the development and testing of hypotheses for the cause(s) [11, 12] that lead to the BLEVEs observed. Unfortunately most of this work has not been able to address the fundamental question as to **why** the BLEVE event exhibits such diverse fluid-vessel reactions; failures range from total catastrophic loss of containment to only the venting of the contents through an arrested crack; a partial loss of containment.

---

<sup>1</sup> Fire Science Centre, Mechanical Engineering Dept., University of New Brunswick, Fredericton, New Brunswick E3B 5A3 Canada.

## Background and the possible BLEVE mechanism

In the fire attack of a PLG vessel flames first heat up the vapor space walls and these increase in temperature more rapidly than the liquid wetted sides since heat transfer here is initially by free convection, and later by subcooled and then saturated pool boiling; only rarely is the critical heat flux exceeded for most fluids and fire exposures. As heating progresses both the liquid and vapor portions of the contents stratify with the temperature of the liquid surface setting the vapor pressure inside the tank. With continued thermal exposure the sub-cooled liquid core can become homogeneous as boiling proceeds from sub-cooled to saturated boiling; this usually occurs within the stratified liquid zone after the pressure relief valve (PRV) opens and later within the bulk liquid upon falling pressure.

With time, the pressure rises to the set pressure of the PRV which opens. Then, dependent upon fill and heating, this may cycle or remain open in its attempt to maintain the pressure of the contents at its design setting. If fill is low, the liquid wetted area is small, the evaporation rate may not exceed the capacity of the valve and the pressure can remain constant with only partial valve lift or the valve may cycle. As fill increases, wetted surface area increases, and the evaporation rate now can exceed the valve's relief capacity, especially since the exiting vapor may be severely superheated due to vapor stratification; in this case there will be an increase in pressure with time until the level falls and along with its the evaporation rate. In all instances the opening of the valve will first depressurize the vapor which will then be followed by the formation of a two-phase swell within the now superheated liquid [11]. If fill is sufficient, the valve intake can continue to be vapor or, with greater swell, two-phase; conditions that will vary with valve size and fire exposure.

Two-phase valve flow can be caused either by entrainment or because the vessel becomes two-phase full. In the entrained case, mist/droplet flow usually results. If the vessel becomes two-phase full, churn-turbulent bubbly two-phase flow through the valve may occur. In any case the choke pressure for such flows is greater, and the choke velocity substantially less, than those for any prior superheated vapor flow. The pressure relieving capacity of the valve can now become compromised as the two-phase fluid exits with a much lower enthalpy, though greater density, compared to the earlier superheated vapor discharge [13].

With continuing fire attack the vapor metal walls weaken and commence plastic deformation at the hottest locations eventually leading to the formation of a crack which will cause further depressurization of the contents and an even greater two-phase swell of the contents. The size of initial fissure formed should be a function of the metal temperature, the fill level and the available energy in the vapor as only it is immediately available to perform the necessary plastic work. Crack development during this process should be relatively slow with choked, nearly isothermal vapor flow ( $\gamma$ , the isentropic index, is just slightly greater than one for propane [14]) conditions being established as the crack lengthens. The crack should arrest locally in stronger, thicker and lower temperature but still very ductile metal.

Once formed the structural stability of such an opening now becomes a matter of vessel loading, the 'dynamics' of the subsequent flow and/or the local cooling of the metal surrounding the crack. If mist/droplet flow issues through the opening cooling times can be long since there will be little liquid contact with the wall. With sufficient fill impact of a low void fraction swell on the superheated head of the vessel can occur and quenching of the hot metal by direct liquid contact and/or its water-hammer like pressure impulse [15] could catastrophically restart the crack. These latter effects may be amplified by the interaction of both the thermal/hydraulic effects and the geometry of the head space (in both horizontal cylindrical and spherical vessels the vapor regions usually comprise convergent sections that lead to any crack).

Whether the cooled crack is now stable, in a fracture mechanics sense due to its size

[16], or becomes unstable due to pressure or fluid impact loading, and/or its imposed thermal stress [17] leads to differing fluid vessel interactions. On one hand we may have a long duration two-phase discharge with the vessel left intact. Alternatively, an apparent instantaneous catastrophic vessel failure can occur. A relatively long time two step LOC failure is also possible. Both of these latter cases will yield a BLEVE. There have been many examples of all types of these adaptive fluid-structure behaviors in the process safety BLEVE literature (eg. [18]).

It is my view, supported by the evidence outlined here, that such a two-step may be the **cause** of all BLEVEs. That is a 'leak before break' (LBB) crack initiator followed by a total loss of containment (LOC) of the PLG vessel is the normal sequence in the development of a BLEVE.

The consequence of such a sequence is that the time delays influence both the pressure at failure and the boiling process within the remaining liquid. If the contents are experiencing a continued increase in pressure despite the additional relief provided by the crack the contents will be subcooled and there will be few bubble nuclei within the bulk. If the pressure was, however, constant or falling the contents would have many uniformly distributed bubbles within the bulk fluid. Upon catastrophic LOC, and the liquid's abrupt depressurization and superheating, the immediate behavior of the internal bubbles can play a significant role in the consequent development of the fireball, since the now high pressure, bubbles will expand and burst, shattering completely their surrounding superheated liquid host, and result in a fine mechanically distributed high velocity evaporating aerosol. Any fireball formed from such a rapidly developing droplet cloud can involve the **total** contents of the vessel and not just the adiabatic flash fraction usually presumed [19]. The nearly instantaneous nature of its deflagration could also develop significant over-pressures such as noted in [18].

Fireball characteristics (sizes, durations and surface emissive powers (SEP)) should thus be functions not only of the mass of the liquid involved [19] but also the time delay from LBB initiator to final LOC and whether the LOC occurs with the contents still increasing in pressure and prior to the liquid contents becoming homogeneous. If vessel LOC occurs with a stratified liquid layer, a sub-cooled core, and increasing pressure the fireball should be less buoyant and have an appreciable flash fraction and/or rain-out and thus a lower SEP than in a case with dropping pressure and thus homogeneous boiling.

Whether the vessel fails completely, as a result of severe 'quenching' of the superheated vapor-space metal, the imposed thermal stresses or the 'dynamics', ie. the water-hammer like impact of the swell upon the already damaged shell and its fracture mechanic 'criticality', the time scales for the two-step process envisaged could range from the near 'zero' to 10's of milliseconds (for an immediate quenching case) to the 10's of seconds (for the mist-flow cooling case). Indeed two-step failures have been noted previously but not explained [12].

Clear examples of all of the above types of BLEVEs may be seen here in this re-examination of the HSL's 2-tonne propane jet fire (JIVE) test records. This information has been supplemented by additional analyses involving physical as well as macro and metallurgical examinations of the tank remnants, frame by frame analysis of the video records and a comprehensive thermo-hydraulic interpretation of the data [21].

## Introduction

As part of the Commission of the European Community (CEC) Science and Technology for Environmental Protection (STEP) programme and with the United Kingdom Health and Safety Executive's (HSE) Technology and Health Sciences Division sponsorship, a joint project (STEP-CT90-098) was set up to investigate the hazard consequences of Jet-fire Interactions with Vessels containing pressurized liquids (JIVE). The HSE's Health and Safety Laboratory (HSL) was contracted to investigate the thermal response of propane tanks when subjected to jet-fire attack and to assess the

effectiveness of mitigation techniques.

The Process Safety Section undertook four field experiments on the thermal response of partially filled two tonne horizontal propane tanks to a jet fire. The jet fire consisted of an ignited, horizontal flashing liquid propane jet at a flow rate of about 1.5 kg/s from a nozzle equivalent to a 12.7 mm diameter hole. The nozzle was placed 4.5 m from the front surface and 1 m below the axial center of the tanks at about the still-air lift-off position of the flame.

The target tanks were standard 1.2 m diameter 4546 liter water capacity (3864 liter propane (85%)) LPG vessels just over 4 m long with semi-ellipsoidal endcaps. The center barrel was 3.276 m long and was constructed of two rolled and longitudinally butt welded plates with a band reinforced circumferential butt weld. The walls were 7.1 mm thick low carbon steel. The tanks were fitted with standard sized (1 1/2" NTP ASME/BS 500 3090) pressure relief valves.

All vessels were fitted with external wall thermocouples (3 mm stainless steel sheathed type K). Interior fluid temperatures, vapor and liquid, were measured on several levels at a single, near central, vertical position corresponding to the fill-level gauge connection with similar, though 1.5 mm, thermocouples. Both vapor and liquid pressures were determined from remote calibrated pressure transducers. The target tank was mounted on a frame supported on four fire protected load cells; these were used to determine the variation in propane mass with PRV action<sup>2</sup>.

All transducers were monitored using a remote computer data acquisition system. There were separate video (2 to 5 cameras) recordings made as well as infra red thermal image records of the fireballs formed. British Gas made wide- and narrow- angle thermal radiation measurements [22].

Commercial grade propane was utilized for both the jet fire fuel and tank contents. Vessel fills of 20, 41, 60, and 85 volume percent were examined under jet fire attack of an ignited flashing discharge of sub-cooled liquid propane at about 0.9 MPa.

Separate HSL documents [1-5, 8] and a video record [6] provide further detail and archive the data obtained. Further physical, macro and micro metallurgical examinations on the tank remnants in addition to extensive video and thermo-hydraulic analyses of the data sets were undertaken by the present author [21] in the preparation of this paper.

## Results

All vessels failed catastrophically in less than five minutes and resulted in Boiling Liquid Expanding Vapor Explosions (BLEVEs) and fireballs.

### *Vessel Failures*

A discussion of the results (Figures 1 to 4), derivations (Tables 1 to 3 [21]) and interpretations of these experiments follows. Examination of the thermo-hydraulic data (Table 1) indicates that as fill level decreases time to first vent increases (multiple vents were observed for the 85% fill), the rate of pressure increase prior to vent decreases, the rate of pressure increase after continuous venting decreases and that the pressure at failure diminishes. Most of this behavior can be explained in terms of the variation in liquid wetted wall with fill level [11] though some observations are in conflict with other workers, most notably Birk [20].

The times to vessel failure are similar (251±28 seconds) all with comparable maximum and mean vapor wall temperatures (810 ± 74° and 611 ± 90°C, Table 2).

Table 3 [21] records measurements and comments on the appearance of the initial ruptures formed in these trials. The derived hoop stress and rupture crack stress intensity factors at commencement of failure are also shown.

<sup>2</sup> It should be noted that PRV discharge thrust indicates an apparent increase in mass.

*Individual Trial Results*

Representative and composite experimental results have been summarized in Tables 1 and 2. Some of the detailed data available for each trial is shown in Figures 1 to 4.

*20% full trial (Tank C [3], Fig. 1)*

In this trial, a 1.52 kg/s flashing liquid propane jet fire brought the 20 % full two tonne propane tank, initially containing 453 kg of commercial propane, to failure after 250 seconds. The PRV opened at a pressure of 18.6 barg at 112 s and then remained partially open, venting its contents at the rate of 1.26 kg/s. At failure the pressure fell to 16.5 barg with a maximum recorded shell temperature of 870°C. Vessel failure was initiated by a longitudinal rupture just to the back side of the top of the tank. This crack was 556 mm long (Table 3) and commenced forming about 635 mm to the right of the left endcap weld some 200 mm circumferentially behind the top. Visual and video observations indicated that when the PRV operated this gave a vertical jet of flame approximately 10 m high with a lift-off distance of about 2 m. After 250 seconds the tank failed catastrophically at a pressure of 16.5 barg as this was slowly falling.

The composite figures of pressure, mass, internal fluid and exterior shell temperatures indicate that at approximately 197 s the recorded pressures (Figure 1(a)) gradually commence falling from 17.2 barg, where they had been constant for over 50 s, until at failure they were 16.5 barg. About the same instant, however, all internal temperatures (Figure 1(b)) rise at least 10 C° in about 8 s and then fall to regain their previous values or trends. All these factors, in addition to the video record, strongly suggest that an initiating fracture developed, and the additional relief provided by its opening, allowed the valve to close; hence the momentary (approximately 16 s) excursion in internal temperatures. These observations suggest that a rupture crack formed around this time and then remained stable for some 40 s prior to catastrophic failure of the vessel by a fast (< 50 ms, ie. one video frame) shear fracture. The time average examination of the video records [6] undertaken by this author [21] confirms this since the films, for all camera angles, show a 6 second period where there is a reduction in flare size and intensity for this interval; such a period very much exceeds the prior and later turbulent flare fluctuations.

The additional depressurization caused by such a mechanism also helps explain the increase in liquid wetted wall temperatures of some 50 C° commencing 40 seconds prior to failure (Figure 1(c)); the progressive reduction in pressure, due to the additional area for discharge, causes more vigorous boiling and an increase in the fluid-wall temperature difference. There was a failure of the automatic recording system for mass and so this record (Figure 1(d)) was logged manually thus little detail can be inferred from the record.

*41% full trial (Tank A [1], Figure 2)*

A 1.38 kg/s flashing liquid propane jet fire brought the 40.9 % full two tonne propane tank, originally containing 926 kg of commercial propane, to failure in just less than 5 minutes. The PRV opened at a pressure of 18.8 barg at 130 s and then remained open, venting its contents at the rate of 1.41 kg/s. The failure pressure was 21.3 barg with a maximum shell temperature of just over 700°C was located near the center top of the shell. Vessel failure was initiated by a longitudinal rupture near the top of the tank. This opening, which was originally 356 mm long, commenced forming about 420 mm to the right of the center weld and some 250 mm circumferentially forward of the top. Visual and video observations indicated that when the PRV operated this gave a vertical jet of flame approximately 10 m high with a lift-off distance of about 2 m. The flare increased in size and intensity after 250 s and the tank failed catastrophically at 285.5 seconds.

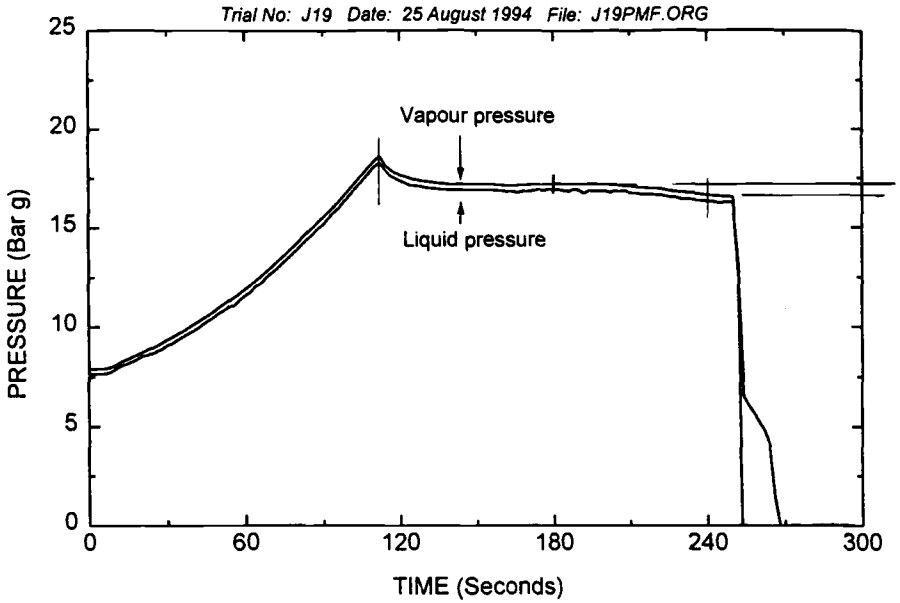


Figure 1(a). Composite results, 20% fill (Tank C): pressure.

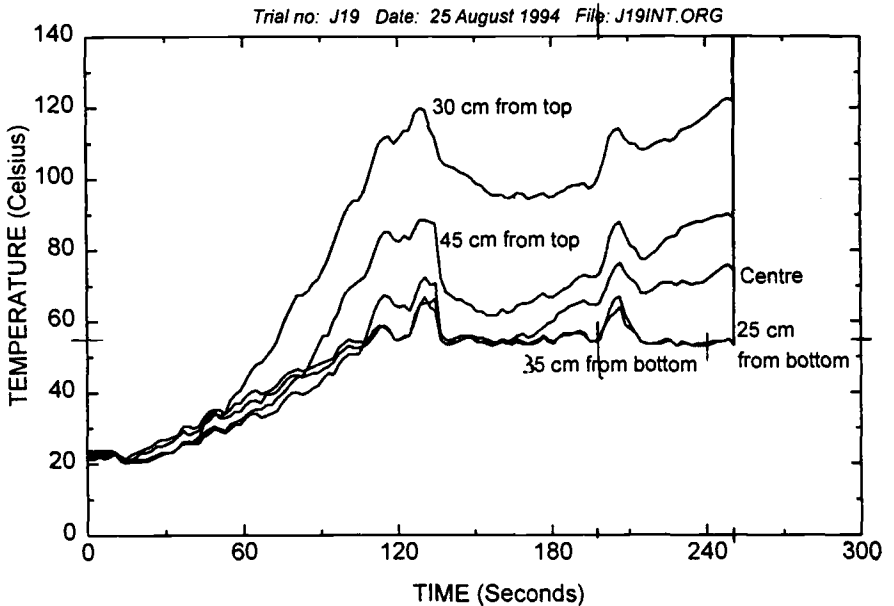


Figure 1(b). Composite results, 20% fill (Tank C): internal temperatures.

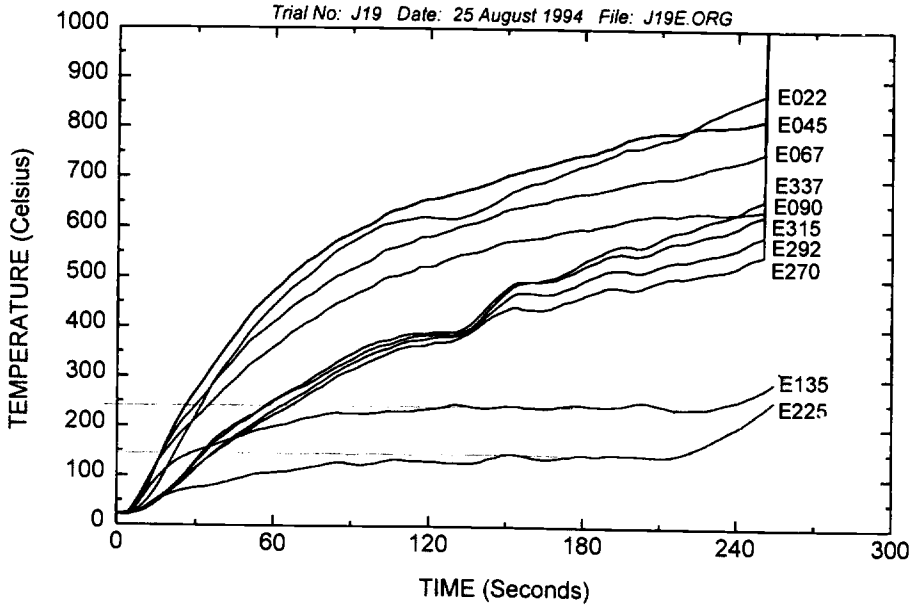


Figure 1(c). Composite results, 20% fill (Tank C): wall temperatures.

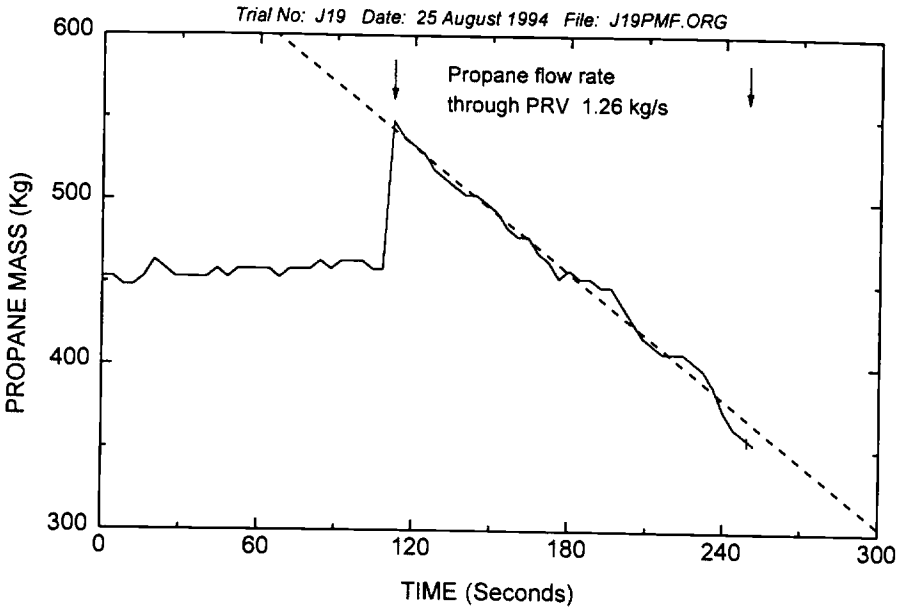


Figure 1(d). Composite results, 20% fill (Tank C): mass.

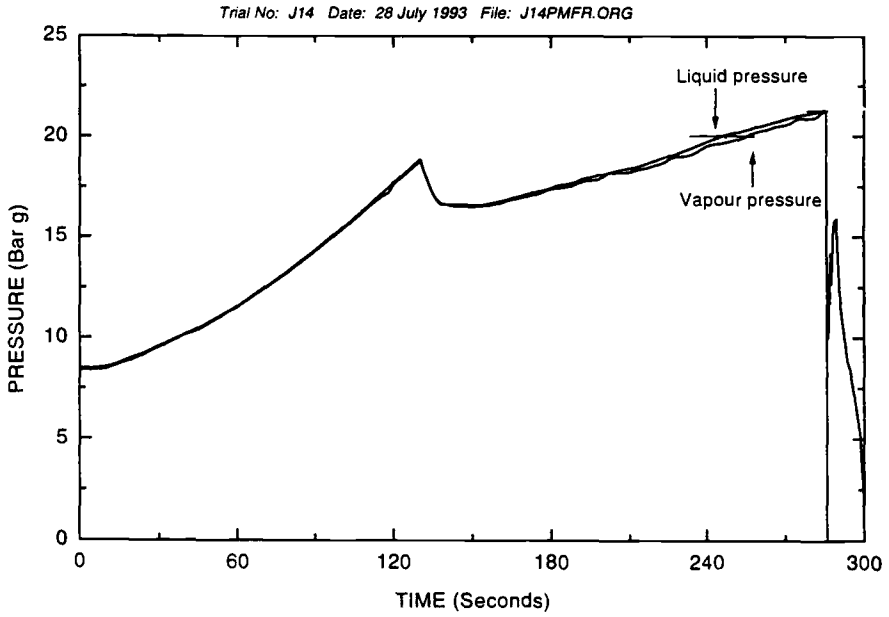


Figure 2(a). Composite results, 41% fill (Tank A): pressure.

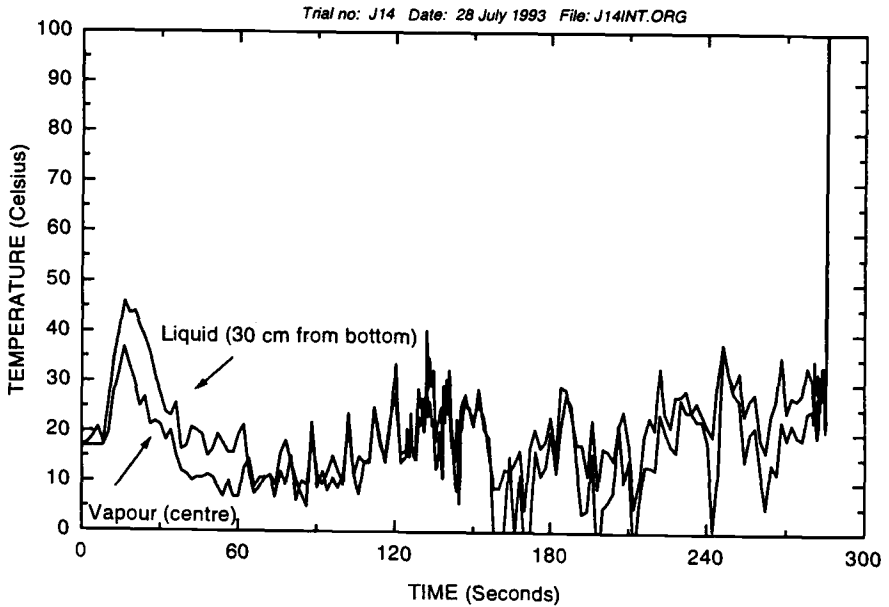


Figure 2(b). Composite results, 41% fill (Tank A): internal temperatures.

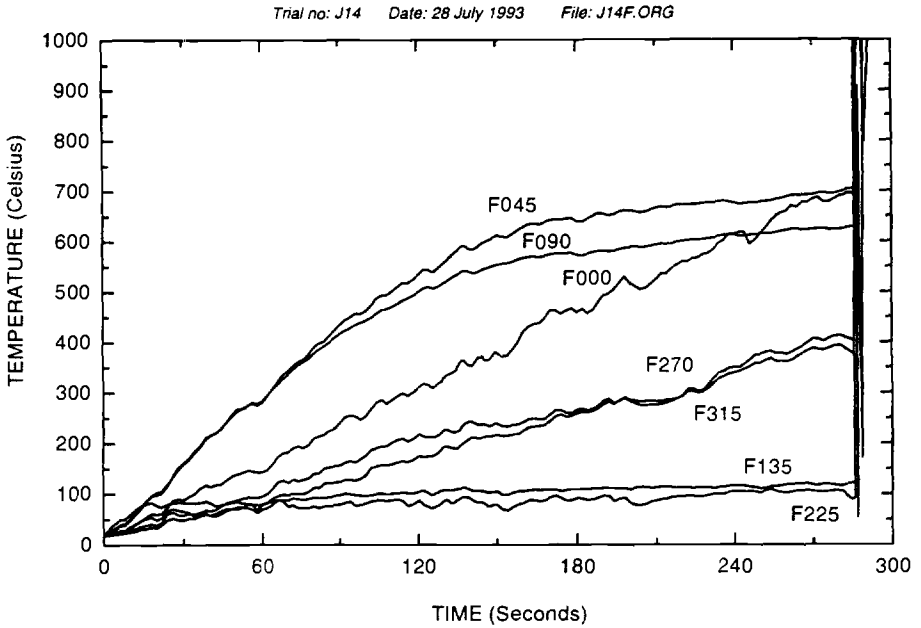


Figure 2(c). Composite results, 41% fill (Tank A): wall temperatures.

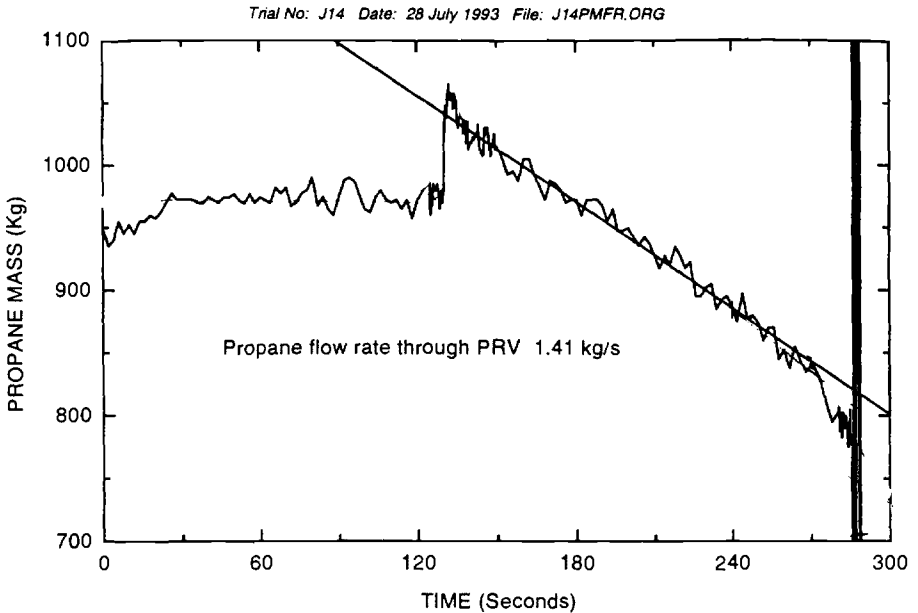


Figure 2(d). Composite results, 41% fill (Tank A): mass.

The composite figures of pressure, temperatures, both interior fluid and exterior shell, Figure 2, indicate that at approximately 250 s there is an inflection point in the recorded liquid pressure (Figure 2(a)) and its rate of increase diminishes. Further, commencing at about the same time there is a progressive increase in the mass flow rate recorded (Figure 2(d)). This is sufficient to suggest that the discharge rate has doubled to over 2.8 kg/s and that the mass at failure is less than the 710 kg noted in [1]. These observations, taken with those determined from a frame by frame analysis of the visual record [21] indicates an increase in PRV flare size and intensity at 250 s, suggesting again that a rupture crack formed around this time and then remained stable for some 30 s prior to catastrophic failure of the vessel by a fast plain stress shear fracture.

Additionally, but perhaps less convincing, evidence comes from the audio track from the video [6]. Here the intensity and pitch of the PRV discharge drops in level at about the same instance as the flare increases in intensity. This observation provides some confirmation to firemen's anecdotal adage when dealing with fires involving PLG's that "when you hear a reduction in pitch of the PRV discharge, run like Hell!".

#### *60% full trial (Tank B [2], Figure 3)*

In this experiment, a 1.59 kg/s flashing liquid propane jet fire brought the 60 % full two tonne propane tank, originally containing 1364 kg of commercial propane, to failure in 217 seconds. The PRV opened at a pressure of 18.1 barg at 109 s and then remained open (Figure 3(a)), venting its contents at the rate of about 0.85 kg/s. There is some evidence to suggest that there was significant entrainment of liquid propane into the valve since the recorded flow rate (Figure 3(d)) is about half that of the earlier trial; as well, in the initial stages of discharge there is an extremely low flow rate. At failure the pressure was 18.6 barg with a maximum recorded shell temperature of just under 800°C (Figure 3(c)). Vessel failure was initiated by a complex series of longitudinal rupture cracks near the top of the tank [21]. These cracks had a combined feather-edged length of some 580 mm and commenced forming about 1200 mm to the right of the center weld and on the top center of the vessel.

Visual and video observations indicated that when the PRV operated this gave a vertical jet of flame approximately 10 m high with a lift-off distance of about 2 m. At 217 s the tank failed catastrophically at a pressure of 18.6 barg. On failure, the tank split into three sections with about the left hand two thirds of the vessel rocketing 447 m, an end cap being thrown 309 m and approximately one third of the barrel opening out flat in the target area.

The composite figures of pressure, mass, internal fluid and external surface temperatures, indicates that at approximately 190 s the recorded liquid and vapor temperatures (Figure 3(b)) all dropped some 20°C in about 15 s and then slightly recovered some 10°C just at failure. Ten seconds prior to failure the propane mass flow rate (Figure 3(d)) increases to about double its previous value; ie. 1.6 kg/s. These observations, all suggest that an opening developed during this time period and the crack so formed remained stable for some 15 s prior to catastrophic failure of the vessel by a fast shear fracture which bifurcated and caused two pieces of the tank to rocket off significant distances.

#### *85% full trial (Tank D [4], Figure 4)*

In this last experiment, a 1.68 kg/s flashing liquid propane jet fire brought the 85 % full two tonne propane tank, initially containing 1932 kg of commercial propane, to failure in 254 seconds. The PRV opened at a pressure of 18.6 barg after 68 s and then cycled open and partially shut at least two times before remaining open (Figure 4(a)), venting its contents at the rate of approximately 1.28 kg/s. At failure the pressure was 24.4 barg with a maximum recorded shell temperature of just under 850°C (Figure 4(c)).

24.4 barg with a maximum recorded shell temperature of just under 850°C (Figure 4(c)). Vessel failure was initiated by a small longitudinal rupture near the top of the tank. This crack, which was 290 mm long, commenced forming about 880 mm to the left of the center weld and about 50 mm circumferentially forward of the top.

Visual and video observations indicated that when the PRV operated this gave a vertical jet of flame approximately 10 m high with a lift-off distance of about 2 m. After 254 seconds the tank failed catastrophically.

The composite figures of pressure, mass, internal fluid and external shell temperatures, indicates no unusual characteristics in the recorded parameters such as were noted previously in the other trials. However, a detailed frame by frame analysis of the video records [21] clearly shows that the fast fracture phase of vessel failure was preceded, by about 1 second (approximately 25-30 video frames), with the formation of a crack which permitted a vapor and then two-phase discharge to occur through the rupture. These video frame sequences seem again to confirm that a two stage process of rupture crack formation and arrest occurs prior to catastrophic failure of the vessel by a fast plain stress shear fracture.

TABLE 1. Thermo-hydraulic Response of Vessels.

Tank (% Volume)	C(20)	A(41)	B(60)	D(85)			
1. Valve operation							
(a) cycles	1	1	1	1	2	3	open
(b) (P/T) <sub>initial</sub> (barg/°C)	7.9/19	8.4/20	7.7/20	8.7/18			
(c) P <sub>open</sub> (barg)	18.6	18.8	18.1	18.3	16.0	14.8	
(d) P <sub>close</sub>	17.2	16.5	14.1	13.9	-		
2. Pressurization (dP/dt)							
(a) before valve open	0.095	0.092	0.106	0.15	-	-	-
(b) after valve open	-ve	0.035	0.047				0.022

TABLE 2. Vessel Thermal Response at Failure.

Tank (Volume %)			C(20)	A(41)	B(60)	D(41)
Tank-wall thickness (mm)			7.1	7.5	7.1	7.1
Liquid space metal temperatures (°C)			257±47	141±68	116±24	159±27
Vapour space metal temperatures (°C)	Front	T <sub>mean</sub>	711±93	645±46	559±49	734±89
		T <sub>min</sub>	516	573	485	644
		T <sub>max</sub>	870	704	641	848
	Back	T <sub>mean</sub>	564±86	424±136	646±94	663±112
		T <sub>min</sub>	479	304	531	508
		T <sub>max</sub>	697	694	798	848
4. Failure Pressure (barg)			16.5	21.3	18.6	24.4

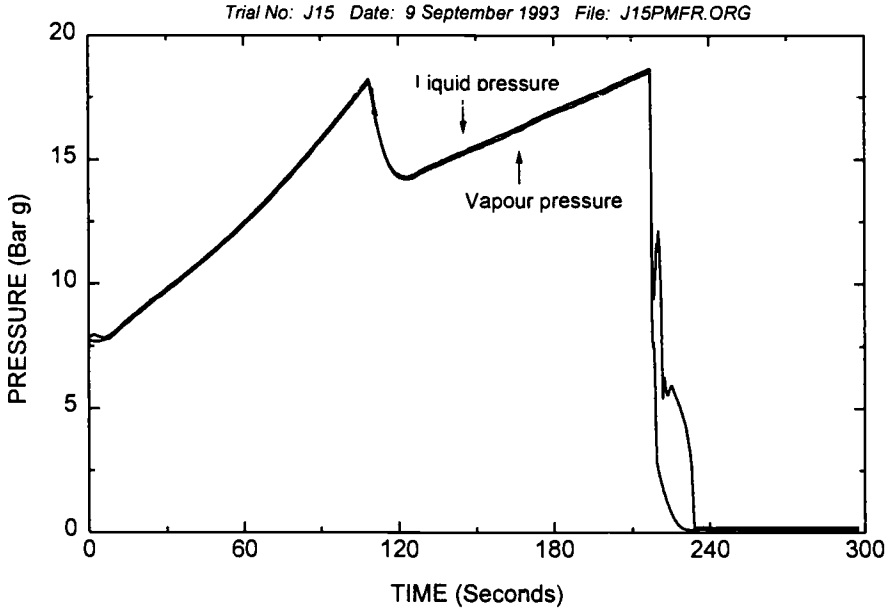


Figure 3(a). Composite results, 60% fill (Tank B): pressure.

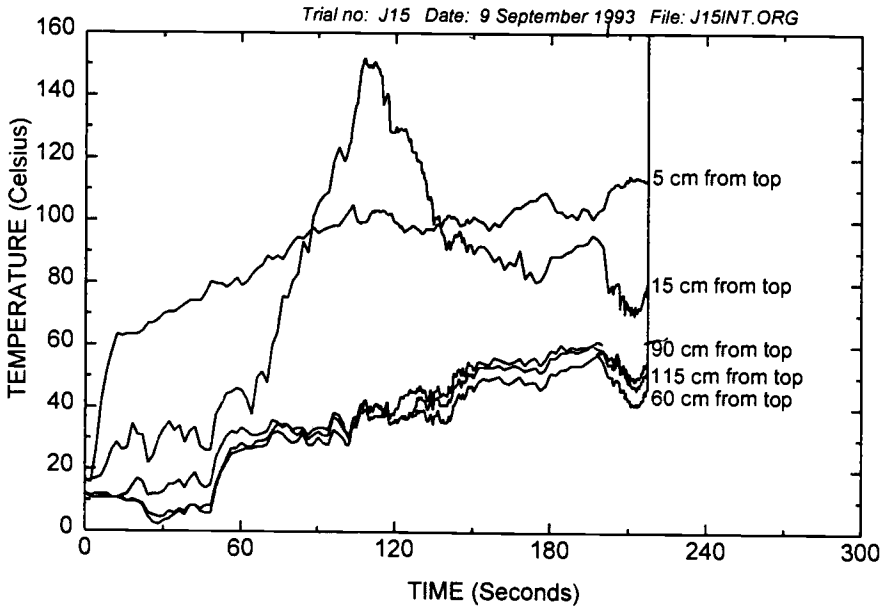


Figure 3(b). Composite results, 60% fill (Tank B): internal temperatures.

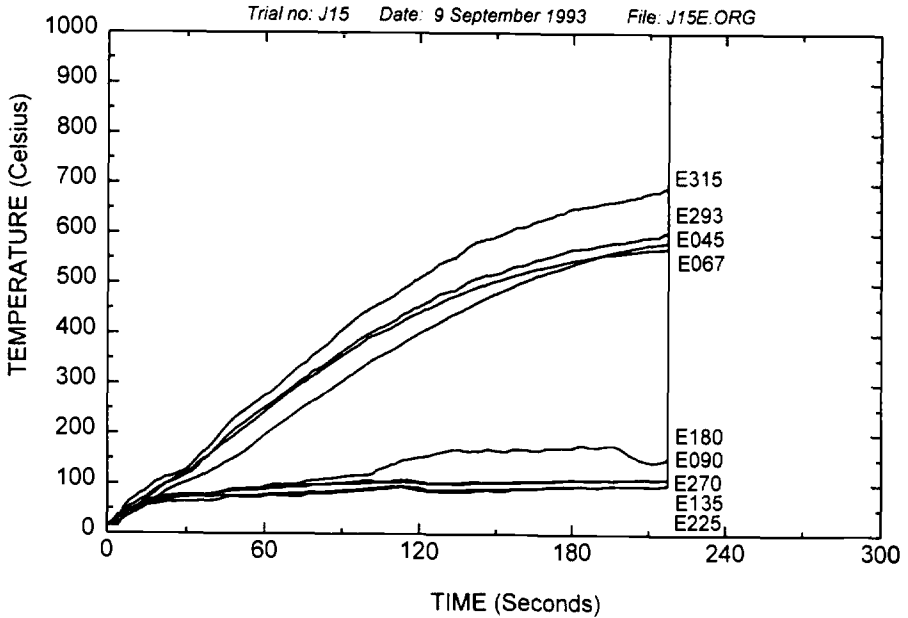


Figure 3(c). Composite results, 60% fill (Tank B): wall temperatures.

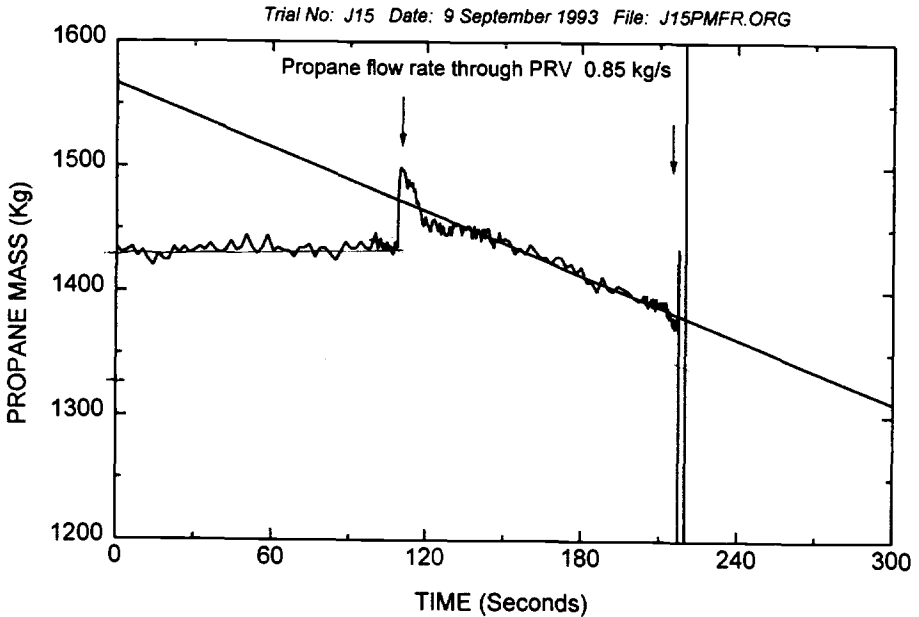


Figure 3(d). Composite results, 60% fill (Tank B): mass.

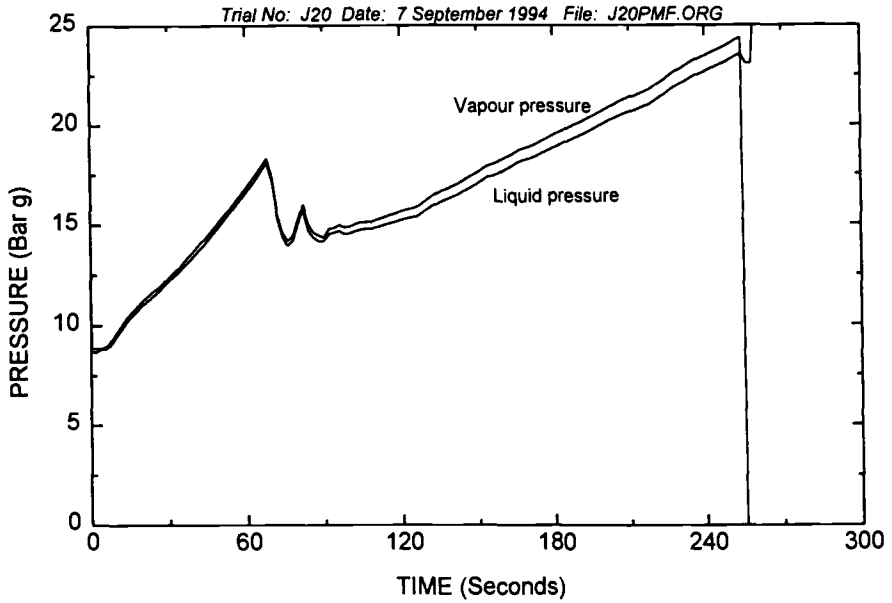


Figure 4(a). Composite results, 85% fill (Tank D): pressure.

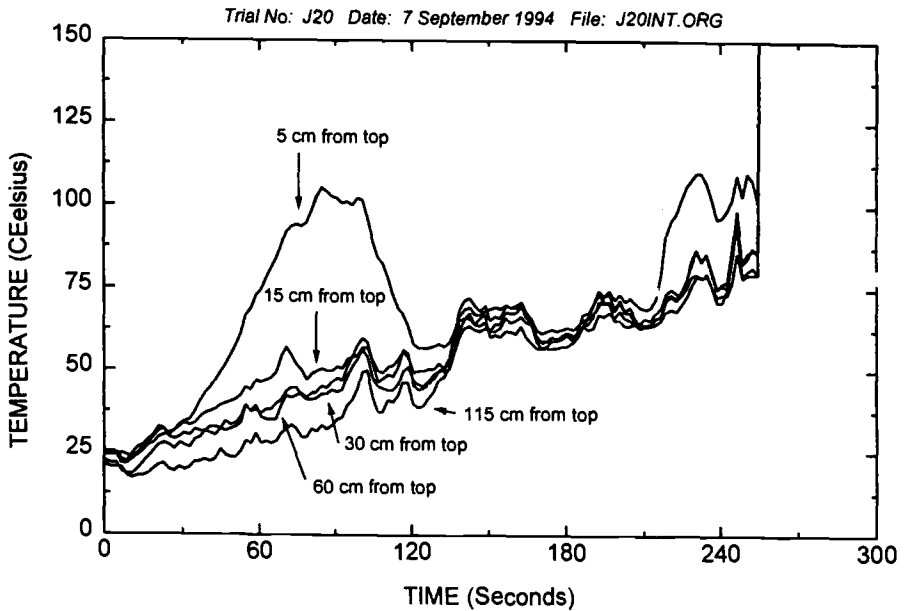


Figure 4(b). Composite results, 85% fill (Tank D): internal temperatures.

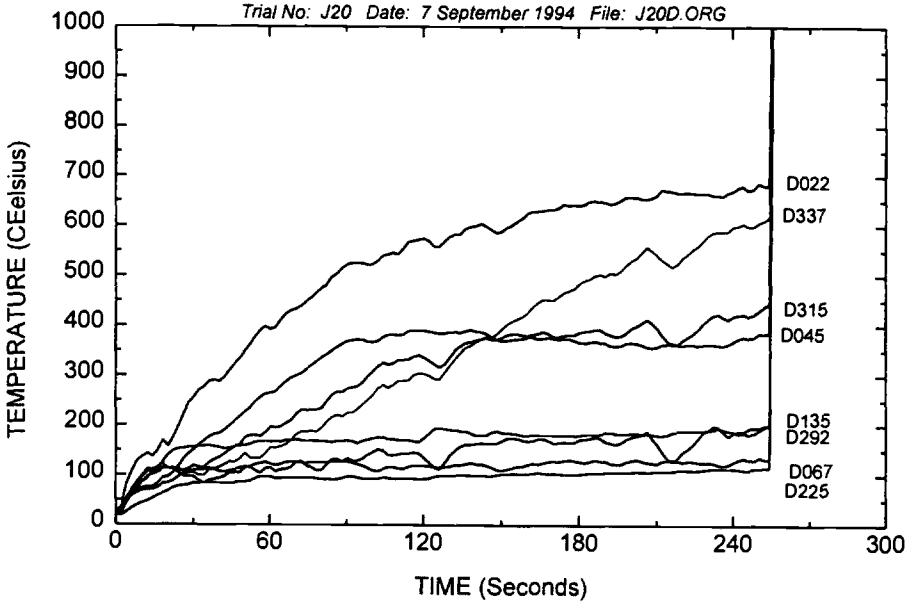


Figure 4(c). Composite results, 85% fill (Tank D): wall temperatures.

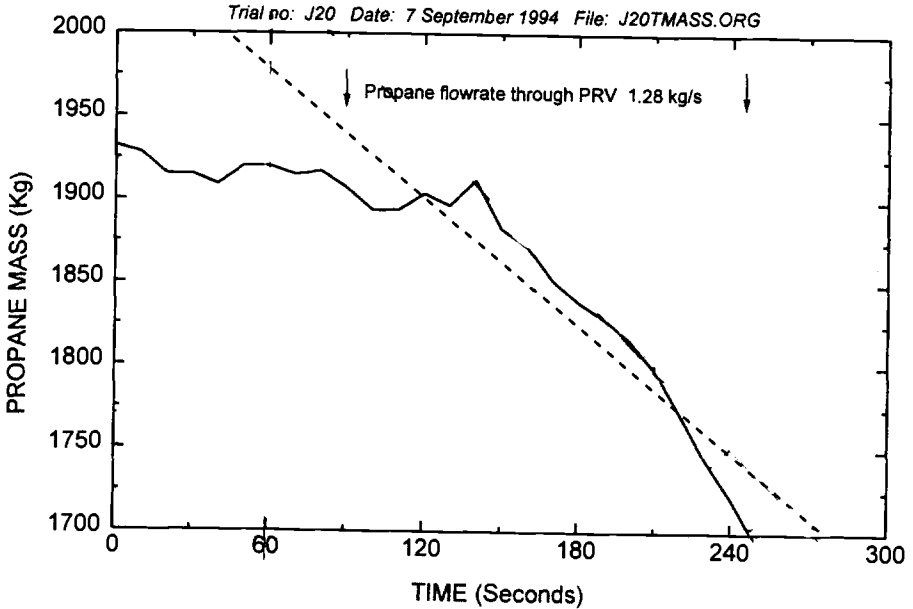


Figure 4(d). Composite results, 85% fill (Tank D): mass.

TABLE 3: Initial crack sizes, failure stresses and stress intensity factors [21].

Tank	$P_f$ (barg)	t (mm)	$\sigma$ (Mpa)	$a_c$ (mm)	$K_I$ (MPa $\sqrt{m}$ )
C(20%)	17.2	7.1	145	278	166
A(41%)	20	7.5	160	178	146
B(60%)	17.5	7.1	148	290	174
D(85%)	24	7.1	203	145	168
mean					164 ± 12
Legend: $P_f$ = initial failure pressure; t = wall thickness; $\sigma$ = hoop stress; $K_I$ = equivalent elastic stress intensity factor ( $K_I = Y\sigma\sqrt{\pi a_c}$ ); $2a_c$ = size of crack					

#### Summary of the results and their interpretation

The thermo-hydraulic evidence and video film analyses summarized above indicates that crack development and propagation during vessel failure occurred in two distinct steps:

- 1.) a rupture stage, where a crack opens up and becomes stable forming an opening for a vapor or two-phase jet discharge additional to that of the PRV, and
- 2.) a final fast fracture stage, where the initial crack rapidly propagates into the metal as a plain stress shear failure along (usually) the entire length of the tank and then circumferentially at the end caps.

The consequence of this type of failure is called a BLEVE (Boiling Liquid Expanding Vapor Explosion). The process causes the remaining contents of the vessel to be rapidly released as a superheated liquid aerosol which may then ignite and form a fireball.

Why does the initiating crack arrest and what causes it to be restart as a fast fracture? What is the influence of this failure mode on the characteristics of the fireballs formed? These are questions that are next addressed.

#### Metallurgical Examination of Fracture Surfaces and other Points of Interest [21]

Vapor wall metal temperatures (Table 2) are extremely variable due to the impact of the jet fire. It was not unusual for temperatures to drop locally by up to 150°C away (< 500 mm) from the initial rupture. Metal strength would thus be affected and any over-pressure crack formed could arrest in this cooler, stronger and tough wall as the vessel unloads due to the local depressurization.

The plastic deformation of all cross sections taken from the initiating crack exhibit a progressive area reduction, with greater amounts occurring on the heated side [21]. This can be attributed to wall thinning and bulging while under the initial biaxial stress state imposed by the internal pressure.

Macro and micro-metallographic examination of metal samples taken near the originating rupture crack tips for three of the four experimental tanks were conducted in order to try to find evidence of quenching such as might be responsible for re-initiation of the arrested cracks.

The contact fluid (two-phase propane) and its cooling rate as well as the hardenability of the steel were such that the micrographs did not show any direct signs of quenching (ie. transformation products, martensite or bainite).

The B (60% fill) tank samples, however, indicated a circumferential rolling direction for the plate forming the section of the barrel where the cracks originated. The originating ruptures formed in this section and may possibly be linked to the early crack bifurcation which was unique to this trial. This process caused the tank to circumferentially separate and rocket nearly 450 meters. Two samples from tank B were taken to observe the region of crack bifurcation. Metallographic examination of this point did not yield any other differentiating features (ie. large inclusion, voids, etc.) in the surrounding grain structure that may have been a direct cause of the bifurcation.

#### *Vicker's Micro-hardness Measurements*

A Leitz **MiniLoad** microhardness tester was used evaluate the hardness of the polished samples cut from the lips of the initial fractures as a function of position [21]. The most reproducible results, consistent with the determination of local effects, were obtained with a load of 100 p. This gave indentation diagonals of 25 to 35  $\mu\text{m}$ . Hardness features located from up to 100  $\mu\text{m}$  from the edges could thus be determined.

There was a general increase in hardness for all samples to its fracture edge. From the central region of the plate values of between 170 to 180 VH were obtained. At the tips of the lips measurements increased to over 200 VH; values as great as 237 VH were obtained within 100  $\mu\text{m}$  of the fracture tips for specimens cut from tanks C and D. No significant differentiation in the transverse directions could be detected that would indicate a greater or lesser cooling of one side relative to the other.

The difference in hardness possible due to quenching in different fluids with this steel was next evaluated. Spare sample coupons, cut from the tanks, were heated in a muffle furnace to 840°C for 4-5 minutes and then quenched or air cooled. Some samples were quenched in water others in R11 (Freon 11). Full cooling of the sample was achieved in less than 15-30 seconds with water; in R11 this required 70-90 seconds. The re-wet, or initiation of film-transition boiling point, also exhibited similar periods. The relevant thermo-physical properties (thermal conductivity of both the liquid and vapor and latent heat) of water are greater, by an order of magnitude, than those for propane or R11. The same properties are comparable between liquid R11 (at atmospheric pressure) and propane at its containment conditions in the HSL experiments. The vapor thermal conductivity for propane at its release condition is, however, greater than twice that for the R11 vapor at atmospheric pressure [14]. A comparison of the cooling times to the re-wet point and the subsequent extremely rapid quench, due to transition and then CHF boiling in propane, would therefore expected to be halved.

The results of these experiments yielded hardness values of about 480 VH for the water quench and 187-200+ VH for the R11 quench. Air cooled samples, taken from the furnace at the same times, gave hardness readings of between 160-170 VH. The hardness and the microstructure of the water quenched samples indicate the severe quench of a steel with about 0.2-0.3 %C as is appropriate for such a pressure vessel. The similarities in hardness achieved with R11 and those recorded at the crack tips of the HSL samples are not at all inconsistent with the quenching mechanism proposed as the possible initiator for the fast fracture phase of tank failure. Since one could expect even higher rates of quenching due to the differences in physical properties between R11 and propane and the velocity and impact of any two-phase discharge (with fills greater than about 20 percent) larger hardness values at the creep crack lips would be anticipated. The relative variations in hardness values observed support this interpretation.

There was significant variability in the transverse hardness of samples taken from tank B consistent with what would be expected for the transverse rolling direction noted for this sheet. This would suggest local variations in strength that may have been

sufficient to cause the developing ruptures to split and perhaps bifurcate in regions of reduced strength. Such a process would support the observations of the circumferential splits observed along the developing longitudinal rupture that eventually allowed one end of the vessel to separate and rocket off.

#### *Fireball Characteristics*

The fireball characteristics, [5, 8] (Table 4), show that as the mass of material involved in the BLEVE increases, the duration and size of the fireball becomes larger; however, its shape becomes less spherical and more vertically elongated. From the video analyses [21] it is also apparent that there is a greater ground flash fraction for large fills and these require significant times before ignition. The mean Surface Emissive Powers (SEP) of the fireballs, at their maximum size, also decrease despite the significant increases in saturation pressure, and thus liquid superheat of the contents. The 85% fill fireball develops much slower and exhibits both an average and a top 10% SEP that is nearly 20% less than that exhibited in the 20% fill experiment.

TABLE 4. HSL JIVE BLEVE fireball characteristics.

Tank and Fill (%)	Mass (kg)	SEP (kW/m <sup>2</sup> )		duration (S)	diameter (m)	Height (m)
		mean	max			
C(20)	279	410	640	3.5	45	45
A(41)	710	278*	484*	5.5	45	70
B(60)	1272	365	550	6.5	55	75
D(85)	1708	350	580	7.0	45	45

\*British Gas Measurements

#### **Discussion**

The analyses and interpretations of the HSL JIVE tank failure data present a coherent and plausible case that can best be explained by the formation of a fracture which arrests and then is re-initiated for some reason and/or now becomes critical. For the transitions to fast fracture that were observed in all the experiments, there must be some physical reason for crack re-initiation. Once cracks are arrested in a ductile material, re-initiation requires significant further energy. It is our view that the thermo-hydraulic, video and physical data support a crack tip quenching mechanism as the most probable cause; the metallurgical data for this is less conclusive, however.

Taken together the situation described is not unlike that envisaged in the highly transient 'rewet' situation in forced convective boiling; however, it now occurs within a stressed and damaged pressure vessel. The dependence of the time delay on liquid fill would appear to be a function of the heat transfer and the distance to the boiling surface. Due to entrainment, flow through the crack could be mist/droplet two-phase flow in the case of low fills; for fills greater than 50 percent impact of the two-phase swell on the hot vapor space walls, as a result of the additional pressure relief from crack formation, is possible [15]. This discharge situation would be similar to a 'churn-turbulent bubbly' flow impacting upon the vessel's hot head space; very rapid cooling of the metal surface could therefore take place due to direct liquid-metal contact.

The influence of such a two-step vessel failure on fireball formation is significant. Some of the observations made here contradict earlier works based upon results from single step failures [7, 19] and thus will have importance to the development of realistic fireball and BLEVE models.

### Conclusion

The thermo-hydraulic, physical and metallurgical evidence presented supports the hypothesis that the catastrophic vessel failures leading to the BLEVEs observed were preceded by an initiating, mostly longitudinal, overpressure rupture crack which arrested in the hot ductile vapor space metal. The location of this point is thought to be where the stresses at the crack tip equalled the local yield stress in the less ductile but still very tough, cooler metal. These cracks are then thought to be reactivated as fast fractures that result in the complete loss of containment of the contents in less than one video frame, i.e. about 50 milliseconds. A possible reason for crack re-initiation is considered to be the thermal tensile stress at the crack tip brought on by rapid quenching of this area by its two-phase discharge.

The failure mode of the vessel and its thermo-hydraulic state exerts a significant influence on the BLEVE process and any fireball formed.

A possible connection between rolling direction and circumferential crack bifurcation was indicated for one trial.

### Acknowledgement

The experimental field work described here was performed as part of the Commission of the European Community (CEC) Science and Technology for Environmental Protection (STEP) program and with the United Kingdom Health and Safety Executive (HSE) Technology Sciences Division sponsorship. The programme (STEP-CT90-098) investigated the hazard consequences of Jet-fire Interactions with Vessels containing pressurized liquids (JIVE). Dr. T.A. Roberts, HSL, Buxton, provided access to the data sets and gave permission for the removal of samples and the metallurgical examinations. Marc LeBlanc helped in the preparation and analyses of the metallographic and hardness specimens. Dr. C. Thornley, New Brunswick Research and Productivity Council, assisted in the examination and analyses of the metallographic samples. The views and interpretations put forward in this report are those of the author alone.

### References

1. Roberts, T., Beckett, H., Cooke, G. & Brown, D.; "Jet fire impingement trial on a 41% full, unprotected, 2 tonne propane tank", HSL Report R04.029, IR/L/PH/95/11, Buxton, UK, July, 1995.
2. Roberts, T., Beckett, H., Cooke, G. & Brown, D.; "Jet fire impingement trial on a 60% full, unprotected, 2 tonne propane tank", HSL Report R04.029, IR/L/PH/95/12, Buxton, UK, Aug., 1995.
3. Roberts, T., Beckett, H., Cooke, G. & Brown, D.; "Jet fire impingement trial on a 20% full, unprotected, 2 tonne propane tank", HSL Report R04.029, IR/L/PH/95/13, Buxton, UK, Oct., 1995.
4. Roberts, T., Beckett, H., Cooke, G. & Brown, D.; "Jet fire impingement trial on a 85% full, unprotected, 2 tonne propane tank", HSL Report R04.029, IR/L/PH/95/14, Buxton, UK, Oct., 1995.

5. Hawksworth, S.J. and Brearley, D.; "Thermal Imaging of propane fireballs as part of the hazardous consequences of jet-fire interactions with vessels containing pressurised liquids project", HSL Report R04.029, IC/06/01, Feb., 1996.
6. Nind, M.J.; "Video record BLEVE Tests (Great Longstone); all camera views from ignition to explosion", HSL Visual Presentation Services, Sheffield, UK, January, 1995 and video July 1996.
7. Johnson, D.M., Pritchard, M.J. & Wickens, M.J., "Large Scale Catastrophic Releases of Flammable Liquids", British Gas Report to the CEC, 1990, Contract EV4T.0014.UK.
8. Roberts, T & Beckett, H.; "Hazard Consequences of Jet-fire Interactions with Vessels Containing Pressurised Liquids: Project Final Report", HSL Report R04.029, PS/96/03, Buxton, UK, Feb., 1996.
9. Birk, A.M. & Cunningham, M.H., "The Boiling Liquid Expanding Vapour Explosion", *J. Loss Prev. Process Ind.*, 7, 6, 1994, pp. 474-480.
10. Venart, J.E.S., Rutledge, G.A., Sumathipala, K. & Sollows, K.; "To BLEVE or Not to BLEVE: anatomy of a Boiling Liquid Expanding Vapor Explosion", *AIChE Process Safety Progress*, 12, 2, April 1993, pp. 67-70.
11. Sumathipala, K., Hadjisophocleous, G., Aydemir, N., Yu, C., Sousa, A., Steward, F. & Venart, J., "Fire Engulfment of Pressure-Liquefied Gas Tanks: Experiments and Modelling", *ASTM STP 1150, Fire Hazard and Fire Risk Assessment*, 1992, pp. 106-121.
12. Birk, A.M., "Scale Effects with Fire Exposure of Pressure-Liquefied Gas Tanks", *J. Loss Prev. Process Ind.*, 8, 5, 1995, pp. 275-290.
13. Sumathipala, K., Venart, J.E.S. & Steward, F.R., "Two-phase swelling and entrainment during pressure relief valve discharge", *J. Hazardous Materials*, 25, 1990, 219-236.
14. Huber, M., Gallagher, J., McLinden, M. & Morrison, G.; "NIST Thermodynamic Properties of Refrigerants and Refrigerant Mixtures Database (REFPROP)", Ver. 5.0, Feb. 1996, U.S. Dept. of Commerce, NIST, SRDP, Gaithersburg, MD.
15. Ramier, S., "Dynamic Top Venting of a PLG Vessel", MScE Thesis, Dept. of Mech. Eng., UNB, 1996.
16. McClintock, F.A. & Argon, A.S., (Eds.), "Mechanical Behavior of Materials", Addison-Wesley, Reading, MA, 1966.
17. Goodier, J.N.; "Thermal Stress and Deformation", *J. Appl. Mech.*, Trans. ASME, Sept. 1957, pp. 467-474.
18. Pietersen, C.M., "Analysis of the LPG-Disaster in Mexico City", *J. Hazard. Materials*, 20, 1988, pp. 85-107.
19. Roberts, A.F., "Thermal radiation hazard from releases of LPG from pressurised storage", *Fire Safety Journal*, 4, 1982, pp. 197-212.

20. Birk, A.M. & Cunningham, M.H., "Liquid Temperature Stratification and its Effect on BLEVEs and their Hazards", *J. Hazard. Materials*, 1996.
21. Venart, J.E.S., "HSL JIVE Tank Failures; Physical and Metallurgical Examinations", UNB Fire Science Centre report UNB FSC: R-96-09-23 (revised) Nov. 7, 1996.
22. Gosse, A.J. & Pritchard, M.J., "A study of the radiative characteristics of the fireball produced following the BLEVE failure of a pressurised LPG vessel; a record of measurements made by British Gas as part of a CEC co-funded research project", British Gas Report GRC R 1197, January 1996.

# **Marine Fires**

Jorman A. Koski<sup>1</sup>, Steven D. Wix<sup>1</sup>, and David E. Beene, Jr.<sup>2</sup>

## **EXPERIMENTAL MEASUREMENT OF A SHIPBOARD FIRE ENVIRONMENT WITH SIMULATED RADIOACTIVE MATERIALS PACKAGES**

---

**REFERENCE:** Koski, J. A., Wix, S. D., and Beene, D. E., Jr., “**Experimental Measurement of a Shipboard Fire Environment with Simulated Radioactive Materials Packages,**” *Very Large-Scale Fires*, ASTM STP 1336, N. R. Keltner, N. J. Alvares, and S. J. Grayson, Eds., American Society for Testing and Materials, 1998.

**ABSTRACT:** Results from a series of eight test fires ranging in size from 2.2 to 18.8 MW conducted aboard the Coast Guard fire test ship *Mayo Lykes* at Mobile, Alabama are presented and discussed. Tests aboard the break-bulk type cargo ship consisted of heptane spray fires simulating engine room and galley fires (across bulkhead assault), wood crib fires simulating cargo hold fires (direct assault), and pool fires staged for comparison to land-based regulatory fire results. Primary instrumentation for the tests consisted of two pipe calorimeters that simulated a typical package shape for radioactive materials packages. The calorimeters were both located adjacent to the fires and on the opposite side of the cargo hold bulkhead nearest the fire. The calorimeters were constructed from 1.5 m length sections of nominal 2 foot diameter schedule 60 steel pipe. Type K thermocouples were attached at 12 locations on the circumference and ends of the calorimeter. Fire heat fluxes to the calorimeter surfaces were estimated with the use of the Sandia SODDIT inverse heat conduction code. Experimental results from all types of tests are discussed, and some comparisons are made between the environments found on the ship and those found in land-based pool fire tests.

**KEYWORDS:** Ship fires, calorimeters, radioactive materials shipments, cargo fires

---

The safety of land transport of radioactive materials packages has been studied for many years. For example the “modal studies” [1] conducted during the 1980s considered truck and rail shipment of radioactive cargoes. Sea shipments of such cargoes, on the other hand, have not been studied to the same level of detail. In an effort to increase the knowledge of the possible fire exposure that a package might receive during sea transport, a series of eight shipboard fire experiments have been conducted aboard an actual break-bulk cargo ship. The tests were intended to measure a range of possible fire exposures for packages on ships, and give some basis for comparison to fires specified in current safety

---

<sup>1</sup> Sandia National Laboratories, Transportation Systems Department, MS-0717, Albuquerque, NM 87185. Sandia is a multiprogram laboratory operated by Sandia Corporation, a Lockheed Martin Company, for the United States Department of Energy under Contract DE-ACO4-94AL85000.

<sup>2</sup> United States Coast Guard Research and Development Center, 1082 Shennecossett Road, Groton, CT 06340-6096

regulations. This paper presents some key results from the tests. More detail in a report format, including plots of all data collected, is available in Reference [2].

Sea shipments of hazardous materials are governed by the International Maritime Dangerous Goods (IMDG) code [3]. For radioactive materials packages, the Irradiated Nuclear Fuel (INF) regulations [4] and the International Atomic Energy Agency Safety Series 6 regulations [5] must also be followed. Together these regulations limit the types of fires that must be considered during sea shipments. For example, the IMDG code specifies that for break-bulk freighters, a watertight bulkhead must separate radioactive cargo from flammable cargo. Thus, the most likely fires on this type of ship are fires with flammable materials in adjacent holds such as engine rooms, galleys and crews quarters, and combustible cargo fires in the same ship hold.

The tests were conducted aboard the *Mayo Lykes*, a World War II Victory class cargo ship, maintained by the United States Coast Guard at Mobile, Alabama, specifically for the purpose of fire testing. Two holds, Holds 4 and 5, at the aft end of the ship were selected for the tests. Level 1 of these holds, immediately below the weather deck, was used for all fires and measurements. In all cases the fires were set in Hold 4. Steel pipe calorimeters representing simulated radioactive materials packages were placed in both Holds 4 and 5. Fires consisted of ignited heptane sprays impinging on the steel bulkhead between Holds 4 and 5, and wood crib fires representing combustible cargo fires. The general experimental arrangement is shown in Fig. 1.

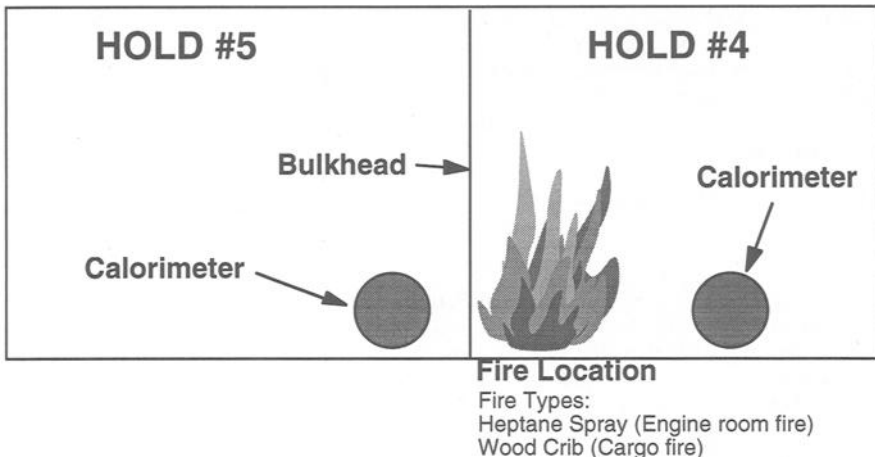


FIG. 1. Sketch of experimental configuration for heptane and wood crib fires.

Land based studies of fire accidents concentrate on the fully engulfing pool fire. This type of fire could occur, for example, if a truck transporting radioactive materials collided with a gasoline tanker truck with a resultant large gasoline spill. Packages for larger quantities of radioactive materials are designed and tested to withstand 30 minutes in a fully engulfing hydrocarbon fire. Filling a ship hold with flammable hydrocarbons with an adequate source of oxygen is a highly unlikely event, but for comparison to land based fires, a pool fire with a simulated package suspended over the pool was conducted as part of the test series to determine if in-hold shipboard pool fires differed from those conducted on land.

A major purpose of the tests was to collect data useful in benchmarking fire calculations for ship fires. In a separate effort, the data collected are being compared to fire simulations made with the use of computational fluid dynamics.

For brevity, this paper will concentrate on the results obtained from the steel pipe calorimeters representing simulated radioactive materials packages. Results such as bulkhead and overhead temperatures, air temperatures in the holds, and flow probe measurements are included in [2]. Over 100 thermocouples, 12 flow probes, two radiometers, two video cameras, and an oxygen sensor were included in the test instrumentation.

### TEST DESCRIPTION AND SEQUENCE

The sequence of eight fires conducted aboard the *Mayo Lykes* is shown in Table 1. A brief description of each type of fire and major fire characteristics follows. Hold 4 measures 17.6 m wide by 21 m long by 3.8 m high. Hold 5 dimensions are 17.6 m wide by 16 m long by 3.8 m high. For all tests the calorimeter in Hold 5 was located with its centerline 0.4 m above the deck and 2 m aft of the Hold 4-5 bulkhead. Detailed descriptions of the ship holds involved and instrumentation locations are included in [2].

To avoid potentially explosive conditions with the heptane spray and in-hold pool fires, adequate oxygen was supplied to Hold 4 via openings in the hull. Measurements indicate that oxygen levels in the vicinity of the fire were usually near normal atmospheric

TABLE 1--*Fire Test Sequence.*

Test Number	Date, Time and Duration	Type of Test	Peak Thermal Power, MW
5037	9/12/95 2:09 PM CDT 60 Minutes	2 burner heptane spray test	2.2
5040	9/14/95 9:13 AM CDT 20 Minutes	Wood crib fire test with 17 L heptane accelerant	4.1
5041	9/14/95 12:21 PM CDT 60 Minutes	2 burner heptane spray test with diesel fuel in drip pans for smoke	2.2
5043	9/15/95 8:26 AM CDT 20 Minutes	Wood crib fire test with 17 L heptane accelerant	4.1
5045	11/13/95 12:02 PM CDT 60 Minutes	4 burner heptane spray test	5.6
5046	11/13/95 2:46 PM CDT 60 Minutes	4 burner heptane spray test with diesel fuel in drip pans for smoke	5.6
5048	11/14/95 3:09 PM CDT 27 Minutes	Diesel pool fire in Hold 4	15.7
5049	11/15/95 2:20 PM CDT 32 Minutes	Diesel pool fire on weather deck	18.8

content. In sealed shiphold fires at sea, oxygen would be more limited, leading to smoldering fires with even lower heat flux levels than experimentally measured. The experimental fires reported here represent conditions more typical of a fire that could occur during ship loading or unloading in port.

### Heptane Spray Tests

The heptane spray fires were intended primarily to simulate a fire in an adjacent ship compartment. For the first series of tests heptane in a pressurized reservoir was fed through nominal 3/8 inch stainless steel tubing to two nozzles located in Hold 4. Stainless steel BETE model P54 fine atomization spray nozzles were used to create a 90° cone shaped fog spray that was manually ignited with a propane torch. The nozzles were located 0.91 m to either side of the hold centerline. The nozzles were located 1 m above the deck, 1 m from the bulkhead between Holds 4 and 5, and were aimed at the bulkhead at an angle of 45° above horizontal. The heat release of a spray nozzle was estimated by correcting the spray nozzle factor,  $k$ , in the equation

$$q = k\sqrt{\Delta p} \quad (1)$$

where  $q$  is the flow in  $\text{m}^3/\text{s}$ ,  $k$  is the nozzle flow constant, and  $\Delta p$  is the pressure drop in MPa. For heptane density rather than the water density data listed in the BETE catalog the factor  $k$  can be modified with the expression

$$k_{\text{heptane}} = k_{\text{water}} \sqrt{\rho_{\text{water}}/\rho_{\text{heptane}}} \quad (2)$$

where  $\rho$  is the density of the fluid. Since heptane is less dense than water, the nozzle flow increases by a factor of about 20 per cent above water flow for the fluid temperatures considered. Pressure drop from the reservoir to the nozzles was estimated with standard fluid pressure drop formulas for flows in piping. For the estimated 0.21 MPa pressure difference across the nozzle, a 0.024 kg/s mass flow rate results through each nozzle. For heptane with a heat of combustion of 44.6 MJ/kg, this gives a thermal output of each nozzle for full combustion of 1.1 MW. The two nozzle configuration doubles this to a total thermal output of the fire to 2.2 MW.

After inspecting the calorimeter results from the first series of two-burner heptane spray tests, a second series with larger nozzles in a four-burner arrangement were conducted. For these tests, in addition to the nozzle locations 0.91 m to each side of the ship centerline, nozzles were located 3.05 m to each side of the centerline. As with the two burner tests, nozzles were 1 m above the deck, 1 m from the Hold 4 and 5 bulkhead, and aimed at the bulkhead at an angle of 45° above horizontal. For the test, the larger BETE P66 nozzles were used with a 0.55 MPa pressure maintained at the fuel reservoir. This gives an estimated nozzle pressure difference of 0.17 MPa and a flow from each nozzle of 0.031 kg/s. This yields an estimated power release of 1.4 MW for each burner, and a total release of 5.6 MW total for all burners.

### Wood Crib Fires

Wood cribs built from clear Douglas fir were used to simulate a cargo fire immediately adjacent to the radioactive cargo. The general arrangement for the crib fires is shown in Figure 2. The general wood crib design is based on UL Standard 711 [6], and is consistent with the size designated as 20-A in that standard. To estimate the heat release

from the crib, equations were taken from Walton [7]. First the cross sectional area of the exposed surface,  $A_E$ , is calculated from the equation

$$A_E = 2nb^2[(2(l/b) + 1)N - n(N - 1)] \tag{3}$$

where  $b$  is the stick thickness in m,  $n$  is the number of sticks per layer,  $N$  is the number of layers and  $l$  is the length of the wood sticks. Since the wood used was rectangular in cross section, the stick thickness  $b$  was taken to be one-fourth of the perimeter dimension. The heat release rate is then obtained from the equation

$$\dot{q} = A_E E C b^{-0.5} \tag{4}$$

where  $\dot{q}$  is the heat release rate in MW,  $A_E$  is the cross-sectional area from Equation (3) in  $m^2$ ,  $E$  is the heat released from the combustion of pyrolysis products in  $kJ/kg$ , and  $C$  is an empirical constant for the mass of pyrolysis product produced per unit surface area and unit time in  $kg/(m^{1.5}s)$ . Walton suggests a  $C$  value of  $0.65 \times 10^{-3} kg/(m^{1.5}s)$  for single cribs of Douglas fir. Application of these equations to the UL 711 size 20-A crib give a heat release of 2.4 MW. The UL standard also specifies that to initiate the fire, 17 L of heptane accelerant are to be ignited in a 1 m square pan under the crib. Observation of the experimental data indicated that this accelerant burned for about five minutes giving an experimental recession rate of  $0.038 kg/(m^2s)$ , and a corresponding output of 1.7 MW. Combining the heat release of the wood crib and the heptane accelerant gives an initial thermal output of 4.1 MW for the first 5 minutes of the fire, then a steady heat release of 2.4 MW as the crib alone burns. Inspection of the data for the calorimeter in Hold 4 indicates that the wood crib heat release decreased rapidly 15 minutes after ignition indicating that most wood had burned.

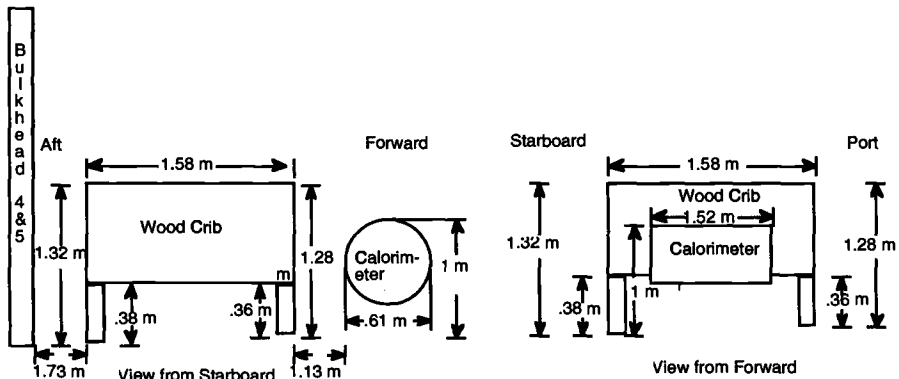


FIG. 2. Sketch of wood crib fire arrangement.

Pool Fires

For this test a 3 m x 3 m pool was constructed on the ship centerline at the aft end of Hold 4, and the steel pipe calorimeter moved to be centered above the pool in a manner consistent with land based regulatory testing. At the start of the burn, the bottom of the calorimeter was 1 m above the fuel surface. Because of its ready availability and usefulness for other purposes if not all the fuel was consumed, diesel fuel was selected for this test. The fuel was floated on a pool of water in the specially built containment area

adjacent to the bulkhead between Holds 4 and 5. To avoid a possible explosion, openings in the hull provided adequate oxygen to the fire. In an actual shipboard fire, this free availability of oxygen is unlikely.

During the test a 7.6 cm depth out of a total depth of 13 cm of diesel fuel were burned before overhead temperatures exceeded the previously agreed upon maximum of 540°C at 24 minutes into the test. At 27 minutes the fire extinguishment with foam was complete. From this information a fuel recession rate of 0.0443 kg/m<sup>2</sup>-s was calculated. With a typical diesel heat of combustion of 42.75 MJ/kg this leads to an average heat release of 15.7 MW during the test.

For the pool fires Directional Flame Thermometers (DFTs) based on a design from Burgess and Fry [8] were used to estimate the temperatures of the engulfing flames. These devices, resembling a vegetable can, have thin metal ends that rapidly approach flame temperatures. Thermocouples attached on the inside of the thin metal ends provide an estimate of flame temperatures in the direction that the end faces in the fire. The cans are filled with insulation to prevent internal heat transfer within the DFT.

For comparison to the in-hold fire test, a 3 m x 3 m pool was built on the weather deck of the *Mayo Lykes* on the port side amidships. The pool was constructed to closely follow the dimensions of the pool built in Hold 4. The calorimeter from Hold 5 was centered above the pool, 1 m above the fuel surface at the start of the test. A depth of 13 cm of diesel fuel gave a 32 minute burn, typical of a regulatory pool fire. Calculation of the recession rate for this fire led to an estimated average thermal output of 18.8 MW. A strong off-shore wind with gusts in excess of 10 m/s tended to lay the fire plume over, often diverting the flames from the calorimeter. This effect, which was visible in the data as highly variable heat fluxes to the calorimeter, is not typical of land based tests that are conducted when the wind is relatively calm.

## PIPE CALORIMETER DESIGN

The pipe calorimeters that simulated the radioactive cargo packages were constructed from two 1.52 m lengths of nominal 2 foot diameter Schedule 60 carbon steel pipe with an outside diameter of 0.61 m and a wall thickness of 0.0244 m. Nominal 1 inch (0.0254 m) thick circular carbon steel plates were bolted to form the ends of the calorimeters. Thermocouples were fastened to the pipe interior and exterior surfaces with thin capacitance-welded Nichrome metal strips at the locations shown in Figure 3. The Nichrome strips were applied so that the thermocouple tip was firmly held and covered by the strip. Calorimeters located in Holds 4 and 5 were identical in construction, with the side containing the larger number of thermocouples facing the bulkhead between Holds 4 and 5. Type K thermocouples were attached in pairs with one interior and one exterior thermocouple at each location. This permitted measurement of the time history of the pipe wall temperature difference at 12 locations as shown in Fig. 3.

As discussed by Keltner and Moya [9], the temperatures measured by a thermocouple must be considered carefully. A surface thermocouple on the calorimeter, for example, when exposed to rapid changes in radiant energy levels, does not respond in the same manner as the steel substrate to which it is attached. With less mass and a contact resistance between the thermocouple and the substrate, the thermocouple bead responds more rapidly than the surface, and, under these rapid heating conditions, does not accurately represent the calorimeter surface temperature. The SODDIT [10] inverse heat conduction program interprets this rapid increase in the bead temperature as the temperature of the steel surface of the calorimeter. The result is an estimated peak in the heat transfer

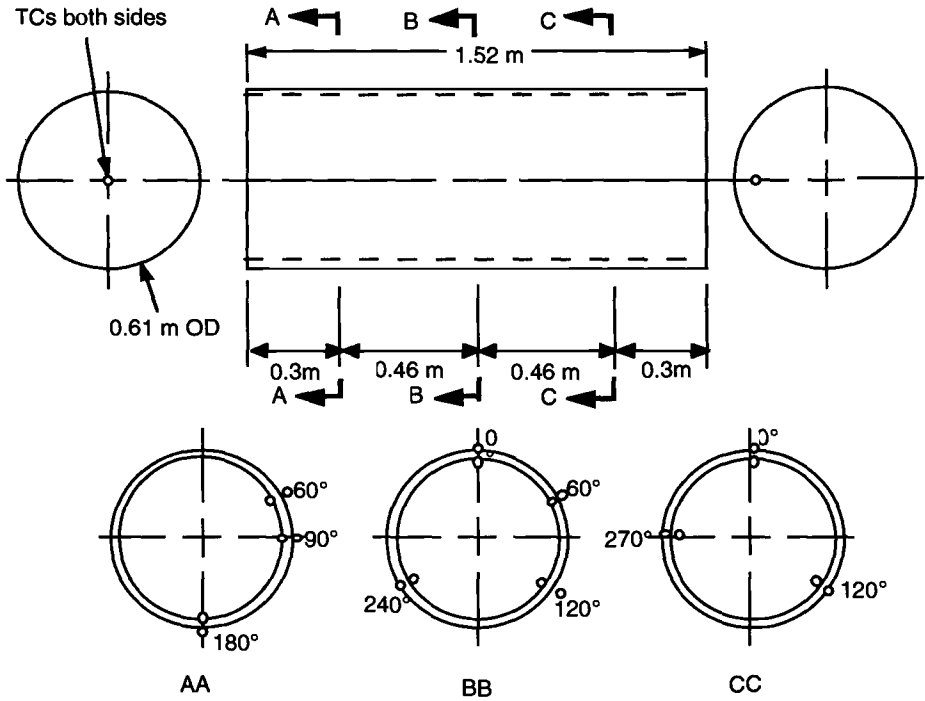


FIG. 3. Calorimeter arrangement with thermocouple locations.

that is significantly higher than when the inside thermocouple alone is used for the data analysis. Where the heating rate is slow, as is the case for the calorimeter located in the adjacent Hold 5, little effect is noticed whether only the inside or both inside and outside thermocouples are used. For the cases in Hold 4 with wood cribs and pool fires in the immediate proximity of the calorimeter, only the inside thermocouple response is typically used to predict heat flux and calorimeter surface temperatures since these estimates do not exhibit the errors that occur during rapid surface heating.

After attachment of the thermocouples, the calorimeter interiors were packed with commercial Kaowool insulation material with a nominal density of 8 pounds per cubic foot (128 kg/m<sup>3</sup>) to provide an insulated boundary condition for data analysis. The insulation also blocked thermal radiation and convection heat transfer inside the calorimeter cavity that would require the complicated interior geometry to be analyzed as part of the data reduction.

Absorbed heat fluxes to the calorimeter were determined with the use of the Sandia One-Dimensional Direct and Inverse Thermal (SODDIT) computer code [10]. This code can be used to solve inverse heat conduction problems, i.e., rather than solving for the temperatures of an object given the boundary conditions, this code estimates the heat flux boundary conditions given object temperatures. As the name implies, the code assumes a one-dimensional geometry for cylinders, spheres or plates. This approach provides good

estimates of the surface heat transfer as long as local peaking of the flux profiles does not produce significant two- or three-dimensional heat transfer near the peak.

As a test of the calorimeter's potential to record accurately the absorbed heat fluxes, a computer simulation under controlled conditions was conducted. First the Topaz2D [11] finite-element computer code was used to generate simulated two-dimensional test data for the calorimeter. The geometry chosen for the test consisted of a circular pipe cross section with a view of a flat, infinite hot wall. With a radiation heat transfer boundary condition, this leads to a peaked heat flux distribution on the side of the calorimeter facing the hot wall. The temperatures calculated by Topaz2D for the inside surface of the calorimeter for this geometry were then treated as pseudo-experimental data in the one-dimensional SODDIT code. The comparison between the Topaz2D heat flux values calculated at the calorimeter surface and the SODDIT predictions at three different times is shown in Fig. 4. Initially, the heat flux is accurately predicted as shown by the small overprediction of the heat flux at one minute in Fig. 4. As time progresses, the SODDIT predictions start to predict peak values lower than the calculated Topaz2D heat fluxes and higher values than Topaz2D at points away from the peak. At 30 minutes, SODDIT predicts about 87 per cent of the Topaz2D peak heat flux, while at 60 minutes, about 80 per cent of the Topaz2D peak heat flux is predicted. The gradual decrease of the predicted values with time is probably due to the circumferential component of thermal conduction in the pipe wall that is included in the Topaz2D model, but neglected by the one-dimensional SODDIT code. For these experiments, this level of measurement accuracy is considered adequate, but all heat flux data presented should be viewed with these effects in mind.

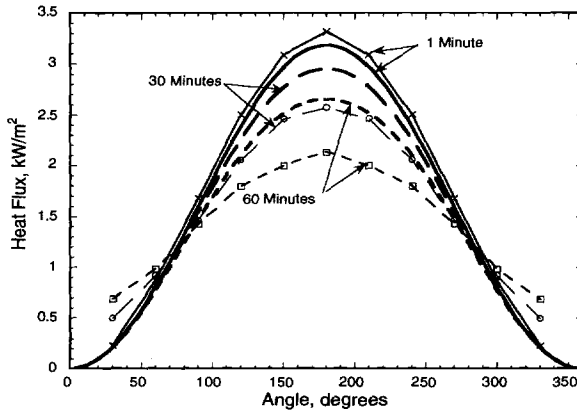


FIG. 4. *Topaz2D calculations compared to SODDIT results. SODDIT results are lighter lines with symbols.*

Another consideration in analysis of calorimeter data is the size of the time step used for the numerical SODDIT calculations. If the time step is too small, the magnitude of the signal noise is comparable to the magnitude of the temperature change, and the code has difficulty separating signal from noise. If the time step chosen is too large, SODDIT, which uses a numerically stable implicit time-stepping algorithm, can obtain inaccurate solutions that yield poor heat flux predictions. For the calorimeters used for these experiments, a 30 s time step proved a good compromise between these two extremes.

## EXPERIMENTAL RESULTS

### Heptane Spray Fires for Trans-bulkhead Exposure

Temperature and heat flux results for the first four-burner heptane spray test designated test 5045 are given in Figs. 5, 6, and 7. These results are typical of the one-hour four-burner heptane spray fires conducted. For these tests the calorimeter located in the adjacent compartment, Hold 5, was heated about 25°C during the one hour duration of the test as shown in Fig. 5. SODDIT, with use of both inside and outside thermocouples at each angular position shows maximum heat fluxes of about 0.8 kW/m<sup>2</sup> on the side of the calorimeter facing the hot bulkhead between Holds 4 and 5 (see Fig. 6). Noise shown in Fig. 6 results from relatively small calorimeter temperature increases that lead to low signal-to-noise ratio conditions. Fig. 7 shows the angular distribution of the heat flux around the circumference of the calorimeter 30 minutes after ignition.

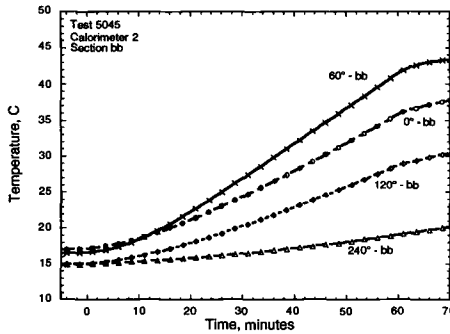


FIG. 5. *Exterior temperatures at center of calorimeter in Hold 5 during four burner heptane test.*

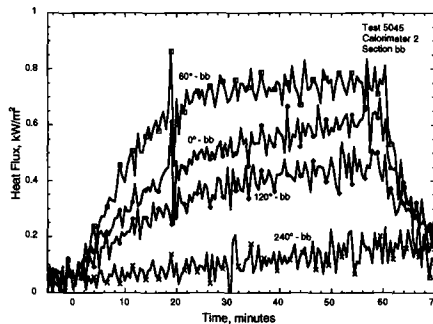


FIG. 6. *Estimated heat fluxes to calorimeter in Hold 5 during four-burner heptane test.*

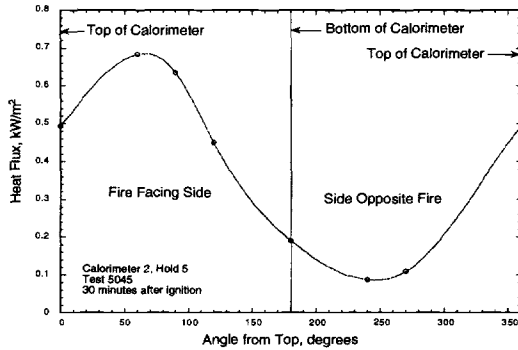


FIG. 7. Heat flux distribution around calorimeter in Hold 5 30 minutes after ignition during four-burner heptane spray test.

Wood Crib Fires for Direct Cargo Exposure

Results for the calorimeter located immediately adjacent to the burning wood crib for the first wood crib test designated as Test 5040 are shown in Figs. 8, 9, 10, and 11. During this test the calorimeter increased in temperature about 200°C. The initial rapid temperature increase at the start of the test is caused by the heptane accelerant used to start the fire. This initial transient results in an initial peak of about 25 kW/m<sup>2</sup> on the calorimeter surface (see Fig. 9) as estimated with SODDIT with the use of the interior thermocouples only. Angular distributions of the heat flux at 4 and 20 minutes after ignition are shown in Figs. 10 and 11.

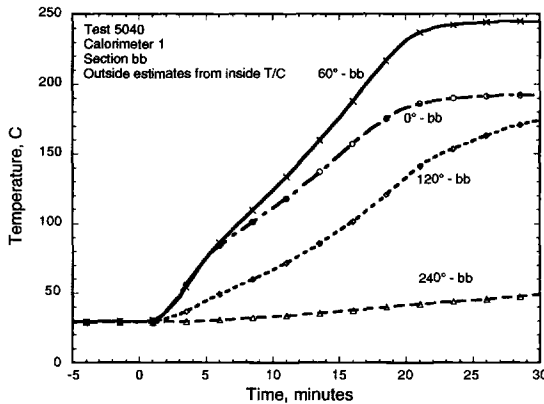


FIG. 8. Temperatures at outside of calorimeter in Hold 4 during wood crib fire test. Temperatures are estimated from inside thermocouple data with use of the SODDIT code.

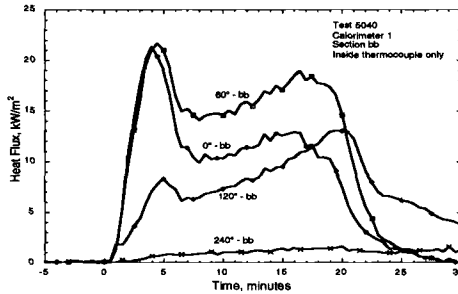


FIG. 9. Heat fluxes estimated by SODDIT code for calorimeter in Hold 4 during wood crib fire test. The initial peak is caused by the heptane fire accelerant.

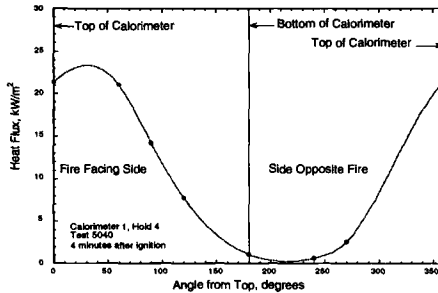


FIG. 10. Heat flux distribution around calorimeter 4 minutes after ignition during wood crib fire test.

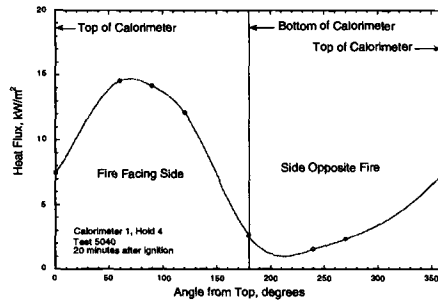


FIG. 11. Heat flux distribution around calorimeter 20 minutes after ignition during wood crib fire test.

Pool Fires for Direct and Trans-bulkhead Exposures

For the in-hold pool fire, the calorimeter was completely engulfed by the pool fire flames. Near the end of this test, cables strung on the deck above the fire hold were damaged, resulting in erratic data swings. As shown in Fig. 12, calorimeter temperature increases of 700 to 800°C were measured during the test. SODDIT calculated brief initial heat flux values between 150 and 200 kW/m<sup>2</sup> for this test as shown in Fig. 13. Directional Flame Thermometers located in the fire zone recorded temperatures between 900 and 1100°C during the fire as shown in Fig. 14. The heat fluxes to the calorimeter in Hold 5 adjacent to the fire compartment remain at about the 1 kW/m<sup>2</sup> level as shown in Fig. 15. At

about 24 minutes, a decision to extinguish the fire was made to avoid damaging the deck immediately above the fire zone.

Because the on-deck outdoor pool fire was conducted during a strong wind, these data are not directly comparable to typical regulatory outdoor pool fires conducted under low wind conditions. For this reason, these data are not presented here. A complete summary of the data is provided in [2].

**CONCLUSIONS**

The fire tests yielded several results that tend to confirm the beliefs held prior to testing. First, the overall heat flux level in typical adjacent-hold and combustible-cargo ship fires is considerably below the initial 65 kW/m<sup>2</sup> heat flux levels implied by regulations such as Safety Series 6 [5]. Even for the in-hold pool fire, initial heat flux levels are comparable to values measured in land-based regulatory fires [12]. For Hold 5, adjacent to the fire hold, the heat fluxes to the calorimeter never exceeded 1.5 kW/m<sup>2</sup>, even with the large 15.7 MW pool fire near the Hold 4-5 bulkhead in Hold 4.

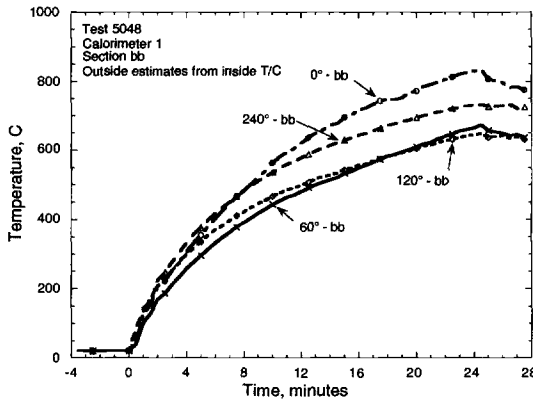


FIG. 12. *Estimated surface temperatures from SODDIT for calorimeter located in fully engulfing in-hold pool fire.*

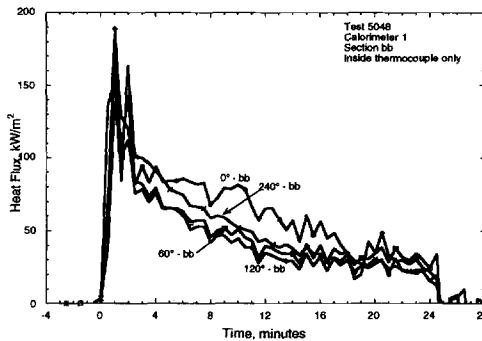


FIG. 13. *Estimated heat fluxes to calorimeter located in pool fire in Hold 4*

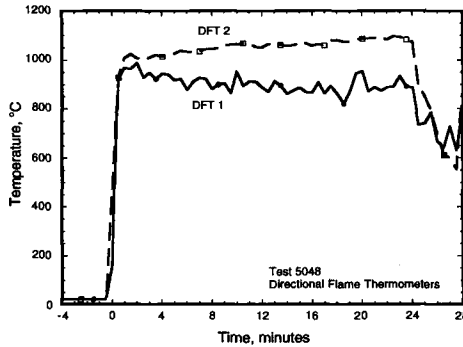


FIG. 14. Directional flame thermometer temperatures for pool fire in Hold 4.

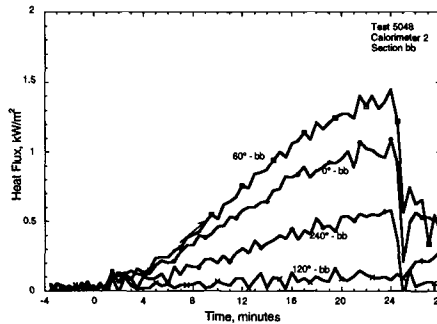


FIG. 15 Estimated heat fluxes to calorimeter in Hold 5 during pool fire in Hold 4.

For both the heptane spray and wood crib fires, analysis of the calorimeter heat flux plots shows that the absorbed heat fluxes are much higher on the side facing the fire. This indicates that thermal radiation is the dominant heat transfer mechanism since convection would lead to a more uniform heating with hot gases flowing around the entire circumference of the calorimeter. Accurate fire simulations with computer models will aid in determining the partitioning of the heat transfer mechanisms involved.

Steel cargo holds typically do not contain the combustible carpets, wall coverings and other easily combustible materials such as furniture and paper that lead to the flashover conditions typical of building fires on land. At the flashover point, room temperatures and thermal radiation combine to ignite simultaneously most combustible materials in the room. This condition was not observed for any of the tests conducted. The calorimeter measurements of heat fluxes, coupled with ignition models, could be used to estimate the time required for spread of a ship-hold fire from one combustible cargo to another.

Inspection of the estimated heat transfer plots for Holds 4 and 5 shows some rapid fluctuations in the estimated heat flux values, especially for Hold 5. Since the heat fluxes to the calorimeter in Hold 5 are generally much lower than the values for the calorimeter in Hold 4, any noise in the Hold 5 data are displayed as proportionately larger variations on the heat flux signal than occur for Hold 4 data. Although the SODDIT code permits multiple time point analyses that smooth the results, the decision was made to display the

single time point analysis results to enable a better understanding of the signal-to-noise ratios involved in the data analysis.

Analysis of the data does not indicate that shipboard fires are likely to lead to increased heat transfer when compared to land based regulatory fires. In general, the heat transfer seems to be lower than for the fully engulfing pool fire considered for land based accidents. This leads to the consideration of the duration of shipboard fires, a study that may be better based on historical data or engineering analysis than on experiment.

These experimental results are primarily intended to serve as a means of confirming and refining analytical heat transfer models of shipboard fires. No general conclusions regarding the adequacy or inadequacy of regulatory tests as applied to the shipboard fire environment can be drawn directly from the tests. Any risk assessment model of fires must also include the probabilities of initiating events, as well as details of crew response and allowances for use of fire suppression systems.

The testing here applies primarily to the break-bulk freighters typically used to transport radioactive materials. The work does not apply to container ships, where the IMDG rules differ from those applied to break-bulk ships. Further investigations are in progress to assess typical fire conditions aboard container cargo ships.

## REFERENCES

- [1] Fischer, L. E., Chou, C. K., Gerhard, M. A., Kimura, C. Y., Martin, R. W., Mensing, R. W., Mount, M. E., and Witte, M. C., "Shipping Container Response to Severe Highway and Railway Accident Conditions," Report NUREG/CR-4829, Lawrence Livermore National Laboratory, Livermore, CA, February 1987.
- [2] Koski, J. A., Bobbe, J. G., Arviso, M., Wix, S. D., Beene, D. E., Jr., Byrd, R., and Graupmann, J., "Experimental Determination of the Shipboard Fire Environment for Simulated Radioactive Material Packages," SAND97-0506, Sandia National Laboratories, Albuquerque, NM, 1997.
- [3] International Maritime Organization, "International Maritime Dangerous Goods Code," International Maritime Organization, London, UK, 1992.
- [4] International Maritime Organization, "Irradiated Nuclear Fuels Code," International Maritime Organization, London, UK, 1995.
- [5] International Atomic Energy Agency, "Regulations for the Safe Transport of Radioactive Waste, Safety Series No. 6," International Atomic Energy Agency, Vienna, 1990.
- [6] Underwriters Laboratories, "Rating and Fire Testing of Fire Extinguishers," Standard for Safety, UL 711, Underwriters Laboratories, 1990.
- [7] Walton, W. D., "Suppression of Wood Crib Fires with Sprinkler Sprays: Test Results," U. S. Dept. of Commerce, NBSIR 88-3696, National Bureau of Standards, National Engineering Laboratory, Gaithersburg, MD, 1988.
- [8] Burgess, M. H., and C. J. Fry, "Fire Testing for Package Approval," *RAMTRANS*, No.1, 1990, pp. 7-16.

- [9] Keltner, N. R., and Moya, J. L., "Defining the Thermal Environment in Fire Tests," *Fire and Materials*, Vol. 14, 1989, pp. 113-138.
- [10] Blackwell, B. F., R. W. Douglas, and H. Wolf, "A User's Manual for the Sandia One-Dimensional Direct and Inverse Thermal (SODDIT) Code," SAND85-2478, Sandia National Laboratories, Albuquerque, NM (1987).
- [11] Shapiro, A. B., "Topaz2D -- A Two-Dimensional Finite Element Code for Heat Transfer Analysis, Electrostatic, and Magnetostatic Problems," UCID-20824, Lawrence Livermore National Laboratory, Livermore, CA, 1986.
- [12] Gregory, J. J., N. R. Keltner and R. Mata, Jr., "Thermal Measurements in Large Pool Fires," *Journal of Heat Transfer*, Vol. 111, 1989, pp., 446-454.

Richard L. Hansen<sup>1</sup>, and Gerald G. Back<sup>2</sup>

## EVALUATION OF LARGE-SCALE MARINE FIRE PROTOCOLS

---

**REFERENCE:** Hansen, R. L. and Back, G. G., "Evaluation of Large-Scale Marine Fire Protocols," *Very Large-Scale Fires, ASTM STP 1336*, N. R. Keltner, N. J. Alvares, and S. J. Grayson, Eds., American Society for Testing and Materials, 1998.

**ABSTRACT:** The United States Coast Guard has been actively involved in the research efforts to identify alternative fire protection methods to replace Halon 1301. The Coast Guard Research & Development Center conducted the first large scale marine fire extinguishment tests of four replacement agents in April, 1994. Large scale evaluation testing has also been performed on the International Maritime Organization's (IMO) Water Mist and Gaseous Agent test protocols. This paper will summarize some of the unique findings of these test programs and the value of large scale testing to the Coast Guard's regulatory authority.

**KEYWORDS:** Halon alternatives, water mist, gaseous agents, maritime, fire protection

---

This document is disseminated under the sponsorship of the Department of Transportation in the interest of information exchange. The United States Government assumes no liability for its content or use thereof.

The United States' Government does not endorse products or manufacturers. Trade or manufacture's names appear herein solely because they are considered essential to the object of this paper.

The contents of this paper reflect the views of the authors who are solely responsible for the facts and accuracy of the data presented. This paper does not constitute a standard, specification, or regulation.

### Introduction

The United States Coast Guard (USCG) is responsible for establishing fire safety standards for its cutters and U.S. flag ships via 46 U.S. Code of Federal Regulations. The U.S. Coast Guard is also active in establishing and enforcing rules for fire safety on

---

<sup>1</sup> Project manager and fire protection engineer, USCG Research & Development Center, Groton, CT 06340-6096

<sup>2</sup> Fire protection engineer, Hughes Associates, Inc., Baltimore, MD 21227-1652

vessels making international voyages by representing the United States at the International Maritime Organization (IMO). Both the U.S. Coast Guard and the IMO have recognized that the phaseout of Halon 1301 due to its ozone depletion potential, has created an urgent need for the development of a replacement agent. For ship board fire protection applications, one of the most critical applications is protection of the machinery spaces.

The chemical, fire protection, and marine industries have developed several potential alternative technologies. Fine water mist and alternative gaseous agents are two alternatives that have shown promise for shipboard applications. Several of these technologies have been tested in smaller scale, no data existed with real shipboard type systems in full scale. Prior to permitting the use of these technologies onboard ships the U.S. Coast Guard and the IMO believe that they must pass a standard, large-scale performance test. Such tests have been proposed during recent meetings of the IMO's Subcommittee on Fire Protection (FP). These draft test protocols, had to be evaluated to verify their effectiveness in testing capabilities and limitations of the candidate technologies.

The tests were conducted by the U.S. Coast Guard Research and Development Center (USCG R&DC) at the request of U.S. Coast Guard Headquarters (G-MSE-4 and/or G-SEN-1) for the purpose of developing input for the U.S. position at the IMO meetings on the proposed test protocol<sup>1</sup> and aiding in assessing cutter protection options. The tests were conducted in cooperation with industry to the maximum extent possible.

## Objectives

The testing conducted was designed to meet five general objectives:

1. Identification of any scale unique attributes for these technologies that would preclude effective qualification being done in smaller scale testing.
2. Establish if there are any limitations in the scalability of the test protocol's results to anticipated actual shipboard installations.
3. Do the proposed test protocols effectively measure the ability of the proposed technology to safely and effectively extinguish machinery space fires.
4. Determine if there are any additional hazards created beyond those created by the fire itself.
5. Is the test biased toward any particular subset of the range of applicable technologies.

In addition to the above U.S. Coast Guard objectives, the testing has provided participating industry with valuable information regarding the performance of their product against the proposed test protocols.

### **Fine Water Mist**

Testing<sup>2</sup> conducted jointly by the U.S. Army and U.S. Navy identified the feasibility of using some fine water mist technologies for machinery space applications. However, those tests also identified some limitations. One limitation is fine water mist's inability to extinguish highly concealed fires, such as could be found in machinery space's bilges. They also identified a general trend that smaller fires were more difficult to extinguish. These tests were conducted in test compartments that had specific limitations for applicability to commercial vessels, such as smaller volumes and lower ceiling heights. The spaces had ceiling heights of 4 and 6 meters. The larger U.S. Navy compartment when closed was an extremely air tight compartment. This degree of tightness would not generally be found on commercial vessels.

Considering the need to evaluate the IMO protocol<sup>1</sup> for fine water mist and the limitations of previous test efforts<sup>2</sup> applicability, the U.S. Coast Guard set up a three phase test series. The first and third phases of the testing for compartment volumes <500 m<sup>3</sup> were conducted at the USCG's Fire & Safety Test Detachment in Mobile, AL. This unique fire test facility allows actual fire tests to be conducted in actual shipboard applications/installations.

The first phase evaluated aspects of the IMO protocol that the earlier efforts had not investigated. They were the effects of higher ceilings (up to 7.3 m), stacking of nozzle arrays, and the role of oxygen depletion in the extinguishment.

Using the IMO's protocol, the second phase evaluated the role of the role of oxygen depletion, ceilings, and walls have on fine water mist in larger spaces (compartment volumes >500 m<sup>3</sup>). The protocol<sup>1</sup> required a test hall with a 300 m<sup>2</sup> open floor area for the tests, and with at least a 10 m ceiling height. These tests were conducted in Factory Mutual Research's Test Center, located in W. Glocester, RI. In this series, a limited number of tests were conducted in a configuration that started with no walls and ceiling as is called for in the IMO protocol<sup>1</sup>. When the results indicated that the fine water mist technologies tested would be unable to extinguish any of these fires, a ceiling and eventually walls were constructed around the 300 m<sup>2</sup> floor area. These tests identified that oxygen depletion is one of fine water mist's extinguishing mechanisms. Oxygen depletion was tied to recirculation of fire byproducts in addition to the previously believed local steam generation at the flame. This result explained why smaller fires were more difficult to extinguish. The smaller fires have little impact on the oxygen concentration in the compartment.

The third phase, conducted at the USCG's Fire & Safety Test Detachment further evaluated the role of oxygen depletion by removing ceiling panels of the test compartment, as well as evaluating the capabilities of four commercially available water mist technologies. They were one high pressure, one twin fluid (water and air), and two low pressure systems.

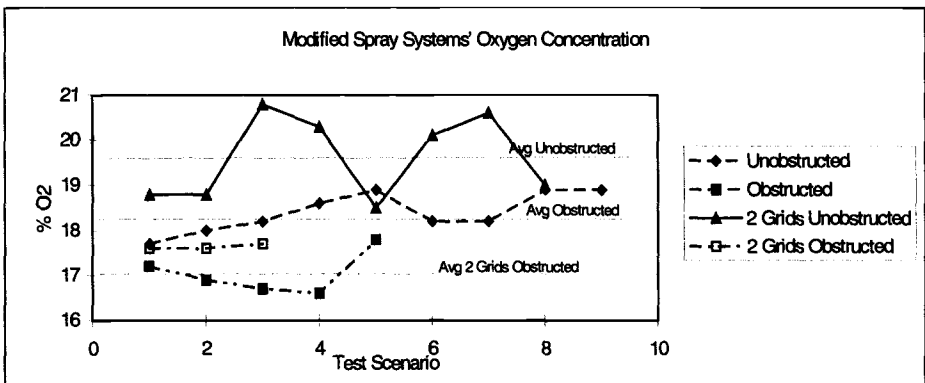
**Fine Water Mist Testing Results**

The results<sup>3</sup> of these large scale tests identified several important findings. The first was that extinguishment is tied to the oxygen concentration in the space. From the thirteen IMO test scenarios, nine (9) especially challenging test scenarios were derived for evaluation<sup>3</sup>. For the various nozzle technologies tested, a specific amount of oxygen depletion was needed before the fires were extinguished. This can be seen by plotting the oxygen concentration at the time of extinguishment for these fire scenarios from the IMO protocol<sup>1</sup>, see Figure 1. Paramagnetic oxygen concentrations of dried samples were taken at a variety of locations in the test compartment. The three horizontal lines superimposed on the plots represent the average oxygen concentration for the three conditions; 2 grids of nozzles with unobstructed fires, 1 grid of nozzles with unobstructed fires, and 1 grid of nozzles with obstructed fires. For the modified Spraying System's nozzle used in this evaluation, the fires were not extinguished until the oxygen concentration at the base of the fire was reduced below these average values.

The phase two tests, conducted in the large unenclosed test area at Factory Mutual's Test Center, identified limitations on scaling the effectiveness results to larger volumes. There is also a corresponding limitation based on the amount of vent losses in the compartment. Both of these limitations are related to the oxygen depletion mechanism. As a result of these test series, the IMO protocol<sup>1</sup> was modified to require testing to the largest protected volume for volumes greater than 500 m<sup>3</sup>.

A model for predicting the critical fire size (size of fire that cannot be extinguished) given the mist system and the compartment's parameters (i.e., size, temperature, ventilation conditions, and materials) has been developed from the results of these tests. The model is used to predict the oxygen concentration history in the space and considers both the oxygen consumption by the fire and the dilution of the oxygen by saturated vapors. This model can be used to predict when extinguishment will occur

*Figure 1  
Oxygen Concentration at Extinguishment for Different Test Scenarios*



based on compartment conditions. It has the potential for regulators and designers to determine how large a fire would not be extinguished by a fine water mist system. These critical fires are relatively small compared to the compartment size. If the critical fire size is small enough to be extinguishable by manual means, regulators should be able to approve the system without requiring large scale testing in a volume of that size or larger.

Other findings include; the ceiling height could be increased from 5.0 m to 7.5 m, and obstructions can have a significant effect on the extinguishment, and a separate protection scheme may be required for highly obstructed areas. These changes were incorporated in the modification of the IMO protocol<sup>1</sup>.

Overall the U.S. Coast Guard is encouraged with the prospects of fine water mist technologies providing safe and effective fire protection for shipboard machinery spaces. There remains some design and engineering work that still needs to be performed. The Coast Guard is still actively working on some of those issues where they meet the Coast Guard's needs.

### Gaseous Agents/Systems Testing

Four alternative gaseous agents/delivery systems were tested using all or part of the fire scenarios in the gaseous agent protocol<sup>4</sup>. Additionally, baseline tests using Halon 1301 were conducted. The agent/distribution systems tested are shown in Table 1. The agents were discharged through systems provided by the agent manufacturer or equipment manufacturer participating in the Cooperative Research and Development Agreements (CRADAs).

The gaseous agent tests<sup>5</sup> were conducted in 1996 onboard the test vessel STATE OF MAINE, located the U.S. Coast Guard's Fire & Safety Test Detachment in Mobile, AL. The ship was modified to comply with the protocol's requirements and allow safe conduct of the tests. The test compartment was 10 x 10 x 5 m for a total volume of 500 m<sup>3</sup>.

*Table 1. Agent/Systems*

Agent	Dissignation	Agent Provided by	Distribution System	No. Of Nozzles
CEA-410™	PFC-410	3M	Thorne Securities	4
Envirogel	Gas/Powder Mix	Powsus, Inc.	Powsus, Inc.	2
FM-200™	HFC-227ea	Kidde-Fenwal, Inc.	Kidde	4
NAF-SIII	HCFC Blend A	Ansul, Inc.	Ansul, Inc.	2

The test compartment was instrumented to measure temperature, pressure, heat flux, and gas concentration. In addition, agent and decomposition product concentrations

Table 2. Tell Tale (Scenario 1) Results

Agent	Agent Conc. (%)	Number of Nozzles	Nozzle Type	Discharge Time (s)	Average Nozzle Pressure (psi)	Extinguishment Results								Overall Performance	
						High Elevation				Low Elevation					
						Forward		Aft		Forward		Aft			
						Port	Stbd	Port	Stbd	Port	Stbd	Port	Stbd		
NAF-SIII	10	2	A-1	11	120	P	P	P	P	P	P	P	P	P	P
NAF-SIII	10	2	N-2	10	130	F	F	P	P	P	P	P	P	P	F
NAF-SIII	10	2	N-2	11	125	F	P	P	P	P	P	P	P	P	F
NAF-SIII	10	2	N-3	11	120	F	P	P	P	P	P	P	P	P	F
NAF-SIII	10	2	N-4	10	130	P	P	P	P	P	P	P	P	P	P
CEA-410™	5.9	4	C-1	10	160	P	P	P	P	P	P	P	P	P	P
FM-200™	6.7	4	F-1	11	100	P	P	P	P	P	P	P	P	P	P
Enviro (134/powder)	3.6/250	2	E-1	?	150	F	F	F	F	P	P	P	P	P	F
Enviro (134/powder)	3.6/250	2	E-2	?	150	F	P	P	F	F	P	P	P	P	F
Enviro (134/powder)	3.6/250	2	E-2	?	150	P	P	P	P	P	P	P	P	P	P
Enviro (125/powder)	3.0/250	2	E-2	7	150	P	P	P	P	F	F	F	P	P	F

P = pass - fire extinguished in less than 30 seconds.  
 F = fail - fire not extinguished or extinguished after 30 seconds.

Table 3. Fire Scenario 2 & 2A Results

Agent	Fire Scenario 2						Fire Scenario 2A		
	NAF-SIII	NAF-SIII	Halon	CEA-410™	FM-200™	FM-200™	NAF-SIII	CEA-410™	FM-200™
Agent Concentration (%)	12	12	5	8.2	8.7	8.7	12	8.2	8.7
Relative Concentration <sup>(1)</sup>	1.1	1.1	1.6	1.6	1.3	1.3	1.1	1.6	1.3
Number of Nozzles	2	2	2	4	4	4	2	4	4
Nozzle Type	A-1	N-4	H-1	C-1	F-1	F-2	A-1	C-1	F-2
Discharge Time (s)	9.5	9.2	9.5	11.0	11.0	9.5	10	10	10
Extinguishment Time (s) <sup>(2)</sup>	10	1	1.5	12	13	9	11	12	12
Heptane pan fire (side)					5				
Extinguishment Time (s) <sup>(2)</sup>	3		2	2		2	4	3	2
Heptane spray fire (top)									
Extinguishment Time (s) <sup>(2)</sup> Diesel spray fire (top)	3	5	2	2	5	2	4	3	2
Average Agent Conc. (%)	11.8	12.2	4.6	7.9	9.0	7.7	12.7	8.6	8.6
Peak HF Conc. (ppm)	2500	4400	100	2300	8100	3600	1600	1200	1500
Positive Compartment Pressure (kPa (IWC))	0.75 (3)	0.5 (2)	0 (0)	0.75 (3)	0.5 (2)	0.5 (2)	0.25 (1)	0 (0)	0.25 (1)
Negative Compartment Pressure (kPa (IWC))	>1.25 (>5)	4.2 (17)	1.5 (6)	6.2 (25)	0.75 (3)	0.75 (3)	0.25 (1)	0.75 (3)	0.75 (3)
Oxygen Conc. after Discharge (%) <sup>(3)</sup>	14.8	14.7	16.5	16.4	15.1	16.6	16.0	17.5	17.0

Notes: (1) Relative concentrations are based on the NRL cup burner concentration for n-heptane.  
 (2) Extinguishment times are measured from the beginning of agent discharge.  
 (3) After agent discharge, the oxygen concentration is relatively uniform throughout the compartment.

Table 4. Fire Scenario 3, 3A & 3B Results

Agent	Fire Scenario 3		Fire Scenario 3A				Fire Scenario 3B				
	CEA-410™	FM-200™	NAF-SIII	CEA-410™	FM-200™	NAF-SIII	NAF-SIII	CEA-410™	Halon	FM-200™	Envirogel
Agent Conc. (%)	8.2	8.7	12	8.2	8.7	12	12	8.2	5	8.7	4.6
Relative Conc.	1.6	1.3	1.1	1.6	1.3	1.1	1.1	1.6	1.6	1.3	.46
No. of Nozzles	4	4	2	4	4	2	2	4	2	4	2
Nozzle Type	C-1	F-2	A-1	C-1	F-2	A-1	N-4	C-1	H-1	F-2	E-2
Disc. Time (s)	10	10	10.5	10	10	9.5	9	10	9.5	10	?
Ext. Time(s)											
Wood crib (deck)	4	4	9	8	7	7	4	8	5	3	10
Ext. Time(s)											
Diesel pan fire (bilge plate) <sup>(2)</sup>	9	12	15	13	9	8	4	8	10	11	10
Ext. Time(s)	9	12	12	13	15	14	4	9	11	9	3:00*
Spray fire (side) <sup>(2)</sup>											
Avg. Agent Conc. (%) 5:00	7.7	8.2	1	1	2	10.8	11.6	7.7	4.8	8.1	5.0
Avg. HF Conc. (Ppm) 5:00	3200	3900	5100	4300	5000	2300	3400	2600	300	3900	5800
Pos. Compt.	0.5 (2)	0.5 (2)	0.5 (2)	0 (0)	0.5 (2)	1.0 (4)	0.37 (1.5)	0.5 (0)	0 (0)	0.5 (2)	0.25 (1)
Neg. Compt.	2.0 (8)	2.25 (9)	2.5 (10)	3.8 (15)	2.8 (11)	>1.25 (>5)	3.0 (12)	3.0 (12)	0 (0)	2.0 (8)	3.0 (12)
O <sub>2</sub> Conc. after Disc. (%) <sup>(3)</sup>	16.0	16.7	15.8	17.5	17.0	15.3	14.3	16.7	17.3	16.3	18.3

Note: (1) Relative concentrations are based on the NRL cup burner concentration for n-heptane.

(2) Extinguishment times are measured from the beginning of agent discharge.

(3) After agent discharge, the oxygen concentration is relatively uniform throughout the compartment.

\* Fire appeared to extinguish due to oxygen depletion.

were measured using two Fourier Transform Infrared Spectrometers (FTIRs) at mid-points in the compartment. Each distribution system was instrumented to measure system pressure and temperature at various locations throughout the network. Video cameras were used to monitor and record the tests.

Prior to fire ignition, natural ventilation was established using two (2) 2m<sup>2</sup> supply vents placed low in the compartment and one (1) 6m<sup>2</sup> exhaust vent in the overhead. Ignition for each fire type was timed to allow preburns of six minutes for wood cribs, two minutes for pan fires, and one minute for spray fires in accordance with the IMO protocol<sup>4</sup>. All vents were closed ten seconds prior to agent discharge. When required by the proposed IMO protocol<sup>4</sup>, an attempt was made to reignite a spray fire fifteen minutes after discharge.

### Gaseous Agent Testing Results

The results of the tests by fire scenario are described below. All agents were not evaluated against every scenario due to logistical restraints. Envirogel was only tested against two scenarios due to agent distribution system problems.

Freeburns of each fire scenario and the individual component fires were also evaluated. The results of these tests showed a reduction in the size of the large fires due to oxygen depletion after 15 seconds. This effect could result in non-representative results for inert gas agents that are allowed a 2 minute discharge time.

The first fire scenario consisted of 8 small heptane 5 cm diameter pan fires (commonly called telltales) which are intended to validate the minimum extinguishing concentration (based on previous cup burner concentrations), and to verify the ability of the nozzles to produce a uniform concentration throughout the space. The results of these tests are shown in Table 2. The failure rate observed suggests that this test is the most challenging. Many agents (NAF-III and Envirogel) used this test scenario for screening candidate nozzles and systems. The tests indicate that a centrally located and obscured telltale would also be beneficial, such as under the engine mockup or bilge plates.

The test results for the second fire scenarios (2 & 2A) shown in Table 3, show that the two spray fires (0.16 kg/s of heptane and 0.05 kg/s of diesel) located on the top of the mockup were extinguished within 5 seconds. They were either blown out or located in an area of localized high agent concentration during discharge. All other component fires were extinguished within 10-15 seconds of discharge. No major differences in extinguishment times were noted when a smaller fire size (0.03 kg/s of heptane) was tested (Scenario 2A). The lower fire size did result in lower decomposition product concentrations.

The test results for the third scenarios (3, 3A, & 3B) are shown in Table 4. The scenarios consists of; a series of Class B spray (0.30 kg/s of heptane) and pan fires (2.0 m<sup>2</sup> diesel, 1.25 m<sup>2</sup> heptane, and 0.25 m<sup>2</sup> heptane), and Class A wood cribs (~300 KW). All fires independent of scenario were extinguished within 15 seconds of discharge except for the one test with Envirogel. Envirogel is a hybrid gaseous/powder agent. Its effectiveness appears to be highly dependent on agent distribution and possibly limited by

obstructions. As in the second scenarios, the pan fires required a longer time to extinguish than the spray fire. There appeared to be no difference in extinguishment times between the two different wood cribs tested.

The test results for fourth scenarios (4 & 4A) are shown in Table 5. The scenarios consist of Class B pan fires (4.0 m<sup>2</sup> diesel, 1.25 m<sup>2</sup> heptane, and 1.25 m<sup>2</sup> diesel). Extinguishment times for these fires ranged from 8-15 seconds independent of fire size or fuel type. Freeburn tests indicate that these fires were burning at about half the expected burning rate due to oxygen starvation. This was confirmed by placing an oxygen probe into the bilge area adjacent to the fire. The measured oxygen concentrations were below 15 % prior to agent discharge. This resulted in lower decomposition product concentration than would be expected for a similar sized fire without oxygen depletion. Due to oxygen starvation and fire locations, the actual fire size of Scenario 4A (planned 4.75 MW) was greater than Scenario 4 (planned 6 MW).

The Hydrogen Fluoride (HF) concentrations measured during these tests are shown in Tables 3 - 5. Hydrogen Chloride (HCl) concentrations for the NAF-SIII agent (the only agent containing chlorine) are shown in Table 6. These concentrations are on the same order as the HF concentrations. For similar fire sizes and discharge times it appears that these halocarbon Halon alternatives produce approximately 5-10 times more HF than Halon 1301. These measured concentrations follow the general trend for fire size to room volume ratios<sup>4&5</sup> previously reported<sup>6</sup>.

### **Gaseous Agent Testing Conclusions**

Based on the results of these tests, the USCG concluded that the proposed protocol<sup>3</sup> provides a reasonable basis for evaluating total flooding halocarbon gaseous agents and distribution systems. It was also concluded that the protocol as drafted could not reasonably evaluate inert gas agents due to the long discharge times they are allowed. Additionally, it is unclear if the protocol<sup>3</sup> is appropriate for hybrid agents such as Envirogenel without additional testing.

On the recommendations submitted by the USCG, the Fire Protection (FP) Subcommittee modified the test protocol and submitted for approval. The Maritime Safety Committee (MSC) approved the protocol as MSC Circular 776 in December 1996.

No unique scaling limitations were found. Results appear to be indicative of expected shipboard performance. The hazard created by the acid gases has been identified and quantified. The protocol<sup>4</sup> as written might not be appropriate for hybrids, like gas/powder mixes. Reviewing all of these tests, the Coast Guard has determined that this protocol<sup>3</sup> is effective and useful for gaseous agent approvals purposes.

Table 5. Fire Scenario 4 &amp; 4A Results

Agent	Fire Scenario 4						Fire Scenario 4A		
	NAF-SIII	NAF-SIII	Halon	CEA-410™	FM-200™	NAF-SIII	CEA-410™	FM-200™	
Agent Conc. (%)	12	12	5	8.2	8.7	12	8.2	8.7	
Relative Concentration <sup>(1)</sup>	1.1	1.1	1.6	1.6	1.3	1.1	1.6	1.3	
Number of Nozzles	2	2	2	4	4	2	4	4	
Nozzle Type	A-1	N-4	H-1	C-1	F-2	A-1	C-1	F-2	
Discharge Time (s)	9.5	9	9	10	10	10.5	10	10	
Ext. Time (s) Heptane pan fire (bilge)						11	8	12	
Ext. Time(s) <sup>(2)</sup> Diesel pan fire (bilge)	10	9	10	12	15	11	9	14	
Ext. Time(s) Heptane spray fire (top)						2	1	2	
Average Agent Conc. (%) 5:00	11.8	10.2	4.7	8.7	8.8	12.311	7.9	8.7	
Average HF Conc. (Ppm) 5:00	1000	9000	400	1400	2400	1900	4500	3700	
Pos. Compt Press. (kPa (IWC))	0.37 (1.5)	0.25 (1)	0.5 (2)	0.75 (3)	0.25 (1)	0.25 (1)	0.25 (1)	0.5 (2)	
Neg. Compt Press. (kPa (IWC))	>1.25 (>5)	2.5 (10)	1.5 (6)	6.25 (25)	2.25 (9)	2.75 (11)	3.5 (14)	3.0 (12)	
O <sub>2</sub> Conc. after Disc. (%) <sup>(3)</sup>	15.1	14.0	17.0	15.0	16.0	13.0 (1)	13.8	14.5	

Note: (1) Relative concentrations are based on the NRL cup burner concentration for n-heptane.

(2) Extinguishment times are measured from the beginning of agent discharge.

(3) After agent discharge, the oxygen concentration is relatively uniform throughout the compartment.

**Table 6. HF and HCl Concentration Results**

<b>Fire Scenario</b>	<b>Fire Size (MW)</b>	<b>Nozzle Type</b>	<b>Discharge Time</b>	<b>Average HF Conc. (ppm)</b>	<b>Average HCL Conc. (ppm)</b>
1	0.025	A-1	10.5	Neg.	Neg.
2	7.95	A-1	9.2	2500	2300
2	7.95	N-4	9.5	4400	4100
2A	2.40	A-1	9.5	1600	1500
3A	3.40	A-1	9.5	5100	5800
3B	3.40	N-4	9.5	3400	2600
3B	3.40	A-1	9.5	2300	2400
4	6.0	A-1	9.5	1000	500
4	6.0	N-4	9.0	9000	10000
4A	4.75	A-1	9.5	1900	1700

**Summary**

The U.S. Coast Guard has established, through the above discribed large scale testing, the effectiveness of these proposed test protocols to evaluate fire protection technologies. The close working relationship between the U.S. Coast Guard and industry during these tests has been extremely valuable to all parties. Through this relationship industry has obtained valuable information concerning the performance of their systems and equipment.

**REFERENCES:**

1. International Maritime Organization, Maritime Safety Committee (MSC) Circular 668
2. Back, G.G., DiNenno, P.L., Hill, S.A., and Leonard, J.T., "Full-Scale Testing of Water Mist Fire Extinguishing Systems for Machinery Spaces on U.S. Army Watercraft," NRL Memo Rpt., 6180-96-7814, 19 February 1996.
3. Back, G.G., Beyler, C.L., DiNenno, P.J., and Hansen, R., "Full-scale Testing of Water Mist Fire Suppression Systems in Machinery Spaces," Final report prepared for the U.S. Coast Guard Research & Development Center, Groton, CT, March 1997
4. International Maritime Organization, "Alternative Arrangements for Halon Fire Extinguishing Systems in Machinery Spaces and Pump-rooms," IMO FP40, 1995
5. Hansen, R., Back, G., Moore, T., "USCG Full-scale Shipboard Testing of Gaseous Agents," Proceedings of the 1994 International CFC and Halon Alternatives Conference
6. Back, G.G., Beyler, C.L., DiNenno, P.J., Peatross, M.J., Hansen, R., Zalosh, R., and Moore, T., "Full-Scale Machinery Space Testing of Gaseous Halon Alternatives," Final report prepared for the U.S. Coast Guard Research & Development Center, Groton, CT, February 1995

# Full-Scale Model Tests of Smoke Movement in Ship Passenger Accommodations (First Report)

---

**REFERENCE:** Yoshida, K., "Full-Scale Model Tests of Smoke Movement in Ship Passenger Accommodations (First Report)," *Very Large-Scale Fires, ASTM STP 1336*, N. R. Keltner, N. J. Alvares, and S. J. Grayson, Eds., American Society for Testing and Materials, 1998.

**ABSTRACT:** Full-scale smoke movement tests were conducted within a model ship accommodation space, which consisted of three deck levels containing a cabin, a corridor, and a stairway. Smoke extraction systems, as well as air supply systems, were installed in the model and used during the tests. A sprinkler system was also installed in a corridor. Cabin fires were simulated by using a burner and a smoke candle placed in a cabin. Temperature, pressure, and smoke movement were observed and analyzed. Numerical simulations using a zone model were also carried out, but the results will be reported in the second report.

**KEYWORDS:** smoke control, ship accommodation space, ship fire

## Introduction

Major fires have occurred in passenger ships throughout the late 1980s and early 1990s. In these fires, smoke was a major threat to the passengers and crew. This fact has been established for building fires. Therefore, smoke control systems, such as smoke extraction ducts and blowers or smoke extraction openings, have been installed in many buildings. However, international regulations regarding the safety of ships (International Convention for the Safety of Life at Sea: SOLAS) do not contain any requirement for smoke control in ships, except for within very large atriums. Therefore, today's ships still have no smoke control systems in their cabin or accommodation areas.

International Maritime Organization (IMO) has started studies and discussions to prepare regulations for smoke control requirements on board ships. The Research Institute of Marine Engineering and Ship-building Research Institute of Japan have started a series of experimental studies on smoke control in ship accommodations in order to develop basic data and contribute to the discussions at IMO.

## Overview of the Study

A full-scale model of a ship accommodation space, which consisted of three deck levels, was constructed. Each deck contained a cabin, a corridor, and a stairway. These decks were connected through the stairway enclosure. A burner and a smoke candle were placed in the cabin on the lowest deck. Hot gas and smoke traveled through the corridors and the stairway enclosure. The cabins and stairway enclosure have air intake systems. The corridors have

---

<sup>1</sup> Head, Fire Safety Division, Research Institute of Marine Engineering, Japan.

air extraction systems. The corridor in the lowest deck has a sprinkler system. Whether these systems are run depends on the given test scenario. Smoke movement in the corridors was observed by video cameras. Gas/air temperature and pressure were measured in the cabins, in the corridors and in the stairway enclosure. The effectiveness of the smoke extraction systems and the sprinkler systems was discussed based on the experimental data. Numerical simulation using a zone model is underway. The results and comparison with test results will be reported later.

## Accommodation Model

### Layout

A full-scale model of ship accommodation space was constructed using 40- and 20-foot freight containers. The model had three deck levels, each of which consisted of a corridor, a cabin, and a stairway enclosure. (See Fig. 1 and Table 1). The walls and ceilings of the spaces were constructed with plywood panels and insulated by glass wool ( $64 \text{ kg/m}^3$ , 25-mm thickness) in the first deck or expanded poly-styrene foam ( $28 \text{ kg/m}^3$ , 25-mm thickness) in the second and third deck. The floor was made of wood plates 25-mm in thickness. The stairway enclosure had openings at the ceilings and decks through which air flowed from one deck to another.

### Openings

Each cabin had a doorway opening 0.7-m wide and 1.9-m high, by which the cabin connects with the corridor. (See Fig. 2). The corridor had a doorway opening 0.9-m wide and 1.9-m high to the stairway enclosure. A door was installed in each of the openings. The cabin in the first deck had another doorway opening to the outside of the model. This opening provided access to the inside the model, and was tightly closed during each test. Except for

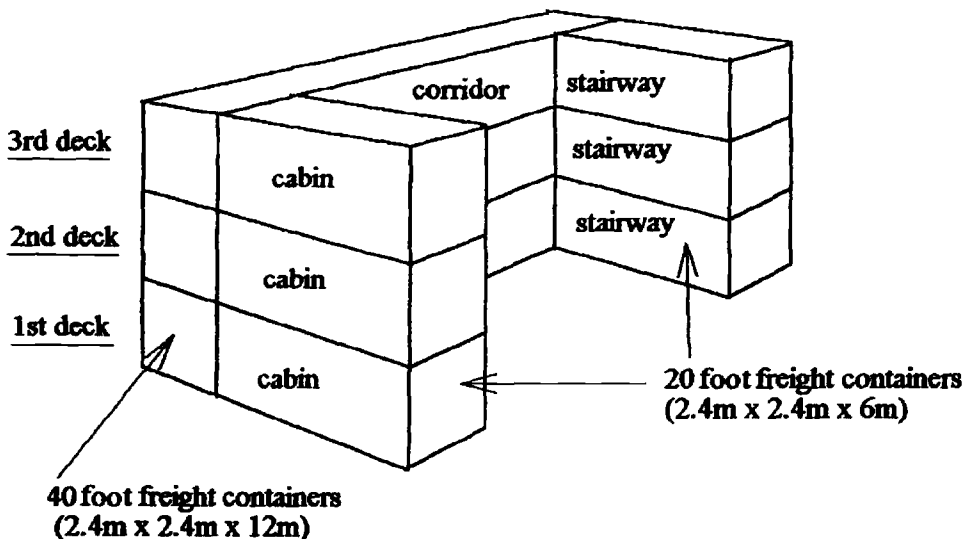


FIG. 1—Model Layout

TABLE 1—Dimensions of spaces of the test model.

Deck	space	width(m)	length(m)	height(m)	volume(m <sup>3</sup> )
1	cabin-1	2.35	4.45	2.35	24.6
1	corridor	1.15	25.00	2.05	58.9
1	stairway	2.35	3.50	2.35	19.3
2	cabin-2	2.35	4.45	2.35	24.6
2	corridor	1.15	11.65	2.05	27.5
2	stairway	2.35	3.70	2.35	20.4
3	cabin-3	2.35	4.45	2.35	24.6
3	corridor	1.15	11.65	2.05	27.5
3	stairway	2.35	3.40	2.35	18.8

the door of the first deck cabin, the model had no opening to the outside, because outside plates of ocean-going ships are usually airtight for safety reasons.

*Ventilation Systems*

In many passenger ships, air is supplied to cabins through duct systems, and extracted from corridors and sanitary spaces of cabins. Stairway enclosures have air supply and extraction systems independent from those of cabins and corridors.

The air supply/extraction systems of the test model attempted to simulate the actual ventilation systems of ships, as far as practicable. (See Fig. 2.) Each cabin of the model had air supply duct and fan systems, but the cabins had no air outlet. The stairway enclosure had

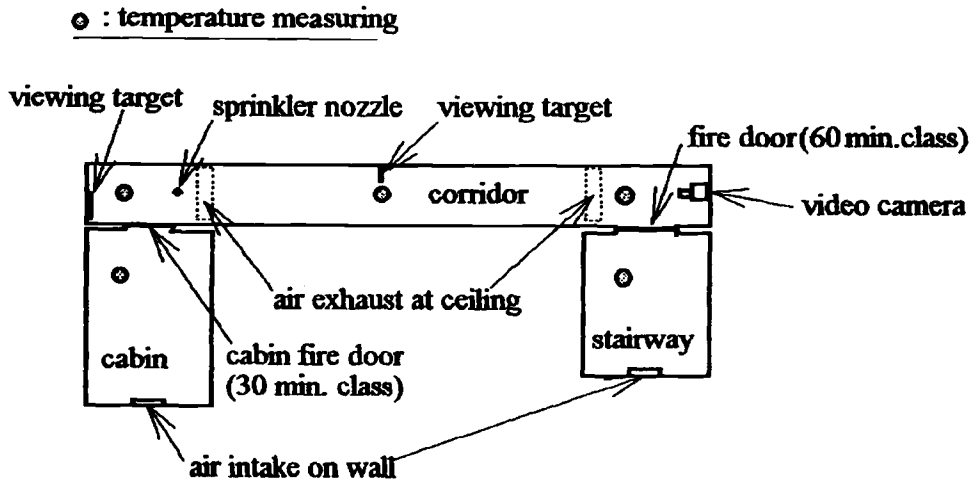


FIG. 2—Arrangements in the Model

three air supply duct and fan systems, one for each deck level. The stairway enclosure had no air outlet. The volume flow rate of the air supply system was controlled. The height of the air inlet in the cabins and stairway enclosure was about 1.5 m from the floor. In the ceiling of the corridor of each deck, there were two air outlets that were connected to a duct and extraction fan system. The flow rate of air extraction was also controlled and could simulate operations of smoke extraction systems.

### *Fire Source*

In real fires, hot gases generated give a driving force to smoke. Therefore, it is necessary to provide a source of hot gas and to mix it with smoke in order to observe smoke movement. An LPG burner was installed in the cabin of the first deck. The LPG supply rate was controlled to obtain a predetermined heat release rate up to 150 kW. Smoke candles were burned beside the LPG burner in order to mix the smoke with hot gas generated by the burner. The purpose of the test was to simulate smoke movement in the early stages of fires.

### *Measurement Devices*

A video camera was installed at one end of each corridor. Observation target marks, which consist of black and white plates 100-mm square, were fitted in the middle and end of the corridor (opposite end to video camera). See Fig. 2.

Vertical temperature profiles were measured in the cabins, corridors, and stairway enclosure by 0.32-mm (diameter) thermocouples. The bare junctions of the thermocouples were placed at the height of 2000-, 1750-, 1500-, 1250- and 1000-mm from the floor.

Air pressure was measured in the cabins, corridors, and stairway enclosure.

### *Sprinkler System*

Passenger ships shall have sprinkler systems in accommodation areas. It is considered that the sprinkler systems, once activated, could reduce the temperature of hot gas developed by fire and this could prevent smoke from spreading through the accommodation area. A sprinkler system was installed in the corridor of the first deck of the test model. The sprinkler head is a fast-response type. The RTI is about 40 and the water delivery rate is about 3 liters/min<sup>2</sup>.

## **Test Conditions**

### *Doorway Openings*

Some preliminary tests were conducted under various open/hot conditions of the doors of the cabin and stairway enclosures. Closed doors prevented smoke from traveling. However, stairway doors may be opened by persons who escape through the doorway. Therefore, in the main tests, all the doors were kept opened to simulate the worst case scenario.

### *Heat Release from LPG Burner*

The maximum heat release rate of the LPG burner was 150 kW. The maximum temperature in the cabin of fire origin reached 350°C by 150 kW output of the burner, and this was

TABLE 2-1—Test conditions and results.

Test No.		12	13	14	16	17	18	19
HRR	(kW)	52	78	104	52	78	104	104
air supply rate to cabin, stairway	air change per hour	0	0	0	10	10	10	10
air extraction from corridor (air change/h)	3rd deck	0	0	0	10	10	10	10
	2nd deck	0	0	0	10	10	10	10
	1st deck	0	0	0	10	10	10	10
increased air extraction from 1 <sup>st</sup> deck corridor	air change per hour	not changed						
	time(sec)							
sprinkler system activation time	(sec)	not used						
Time to smoke arrival 1st deck	in cabin	8	10	8	6	8	10	10
	corridor near cabin	12	16	12	12	12	14	16
	corridor center	20	20	20	20	18	22	20
	corridor near stairway	28	30	30	34	30	32	30
	in stairway	42	42	40	50	44	44	42
Time to smoke arrival 2nd deck	in cabin	—	220	188	356	340	280	316
	corridor near cabin	—	132	116	164	160	136	148
	corridor center	—	112	100	156	132	108	120
	corridor near stairway	—	96	88	144	124	96	108
	in stairway	—	76	64	100	88	72	76
Time to smoke arrival 3rd deck	in cabin	—	220	292	420	—	—	—
	corridor near cabin	372	132	192	392	372	288	344
	corridor center	324	112	168	368	292	240	248
	corridor near stairway	256	96	140	224	220	172	136
	in stairway	232	76	128	288	284	124	—

the acceptable upper limit for the model due to its wooden construction. This heat release rate is relatively small, but is believed to simulate the early stage of a fire.

#### *Air Supply/Extraction*

The air supply rate to the cabins and stairway enclosure was set to a rate to simulate 10 times air change per hour of each space. The air supply systems were not used in some tests, or stopped during the test. It is a common practice for the crew to stop ventilation in case of fire.

The air extraction rate was set at 10 air changes per hour for tests to simulate normal air conditioning. The extraction rate was increased during the test, up to a rate of 50 air changes per hour to simulate the operation of smoke extraction systems.

TABLE 2-2—Test conditions and results.

Test No.	(kW)	22	23	24	28	32	34	38	42	44	48	52	54	58	
HRR		52	78	104	104	52	104	104	52	104	104	52	104	104	
air supply rate to cabin, stairway	air change per hour	10	10	10	10	10	10	10	10	10	10	10	10	10	
air extraction from 3 <sup>rd</sup> deck		10	10	10	10	10	10	10	10	10	10	10	10	10	
corridor	air extraction from 2 <sup>nd</sup> deck	10	10	10	10	10	10	10	10	10	10	10	10	10	
(air change/h)	air extraction from 1 <sup>st</sup> deck	10	10	10	10	10	10	10	10	10	10	10	10	10	
increased air extraction from 1 <sup>st</sup> deck	air change per hour	20	20	20	20	30	30	30	40	40	40	50	50	50	
corridor	time(sec)	66	55	40	161	66	38	149	66	40	158	69	40	158	
sprinkler system activation time	(sec)	not used													
Time to smoke arrival 1st deck	in cabin	10	8	10	10	8	8	10	6	8	8	8	10	8	
corridor near 1st deck	near cabin	16	14	14	14	14	12	14	14	12	14	14	14	14	
corridor near stairway	center	22	20	18	20	20	18	20	20	16	18	20	20	20	
in stairway	near stairway	34	30	28	30	32	28	28	30	26	28	32	28	28	
Time to smoke arrival 2nd deck	in cabin	50	42	40	40	46	38	38	48	34	38	44	38	38	
corridor near 2nd deck	near cabin	---	248	232	240	---	448	320	---	---	---	---	---	---	
corridor near stairway	center	400	128	124	128	296	172	128	---	320	132	---	---	128	
in stairway	near stairway	296	120	112	108	244	132	108	---	224	108	---	---	104	
Time to smoke arrival 3rd deck	in cabin	280	104	100	100	212	116	96	---	212	96	---	---	92	
corridor near 3rd deck	near cabin	136	68	68	72	116	80	68	352	108	72	---	---	68	
in stairway	center	---	212	444	---	---	---	---	---	---	---	---	---	---	
Time to smoke arrival 3rd deck	near cabin	---	228	232	264	---	---	296	---	---	---	---	---	---	
corridor near 3rd deck	center	---	216	212	172	---	328	184	---	---	---	---	---	---	
in stairway	near stairway	448	136	152	136	---	216	124	---	452	132	---	108	124	
Time to smoke arrival 3rd deck	in stairway	---	176	180	168	---	300	264	---	---	---	332	84	---	

TABLE 2-3—Test conditions and results.

Test No.		61	62	63	64	65	66	67	68	69
<b>HRR</b>	<b>(kW)</b>	52	52	52	78	104	104	104	104	104
air supply rate to cabin, stairway	air change per hour	10	10	10	10	10	10	10	10	10
air extraction from corridor (air change/h)	3 <sup>rd</sup> deck	10	10	10	10	10	10	10	10	10
	2 <sup>nd</sup> deck	10	10	10	10	10	10	10	10	10
	1 <sup>st</sup> deck	10	10	10	10	10	10	10	10	10
increased air extraction from 1 <sup>st</sup> deck corridor	air change per hour	not changed					40	40	30	20
	time(sec)						44	162	44	42
sprinkler system activation time	(sec)	no use	52	52	58	44	44	42	44	42
sprinkler head type			1	7	7	7	7	7	7	7
Time to smoke arrival 1st deck	in cabin	6	8	8	12	8	10	8	8	8
	corridor near cabin	14	14	16	20	18	14	14	16	14
	corridor center	24	24	24	30	24	22	20	22	20
	corridor near stairway	36	36	36	38	32	30	30	30	28
	in stairway	60	64	56	58	50	54	44	52	50
Time to smoke arrival 2nd deck	in cabin	392	472	---	344	252	---	---	428	308
	corridor near cabin	200	208	308	172	132	428	136	224	136
	corridor center	164	172	228	136	108	376	108	184	112
	corridor near stairway	156	140	200	132	104	372	104	156	108
	in stairway	96	96	108	96	68	300	72	92	76
Time to smoke arrival 3rd deck	in cabin	---	---	---	---	---	---	---	---	---
	corridor near cabin	---	---	---	404	328	---	---	---	364
	corridor center	420	456	---	356	208	---	---	460	336
	corridor near stairway	28	204	344	248	148	---	152	404	228
	in stairway	304	356	---	364	240	---	---	---	260

*Sprinkler System Operation*

The sprinkler system was used in some tests. The sprinkler head was activated automatically. Duration of sprinkling water was about 5 min.

**Tests Results and Conclusions**

It was observed that temperature increase accompanied the arrival of smoke. Therefore, "time to smoke arrival" was defined as "time when temperature at 2-m height rises 3°C." Tables 2-1, 2-2, and 2-3 show the test conditions and test results.

Figure 3 shows the relationship between time-to-smoke-arrival and heat-release rate or air-extraction rate. The air change rate is converted into an air volume extraction rate (total volume of cabin and stairway enclosure at each deck level is approximately 45 m<sup>3</sup>).

Analysis of the pressure data and video observation is still underway. Numerical simulation using a zone model is underway. These results will be reported at a later date.

The following conclusions are derived from the experimental results obtained so far:

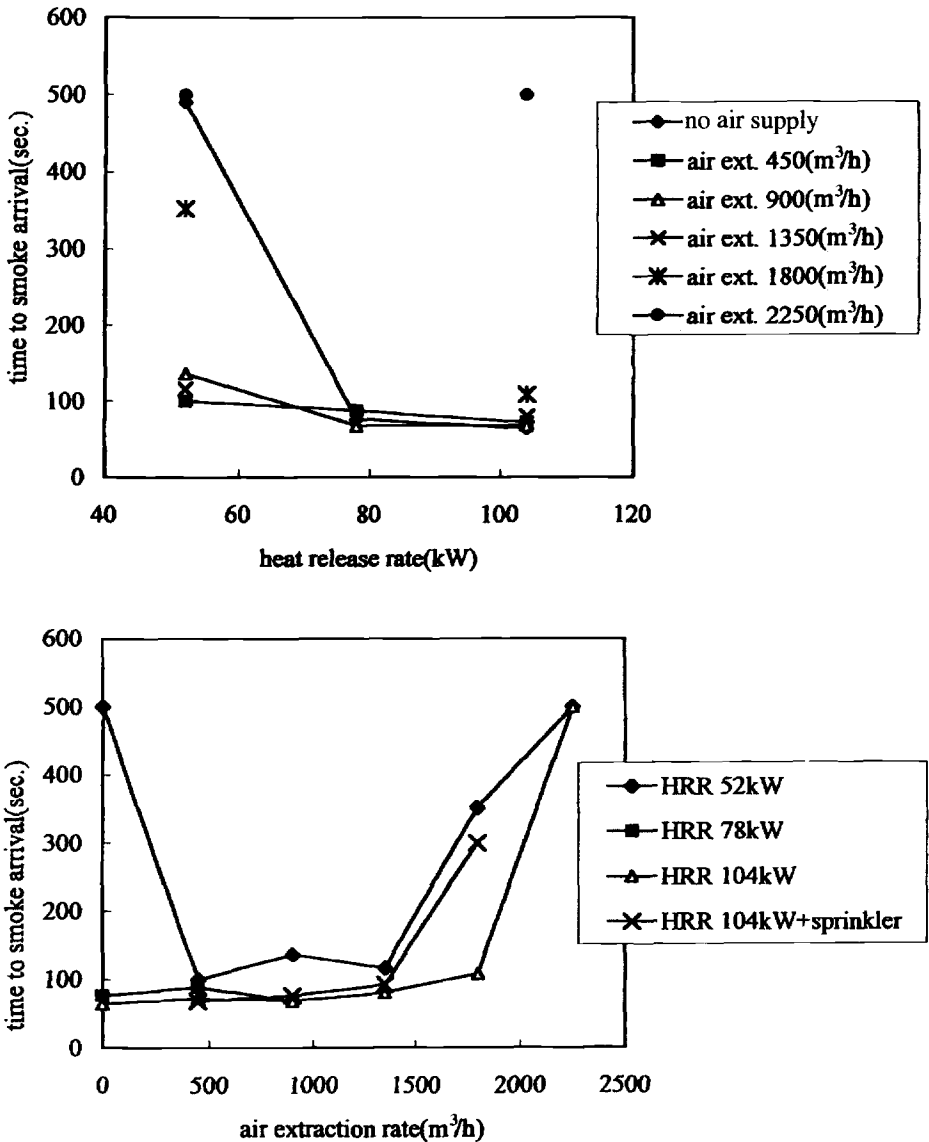


FIG. 3—Time to smoke arrival at second deck stairway.

- (1) It is a typical crew response to stop the air conditioning system when a fire occurs. However, this operation does not stop smoke movement, except in cases of very low heat release.
- (2) Increased smoke extraction may prevent the passage of smoke to upper decks.

The following will be discussed when the results of further analysis are available, including zone model calculations:

- (a) Whether pressurization of the stairway enclosure may be effective, even when the doors are open,
- (b) Whether the sprinkler system may be effective for preventing or reducing smoke movement.